

**ORGANISATION EUROPÉENNE POUR LA RECHERCHE NUCLÉAIRE
CERN EUROPEAN ORGANIZATION FOR NUCLEAR RESEARCH**

**Handbook of LHC Higgs cross sections:
4. Deciphering the nature of the Higgs sector**

Report of the LHC Higgs Cross Section Working Group

Editors: C. Anastasiou
D. de Florian
C. Grojean
F. Maltoni
C. Mariotti
A. Nikitenko
M. Schumacher
R. Tanaka

³

Part I

⁴

Standard Model Predictions¹

¹B. Mellado, P. Musella, M. Grazzini, R. Harlander (eds.); plus Authors

5 Chapter 1

6 VBF and VH¹

7 The production of a Standard Model Higgs boson in association with two hard jets in the forward and
8 backward regions of the detector, frequently quoted as the “vector-boson fusion” (VBF) channel, and the
9 production of a Higgs boson in association with a W or Z boson, known as “VH production” or “Higgs-
10 strahlung”, represent cornerstones in a comprehensive study of Higgs-boson couplings at the LHC. These
11 production channels do not only provide valuable information on the couplings of Higgs bosons to the
12 massive gauge bosons by themselves, but also allow for the isolation of the Higgs-boson decays into
13 τ -lepton or bottom-quark pairs, whose investigation is essential in the Higgs couplings analysis.

14 In the previous reports [1–3], state-of-the-art predictions and error estimates for the total and
15 differential cross sections for $pp \rightarrow H + 2\text{ jets}$ and $pp \rightarrow HW/Z \rightarrow H + 2\text{ leptons}$ were compiled, but
16 the process of improving and refining predictions is still ongoing, even within the Standard Model. In this
17 contribution we update the cross-section predictions for VBF and VH production, covering integrated
18 total and fiducial cross sections as well as differential distributions. In detail, the presented state-of-
19 the-art predictions include QCD corrections up to next-to-next-to-leading order (NNLO), electroweak
20 (EW) corrections up to next-to-leading order (NLO), and contributions from specific partonic channels
21 that open at higher perturbative orders, such as photon-induced collisions or gluon-fusion contributions.
22 Apart from collecting numerical results, we give recommendations as to how to combine the individual
23 components and to assess conservative estimates of remaining theoretical uncertainties. Moreover, issues
24 connected to the matching and the impact of parton showers (PS) are discussed.

25 1 VBF cross-section predictions

26 1.1 Programs and tools for VBF

27 1.1.1 HAWK

28 HAWK [4, 5] is a parton-level event generator for Higgs production in vector-boson fusion [6, 7], $pp \rightarrow$
29 $H + 2\text{ jets}$, and Higgs-strahlung [8], $pp \rightarrow HW/Z \rightarrow H + 2\text{ leptons}$. Here we summarise its most
30 important features for the VBF channel.

31 HAWK includes the complete NLO QCD and EW corrections and all weak-boson fusion and
32 quark–antiquark annihilation diagrams, i.e. t -channel and u -channel diagrams with VBF-like vector-
33 boson exchange and s -channel Higgs-strahlung diagrams with hadronic weak-boson decay, as well as all
34 interferences. HAWK allows for an on-shell Higgs boson or for an off-shell Higgs boson (with optional
35 decay into a pair of gauge singlets). The EW corrections include also the contributions from photon-
36 induced channels, but contributions from effective Higgs–gluon couplings, which are part of the QCD
37 corrections to Higgs production via gluon fusion, are not taken into account. External fermion masses
38 are neglected and the renormalisation and factorisation scales are set to M_W by default. Since version
39 2.0, HAWK includes anomalous Higgs-boson–vector-boson couplings. Further features of HAWK are
40 described in Ref. [4] and on its web page [5].

¹S. Dittmaier, P. Govoni, B. Jäger, J. Nielsen, L. Perrozzi, E. Pianori, A. Rizzi, F. Tramontano (eds.): W.A. Astill, J. Bellm, W.J. Bizon, F. Campanario, J. Campbell, A. Denner, F.A. Dreyer, R.K. Ellis, G. Ferrera, T. Figy, M. Grazzini, R. Harlander, S. Kallweit, A. Karlberg, A. Kulesza, A. Mück, S. Plätzer, E. Re, G.P. Salam, P. Schichtel, M. Sjödahl, V. Theeuwes, C. Williams, G. Zanderighi, M. Zaro, T. Zirke.

41 **1.1.2 *MadGraph5_aMC@NLO***

42 Higgs production through VBF, possibly in association with extra jets, can be generated automatically
43 in **MADGRAPH5_AMC@NLO**, and is thus exactly on the same footing as any other generic process. A
44 phenomenology study of H+2jet VBF production has been presented in Ref. [9], where NLO QCD re-
45 sults matched to different parton showers (HERWIG6, HERWIG++ and virtuality-ordered PYTHIA6)
46 have been compared to fixed-order NLO predictions and the corresponding POWHEG-matched ones.
47 Predictions for VBF matched to PYTHIA8 have been successively presented in Ref. [10]. The code for
48 simulating VBF Higgs production at the NLO(+PS) accuracy can be generated and run via the commands

```
generate p p > h j j $$ w+ w- z [QCD]
output VBF-MG5_aMC
launch
```

49 where the $\$\$$ syntax forbids s -channel W and Z bosons. Virtual corrections featuring electroweak bosons
50 in the loop (pentagons) are not included when using the above command lines. Note that diagrams
51 of this class are either zero, or negligible for all practical purposes.² As the default Standard Model
52 in **MADGRAPH5_AMC@NLO** assumes a non-vanishing bottom mass, no b quark is included in the
53 definition of the p and j multiparticles. In order to include b quarks, it is sufficient to load the ‘loop_sm-
54 no_b_mass’ model before generating the code, with the command

```
import model loop_sm-no_b_mass
```

55 In both cases, a $V_{CKM} = 1$ is assumed and the Higgs boson is kept on its mass shell.

56 For what concerns Higgs plus three jets production in VBF, predictions for the third and the veto jet at
57 NLO+PS accuracy have been presented in Ref. [10], considering t -channel modes only. The relevant
58 code can be generated and executed with the commands

```
generate p p > h j j j $$ w+ w- z [QCD]
output VBF-MG5_aMC
launch
```

59 **1.1.3 *POWHEG***

60 The POWHEG BOX is a program package that allows for the matching of NLO QCD calculations
61 with parton-shower generators using the POWHEG method. VBF-induced Higgs production has been
62 implemented in the POWHEG BOX in the factorized approximation, where cross-talk between the
63 fermion lines is neglected, in Ref. [11]. More recently, also an implementation of Higgs production
64 in association with three jets via VBF, based on the NLO QCD calculation of Ref. [12], has become
65 available [13].

66 Both implementations are based on the respective NLO QCD calculations for genuine weak-boson
67 fusion topologies, i.e. the VBF approximation. Quark–antiquark annihilation and interference contribu-
68 tions between t - and u -channel contributions are disregarded. The CKM matrix elements can be assigned
69 by the user. External fermion masses are neglected throughout. For the choice of renormalization and
70 factorization scales, various options are available. For this report, fixed scales, $\mu_F = \mu_R = M_W$, are
71 used, and contributions from external bottom and top quarks are entirely disregarded.

72 **1.1.4 *proVBFH***

73 **proVBFH** is a parton-level Monte Carlo program for the calculation of differential distributions for VBF
74 Higgs production to NNLO QCD accuracy. It is based on POWHEG’s fully differential NLO QCD

²For this reason, the internal check of pole cancellation fails. In order to disable these checks, the parameters `IRPoleCheckThreshold` and `PrecisionVirtualAtRunTime` inside `Cards/FKS_params.dat` must be set to -1.

75 calculation for Higgs production in association with three jets via VBF [12, 13], and an inclusive NNLO
 76 QCD calculation [14], both taken in the structure-function approximation, which are combined using the
 77 projection-to-Born method described in Ref. [15].

78 proVBFH uses a diagonal CKM matrix, Breit–Wigner distributions for the W and Z bosons, and
 79 neglects fermion masses. It is based on the structure-function approach, which assumes that there is no
 80 cross-talk between the upper and lower hadronic sectors. For this report, the factorisation and renormal-
 81 isation scales are set to the W-boson mass, $\mu_R = \mu_F = M_W$.

82 **1.1.5 VBFNLO**

83 VBFNLO [16] is a parton-level Monte Carlo generator for the simulation of various processes with weak
 84 bosons at NLO QCD accuracy. In particular, Higgs production in association with two [17] or three
 85 jets [12] via VBF is implemented with different options for the decays of the Higgs boson. For VBF
 86 Higgs production in association with two jets, in addition to the default SM implementation, options are
 87 available for the inclusion of anomalous coupling effects [18] and VBF Higgs production in the context of
 88 the MSSM [19]. NLO EW corrections to VBF can also be computed [19]. Quark–antiquark annihilation
 89 and interference contributions between t - and u -channel contributions are not taken into account. In the
 90 following we will refer to this setup as “VBF approximation”.

91 **1.1.6 VBF@NNLO**

92 VBF@NNLO [14, 20] computes VBF total Higgs cross sections at LO, NLO, and NNLO in QCD via the
 93 structure-function approach. This approach [21] consists in considering VBF process as a double deep-
 94 inelastic scattering (DIS) attached to the colourless pure electroweak vector-boson fusion into a Higgs
 95 boson. According to this approach one can include NLO QCD corrections to the VBF process employing
 96 the standard DIS structure functions $F_i(x, Q^2)$; $i = 1, 2, 3$ at NLO [22] or similarly the corresponding
 97 structure functions at NNLO [23–26].

98 The effective factorisation underlying the structure-function approach does not include all types
 99 of contributions. At LO an additional contribution arises from the interferences between identical final-
 100 state quarks (e.g., $uu \rightarrow Huu$) or between processes where either a W or a Z can be exchanged (e.g.,
 101 $ud \rightarrow Hud$). These LO contributions have been added to the NNLO results presented here, even if they
 102 are very small. Apart from such contributions, the structure-function approach is exact also at NLO. At
 103 NNLO, however, several types of diagrams violate the underlying factorisation. Their impact on the total
 104 rate has been computed or estimated in Ref. [20] and found to be negligible. Some of them are colour
 105 suppressed and kinematically suppressed [12, 27, 28], others have been shown in Ref. [29] to be small
 106 enough not to produce a significant deterioration of the VBF signal.

107 At NNLO QCD, the theoretical QCD uncertainty is reduced to less than 2%. Electroweak correc-
 108 tions, which are at the level of 5%, are not included in VBF@NNLO. The Higgs boson can either be
 109 produced on its mass-shell, or off-shell effects can be included in the complex-pole scheme.

110 **1.2 VBF parameters and cuts**

The numerical results presented in the next section have been computed using the values of the EW
 parameters given in Section ???. The electromagnetic coupling is fixed in the G_F scheme,

$$\alpha_{G_F} = \sqrt{2} G_F M_W^2 (1 - M_W^2/M_Z^2)/\pi, \quad (1.1)$$

and the weak mixing angle, θ_w , is defined in the on-shell scheme,

$$s_w^2 \equiv \sin^2 \theta_w = 1 - M_W^2/M_Z^2. \quad (1.2)$$

The renormalisation and factorisation scales are set equal to the W-boson mass,

$$\mu = \mu_R = \mu_F = M_W, \quad (1.3)$$

111 and both scales are varied in the range $M_W/2 < \mu < 2M_W$ keeping $\mu_F = \mu_R$, which catches the full
 112 scale uncertainty of integrated cross sections (and of differential distributions in the essential regions).

113 In the calculation of the QCD-based cross sections, we have used the PDF4LHC15_nnlo_100
 114 PDFs [30], for the calculation of the EW corrections we have employed the NNPDF2.3QED PDF
 115 set [31], which includes a photon PDF. Note, however, that the relative EW correction factor, which
 116 is used in the following, hardly depends on the PDF set, so that the uncertainty due to the mismatch in
 117 the PDF selection is easily covered by the other remaining theoretical uncertainties.

For the fiducial cross section and for differential distributions the following reconstruction scheme
 and cuts have been applied. Jets are constructed according to the anti- k_T algorithm [32] with $D = 0.4$,
 using the default recombination scheme (E scheme). Jets are constructed from partons j with

$$|\eta_j| < 5, \quad (1.4)$$

118 where η_j denotes the pseudo-rapidity. Real photons, which appear as part of the EW corrections, are an
 119 input to the jet clustering in the same way as partons. Thus, in real photon radiation events, final states
 120 may consist of jets only or jets plus a real identifiable photon, depending on whether the photon was
 121 merged into a jet or not, respectively. Both events with and without isolated photons are kept.

Jets are ordered according to their p_T in decreasing progression. The jet with highest p_T is called
 leading jet (j_1), the one with next highest p_T subleading jet (j_2), and both are the tagging jets. Only
 events with at least two jets are kept. They must satisfy the additional constraints

$$p_{Tj} > 20 \text{ GeV}, \quad |y_j| < 5, \quad |y_{j_1} - y_{j_2}| > 3, \quad M_{jj} > 130 \text{ GeV}, \quad (1.5)$$

122 where $y_{j_{1,2}}$ are the rapidities of the two leading jets. The cut on the 2-jet invariant mass M_{jj} is sufficient
 123 to suppress the contribution of s -channel diagrams to the VBF cross section to the level of 1–2%, so
 124 that the DIS approximation of taking into account only t - and u -channel contributions is justified. In the
 125 cross sections given below, the s -channel contributions will be given for reference, although they are not
 126 included in the final VBF cross sections by default.

127 While the VBF cross sections in the DIS approximation are independent of the CKM matrix,
 128 quark mixing has some effect on s -channel contributions. For the calculation of the latter we employed
 129 a Cabibbo-like CKM matrix (i.e. without mixing to the third quark generation) with Cabibbo angle,
 130 θ_C , fixed by $\sin \theta_C = 0.225$. Moreover, we note that we employ complex W- and Z-boson masses
 131 in the calculation of s -channel and EW corrections in the standard HAWK approach, as described in
 132 Refs. [6, 7].

133 The Higgs boson is treated as on-shell particle in the following consistently, since its finite-width
 134 and off-shell effects in the signal region are suppressed in the SM.

135 1.3 Integrated VBF cross sections

The final VBF cross section σ^{VBF} is calculated according to:

$$\sigma^{\text{VBF}} = \sigma_{\text{NNLOQCD}}^{\text{DIS}}(1 + \delta_{\text{EW}}) + \sigma_\gamma, \quad (1.6)$$

136 where $\sigma_{\text{NNLOQCD}}^{\text{DIS}}$ is the NNLO QCD prediction for the VBF cross section in DIS approximation, based
 137 on the calculation of Ref. [15] with PDF4LHC15_nnlo_100 PDFs. The relative NLO EW correction
 138 δ_{EW} is calculated with HAWK, but taking into account only t - and u -channel diagrams corresponding
 139 to the DIS approximation. The contributions from photon-induced channels, σ_γ , and from s -channel
 140 diagrams, $\sigma_{s\text{-channel}}$ are obtained from HAWK as well, where the latter includes NLO QCD and EW
 141 corrections. To obtain σ^{VBF} , the photon-induced contribution is added linearly, but $\sigma_{s\text{-channel}}$ is left out
 142 and only shown for reference, since it is not of true VBF origin (like other contributions such as H+2jet
 143 production via gluon fusion).

Table 1.1: Total VBF cross sections including QCD and EW corrections and their uncertainties for different proton–proton collision energies \sqrt{s} for a Higgs-boson mass $M_H = 125$ GeV.

$\sqrt{s}[\text{GeV}]$	$\sigma^{\text{VBF}}[\text{fb}]$	$\Delta_{\text{scale}}[\%]$	$\Delta_{\text{PDF}/\alpha_s/\text{PDF} \oplus \alpha_s}[\%]$	$\sigma_{\text{NNLOQCD}}^{\text{DIS}}[\text{fb}]$	$\delta_{\text{EW}}[\%]$	$\sigma_\gamma[\text{fb}]$	$\sigma_{s\text{-channel}}[\text{fb}]$
7	1241.4(1)	$^{+0.19}_{-0.21}$	$\pm 2.1 / \pm 0.4 / \pm 2.2$	1281.1(1)	-4.4	17.1	584.5(3)
8	1601.2(1)	$^{+0.25}_{-0.24}$	$\pm 2.1 / \pm 0.4 / \pm 2.2$	1655.8(1)	-4.6	22.1	710.4(3)
13	3781.7(1)	$^{+0.43}_{-0.33}$	$\pm 2.1 / \pm 0.5 / \pm 2.1$	3939.2(1)	-5.3	51.9	1378.1(6)
14	4277.7(2)	$^{+0.45}_{-0.34}$	$\pm 2.1 / \pm 0.5 / \pm 2.1$	4460.9(2)	-5.4	58.5	1515.9(6)

Table 1.2: Fiducial VBF cross sections including QCD and EW corrections and their uncertainties for different proton–proton collision energies \sqrt{s} for a Higgs-boson mass $M_H = 125$ GeV.

$\sqrt{s}[\text{GeV}]$	$\sigma^{\text{VBF}}[\text{fb}]$	$\Delta_{\text{scale}}[\%]$	$\Delta_{\text{PDF}/\alpha_s/\text{PDF} \oplus \alpha_s}[\%]$	$\sigma_{\text{NNLOQCD}}^{\text{DIS}}[\text{fb}]$	$\delta_{\text{EW}}[\%]$	$\sigma_\gamma[\text{fb}]$	$\sigma_{s\text{-channel}}[\text{fb}]$
7	602.4(5)	$^{+1.3}_{-1.6}$	$\pm 2.3 / \pm 0.3 / \pm 2.3$	630.8(5)	-6.1	9.9	8.2
8	795.9(6)	$^{+1.3}_{-1.3}$	$\pm 2.3 / \pm 0.3 / \pm 2.3$	834.8(7)	-6.2	13.1	11.1
13	1975.4(9)	$^{+1.3}_{-1.2}$	$\pm 2.1 / \pm 0.4 / \pm 2.2$	2084.2(10)	-6.8	32.3	29.0
14	2236.6(26)	$^{+1.5}_{-1.3}$	$\pm 2.1 / \pm 0.4 / \pm 2.1$	2362.2(28)	-6.9	36.7	33.1

Tables 1.1 and 1.2 summarize the total and fiducial Standard Model VBF cross sections and the corresponding uncertainties for the different proton–proton collision energies for a Higgs-boson mass $M_H = 125$ GeV. The scale uncertainty, Δ_{scale} , results from a variation of the factorization and renormalization scales (1.3) by a factor of 2 keeping $\mu_F = \mu_R$, as indicated above, and the combined $\text{PDF} \oplus \alpha_s$ uncertainty $\Delta_{\text{PDF} \oplus \alpha_s}$ is obtained following the PDF4LHC recipe [30]. Both Δ_{scale} and $\Delta_{\text{PDF} \oplus \alpha_s}$ are actually obtained from $\sigma_{\text{NNLOQCD}}^{\text{DIS}}$, but this QCD-driven uncertainties can be taken over as uncertainty estimates for σ^{VBF} as well. The theoretical uncertainties of integrated cross sections originating from unknown higher-order EW effects can be estimated by

$$\Delta_{\text{EW}} = \max\{0.5\%, \delta_{\text{EW}}^2, \sigma_\gamma / \sigma^{\text{VBF}}\}. \quad (1.7)$$

The first entry represents the generic size of NNLO EW corrections, while the second accounts for potential enhancement effects. Note that the whole photon-induced cross-section contribution σ_γ is treated as uncertainty here, because the PDF uncertainty of σ_γ is estimated to be 100% with the NNPDF2.3QED PDF set. At present, this source, which is about 1.5%, dominates the EW uncertainty of the integrated VBF cross section

Results for the VBF cross sections from a scan over the SM Higgs-boson mass M_H can be found in Appendix A.

1.4 Differential VBF cross sections

Figures 1–5 show the most important differential cross sections for Higgs production via VBF in the SM. The upper panels show the LO cross section as well as the best fixed-order prediction, based on the analogue of Eq. (1.6) for differential cross sections. The lower panels illustrate relative contributions and the ratios $(\text{NLO}/\text{LO})_{\text{qcd}}$ and $(\text{NNLO}/\text{NLO})_{\text{qcd}}$ of QCD predictions when going from LO to NLO QCD to NNLO QCD. Moreover, the relative EW correction to the (anti)quark–(anti)quark channels ($\delta_{\text{EW}} = \sigma_{\text{EW}} / \sigma_{\text{LO}}$) and the relative correction induced by initial-state photons ($\delta_\gamma = \sigma_\gamma / \sigma_{\text{LO}}$) are shown. Finally, the relative size of the s -channel contribution for Higgs+2jet production ($\delta_{s\text{-channel}} =$

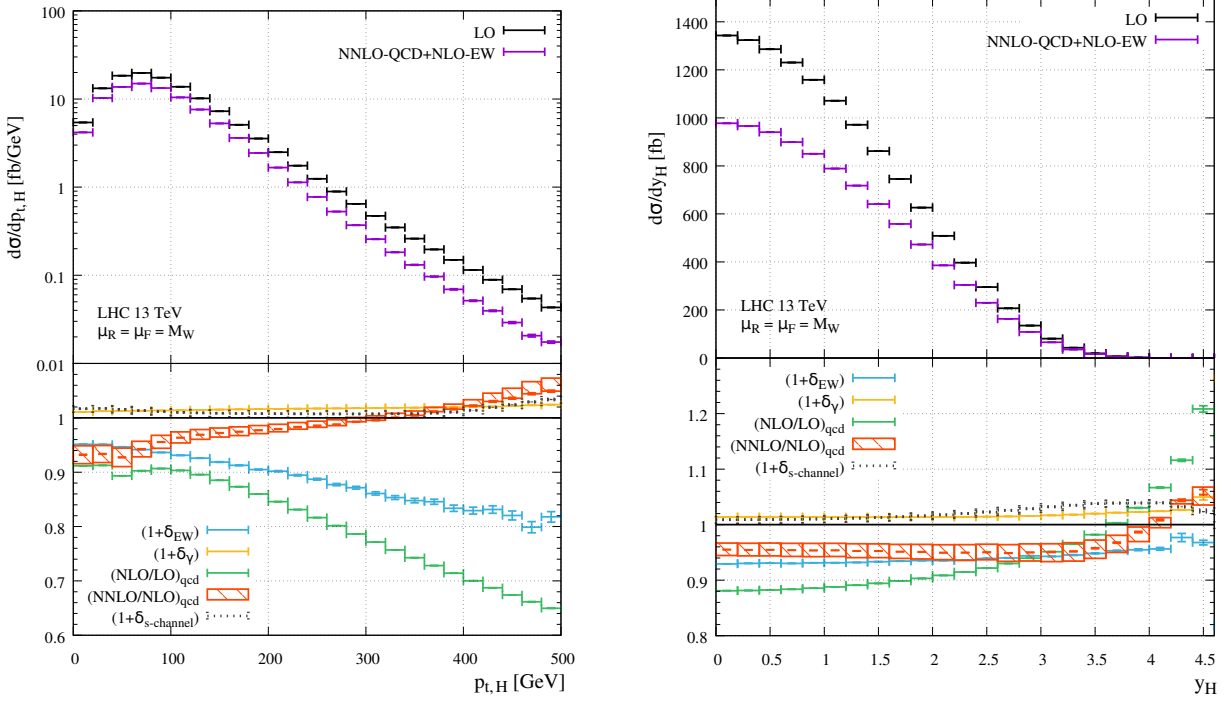


Fig. 1: Transverse-momentum and rapidity distributions of the Higgs boson in VBF at LO and including NNLO QCD and NLO EW corrections (upper plots) and various relative contributions (lower plots) for $\sqrt{s} = 13$ TeV and $M_H = 125$ GeV.

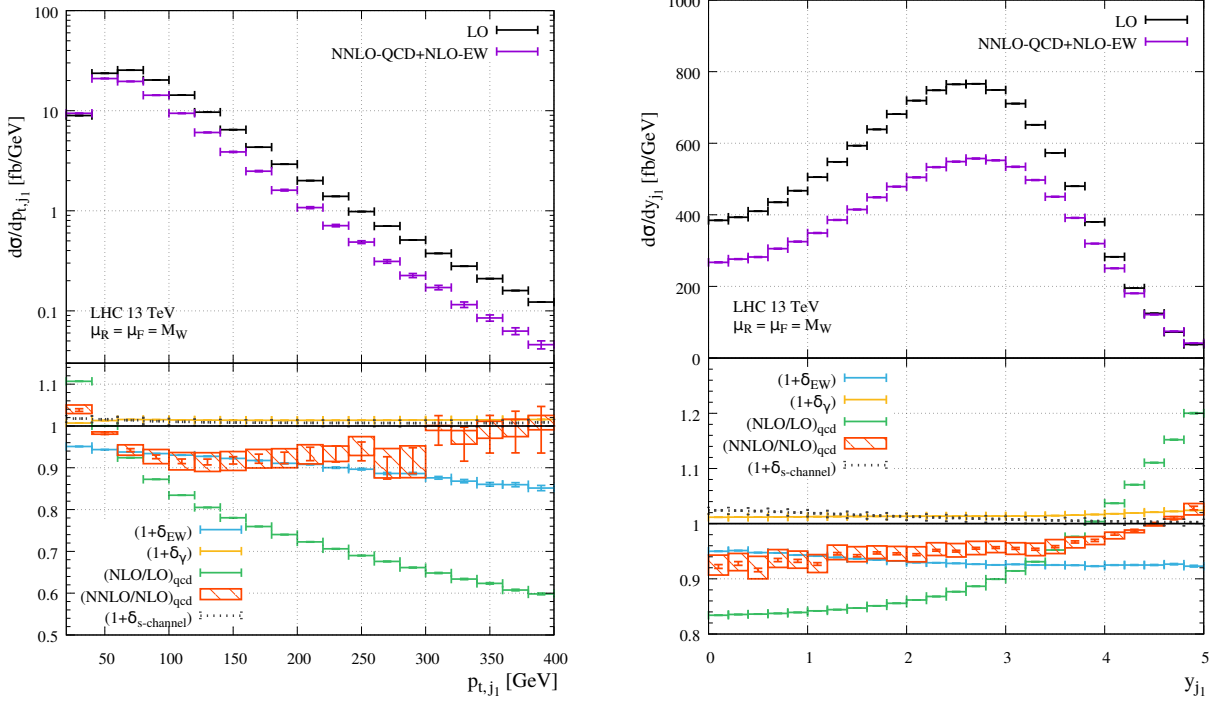


Fig. 2: Transverse-momentum and rapidity distributions of the leading jet in VBF at LO and including NNLO QCD and NLO EW corrections (upper plots) and various relative contributions (lower plots) for $\sqrt{s} = 13$ TeV and $M_H = 125$ GeV.

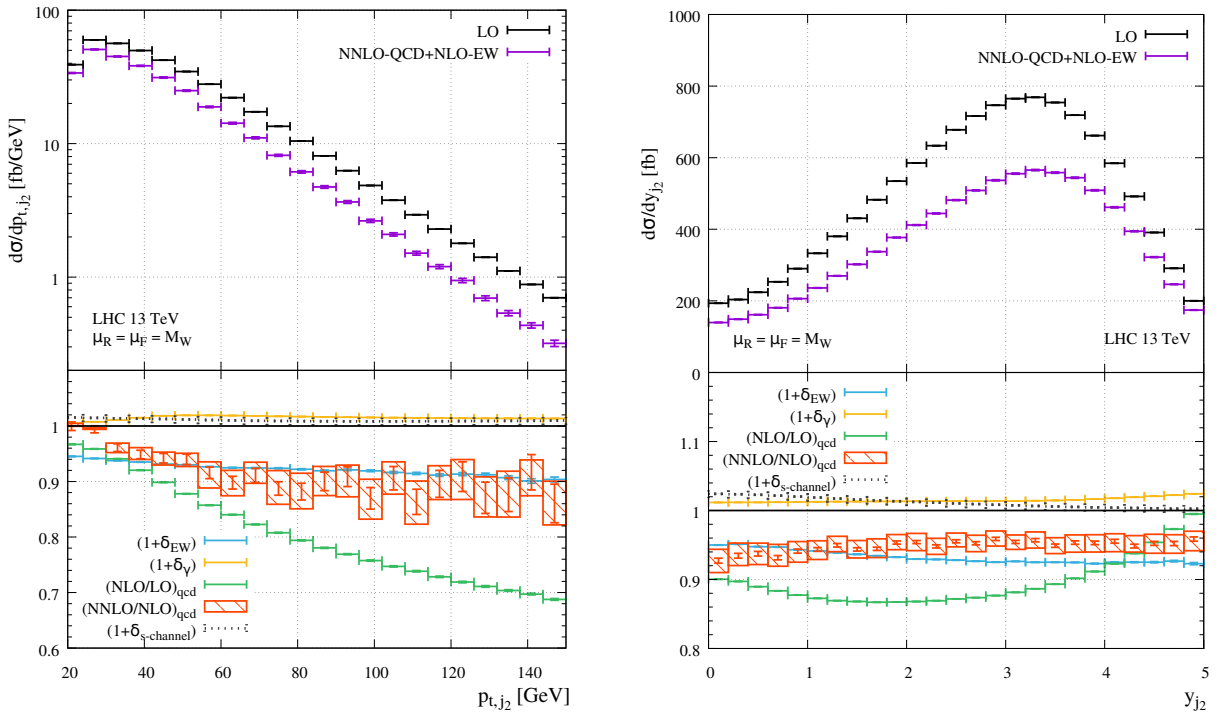


Fig. 3: Transverse-momentum and rapidity distributions of the subleading jet in VBF at LO and including NNLO QCD and NLO EW corrections (upper plots) and various relative contributions (lower plots) for $\sqrt{s} = 13$ TeV and $M_H = 125$ GeV.

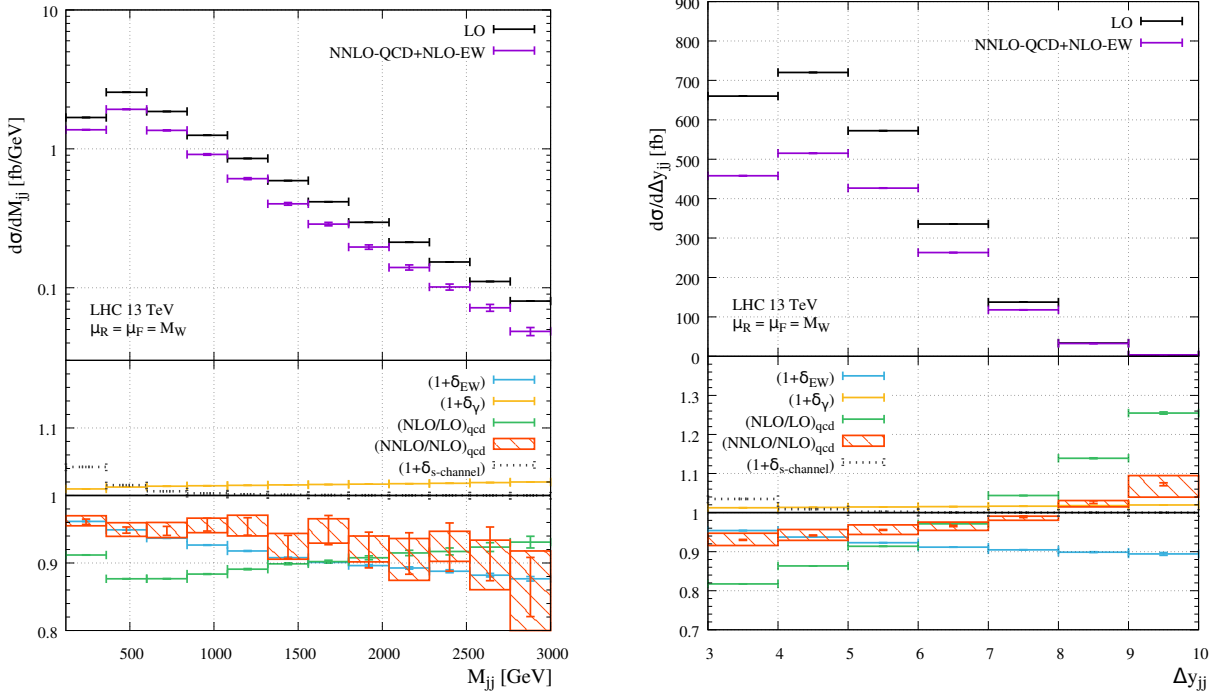


Fig. 4: Distributions in the invariant mass and in the rapidity difference of the first two leading jets in VBF at LO and including NNLO QCD and NLO EW corrections (upper plots) and various relative contributions (lower plots) for $\sqrt{s} = 13$ TeV and $M_H = 125$ GeV.

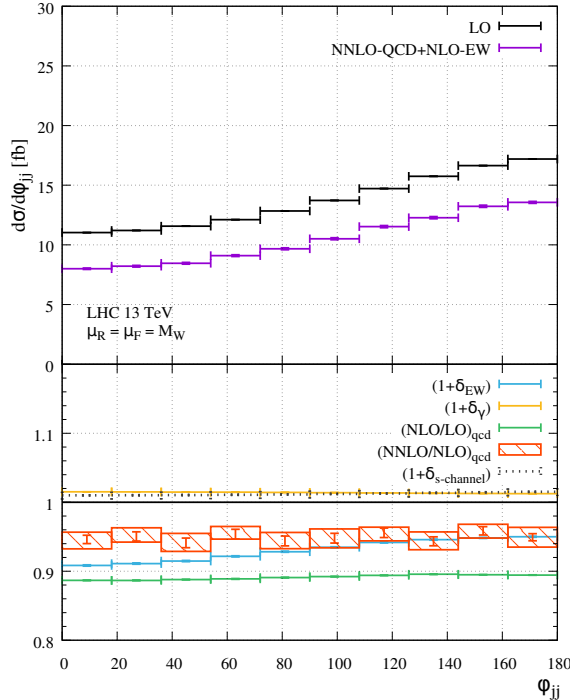


Fig. 5: Distribution in the azimuthal-angle difference of the first two leading jets in VBF at LO and including NNLO QCD and NLO EW corrections (upper plots) and various relative contributions (lower plots) for $\sqrt{s} = 13$ TeV and $M_H = 125$ GeV.

¹⁵⁹ $\sigma_{s\text{-channel}}/\sigma_{\text{LO}}$) is depicted as well, although it is not included in the definition of the VBF cross section.
¹⁶⁰ Integrating the differential cross sections shown in the following, and all its individual contributions,
¹⁶¹ results in the fiducial cross sections discussed in the previous section.

¹⁶² The ratio $(\text{NLO}/\text{LO})_{\text{qcd}}$ shows a quite large impact of NLO QCD corrections, an effect that can be
¹⁶³ traced back to the scale choice $\mu = M_W$, which is on the low side if mass scales such as p_T and M_{jj} get
¹⁶⁴ large in some distributions. The moderate ratio $(\text{NNLO}/\text{NLO})_{\text{qcd}}$, however, indicates nice convergence
¹⁶⁵ of perturbation theory at NNLO QCD. The band around the ratio $(\text{NNLO}/\text{NLO})_{\text{qcd}}$ illustrates the scale
¹⁶⁶ uncertainty of the NNLO QCD cross section, which also applies to σ^{VBF} .

¹⁶⁷ The EW corrections δ_{EW} to (pseudo)rapidity and angular distributions are rather flat, resembling
¹⁶⁸ the correction to the integrated (fiducial) cross section. In the high-energy tails of the p_T and M_{jj}
¹⁶⁹ distributions, δ_{EW} increases in size to 10–20%, showing the onset of the well-known large negative EW
¹⁷⁰ corrections that are enhanced by logarithms of the form $(\alpha/s_w^2) \ln^2(p_T/M_W)$. The impact of the photon-
¹⁷¹ induced channels uniformly stays at the generic level of 1–2%, i.e. they cannot be further suppressed by
¹⁷² cuts acting on the variables shown in the distributions.

¹⁷³ The contribution of s -channel (i.e. VH-like) production uniformly shows the relative size of about
¹⁷⁴ 1.5% observed in the fiducial cross section, with the exception of the M_{jj} and Δy_{jj} distributions, where
¹⁷⁵ this contribution is enhanced at the lower ends of the spectra. Tightening the VBF cuts at these ends,
¹⁷⁶ would further suppress the impact of $\sigma_{s\text{-channel}}$, but reduce the signal at the same time. As an alternative
¹⁷⁷ to decreasing $\sigma_{s\text{-channel}}$, a veto on subleading jet pairs with invariant masses around M_W or M_Z may
¹⁷⁸ be promising. Such a veto, most likely, would reduce the photon-induced contribution δ_γ , and thus the
¹⁷⁹ corresponding uncertainty, as well.

The theoretical uncertainties of differential cross sections originating from unknown higher-order EW effects can be estimated by

$$\Delta_{\text{EW}} = \max\{1\%, \delta_{\text{EW}}^2, \sigma_\gamma/\sigma^{\text{VBF}}\}, \quad (1.8)$$

180 i.e. Δ_{EW} is taken somewhat more conservative than for integrated cross sections, accounting for possible
181 enhancements of higher-order effects due to a kinematical migration of events in distributions. Note that
182 δ_{EW}^2 , in particular, covers the known effect of enhanced EW corrections at high momentum transfer
183 (EW Sudakov logarithms, etc.). As discussed for integrated cross sections in the previous section, the
184 large uncertainty of the current photon PDF forces us to include the full contribution σ_γ in the EW
185 uncertainties.

186 **2 VH cross-section predictions**

187 **2.1 Programs and tools for VH**

188 **2.1.1 HAWK**

189 HAWK [4, 5] is a parton-level event generator for Higgs production in vector-boson fusion [6, 7], $pp \rightarrow$
190 Hjj , and Higgs-strahlung [8], $pp \rightarrow HW/Z \rightarrow H + 2$ leptons. Here we summarise its most important
191 features for the VH channel.

192 HAWK calculates the complete NLO QCD and EW corrections to the processes $pp \rightarrow WH \rightarrow$
193 $v_1 l H$ and $pp \rightarrow ZH \rightarrow l^- l^+ H / v_1 \bar{v}_1 H$, i.e. the leptonic decays and all off-shell effects of the W/Z bosons
194 are included. The Higgs boson can be taken as on-shell or off-shell (with optional decay into a pair
195 of gauge singlets). The EW corrections include also the contributions from photon-induced channels,
196 but gluon-fusion contributions ($gg \rightarrow ZH$) are not taken into account. External fermion masses are
197 neglected, and the renormalisation and factorisation scales are set to $M_V + M_H$ ($V = W, Z$) by default.
198 Since version 2.0, HAWK includes anomalous Higgs-boson–vector-boson couplings. Further features
199 of HAWK are described in Ref. [4] and on its web page [5].

200 **2.1.2 MadGraph5_aMC@NLO**

201 Similar to the generation of any generic process, also Higgs-boson production in association with a vector
202 boson can be generated automatically with MADGRAPH5_AMC@NLO. At the NLO QCD accuracy,
203 multiple jets can also be included using the FxFx merging technique [33]. In Ref. [10] the example of
204 $He^+ \nu_e + 0, 1j$ jets has been presented, and adding a further jet at the NLO is feasible with a small-scale
205 cluster. The situation is entirely similar for the case of ZH (possibly plus jet) production. The commands
206 to generate the corresponding codes are

```
import model loop_sm-no_b_mass
define l+ = e+ mu+ ta+
define l- = e- mu- ta-
define vl~ = ve~ vm~ vt~
define vl = ve vm vt
generate p p > h l+ l- [QCD] @0
add process p p > h l+ vl [QCD] @0
add process p p > h l- vl [QCD] @0
add process p p > h l+ l- j [QCD] @1
add process p p > h l+ vl j [QCD] @1
add process p p > h l- vl~ j [QCD] @1
add process p p > h l+ l- j j [QCD] @2
add process p p > h l+ vl j j [QCD] @2
add process p p > h l- vl~ j j [QCD] @2
output VH-MG5_aMC
```

207 The first command loads a five-flavour scheme model (the MG5_AMC default uses a four-flavour
208 scheme model), which sets the b-quark mass to zero and includes it in the definition of the p and j multi-
209 particle labels. The next four commands define the multi-particle labels for the leptons and neutrinos used
210 in the generate and add process commands. After writing the code to disk (with the output com-
211 mand) the event generation can be started by executing the command launch. The FxFx merging algo-
212 rithm is available when matching to HERWIG6, PYTHIA8, or HERWIG++ partons showers [33, 34],
213 and can be turned on by setting the ickkw parameter to 3 in the file run_card.dat.

214 **2.1.3 MCFM**

215 The calculation is performed at NNLO QCD and includes the decays of the unstable Higgs and vector
216 bosons. We also include all $\mathcal{O}(\alpha_s^2)$ contributions that occur in production for these processes: those

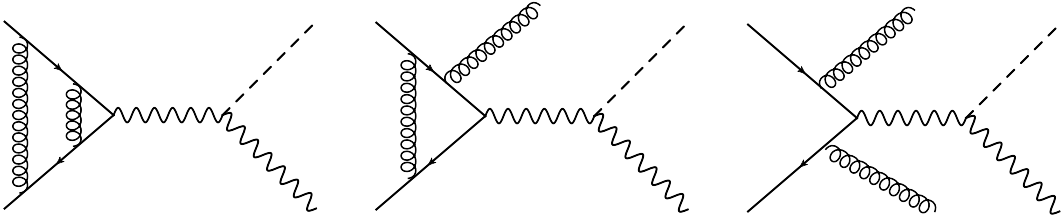


Fig. 6: Drell–Yan-like production modes for the associated production of a Higgs boson. Shown are representative Feynman diagrams needed to compute the $\mathcal{O}(\alpha_s^2)$ corrections to the process. Examples are shown for each of the 0-, 1-, and 2-parton phase-space configurations.

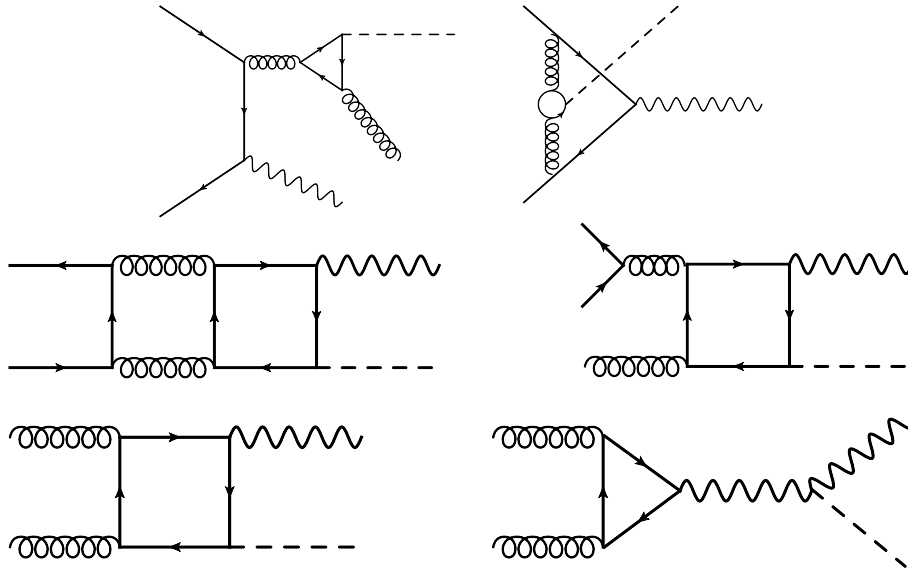


Fig. 7: Diagrams representing associated production of a Higgs boson that are sensitive to the top Yukawa coupling y_t . The topologies indicated in the top line occur for either WH or ZH production and interfere with the LO amplitude. The remaining topologies only occur for ZH production. The $gg \rightarrow ZH$ contribution represented in the bottom line is not proportional to y_t , as can be seen from the examples on the left (y_t -dependent) and right (no y_t).

217 mediated by the exchange of a single off-shell vector boson in the s -channel, and those which arise from
218 the coupling of the Higgs boson to a closed loop of fermions.

219 Examples of diagrams that contribute at NNLO QCD are shown in Figs. 6 and 7. The first type
220 of contributions has the same structure as single vector-boson production, c.f. Fig. 6. Diagrams of the
221 second type, shown in Fig. 7, all contain a closed loop of fermions and, in general, represent the Higgs
222 boson coupling directly to a heavy quark (predominantly a top-quark). Note that some of the contribu-
223 tions shown in Fig. 7 only occur for the case of ZH production and, for the $gg \rightarrow ZH$ contributions, not
224 all diagrams are proportional to the top-quark Yukawa coupling. Each of these contributions results in
225 NNLO QCD corrections at the few percent level for typical cuts, so that inclusion of them all is necessary
226 in order to obtain sufficient theoretical control of this process. A further complication is the inclusion
227 of decays of the Higgs boson into bottom quarks, which we consider. Our calculation also includes the
228 significant impact of NLO QCD corrections in this decay, using the factorized approach described in
229 Refs. [35, 36]. This method takes advantage of improved descriptions of the total decay rate that are
230 available in the HDECAY code [37]. The assembly of a complete calculation at NNLO QCD requires
231 the regularization of infrared singularities, which we handle using the recently-developed “jettiness sub-

²³² traction” procedure [38–41] that has been implemented in the Monte Carlo program MCFM [42–44]. A
²³³ detailed description of our calculation can be found in Ref. [45].

²³⁴ 2.1.4 VHNNLO

²³⁵ VHNNLO [35, 36, 46] is a parton level program for the calculation of fully differential cross sections
²³⁶ for $pp \rightarrow WH$ and $pp \rightarrow ZH$ including up to second order QCD corrections and the decays of the weak
²³⁷ bosons to leptons and of the Higgs boson to bottom quarks.

²³⁸ 2.1.5 VH@NNLO

²³⁹ VH@NNLO [47, 48] calculates the total inclusive cross section for $pp \rightarrow WH$ and $pp \rightarrow ZH$ pro-
²⁴⁰ duction, including all available QCD corrections through $\mathcal{O}(\alpha_s^2)$, i.e. NNLO.³ Specifically, these are the
²⁴¹ Drell–Yan-like terms (see Fig. 6), given by the process $q\bar{q} \rightarrow HW/Z$ plus radiative corrections due to vir-
²⁴² tual and real gluon and/or quark radiation [49, 50], as well as terms involving closed top or bottom loops
²⁴³ (see Fig. 7). For the latter, we distinguish those that interfere with the lowest-order $q\bar{q} \rightarrow HW/Z(g)$ am-
²⁴⁴ plitude (plus crossings) and which we simply denote as “top-loop” terms $\sigma_{t\text{-loop}}$ [51], and the $gg \rightarrow HZ$
²⁴⁵ process [50, 52–54]. VH@NNLO also includes the NLO corrections for this latter process, which are
²⁴⁶ of order α_s^3 [55]. The NLO+NLL corrections for that process quoted below are not yet included in
²⁴⁷ VH@NNLO [56].

²⁴⁸ 2.2 VH parameters and cuts

The numerical results presented in the next section have been computed using the values of the EW parameters given in Section ???. The electromagnetic coupling is fixed in the G_F scheme,

$$\alpha_{G_F} = \sqrt{2}G_FM_W^2(1 - M_W^2/M_Z^2)/\pi, \quad (1.9)$$

and the weak mixing angle is defined in the on-shell scheme,

$$\sin^2 \theta_w = 1 - M_W^2/M_Z^2. \quad (1.10)$$

In the calculation of the QCD-based cross sections, the renormalisation and factorisation scales are set equal to the invariant mass of the VH system,

$$\mu = \mu_R = \mu_F = M_{VH}, \quad M_{VH}^2 \equiv (p_V + p_H)^2, \quad (1.11)$$

²⁴⁹ and both scales are varied independently in the range $M_{VH}/3 < \mu < 3M_{VH}$. The PDFs are taken from
²⁵⁰ the set PDF4LHC15_nnlo_mc PDFs.

²⁵¹ For the calculation of the EW corrections we employed the NNPDF2.3QED PDF set [31], which
²⁵² includes EW corrections and a photon PDF. For the calculation of photon-induced contributions to the
²⁵³ cross sections with a realistic error estimate we took into account the photon PDF of the MRST2004qed
²⁵⁴ PDF set [57] as well. Note, however, that the relative EW correction factor, which is used in the fol-
²⁵⁵ lowing, hardly depends on the PDF set, so that the uncertainty due to the mismatch in the PDF selection
²⁵⁶ is easily covered by the other remaining theoretical uncertainties. Moreover, the EW corrections show
²⁵⁷ a very small dependence on the factorization scale, so that the use of $\mu_F = M_V + M_H$ is acceptable,⁴
²⁵⁸ although full consistency would require to use equal QCD and QED factorization scales.

For the fiducial cross section and for differential distributions the following reconstruction scheme and cuts have been applied. Jets are constructed according to the anti- k_T algorithm [32] with $D = 0.4$, using the default recombination scheme (E scheme). Jets are constructed from partons j with

$$|\eta_j| < 5, \quad (1.12)$$

³Large parts of VH@NNLO are taken over from ZWPROD by W. van Neerven [49].

⁴In its present version, HAWK does not support dynamical scales.

Table 1.3: Total $W^+(\rightarrow l^+ \nu_l)H$ cross sections including QCD and EW corrections and their uncertainties for different proton–proton collision energies \sqrt{s} for a Higgs-boson mass $M_H = 125$ GeV.

$\sqrt{s}[\text{GeV}]$	$\sigma[\text{fb}]$	$\Delta_{\text{scale}}[\%]$	$\Delta_{\text{PDF}/\alpha_s/\text{PDF}+\alpha_s}[\%]$	$\sigma_{\text{NNLOQCD}}^{\text{DY}}[\text{fb}]$	$\sigma_{\text{t-loop}}[\text{fb}]$	$\delta_{\text{EW}}[\%]$	$\sigma_\gamma[\text{fb}]$
7	40.99	$^{+0.7}_{-0.9}$	$\pm 1.9 / \pm 0.7 / \pm 2.0$	42.78	0.42	-7.2	$0.88^{+1.10}_{-0.10}$
8	49.52	$^{+0.6}_{-0.9}$	$\pm 1.8 / \pm 0.8 / \pm 2.0$	51.56	0.53	-7.3	$1.18^{+1.38}_{-0.14}$
13	94.26	$^{+0.5}_{-0.7}$	$\pm 1.6 / \pm 0.9 / \pm 1.8$	97.18	1.20	-7.4	$3.09^{+3.33}_{-0.37}$
14	103.63	$^{+0.3}_{-0.8}$	$\pm 1.5 / \pm 0.9 / \pm 1.8$	106.65	1.36	-7.4	$3.55^{+3.72}_{-0.43}$

Table 1.4: Total $W^-(\rightarrow l^- \bar{\nu}_l)H$ cross sections including QCD and EW corrections and their uncertainties for different proton–proton collision energies \sqrt{s} for a Higgs-boson mass $M_H = 125$ GeV.

$\sqrt{s}[\text{GeV}]$	$\sigma[\text{fb}]$	$\Delta_{\text{scale}}[\%]$	$\Delta_{\text{PDF}/\alpha_s/\text{PDF}+\alpha_s}[\%]$	$\sigma_{\text{NNLOQCD}}^{\text{DY}}[\text{fb}]$	$\sigma_{\text{t-loop}}[\text{fb}]$	$\delta_{\text{EW}}[\%]$	$\sigma_\gamma[\text{fb}]$
7	23.04	$^{+0.6}_{-0.8}$	$\pm 2.2 / \pm 0.6 / \pm 2.3$	23.98	0.24	-7.0	$0.51^{+0.69}_{-0.05}$
8	28.62	$^{+0.6}_{-0.8}$	$\pm 2.1 / \pm 0.6 / \pm 2.1$	29.71	0.31	-7.1	$0.70^{+0.94}_{-0.07}$
13	59.83	$^{+0.4}_{-0.7}$	$\pm 1.8 / \pm 0.8 / \pm 2.0$	61.51	0.78	-7.3	$2.00^{+2.34}_{-0.22}$
14	66.49	$^{+0.5}_{-0.6}$	$\pm 1.7 / \pm 0.9 / \pm 1.9$	68.24	0.89	-7.3	$2.32^{+2.65}_{-0.26}$

where y_j denotes the rapidity of the (massive) jet. In the presence of phase-space cuts and in the generation of differential distributions, the treatment of real photons, which appear as part of the NLO EW corrections, has to be specified. In the following we assume perfect isolation of photons from leptons.⁵ The charged leptons l have to pass the following acceptance cuts,

$$p_{Tl} > 15 \text{ GeV}, \quad |y_l| < 2.5. \quad (1.13)$$

For ZH production with $Z \rightarrow l^+ l^-$ the invariant mass of the two leptons should further concentrate around the Z pole,

$$75 \text{ GeV} < M_{ll} < 105 \text{ GeV}. \quad (1.14)$$

While the ZH cross sections are independent from the CKM matrix, quark mixing has some effect on WH production. For the calculation of the latter we employed a Cabibbo-like CKM matrix (i.e. without mixing to the third quark generation) with Cabibbo angle θ_C fixed by $\sin \theta_C = 0.225$. Moreover, we note that we employ complex W- and Z-boson masses in the calculation of the EW corrections in the standard HAWK approach, as described in Ref. [8].

The Higgs boson is treated as on-shell particle in the following consistently, since its finite-width and off-shell effects in the signal region are suppressed in the Standard Model.

2.3 Total VH cross sections

Tables 1.3 and 1.4 summarize the total Standard Model $W^\pm H$ cross sections with $W^+ \rightarrow l^+ \nu_l$ and $W^- \rightarrow l^- \bar{\nu}_l$ as well as the corresponding uncertainties for different proton–proton collision energies for a Higgs-boson mass $M_H = 125$ GeV. Tables 1.5 and 1.6 likewise show the respective results on the total Standard Model ZH cross sections with $Z \rightarrow l^+ l^-$ and $Z \rightarrow \nu \bar{\nu}$ (summed over three neutrino generations).

⁵Perfect isolation to some extent applies to muons going out into the muon chamber. A simulation of radiation off electrons requires some recombination of collinear electron–photon pairs, mimicking the inclusive treatment of electrons within electromagnetic showers in the detector. The two different treatments were compared in Ref. [8], revealing differences at the 1% level for the relevant physical observables.

Table 1.5: Total ZH cross sections with $Z \rightarrow l^+l^-$ including QCD and EW corrections and their uncertainties for different proton–proton collision energies \sqrt{s} for a Higgs-boson mass $M_H = 125$ GeV.

$\sqrt{s}[\text{GeV}]$	$\sigma[\text{fb}]$	$\Delta_{\text{scale}}[\%]$	$\Delta_{\text{PDF}/\alpha_s/\text{PDF}+\alpha_s}[\%]$	$\sigma_{\text{NNLOQCD}}^{\text{DY}}[\text{fb}]$	$\sigma_{\text{NLO+NLL}}^{\text{ggZH}}[\text{fb}]$	$\sigma_{\text{t-loop}}[\text{fb}]$	$\delta_{\text{EW}}[\%]$	$\sigma_\gamma[\text{fb}]$
7	11.43	$^{+2.6}_{-2.4}$	$\pm 1.6 / \pm 0.7 / \pm 1.7$	10.91	0.94	0.11	-5.2	$0.03^{+0.04}_{-0.00}$
8	14.18	$^{+2.9}_{-2.4}$	$\pm 1.5 / \pm 0.8 / \pm 1.7$	13.36	1.33	0.14	-5.2	$0.04^{+0.05}_{-0.00}$
13	29.82	$^{+3.8}_{-3.1}$	$\pm 1.3 / \pm 0.9 / \pm 1.6$	26.66	4.14	0.31	-5.3	$0.11^{+0.12}_{-0.01}$
14	33.27	$^{+3.8}_{-3.3}$	$\pm 1.3 / \pm 1.0 / \pm 1.6$	29.47	4.87	0.36	-5.3	$0.12^{+0.13}_{-0.01}$

Table 1.6: Total ZH cross sections with $Z \rightarrow \nu\bar{\nu}$ (summed over three neutrino generations) including QCD and EW corrections and their uncertainties for different proton–proton collision energies \sqrt{s} for a Higgs-boson mass $M_H = 125$ GeV.

$\sqrt{s}[\text{GeV}]$	$\sigma[\text{fb}]$	$\Delta_{\text{scale}}[\%]$	$\Delta_{\text{PDF}/\alpha_s/\text{PDF}+\alpha_s}[\%]$	$\sigma_{\text{NNLOQCD}}^{\text{DY}}[\text{fb}]$	$\sigma_{\text{NLO+NLL}}^{\text{ggZH}}[\text{fb}]$	$\sigma_{\text{t-loop}}[\text{fb}]$	$\delta_{\text{EW}}[\%]$	$\sigma_\gamma[\text{fb}]$
7	68.18	$^{+2.6}_{-2.4}$	$\pm 1.6 / \pm 0.7 / \pm 1.7$	64.70	5.59	0.64	-4.3	-0.00
8	84.56	$^{+2.9}_{-2.4}$	$\pm 1.5 / \pm 0.8 / \pm 1.7$	79.25	7.89	0.81	-4.3	-0.00
13	177.62	$^{+3.8}_{-3.1}$	$\pm 1.3 / \pm 0.9 / \pm 1.6$	158.10	24.57	1.85	-4.4	-0.00
14	198.12	$^{+3.8}_{-3.3}$	$\pm 1.3 / \pm 1.0 / \pm 1.6$	174.77	28.88	2.11	-4.4	-0.00

The total VH cross sections σ^{VH} are calculated according to

$$\sigma^{\text{WH}} = \sigma_{\text{NNLOQCD}}^{\text{WH,DY}}(1 + \delta_{\text{EW}}) + \sigma_{\text{t-loop}} + \sigma_\gamma, \quad (1.15)$$

$$\sigma^{\text{ZH}} = \sigma_{\text{NNLOQCD}}^{\text{ZH,DY}}(1 + \delta_{\text{EW}}) + \sigma_{\text{t-loop}} + \sigma_\gamma + \sigma^{\text{ggZH}}, \quad (1.16)$$

where $\sigma_{\text{NNLOQCD}}^{\text{VH,DY}}$ is the Drell–Yan-like part of the NNLO QCD prediction for the VH cross section, based on the calculation of Ref. [50] with NNLO PDFs. Since we include the leptonic decays of the W/Z bosons, we multiply the cross sections from VH@NNLO with the branching ratios

$$\text{BR}_{\text{LO}}(\text{W} \rightarrow l\nu_l) = 0.108894, \quad \text{BR}_{\text{LO}}(\text{Z} \rightarrow l^+l^-) = 0.0335950, \quad \text{BR}_{\text{LO}}(\text{Z} \rightarrow \nu\bar{\nu}) = 0.199218, \quad (1.17)$$

which are the ratios of the LO partial widths and the total widths as defined in Section ???. With these branching ratios our combination of QCD and EW corrections results in NNLO QCD + NLO EW accuracy. The relative NLO EW correction δ_{EW} is calculated with HAWK. Note that there is no issue with photon isolation in the calculation of the total cross section, where all mass singularities from collinear photon emission off leptons vanish owing to the KLN theorem. The contributions from photon-induced channels, σ_γ are obtained from HAWK as well and added linearly to the cross section. It is important to notice that σ_γ is based on the average of the median of the cross sections obtained with PDF replicas of NNPDF2.3QED PDFs and the cross section obtained with MRST2004qed PDFs “set 1”. The lower error corresponds to the lower limit of all NNPDF2.3QED PDFs, the upper error to the maximum of the 68% smallest cross sections from the NNPDF2.3QED set and the cross section obtained with MRST2004qed “set 0”. Since the photon PDF is constrained by data rather loosely, the error on σ_γ is large and non-Gaussian. In fact the mean value of σ_γ calculated with NNPDF2.3QED PDF replicas is larger than the shown median by factors ~ 2 – 2.5 .

The contribution σ^{ggZH} of the gluon-fusion channel is calculated through NLO using VH@NNLO [47, 48, 55]; the NLL effects are added on top of that, following Ref. [56]. The scale uncertainty Δ_{scale} results from a variation of the factorization and renormalization scales (1.11) by a factor of 3, as indicated

above. The errors Δ_{PDF} and Δ_{α_s} induced by uncertainties in the PDFs and α_s , respectively, are given separately together with the combined version $\Delta_{\text{PDF} \oplus \alpha_s}$, which is calculated from the 68% CL interval using the PDF4LHC15_nnlo_mc PDF set. The Δ_{scale} and $\Delta_{\text{PDF} \oplus \alpha_s}$ are evaluated without taking into account EW effects.

The theoretical uncertainties of integrated cross sections originating from unknown higher-order EW effects can be estimated by

$$\Delta_{\text{EW}} = \max\{0.5\%, \delta_{\text{EW}}^2, \Delta_\gamma\}. \quad (1.18)$$

This estimate is based on the maximum of the generic size $\sim 0.5\%$ of the neglected NNLO EW effects, taking into account a possible systematic enhancement $\sim \delta_{\text{EW}}^2$, and the potentially large relative uncertainty $\Delta_\gamma = \Delta\sigma_\gamma/\sigma$ of the photon-induced contribution σ_γ , whose absolute uncertainty $\Delta\sigma_\gamma$ can be read from the tables.

In order to extract the total VH production cross sections without leptonic W/Z decays in NNLO QCD + NLO EW accuracy (neglecting off-shell effects), one should divide the results on total cross sections by the respective leptonic W/Z branching ratios in NLO EW accuracy. These are given by

$$\text{BR}_{\text{NLO}}(W \rightarrow l\nu_l) = 0.108535, \quad \text{BR}_{\text{NLO}}(Z \rightarrow l^+l^-) = 0.0335962, \quad \text{BR}_{\text{NLO}}(Z \rightarrow \nu\bar{\nu}) = 0.201030, \quad (1.19)$$

calculated from the ratios of the NLO partial widths (calculated in the HAWK setup) and the total widths as defined in Section ???. In this extraction, one should subtract the photon-induced contributions σ_γ from the cross sections before dividing through the branching ratio, since σ_γ receives a significant contribution from incoming photons coupling to the charged leptons of the W or Z decays. Thus, σ_γ/BR is an uncertainty of the resulting VH cross section, which is quite significant in the WH case.

Results for the total VH cross sections from a scan over the SM Higgs-boson mass M_H can be found in Appendix B.

2.4 Fiducial and differential VH cross sections

Tables 1.7 and 1.8 summarize the fiducial Standard Model $W^\pm H$ cross sections with $W^+ \rightarrow l^+\nu_l$ and $W^- \rightarrow l^-\bar{\nu}_l$ as well as the corresponding uncertainties for the proton–proton collision at $\sqrt{s} = 13$ TeV for a Higgs-boson mass $M_H = 125$ GeV. Table 1.9 likewise shows the respective results on the total Standard Model ZH cross sections with $Z \rightarrow l^+l^-$. The fiducial cross sections are calculated as follows: For QCD corrections we have used VHNNLO with the NNPDF3.0_nnlo_as_0118 PDF set. Renormalization and factorization scales are varied independently by factors of 2 and 1/2 including 7 combinations, avoiding the cases (2, 1/2) and (1/2, 2). The envelope is taken as a scale uncertainty to parametrize missing higher-order QCD corrections. A representation of the PDF error for the QCD part in VH production has been obtained with SMPDF [58] starting from a prior of NNPDF3.0NNLO. The SMPDF derived in [58] for VH processes adopted an analysis very close to the one used here and contains in total five symmetric eigenvectors. The EW corrections are again calculated with HAWK in the same way as described for the total cross section. Moreover, the recipe (1.18) for estimating the EW uncertainty Δ_{EW} applies for the fiducial cross section as well.

The combination of QCD and EW corrections has been done following the same procedure as described in Eqs. (1.15) and (1.16), as far as the corresponding contributions are available (see tables). The Δ_{scale} and Δ_{PDF} are evaluated without taking into account EW effects; the uncertainties of the latter can be estimated again following Eq. (1.18).

Differential cross section results in NNLO QCD + NLO EW accuracy have been computed following the same procedure as outlined above for the fiducial cross section. QCD corrections are calculated with VHNNLO using the settings reported above for the computation of the fiducial cross sections. The EW corrections are again calculated with HAWK as in the previous section, with the only difference

Table 1.7: Fiducial $W^+(\rightarrow l^+ \nu_l)H$ cross sections including QCD and EW corrections and their uncertainties for proton–proton collisions at $\sqrt{s} = 13\text{TeV}$ for a Higgs-boson mass $M_H = 125\text{ GeV}$.

$\sqrt{s}[\text{GeV}]$	$\sigma[\text{fb}]$	$\Delta_{\text{scale}}[\%]$	$\Delta_{\text{PDF}}[\%]$	$\sigma_{\text{NNLOQCD}}^{\text{DY}}[\text{fb}]$	$\delta_{\text{EW}}[\%]$	$\sigma_\gamma[\text{fb}]$
13	73.90	$^{+0.3}_{-0.3}$	± 1.4	78.61	-8.3	$1.81^{+1.10}_{-0.23}$

Table 1.8: Fiducial $W^-(\rightarrow l^- \bar{\nu}_l)H$ cross sections including QCD and EW corrections and their uncertainties for proton–proton collisions at $\sqrt{s} = 13\text{TeV}$ for a Higgs-boson mass $M_H = 125\text{ GeV}$.

$\sqrt{s}[\text{GeV}]$	$\sigma[\text{fb}]$	$\Delta_{\text{scale}}[\%]$	$\Delta_{\text{PDF}}[\%]$	$\sigma_{\text{NNLOQCD}}^{\text{DY}}[\text{fb}]$	$\delta_{\text{EW}}[\%]$	$\sigma_\gamma[\text{fb}]$
13	42.77	$^{+0.2}_{-0.3}$	± 1.8	45.29	-8.0	$1.11^{+0.65}_{-0.12}$

Table 1.9: Fiducial ZH cross sections with $Z \rightarrow l^+l^-$ including QCD and EW corrections and their uncertainties for proton–proton collisions at $\sqrt{s} = 13\text{TeV}$ for a Higgs-boson mass $M_H = 125\text{ GeV}$.

$\sqrt{s}[\text{GeV}]$	$\sigma[\text{fb}]$	$\Delta_{\text{scale}}[\%]$	$\Delta_{\text{PDF}}[\%]$	$\sigma_{\text{NNLOQCD}}^{\text{DY}}[\text{fb}]$	$\sigma^{\text{ggZH}}[\text{fb}]$	$\delta_{\text{EW}}[\%]$	$\sigma_\gamma[\text{fb}]$
13	16.08	$^{+2.2}_{-1.4}$	± 1.2	16.21	1.36	-9.2	0.00

325 in the calculation of the photon-induced contribution. Instead of the cumbersome procedure of working
 326 with many PDF replicas we have calculated σ_γ with the central PDF of NNPDF2.3qed. In order to obtain
 327 σ_γ in the same setup as for the integrated cross sections of the previous section (for $\sqrt{s} = 13\text{ TeV}$), the
 328 shown results on σ_γ in WH production should be rescaled by a factor of 0.7. This rescaling is based on
 329 the corresponding integrated results for σ_γ . Taking over the relative uncertainty from the integrated cross
 330 section as well, we get the estimate $\Delta_\gamma \sim 1.5\%$. For ZH production σ_γ and Δ_γ have a phenomenologically
 331 negligible impact.

The theoretical uncertainties of differential cross sections originating from unknown higher-order
 332 EW effects can be estimated by

$$\Delta_{\text{EW}} = \max\{1\%, \delta_{\text{EW}}^2, \Delta_\gamma\}, \quad (1.20)$$

332 i.e. Δ_{EW} is taken somewhat more conservative than for integrated cross sections, accounting for possible
 333 enhancements of higher-order effects due to a kinematical migration of events in distributions. Note that
 334 δ_{EW}^2 , in particular, covers the known effect of enhanced EW corrections at high momentum transfer (EW
 335 Sudakov logarithms, etc.).

336 Figures 8–12 show the impact of radiative corrections of the most important differential distribu-
 337 tions for Higgs production via WH mode in the SM, while in Figs. 13–15 the same effects are shown
 338 for the Higgs boson production in association with a Z boson. The figures generically show the known
 339 size of the NLO QCD corrections at the level of $\sim 20\text{--}30\%$ in the most important phase-space regions.
 340 At NNLO, the QCD corrections amount to some percent in the dominating regions, but can grow to
 341 $10\text{--}20\%$ in the tails of distributions. In those regions the QCD scale uncertainty accordingly grows to
 342 $\sim 5\%$ or more. The EW corrections are generically flat in (pseudo)rapidity distributions, where they
 343 resemble the EW corrections to the fiducial cross sections. In transverse-momentum distributions the
 344 EW correction grow further negative to $-(10\text{--}20)\%$ for p_T of some 100 GeV. The photon-induced
 345 corrections turn out to be only significant for WH production. They have a tendency to grow in the tails
 346 of distributions as well, but do hardly exceed the 5% level there.

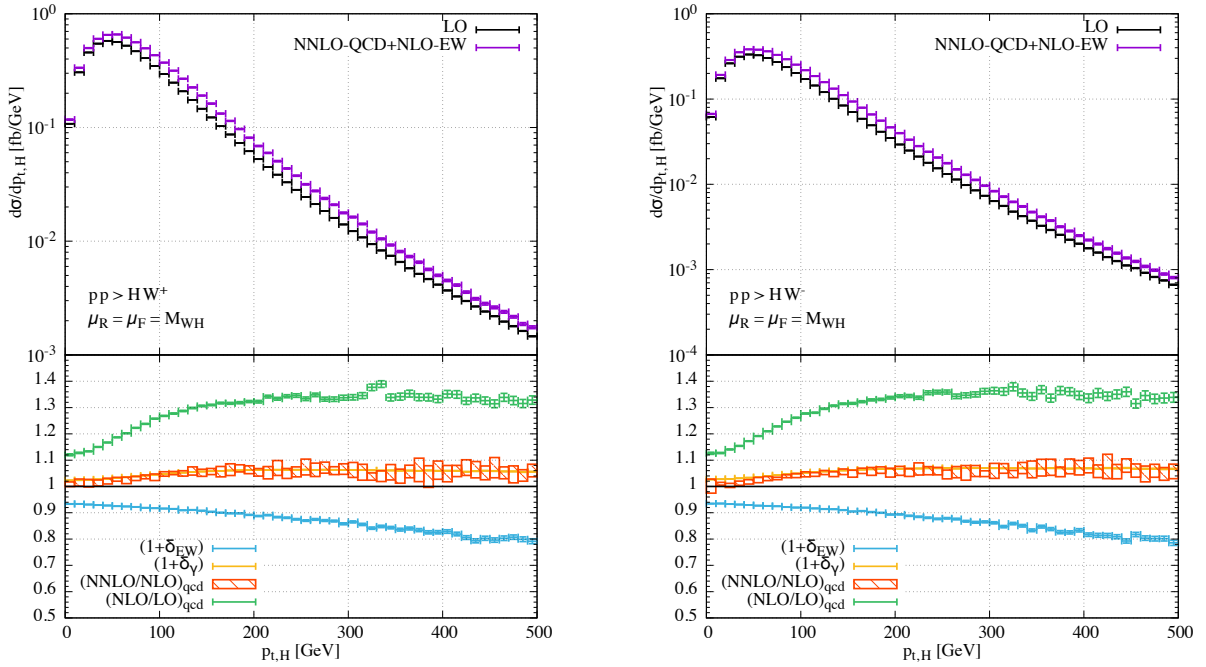


Fig. 8: Left: transverse-momentum distributions of the Higgs boson in W^+H production at LO and including NNLO QCD and NLO EW corrections (upper plots) and relative higher-order contributions (lower plots) for $\sqrt{s} = 13$ TeV and $M_H = 125$ GeV. Right: the same for W^-H production. Note that δ_γ is based on the central value of the photon PDF of NNPDF2.3qed, while σ_γ in Tables 1.3–1.9 is based on combined results using the median and the photon PDF of MRST2004qed (and smaller by a factor 0.7), see text.

Finally, we emphasize that the contributions $\sigma_{t\text{-loop}}$ are not included in the discussion of fiducial cross sections and differential distributions presented here, while the contribution σ^{ggZH} are included at leading order (α_s^2).

2.5 Cross-section predictions including the decay $H \rightarrow b\bar{b}$

We use the Standard Model parameters as recommended by the LHCHXSWG, supplemented by CKM matrix elements $V_{ud} = 0.975$ and $V_{cs} = 0.222$. For the parton distribution functions we use the NNLO CT14 set and associated strong coupling, $\alpha_s(M_Z) = 0.118$ with 3-loop running. Central predictions correspond to the scale choice $\mu_R = \mu_F = \mu_0$ where $\mu_0 = M_V + M_H$ and we consider an envelope of variations around this choice to define the scale uncertainty. For $W^\pm H$ production the extreme choices correspond to $\mu_R = 2\mu_0$, $\mu_F = \mu_0/2$ and $\mu_R = \mu_0/2$, $\mu_F = 2\mu_0$. For ZH production the extrema are instead represented by $\mu_F = \mu_R = 2\mu_0$ and $\mu_F = \mu_R = \mu_0/2$. Our results are obtained for the LHC operating at $\sqrt{s} = 13$ TeV.

We cluster all jets according to the anti- k_T jet algorithm with distance parameter $R = 0.4$. We subsequently require that two of the jets contain the b and \bar{b} quarks from the Higgs-boson decay and that these jets satisfy,

$$p_T(\text{b-jet}) > 25 \text{ GeV}, \quad |\eta(\text{b-jet})| < 2.5. \quad (1.21)$$

Note that the calculation of the $H \rightarrow b\bar{b}$ decay is performed at NLO QCD.

We begin by considering the $W^\pm H$ process, with the W boson decaying to a lepton and a neutrino. The acceptance cuts for the decay products are,

$$p_T(\text{lepton}) > 15 \text{ GeV}, \quad |\eta(\text{lepton})| < 2.5, \quad p_T(\text{neutrino}) > 15 \text{ GeV}. \quad (1.22)$$

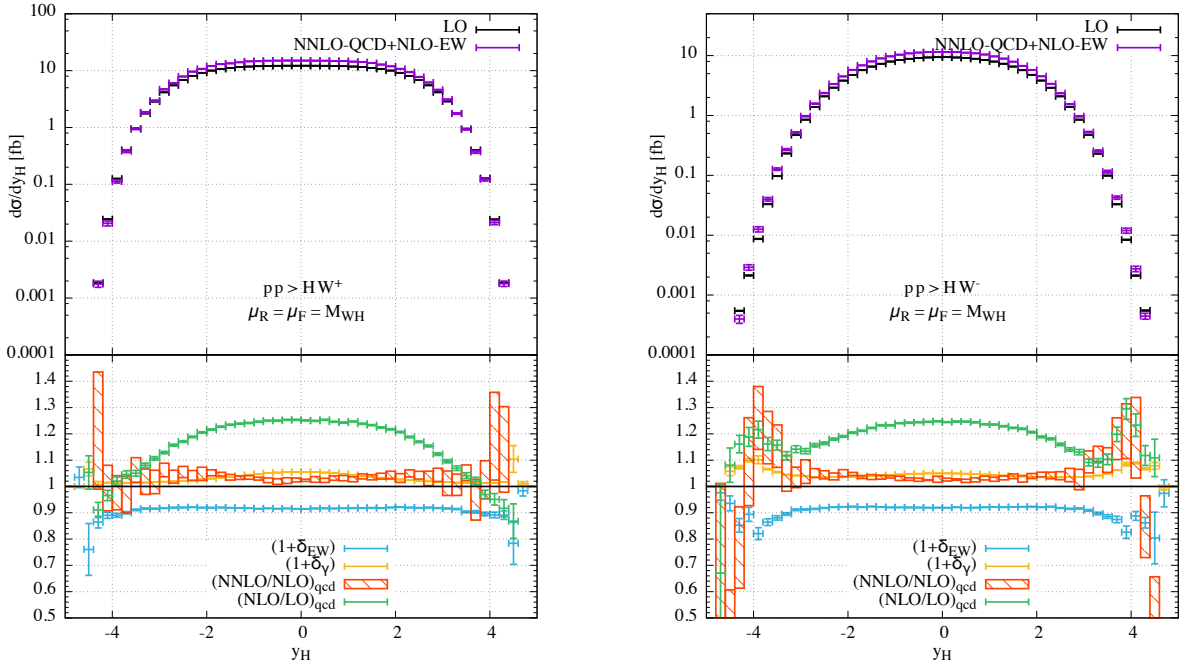


Fig. 9: Left: rapidity of the Higgs boson in W^+H production at LO and including NNLO QCD and NLO EW corrections (upper plots) and relative higher-order contributions (lower plots) for $\sqrt{s} = 13$ TeV and $M_H = 125$ GeV. Right: the same for W^-H production. Note that δ_γ is based on the central value of the photon PDF of NNPDF2.3qed, while σ_γ in Tables 1.3–1.9 is based on combined results using the median and the photon PDF of MRST2004qed (and smaller by a factor 0.7), see text.

The cross sections under these cuts, using NNLO PDFs, are found to be

$$\begin{aligned}\sigma^{\text{NLOQCD}}(W^+H) &= 23.56 \text{ fb}, & \sigma^{\text{NNLOQCD}}(W^+H) &= 24.18^{+0.36}_{-0.64} \text{ fb}, \\ \sigma^{\text{NLOQCD}}(W^-H) &= 15.49 \text{ fb}, & \sigma^{\text{NNLOQCD}}(W^-H) &= 15.87^{+0.26}_{-0.46} \text{ fb}.\end{aligned}\quad (1.23)$$

360 The NNLO QCD corrections under these cuts are small and positive, increasing the NLO QCD cross
361 sections by less than 1%. The scale uncertainty at NNLO QCD is at the 3% level.

For the ZH process we consider the decay of the Z boson into a single family of leptons and apply the cuts,

$$\begin{aligned}p_T(\text{lepton}) &> 15 \text{ GeV}, & |\eta(\text{lepton})| &< 2.5, \\ 75 \text{ GeV} &< M_{ll} < 105 \text{ GeV}.\end{aligned}\quad (1.24)$$

These result in the following cross sections,

$$\sigma^{\text{NLOQCD}}(\text{ZH}) = 6.041 \text{ fb}, \quad \sigma^{\text{NNLOQCD}}(\text{ZH}) = 6.891^{+0.101}_{-0.162} \text{ fb}. \quad (1.25)$$

362 In this case the NNLO corrections increase the NLO cross section by about 15% and the scale uncertainty
363 at NNLO QCD is around 2%.

Differential predictions for the final state $V(\rightarrow l_1 l_2)H(\rightarrow b\bar{b})$ are presented in Figs. 16–20. For $W^\pm H$ production we present the differential observables side-by-side on the same scale, so that the relative suppression of W^- compared to W^+ is readily apparent. Figure 16 presents the p_T of the Higgs-boson candidate, whose four-momentum is defined as the sum of those of the identified b-jets.

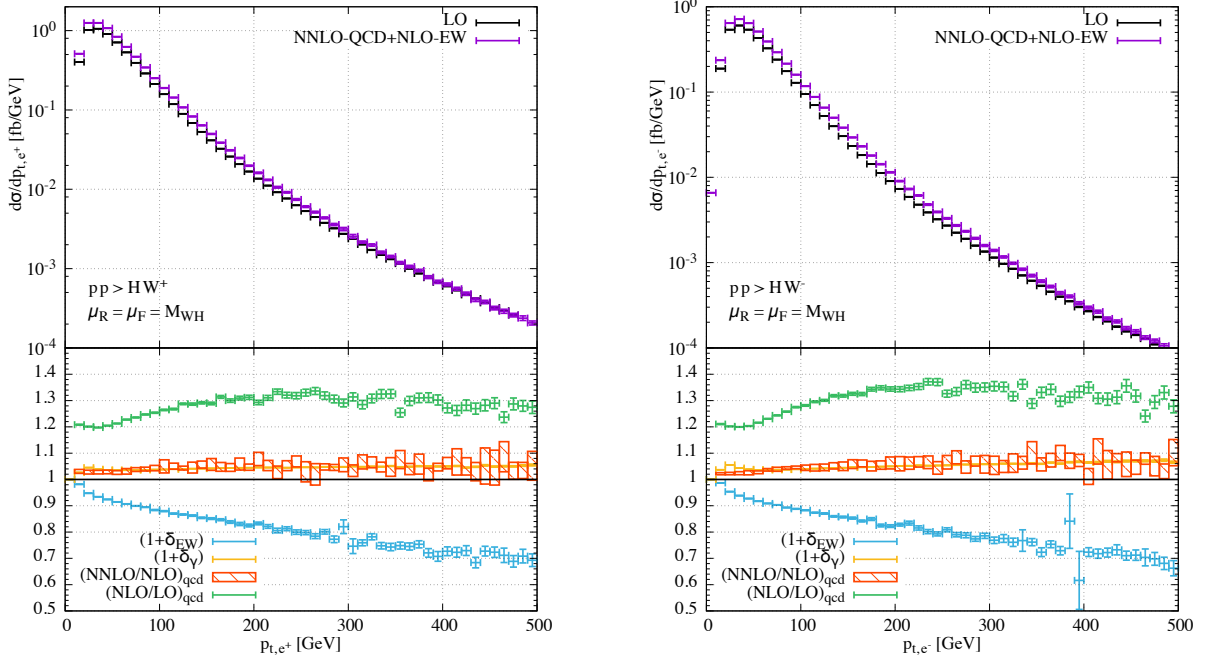


Fig. 10: Left: transverse-momentum distribution of the charged lepton in W^+H production at LO and including NNLO QCD and NLO EW corrections (upper plots) and relative higher-order contributions (lower plots) for $\sqrt{s} = 13$ TeV and $M_H = 125$ GeV. Right: the same for W^-H production. Note that δ_γ is based on the central value of the photon PDF of NNPDF2.3qed, while σ_γ in Tables 1.3–1.9 is based on combined results using the median and the photon PDF of MRST2004qed (and smaller by a factor 0.7), see text.

We present predictions for a variety of selection cuts. The red curve corresponds to an “inclusive” p_T^V selection while the remaining curves slice the phase space into various p_T^V bins:

$$\begin{aligned}
 \text{red: } & p_T^V \text{ inclusive,} \\
 \text{blue: } & 0 < p_T^V < 150 \text{ GeV,} \\
 \text{green: } & 150 < p_T^V < 250 \text{ GeV,} \\
 \text{magenta: } & p_T^V > 250 \text{ GeV.}
 \end{aligned} \tag{1.26}$$

The inclusive curve is thus recovered by summing over all of the remaining curves. At leading order $p_T^V \equiv p_T^H$, with departures from this equality the result of additional radiation that is inherent in the higher-order corrections. The discontinuities that are apparent in the regions of phase space around $p_T^V = p_T^H$, namely at $p_T^H = 150, 250$ GeV, are indicators of the fact that perturbation theory is unreliable at such boundaries. The situation is exacerbated by the inclusion of higher-order corrections in the Higgs-boson decay, since boundary logarithms also appear due to radiation in the decay [35, 36, 45]. The differences between the W^+H and W^-H predictions are most clear in the y_H observable (Figure 17). This observable is sensitive to the valence/sea quark distribution inside the proton. The valence u distribution is more favored for W^+H , and stiffens the y_H distribution by favoring more forward regions of phase space. On the other hand W^-H production is associated with the production of more central Higgs bosons. We present the leptonic observables in Figure 18. As the p_T^V cut is increased the p_T^l distribution flattens out. Finally in Figures 19–20 we present the differential predictions for ZH . The conclusions are broadly similar, although the phase-space boundary effects are somewhat damped for this process. This is due to the presence of $gg \rightarrow ZH$ contributions that provide a sizable correction to the cross section at NNLO. Since this switches-on in the LO phase space, the large negative bin is partially compensated

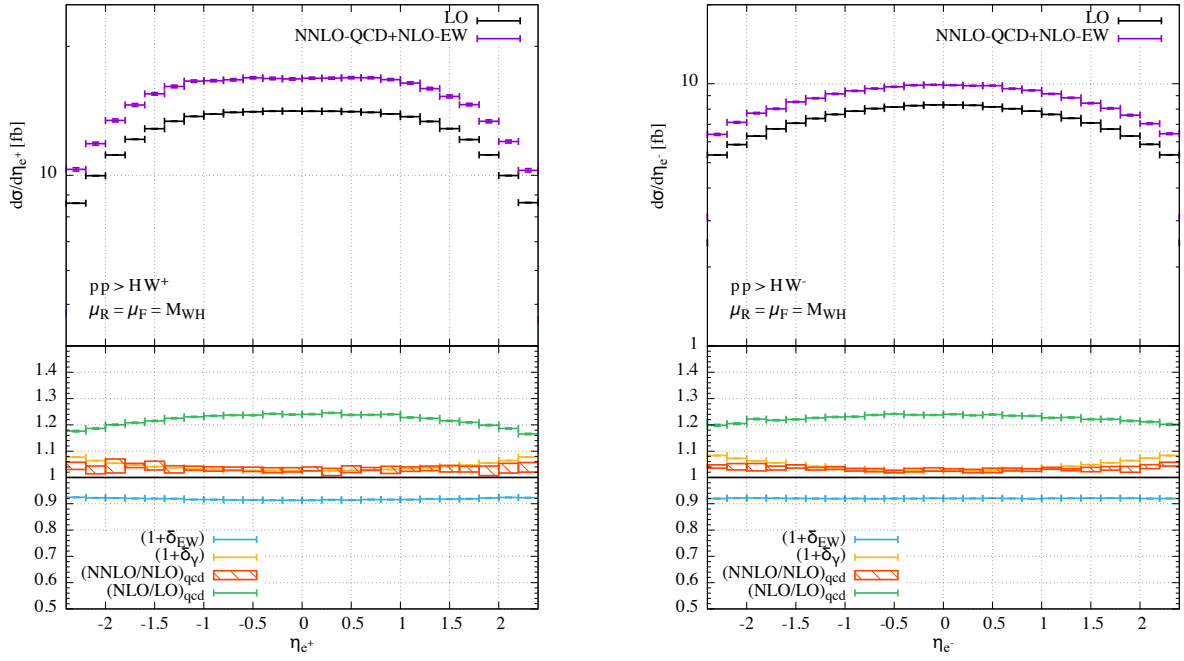


Fig. 11: Left: pseudorapidity distribution of the charged lepton in W^+H production at LO and including NNLO QCD and NLO EW corrections (upper plots) and relative higher-order contributions (lower plots) for $\sqrt{s} = 13$ TeV and $M_H = 125$ GeV. Right: the same for W^-H production. Note that δ_γ is based on the central value of the photon PDF of NNPDF2.3qed, while σ_γ in Tables 1.3–1.9 is based on combined results using the median and the photon PDF of MRST2004qed (and smaller by a factor 0.7), see text.

379 by the inclusion of these pieces. There is a noticeable inflection in the p_T^H spectrum at around $p_T^H \sim m_t$,
 380 which is where these pieces begin to become important.

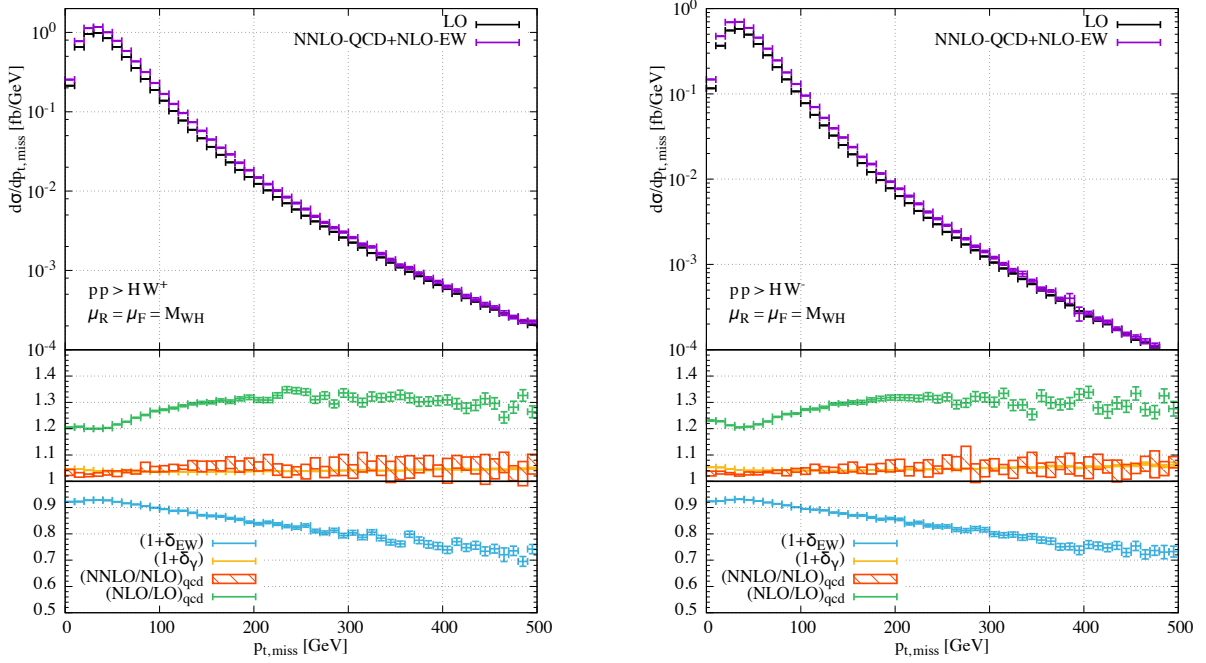


Fig. 12: Left: missing transverse momentum in W^+H production at LO and including NNLO QCD and NLO EW corrections (upper plots) and relative higher-order contributions (lower plots) for $\sqrt{s} = 13$ TeV and $M_H = 125$ GeV. Right: the same for W^-H production. Note that δ_γ is based on the central value of the photon PDF of NNPDF2.3qed, while σ_γ in Tables 1.3–1.9 is based on combined results using the median and the photon PDF of MRST2004qed (and smaller by a factor 0.7), see text.

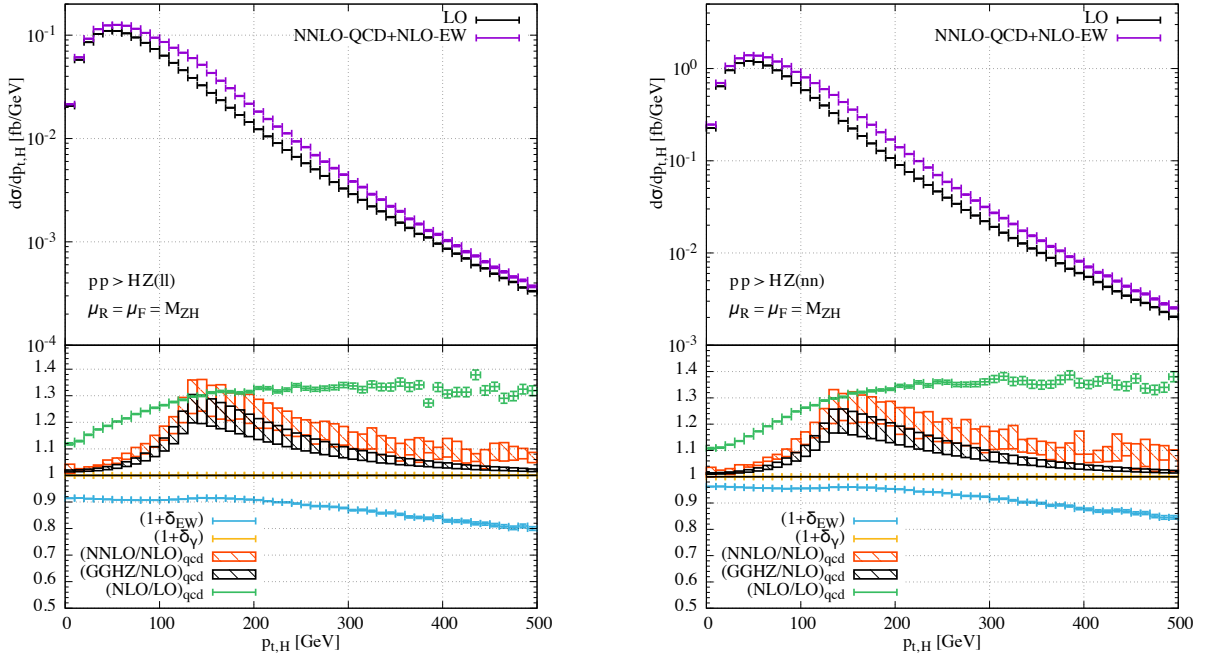


Fig. 13: Left: transverse-momentum distributions of the Higgs boson in $Z(\rightarrow 1^+1^-)H$ production at LO and including NNLO QCD and NLO EW corrections (upper plots) and relative higher-order contributions (lower plots) for $\sqrt{s} = 13$ TeV and $M_H = 125$ GeV. Right: the same for $Z(\rightarrow \nu\bar{\nu})H$ production.

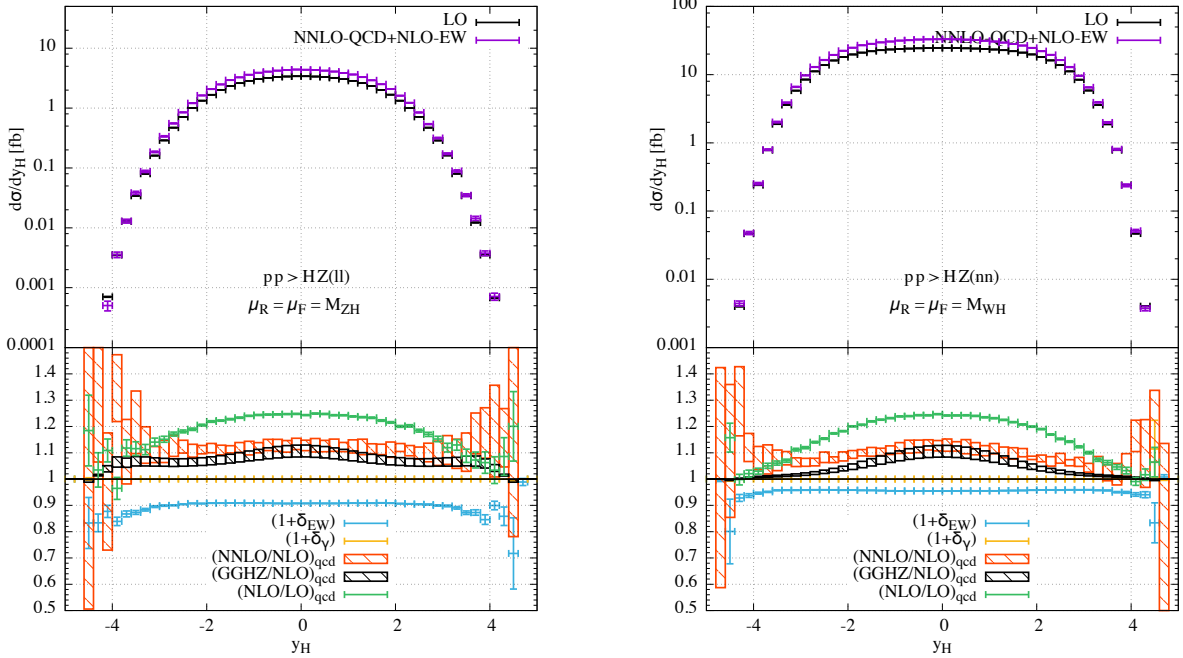


Fig. 14: Left: rapidity distributions of the Higgs boson in $Z \rightarrow 1^+1^-$ H production at LO and including NNLO QCD and NLO EW corrections (upper plots) and relative higher-order contributions (lower plots) for $\sqrt{s} = 13$ TeV and $M_H = 125$ GeV. Right: the same for $Z \rightarrow \nu\bar{\nu}$ H production.

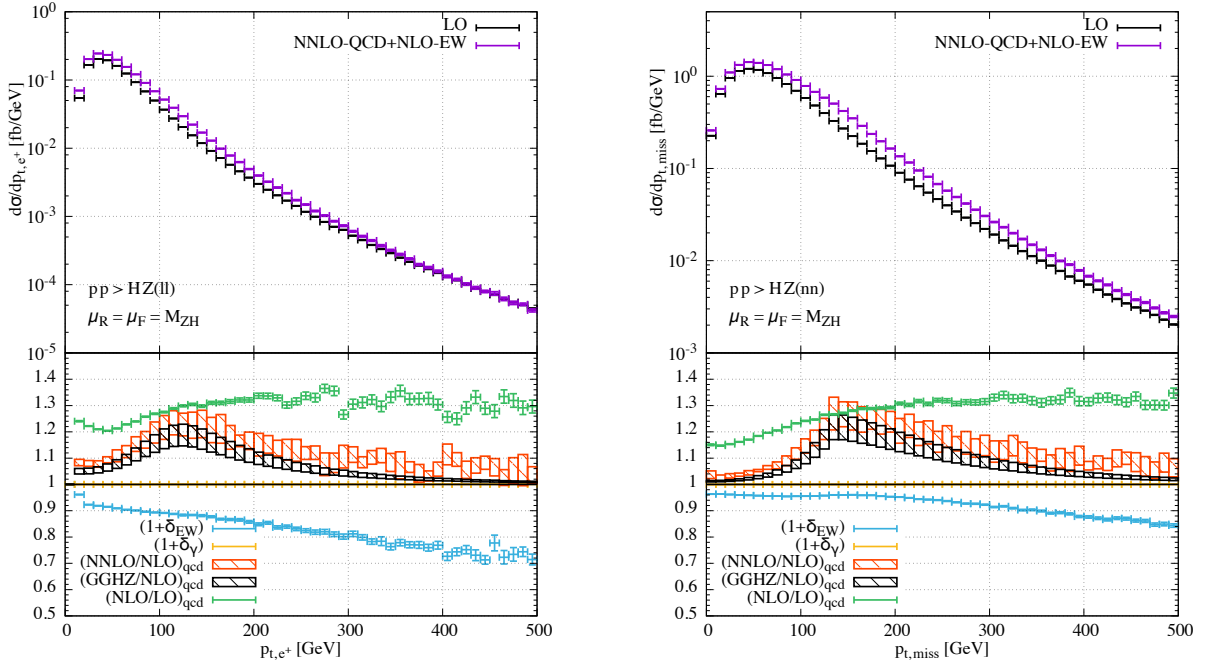


Fig. 15: Left: transverse-momentum distributions of the positive charged lepton in $Z \rightarrow 1^+1^-$ H production at LO and including NNLO QCD and NLO EW corrections (upper plots) and relative higher-order contributions (lower plots) for $\sqrt{s} = 13$ TeV and $M_H = 125$ GeV. Right: the same for the missing-transverse-momentum distribution in $Z \rightarrow \nu\bar{\nu}$ H production.

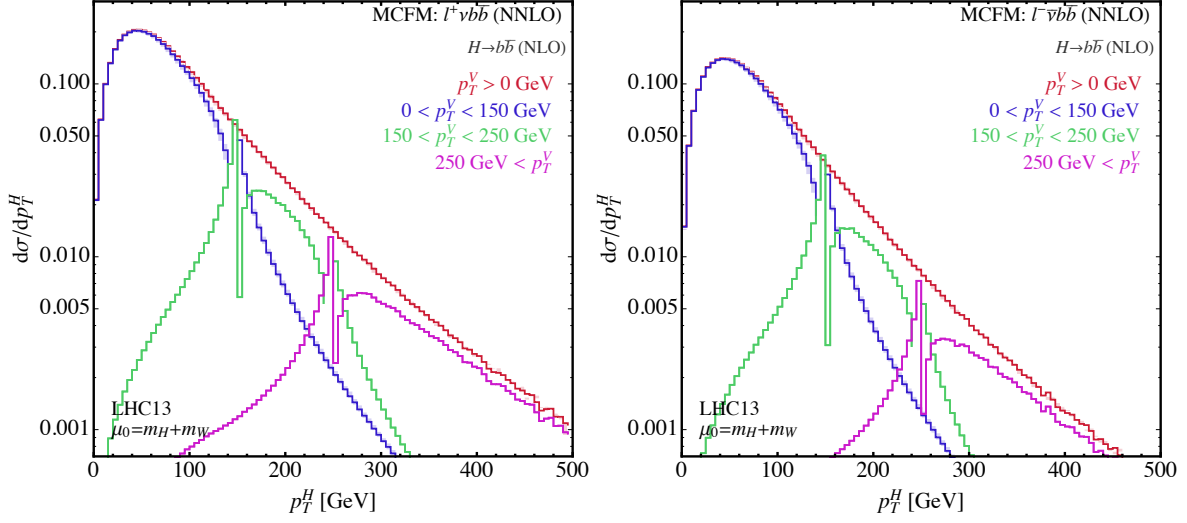


Fig. 16: The transverse momentum $p_T^{b\bar{b}}$ for W^+H (left) and W^-H (right) at the 13 TeV LHC, phase space cuts are described in the text.

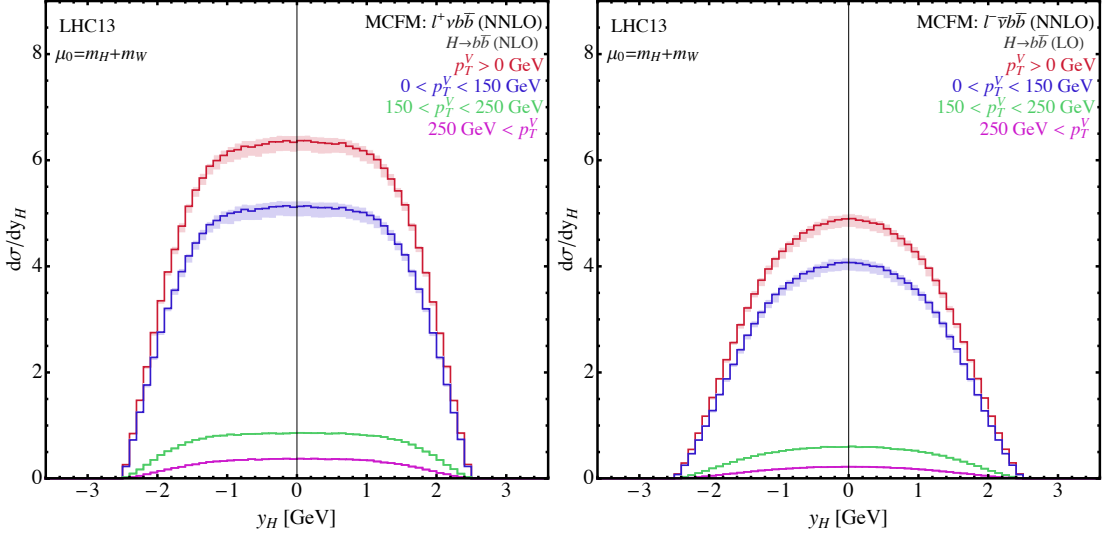


Fig. 17: The rapidity of the $b\bar{b}$ pair for W^+H (left) and W^-H (right) at the 13 TeV LHC, phase space cuts are described in the text.

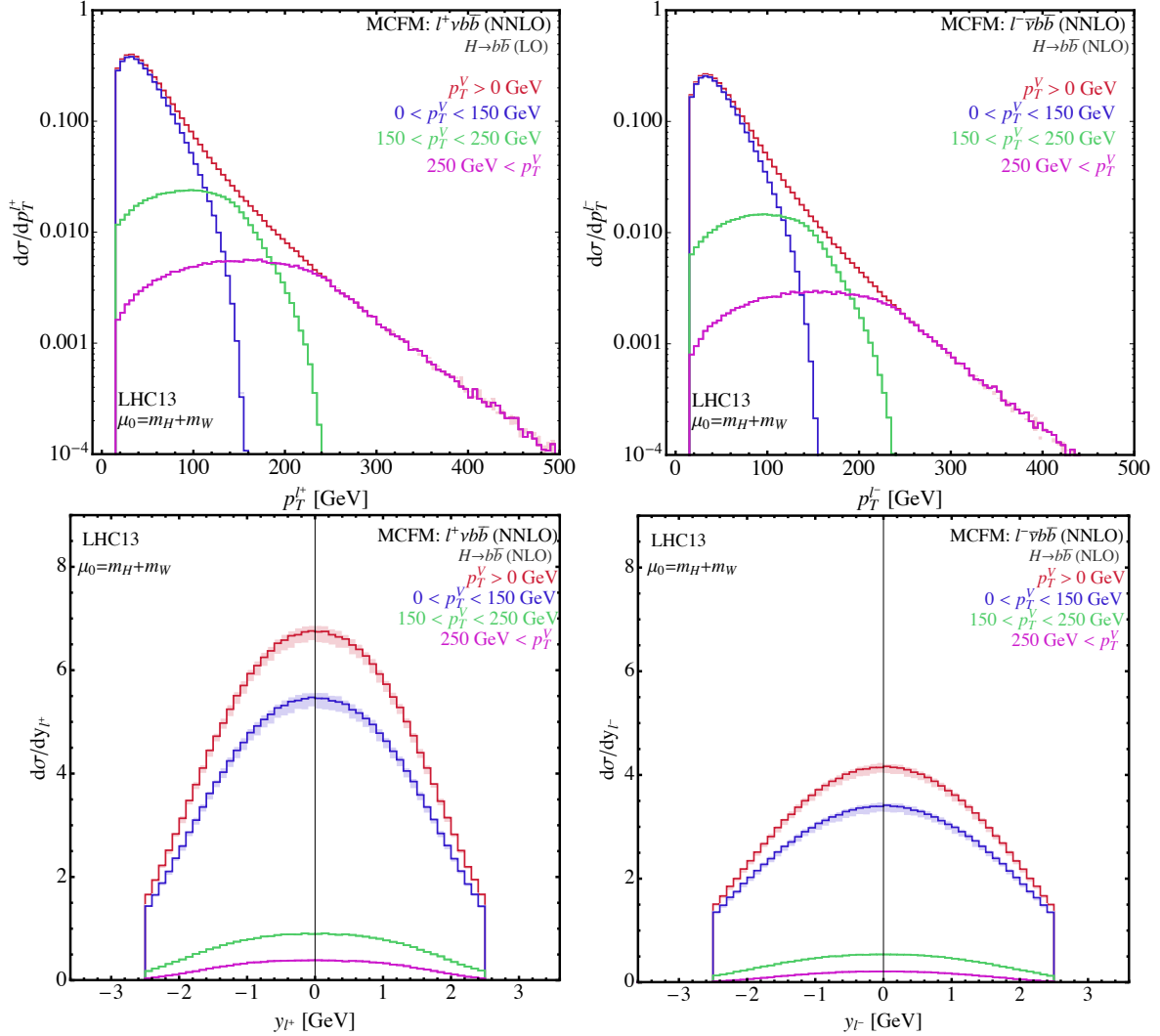


Fig. 18: The transverse momentum p_T^1 for W^+H (left, upper) and W^-H (right, upper) and lepton rapidity W^+H (left, lower) and W^-H (right, lower) at the 13 TeV LHC, phase space cuts are described in the text.

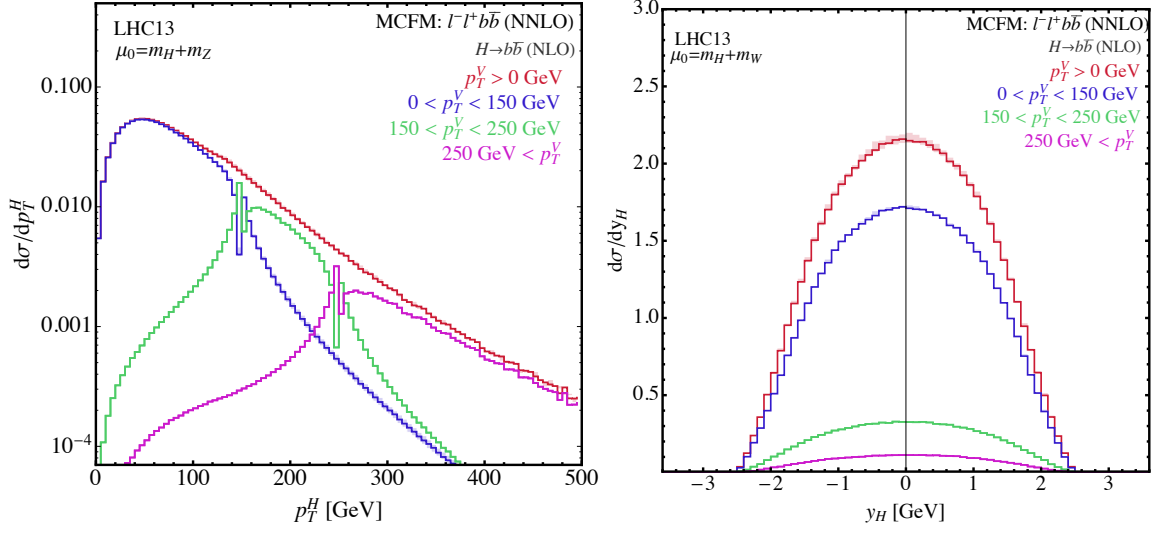


Fig. 19: The transverse momentum and rapidity of the $b\bar{b}$ pair for ZH at the 13 TeV LHC, phase space cuts are described in the text.

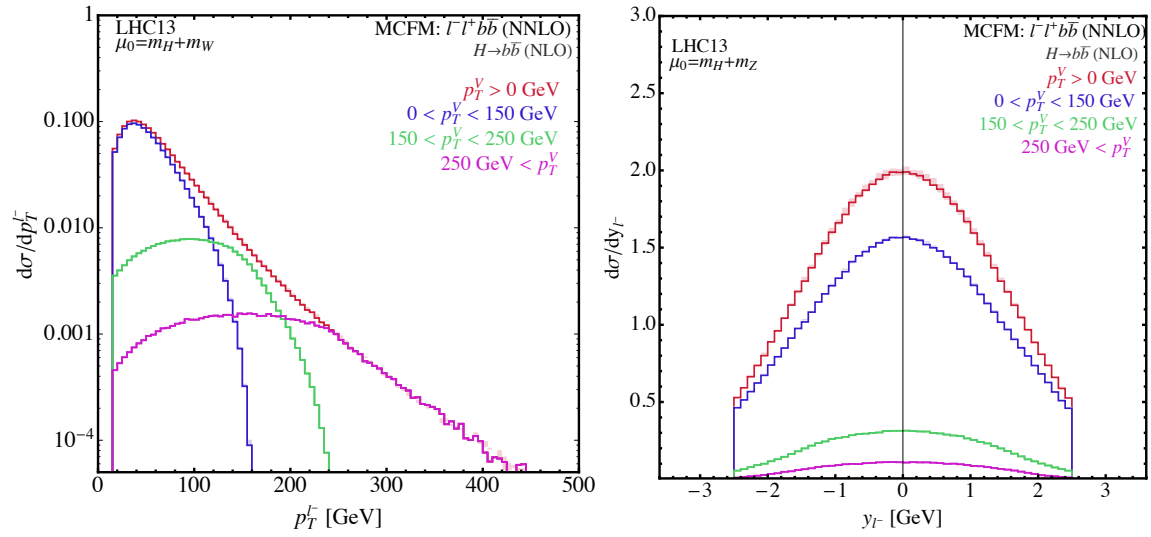


Fig. 20: The lepton transverse momentum and rapidity for ZH at the 13 TeV LHC, phase space cuts are described in the text.

381 **3 Electroweak H+3jets production at NLO+PS**

382 Electroweak production of a Higgs boson in association with three jets has first been considered at NLO-
383 QCD accuracy in Ref. [12] in the VBF approximation. A matching of this calculation to parton-shower
384 programs in the framework of the POWHEG BOX has been presented in [13]. In Ref. [59], NLO-QCD
385 corrections have been provided without resorting to the VBF approximation. This latter calculation is
386 based on spinor helicity techniques in combination with the methods developed in the context of [60].
387 For its implementation, a module has been developed: HJets++ [?] is a plugin to HERWIG7’s Match-
388 box [61,62] module, providing amplitudes for calculating the production of a Higgs boson in association
389 with $n_{\text{jet}} = 2, 3$ jets at next-to-leading order in QCD, *i.e.* at $\mathcal{O}(\alpha^3 \alpha_s^{n_{\text{jet}}-1})$ ⁶. The plugin nature of this
390 module enables the amplitudes to be directly used in an NLO-plus-parton-shower matched simulation,
391 with both subtractive (MC@NLO-type) and multiplicative (POWHEG-type) matchings being available.
392 Either of the two parton showers available in HERWIG7 can be used in the matching.

Here, results obtained with the HJets++ module matched through the subtractive matching algorithm with the default HERWIG7 angular ordered shower are presented and compared to those obtained with the POWHEG BOX implementation. Multiple partonic interactions and hadronization are disregarded throughout. Contributions from external top- and bottom quarks are neglected and, consistently, the CT10 four-flavour PDF set is used [63]. In addition to the selection cuts of Eqs. (1.4)–(1.5) a third jet is required with

$$p_{Tj} > 20 \text{ GeV}, \quad |y_j| < 5. \quad (1.27)$$

393 Results for the transverse-momentum and rapidity distributions of the Higgs boson and the hardest tag-
394 ging jet are shown in Figs. 21 and 22, respectively. In addition, the respective distributions of the third-
395 hardest jet are illustrated in Fig. 23. For the given setup results obtained with the POWHEG BOX code
396 that resorts to the VBF approximation are in good agreement with the full calculation of the HJets++
397 implementation. A comparison of the HJets++ at NLO QCD and at NLO QCD matched with parton
398 shower reveals that parton-shower effects are moderate for the considered observables.

⁶In this approach, Yukawa couplings are counted as a separate expansion parameter; thus finite heavy quark loop contributions are to be considered separately.

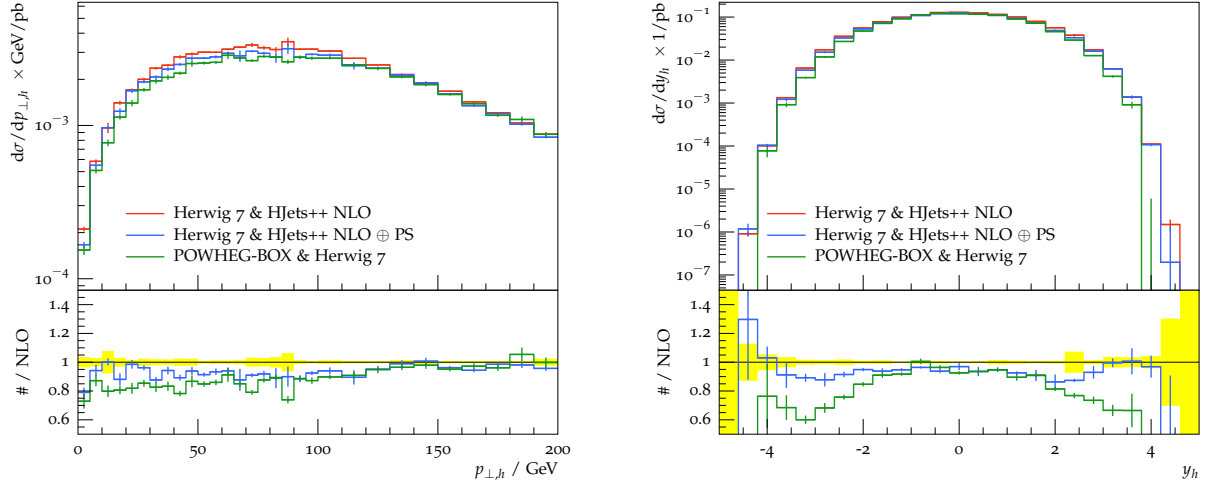


Fig. 21: Transverse-momentum and rapidity distributions of the Higgs boson in EW H+3 jet production at NLO QCD (red line) as obtained from using the Matchbox framework of HERWIG7 with the HJets++ plugin, and at NLO QCD matched with the HERWIG7 angular ordered parton shower in the same framework (blue line), and with the POWHEG BOX (green line), respectively. The lower panels show the respective ratios of the NLO+PS to the fixed-order NLO QCD result for $\sqrt{s} = 13$ TeV and $M_H = 125$ GeV. The yellow bands indicate the statistical uncertainty of the NLO result.

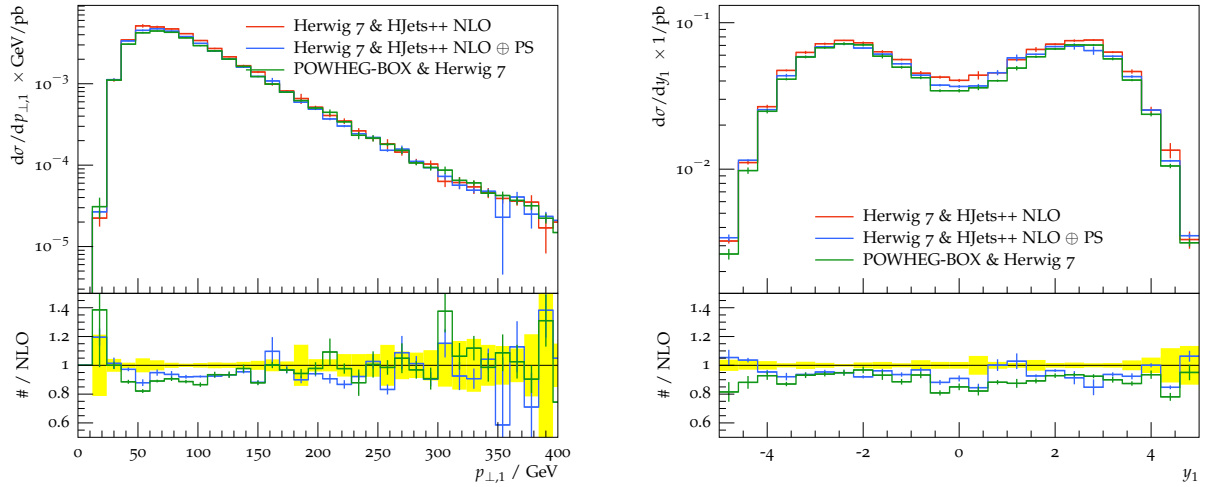


Fig. 22: Transverse-momentum and rapidity distributions of the hardest tagging jet in EW H+3 jet production at NLO QCD (red line) as obtained from using the Matchbox framework of HERWIG7 with the HJets++ plugin, and at NLO QCD matched with the HERWIG7 angular ordered parton shower in the same framework (blue line), and with the POWHEG BOX (green line), respectively. The lower panels show the respective ratios of the NLO+PS to the fixed-order NLO QCD result for $\sqrt{s} = 13$ TeV and $M_H = 125$ GeV. The yellow bands indicate the statistical uncertainty of the NLO result.

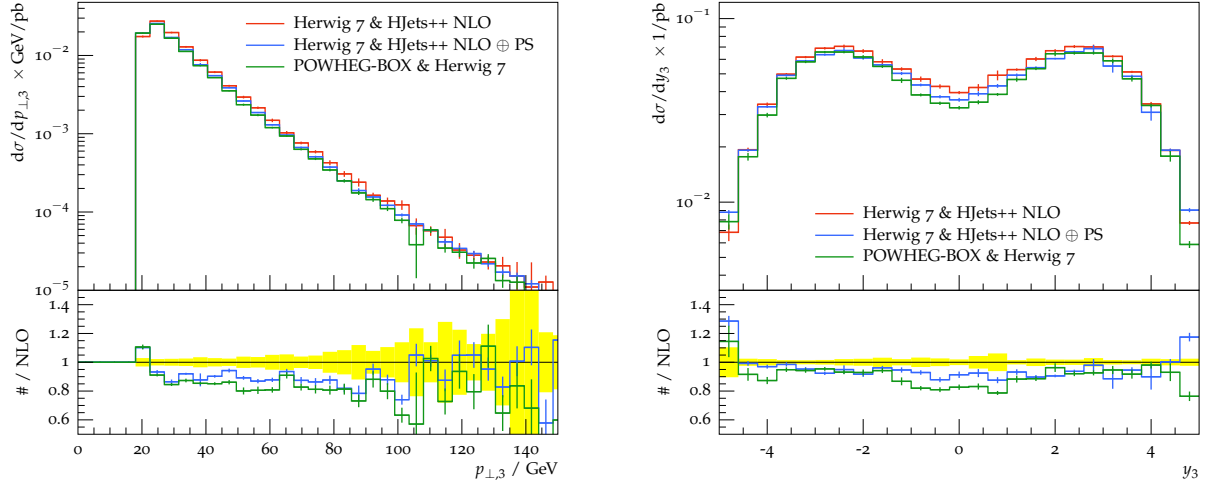


Fig. 23: Transverse-momentum and rapidity distributions of the third jet in EW H+3 jet production at NLO QCD (red line) as obtained from using the Matchbox framework of HERWIG7 with the Hjets++ plugin, and at NLO QCD matched with the HERWIG7 angular ordered parton shower in the same framework (blue line), and with the POWHEG BOX (green line), respectively. The lower panels show the respective ratios of the NLO+PS to the fixed-order NLO QCD result for $\sqrt{s} = 13$ TeV and $M_H = 125$ GeV. The yellow bands indicate the statistical uncertainty of the NLO result.

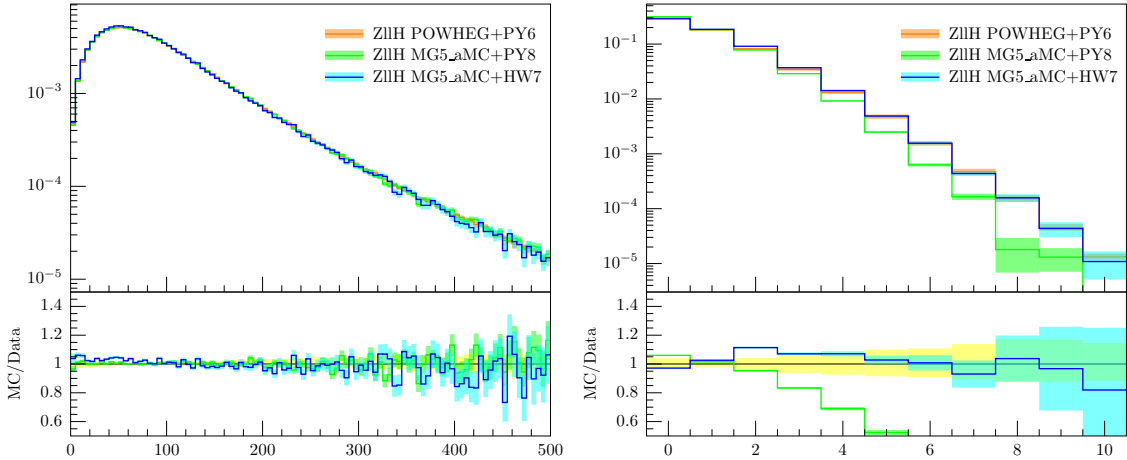


Fig. 24: Comparison of the boson p_T (left) and number of additional jets (right) in the inclusive case for $Z(l)lH$.

399 4 VH production at NLO+PS

400 Calculations for the VH process matched to parton-shower programs are available at NLO accuracy with
 401 POWHEG BOX [11] and MG5_AMC [] with FxFx merging [33, 34], for ZH and WH, and at LO for
 402 ggZH.

403 A systematic comparison of these calculation has been carried out in several regions of the phase
 404 space making use of several Rivet [64] analyses, differing for the vector boson and Higgs candidate
 405 selection. The $Z(l)lH(bb)$ process is studied in the following Z pT bins: inclusive, [0-100] GeV, (100-
 406 200] GeV, >200 GeV. The Z leptons are selected with the following cuts: $|\eta| < 2.5$, $p_T > 15$ GeV.
 407 The dilepton invariant mass m_{ll} is required to be in the range [75-105] GeV. The $Z(\nu\nu)H(bb)$ process
 408 is studied in the following Z pT bins: inclusive, [0-150] GeV, (150-250] GeV, >250 GeV. The Z pT is
 409 evaluated through the missing transverse energy of the event. The $W(l\nu)H(bb)$ process is studied in the
 410 following W pT bins: inclusive, [0-150] GeV, (150-250] GeV, >250 GeV. The W lepton is required to
 411 have $|\eta| < 2.5$, $p_T > 15$ GeV. The neutrino p_T , evaluated through the missing transverse energy of the
 412 event, is required to be above 15 GeV.

413 The processes are studied as a function of the numer of additional jets, defined as ak5 jets recon-
 414 structed with fastjet [] and selected to have $p_T > 20$ GeV and $|\eta| < 4.5$. The jet counting is used to
 415 define the exclusive VH+0-jet and VH+1-jet regions, used in the experimental analyses [?, ?].

416 For each process, the Higgs p_T and rapidity, the lepton p_T and rapidity, and the neutrino p_T are
 417 compared in each of the boson p_T bins, for different bins of additional jets.

418 The results obtained with POWHEG BOX matched with the default PYTHIA6 (POWHEG+PY6)
 419 shower are presented and compared to those obtained with the MG5_AMC implementationm matched
 420 with both default PYTHIA8 (MG5_AMC+PY8) and default HERWIG7 (MG5_AMC+HW7). Com-
 421 parisons are made while keeping the Higgs stable. When the Higgs is decayed into b-quarks, the Higgs
 422 candidate is reconstructed by selecting the leading b-jet pair p_T , where the b-jets are required to have
 423 $|\eta| < 2.5$ and $p_T > 25$ GeV. The comparisons are performed after normalizing the total inclusive cross
 424 section to unity.

425 The boson p_T and additional jet multiplicity distributions in the inclusive case are shown in Fig. 24.
 426 A very small trend is visible in the boson p_T for MG5_AMC+HW7 when compared with POWHEG+PY6
 427 and MG5_AMC+PY8, while the distribution of selected additional jets for MG5_AMC+PY8 deviates
 428 at high multiplicity when compared with the other two cases.

429 In the phase space characterized by inclusive boson p_T and additional jets selection, the Higgs

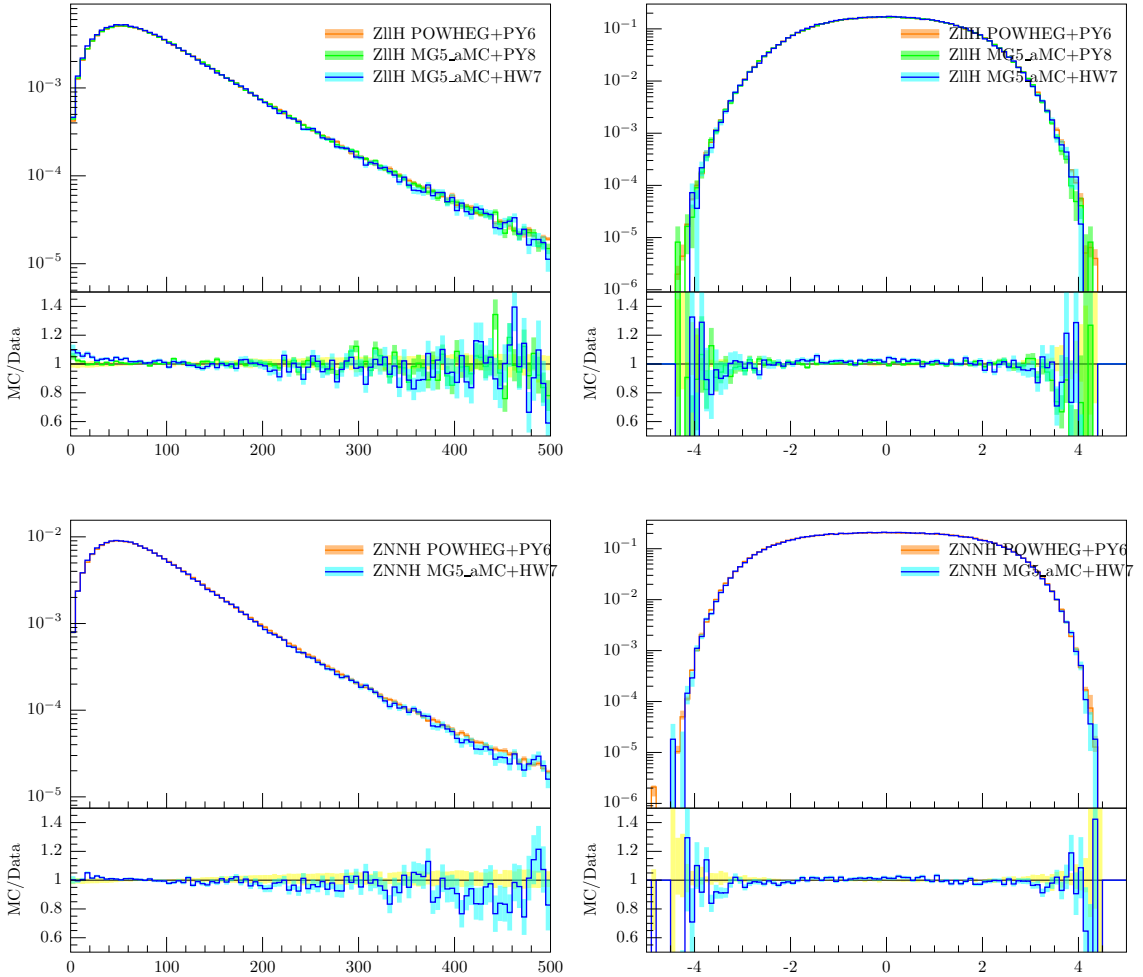


Fig. 25: Comparison of the boson p_T (left) and rapidity (right) in $Z(l\bar{l})H$ events (top) and $Z(\nu\bar{\nu})H$ events (bottom) in the inclusive jet region.

430 p_T for MG5_AMC+HW7 exhibits the same trend visible for the boson p_T , while the rapidity shapes are
 431 well compatible as shown in Fig. 25.

432 This discrepancies clearly indicate the need for a careful choice of the underlying event tune while
 433 performing analyses which require categories with exclusive number of jets.

434 In the phase space characterized by an inclusive boson p_T and the explicit request for 0 additional
 435 jets, the shapes are once more very similar but a different normalization can be observed, as reflection of
 436 the different distribution of additional jets. While requiring the inclusive boson p_T but exactly 1 additional
 437 jet, the p_T shapes start to deviate a bit, both for the lepton p_T and Higgs p_T . Finally, when requiring the
 438 inclusive boson p_T and at least 1 additional jet the p_T shapes deviate a bit more (both for lepton p_T and
 439 Higgs p_T), as well as the overall normalization due to the different additional jet distribution as stated
 440 above.

441 In the low boson p_T region, very similar shapes are observed for the inclusive jet selection, apart
 442 from some mild trend in the low Higgs p_T region especially for HW7. Very similar shapes for the 0
 443 jet phase space but normalization offset due to usual different distribution int he number of jets. Very
 444 similar shapes for exactly 1 jet phase space apart from some trend in the Higgs low pT region especially
 445 for HW7. Very similar shapes are also observed while requiring at least 1 jet, apart from some trend

⁴⁴⁶ in the low Higgs low p_T region especially for HW7, and the normalization offset due to usual different
⁴⁴⁷ distribution in the number of jets.

⁴⁴⁸ The considerations expressed above for the low boson p_T are valid while selecting both the medium
⁴⁴⁹ and high boson p_T regions, in all the jet categories.

⁴⁵⁰ 5 NNLOPS for VH

We report about a study of the Higgs boson production in association with a W^+ boson at next-to-next-to-leading order accuracy including parton shower effects (NNLOPS)

$$pp \rightarrow HW^+ \rightarrow Hl^+\nu_l, \quad (1.28)$$

where $l = \{e, \mu\}$. To achieve NNLOPS accuracy we have implemented a reweighting method similar to the one introduced in HNNLOPS [65] and DYNNLOPS [66]. We reweight events obtained with the POWHEG NLO+PS accurate calculation of HW in association with a jet, and upgraded with the MiNLO procedure (HWJ-MiNLO) [67], by a factor:

$$\begin{aligned} \mathcal{W}(\Phi_{HW}, p_T) &= h(p_T) \frac{\int d\sigma^{\text{NNLO}} \delta(\Phi_{HW} - \Phi_{HW}(\Phi)) - \int d\sigma_A^{\text{MINLO}} \delta(\Phi_{HW} - \Phi_{HW}(\Phi))}{\int d\sigma_A^{\text{MINLO}} \delta(\Phi_{HW} - \Phi_{HW}(\Phi))} \\ &+ (1 - h(p_T)), \end{aligned} \quad (1.29)$$

where $d\sigma^{\text{NNLO}}$ and $d\sigma_{A/B}^{\text{MINLO}}$ are multi-differential distributions obtained at pure NNLO level and by analysing produced HWJ-MiNLO events, respectively. The function $h(p_T)$ is defined as

$$h(p_T) = \frac{(M_H + M_W)^2}{(M_H + M_W)^2 + p_T^2}, \quad (1.30)$$

where p_T is the transverse momentum of the leading jet, and it is used to split the MiNLO cross section into

$$d\sigma_A^{\text{MINLO}} = d\sigma^{\text{MINLO}} h(p_T), \quad d\sigma_B^{\text{MINLO}} = d\sigma^{\text{MINLO}} (1 - h(p_T)). \quad (1.31)$$

⁴⁵¹ Therefore the function $h(p_T)$ ensures that the reweighting is smoothly turned off when the leading jet is
⁴⁵² hard since in that region the HWJ-MiNLO generator is already NLO accurate, as is the NNLO calcula-
⁴⁵³ tion of HW.

For the process in eq. (1.28) the Born kinematics is fully specified by 6 independent variables. We have chosen them to be: the transverse momentum of Higgs boson ($p_{T,H}$); the rapidity of HW system (y_{HW}); the difference of Higgs rapidity and the W^+ rapidity (Δy_{HW}); the invariant mass of $e^+\nu_e$ system ($m_{e\nu}$); and the two Collins-Soper angles (θ^*, ϕ^*) [68]:

$$\Phi_B = \{p_{T,H}, y_{HW}, \Delta y_{HW}, m_{e\nu}, \theta^*, \phi^*\}. \quad (1.32)$$

In this setup the multi-differential cross-section can be written in the form:

$$\begin{aligned} \frac{d\sigma}{d\Phi_B} &= \frac{d^6\sigma}{dp_{t,H} dy_{HW} d\Delta y_{HW} dm_{e\nu} d\theta^* d\phi^*} \\ &= \frac{3}{16\pi} \left(\frac{d\sigma}{d\Phi_{HW^*}} (1 + \cos^2 \theta^*) + \sum_{i=0}^7 A_i(\Phi_{HW^*}) f_i(\theta^*, \phi^*) \right), \end{aligned} \quad (1.33)$$

where $\Phi_{HW^*} = \{p_{T,H}, y_{HW}, \Delta y_{HW}, m_{e\nu}\}$, and the angular dependence is encoded in the coefficients $A_i(\Phi_{HW^*})$ and the functions:

$$f_0(\theta^*, \phi^*) = (1 - 3 \cos^2 \theta^*) / 2, \quad f_1(\theta^*, \phi^*) = \sin 2\theta^* \cos \phi^*,$$

$$\begin{aligned}
f_2(\theta^*, \phi^*) &= (\sin^2 \theta^* \cos 2\phi^*)/2, & f_3(\theta^*, \phi^*) &= \sin \theta^* \cos \phi^*, \\
f_4(\theta^*, \phi^*) &= \cos \theta^*, & f_5(\theta^*, \phi^*) &= \sin \theta^* \sin \phi^*, \\
f_6(\theta^*, \phi^*) &= \sin 2\theta^* \sin \phi^*, & f_7(\theta^*, \phi^*) &= \sin^2 \theta^* \sin 2\phi^*.
\end{aligned} \tag{1.34}$$

454 Since the angular dependence is fully expressed in terms of the $f_i(\theta^*, \phi^*)$ functions, the coefficients
455 of the expansion $A_i(\Phi_{HW^*})$ depend only on the remaining kinematic variables. Using orthogonality
456 properties of spherical harmonics we can extract these coefficients.

457 In our work we have simplified our procedure by noting that the $m_{e\nu}$ invariant mass distribution
458 has a flat K-factor. This is true even when examining the $d\sigma/dm_{e\nu}$ distribution in different bins of
459 $\Phi_{HW} = \{p_{T,H}, y_{HW}, \Delta y_{HW}\}$. Therefore, in eq. (1.33) we replace the 4-dimensional Φ_{HW^*} with the
460 3-dimensional Φ_{HW} . This is an approximation, however we believe that it works extremely well as
461 discussed in ref. [?]. In our work we obtain $\frac{d\sigma}{d\Phi_{HW}}$ and $A_i(\Phi_{HW})$ ($i = 0, 7$) at pure NNLO level by
462 running the HVNNLO code [?, 35, 46], and we obtain the results at MiNLO level by running HWJ-
463 MiNLO [67]. We store the results in 9 three-dimensional tables. Following this step, we use these
464 tables along with eq. (1.33) to obtain the function eq. (1.29) to reweight each produced event. The final
465 ensemble of events is NNLO accurate for all observables at Born level and a parton shower can now be
466 applied without affecting the NNLO accuracy.

In the following we show results for 13 TeV LHC collisions applying the lepton cuts reported in Eq. (1.13). Jets have been clustered using the anti- k_t algorithm with $R = 0.4$ [32] as implemented in FASTJET [69, 70] and count if they fullfil the following conditions:

$$p_T(\text{jet}) > 20 \text{ GeV}, \quad |\eta(\text{jet})| < 4.5. \tag{1.35}$$

467 As for the PDF, we have used the MMHT2014nnlo68cl set [71], corresponding to a value of $\alpha_s(M_Z) =$
468 0.118. For HWJ-MiNLO events, the scale choice is dictated by the MiNLO procedure, while for the
469 NNLO we have used for the central renormalisation and factorisation scales $\mu_0 = M_H + M_W$. To
470 estimate uncertainties we calculate both the fixed order NNLO and HWJ-MiNLO results at 7 scales,
471 each with renormalization and factorization scale varied independently up and down by a factor of 2.
472 When these results are then used in eq. (1.29) this gives 49 combinations for the NNLOPS results. We
473 define our perturbative uncertainty as the envelope of these 49 variations.

474 To shower partonic events, we have used PYTHIA8 [72] (version 8.185) with the “Monash
475 2013” [73] tune. We consider events after parton showering and hadronization effects, unless other-
476 wise stated. Underlying event and multiple parton interactions were kept switched off. To define leptons
477 from the boson decays we use the Monte Carlo truth, *i.e.* we assume that if other leptons are present, the
478 ones coming from the W decay can be identified correctly. To obtain the results shown in the following,
479 we have switched on the “doublefsr” option introduced in ref. [74]. The plots shown throughout this
480 study have been obtained keeping the veto scale equal to the default POWHEG prescription. We also
481 present comparisons among our results and HVNNLO.

482 In Fig. 26 we show distributions for the transverse momenta of the W boson and the WH system,
483 respectively. NNLO results (from HVNNLO) are compared against those obtained with HWJ-MiNLO
484 and HVNNLOPS. For observables that are fully inclusive over QCD radiation, as $p_{T,W}$, the agreement
485 among the HVNNLO and NNLOPS predictions is perfect, as expected. One also notices the sizeable
486 reduction of the uncertainty band when HWJ-MiNLO results are upgraded to NNLOPS. As no par-
487 ticularly tight cuts are imposed, the NNLO/NLO K-factor is almost exactly flat. The right panel shows
488 instead the effects due to the Sudakov resummation. At small transverse momenta, the NNLO cross
489 section becomes larger and larger due to the singular behaviour of the matrix elements for HW produc-
490 tion in association with arbitrarily soft-collinear emissions. The MiNLO method resums the logarithms
491 associated to these emissions, thereby producing the typical Sudakov peak, which for this process is
492 located at $1 \text{ GeV} \lesssim p_{T,HW} \lesssim 4 \text{ GeV}$, as expected from the fact that the LO process is Drell-Yan like. It
493 is also interesting to notice here two other features that occur away from the collinear singularity, and

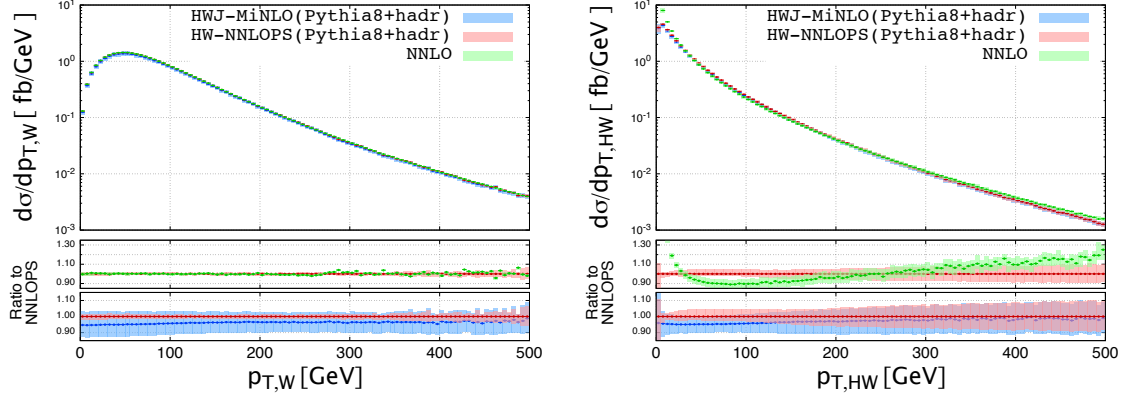


Fig. 26: Comparison of HWJ-MiNLO (PYTHIA8+HADR) (blue), NNLO (green), and HW-NNLOPS (PYTHIA8+HADR) (red) for $p_{T,W}$ (left) and $p_{T,HW}$ (right).

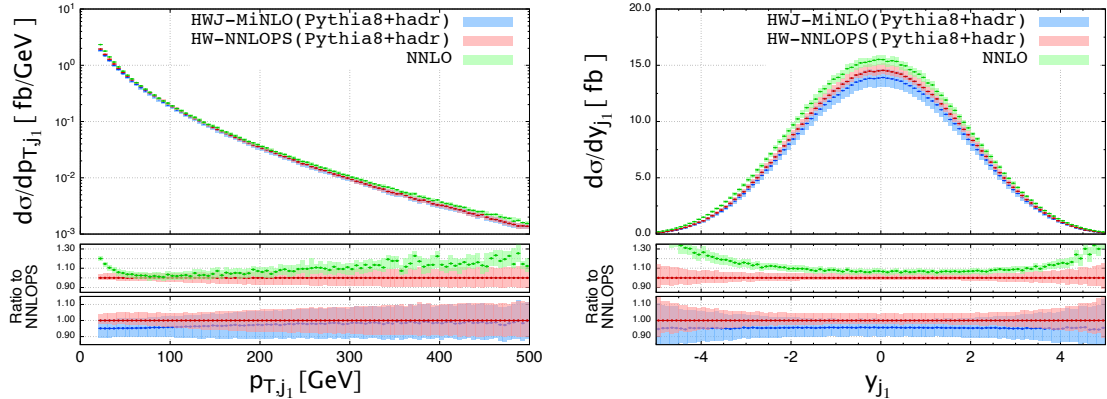


Fig. 27: Comparison of HWJ-MiNLO (PYTHIA8+HADR) (blue), NNLO (green), and HW-NNLOPS (PYTHIA8+HADR) (red) for p_{T,j_1} (left) and y_{j_1} (right).

which are useful to understand plots to be shown in the following. Firstly, the p_T -dependence of the NNLO reweighting can be explicitly seen in the bottom panel, where one can also appreciate that at very large values not only the NNLOPS and MiNLO results approach each other, but also that the uncertainty band of HVNNLOPS becomes progressively larger (in fact, in this region, the nominal accuracy is NLO). Secondly, in the region $30 \text{ GeV} \lesssim p_{T,\text{HW}} \lesssim 200 \text{ GeV}$, the NNLO and NNLOPS lines show deviations of up to 10 %: these are due both to the compensation that needs taking place in order for the two results to integrate to the same total cross section, as well as to the fact that the scale choices are different (fixed for the NNLO line, dynamic and set to $p_{T,\text{HW}}$ in MiNLO). At $p_{T,\text{HW}} \simeq 200 - 250 \text{ GeV}$ the two predictions agree quite well, since this is the region of phase space where the MiNLO scale approaches that used at NNLO ($\mu = M_H + M_W$). The two lines don't cross at $p_T \simeq M_H + M_W$ but rather at slightly larger values, because the effects of spreading the NNLO/NLO K factor not uniformly in p_T are still noticeable, although small, at 200 GeV.

In Fig. 27 we show the transverse momentum and the rapidity of the hardest jet. Most of the differences among these three predictions can be easily explained by the considerations made above on the $p_{T,\text{HW}}$ spectrum, although here effects due to multiple radiation as well as hadronization are bound to play some role too. In Fig. 27 we notice that, for large values of $|y_{j_1}|$, there are large differences among the NNLO result and those containing Sudakov resummation: this is expected, since a large-rapidity jet has on average a smaller transverse momentum, hence the singular nature of the NNLO result is more evident in these kinematics configurations.

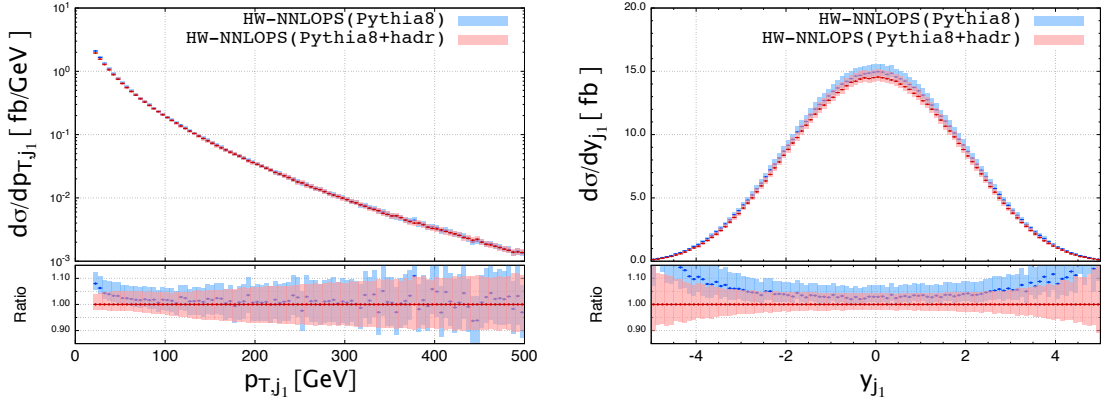


Fig. 28: Comparison of HW-NNLOPS with (red) and without (blue) hadronization for p_{T,j_1} (left) and y_{j_1} (right).

513 Next we find it interesting to examine the size of non-perturbative effects. As shown in Fig. 28,
 514 hadronization has a sizeable impact on the shapes of jet distributions: differences up to 7 – 8 % can be
 515 seen in the jet p_T spectrum at small values, and are still visible at a few percent level till when relatively
 516 hard jets are required ($p_{T,j_1} > 100$ GeV). Even larger effects can be seen in the rapidity distribution (right
 517 panel) at large rapidities. The HVNNLOPS generator allows us to simulate these features in a fully-
 518 exclusive way, retaining at the same time all the virtues of an NNLO computation for fully inclusive
 519 observables, as well as resummation effects, thanks to the interplay among POWHEG, MiNLO and
 520 parton showering.

521 In Fig. 29 we show the transverse momentum and rapidity distributions of the Higgs boson and the
 522 charged lepton, as predicted by the HVNNLOPS code and by the underlying HWJ-MiNLO simulation.
 523 No particular feature needs be commented in these plots: since no cuts are applied on extra radiation, the
 524 inclusion of higher order corrections just makes the HVNNLO predictions more accurate, as expected.
 525 On the other hand it is interesting to see how these distributions are affected by requiring further cuts,
 526 like imposing a jet veto or requiring the presence of at least one jet, whilst restricting at the same time
 527 the phase space to different windows for $p_{T,W}$. Figs. 30, 31 and 32 display the Higgs boson transverse
 528 momentum and rapidity in the three following cases:

- 529 – no jet (“jet veto”), $p_{T,W} < 150$ GeV
- 530 – at least 1 jet, $p_{T,W} < 150$ GeV
- 531 – at least 1 jet, 150 GeV $< p_{T,W} < 250$ GeV

532 The first thing to notice is that, in general, the uncertainty band of the NNLOPS-accurate prediction is
 533 not as narrow as in fig. 29: this is expected and physically sound, because the phase space is not fully
 534 inclusive with respect to the QCD activity, due to the requirements on jets. In the jet-veto case, however,
 535 the results show that the inclusion of NNLO corrections within a MiNLO-based simulation is important,
 536 since the uncertainty band of HVNNLOPS, although larger than in Fig. 29, is still narrower than the
 537 HWJ-MiNLO one.

538 The second thing to notice is that, when jets are required, the HVNNLOPS predictions display
 539 larger uncertainties, a bit smaller but in general similar to those obtained with HWJ-MiNLO. This
 540 is expected, since this is exactly the phase space region where both computations are formally NLO
 541 accurate. The effect of the NNLO/NLO reweighting is still quite visible (both in the overall normalization
 542 and in the slightly smaller bands) though, due to the fact that the cut on the jet transverse momentum
 543 is relatively small. This also means that the HWJ-MiNLO and HVNNLOPS results are likely to be
 544 different from fixed order computations, since the use of dynamic scales in MiNLO and its interplay
 545 with resummation has an impact in this phase space region, as shown in Fig. 27 for the associated jet
 546 distributions.

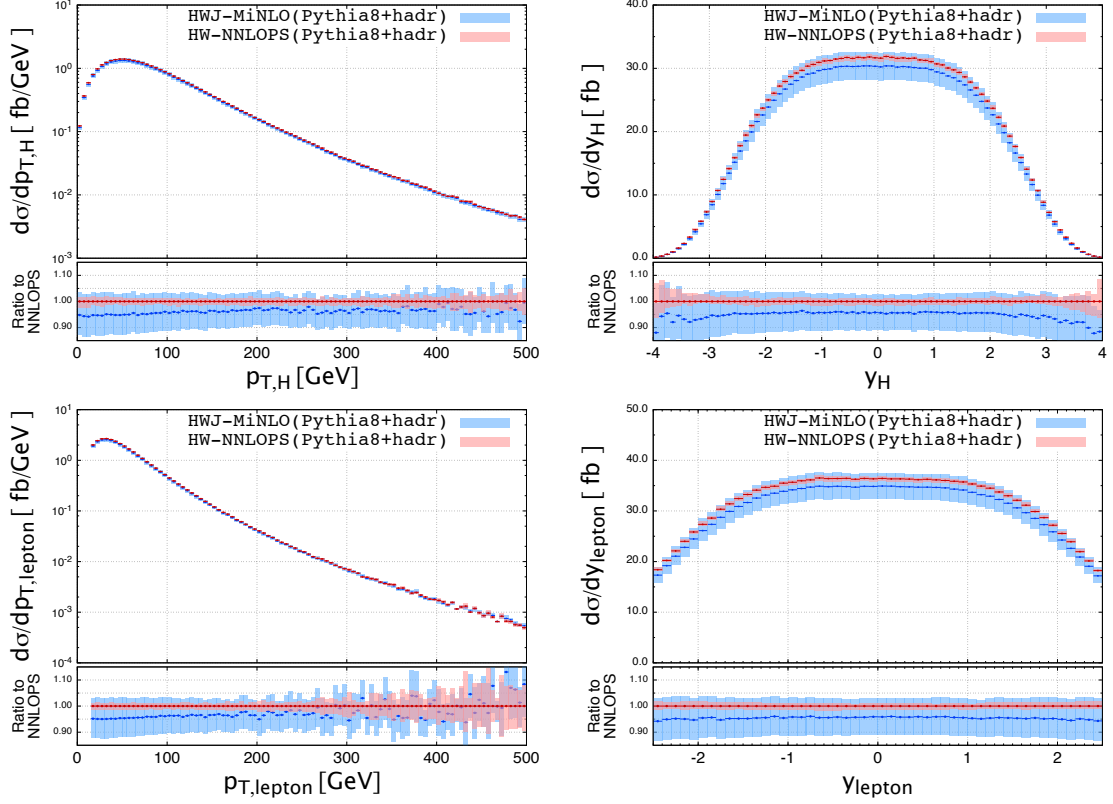


Fig. 29: Comparison of HWJ-MiNLO (PYTHIA8+HADR) (blue) and HW-NNLOPS (PYTHIA8+HADR) (red) for p_T (left) and rapidity (right) for Higgs (upper) and lepton (lower).

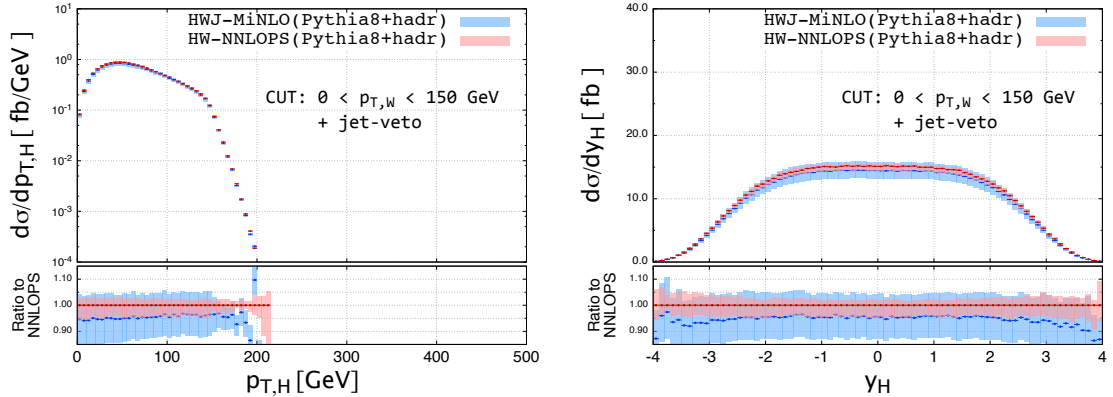


Fig. 30: Comparison of HWJ-MiNLO (PYTHIA8+HADR) (blue) and HW-NNLOPS (PYTHIA8+HADR) (red) for p_T^ϕ (left) and y_H (right) for $p_{T,w} < 150 \text{ GeV}$ and no jet.

547 The final thing to notice, and the one exception to the general trend in the previous observations,
548 is the shrinking of the uncertainty band at intermediate values of p_T^ϕ in Figs. 31 and 32, which is even
549 more noticeable in the y_H distributions, the latter being dominated by the kinematics where p_T^ϕ peaks.
550 This feature is due to the requirement on $p_{T,W}$, and can be explained as follows. For a fully inclusive
551 kinematics, the transverse momenta of the W and H boson are typically balanced, with a value of about
552 40 GeV (see *e.g.* the peak in Figs. 26 and 29). When jets are required, at least the hardest jet p_T will
553 play a role in the momentum conservation in the transverse plane: its typical value, however, depends
554 on the requirements on the massive bosons kinematics. From this observation the band shrinking in the

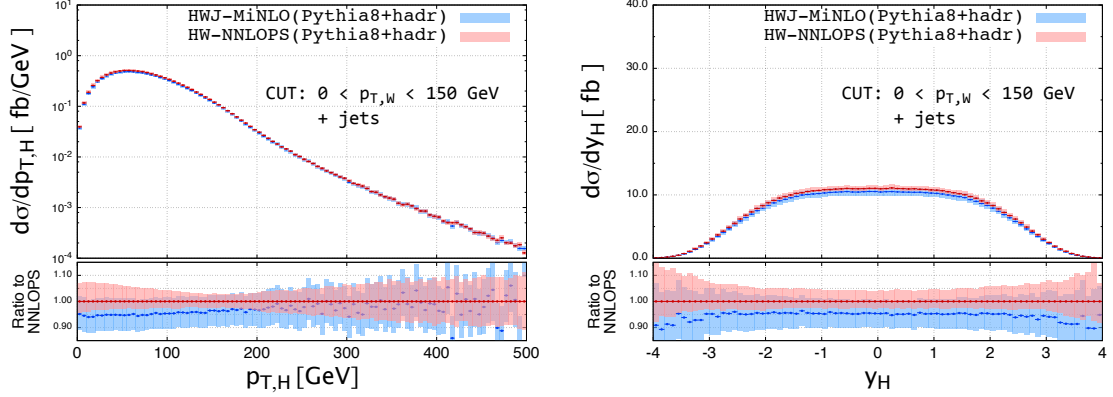


Fig. 31: Comparison of HWJ-MiNLO (PYTHIA8+HADR) (blue) and HW-NNLOPS (PYTHIA8+HADR) (red) for p_T^ϕ (left) and y_H (right) for $p_{T,W} < 150$ GeV and at least 1 jet.

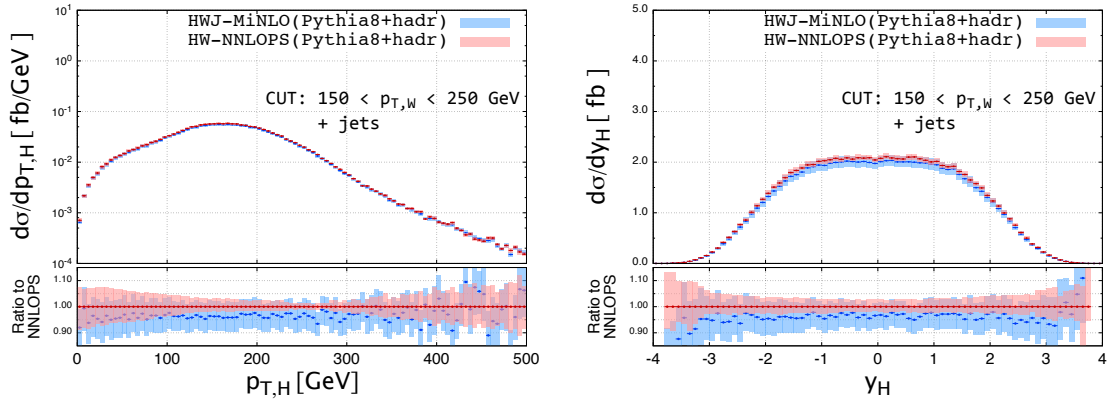


Fig. 32: Comparison of HWJ-MiNLO (PYTHIA8+HADR) (blue) and HW-NNLOPS (PYTHIA8+HADR) (red) for p_T^ϕ (left) and y_H (right) for $150 \text{ GeV} < p_{T,W} < 250 \text{ GeV}$ and at least 1 jet

555 p_T^ϕ spectrum can be understood. For instance, in Fig. 31, when p_T^ϕ approaches values close to the larger
 556 values available for $p_{T,W}$, one enters a region where the jet has to be just above its minimum allowed
 557 value: this is the region where the uncertainty band in the jet p_T spectrum is minimal, as shown in
 558 Fig. 27. As soon as larger p_T^ϕ values are probed whilst keeping $p_{T,W} < 150$ GeV, harder jets are required
 559 by momentum conservation, hence the uncertainty band from HVNNLOPS rapidly approach the one
 560 from HWJ-MiNLO. This effect is even more evident in Fig. 32: if p_T^ϕ is relatively small, then momentum
 561 conservation doesn't constrain p_{T,j_1} very strongly, yielding a standard uncertainty band, relatively similar
 562 to HWJ-MiNLO. In the region where cuts push $p_{T,W}$ and p_T^ϕ to similar values, once more the jet must
 563 be close to its threshold region, and hence the uncertainty band is reduced.

564 6 gg \rightarrow Zh+jet (recommendation and uncertainties)

⁵⁶⁵ **Chapter 2**

⁵⁶⁶ **Conclusions** ¹

⁵⁶⁷ Here come the conclusions.

⁵⁶⁸ Finally, no small set of individuals among the hundreds who have worked collaboration to produce
⁵⁶⁹ this volume can take enough of the credit to single them out, even less the editors.

⁵⁷⁰ ?

Babis, Chiara, Christophe, Daniel, Fabio, Markus, Reisaburo and Sasha

¹C. Anastasiou, D. de Florian, C. Grojean, F. Maltoni, C. Mariotti, A. Nikitenko, M. Schumacher, R. Tanaka

571 Acknowledgements

572 Here come the acknowledgements.

573 We are obliged to CERN, in particular to the IT Department and to the Theory Unit and the LPCC
574 for the support with logistics and technical assistance.

575 Here come the list of grants that supported the various people who contributed

576 M. Zaro is supported by the European Union's Horizon 2020 research and innovation programme
577 under the Marie Skłodowska-Curie grant agreement No 660171 and in part by the ILP LABEX (ANR-
578 10-LABX-63), in turn supported by French state funds managed by the ANR within the "Investissements
579 d'Avenir" programme under reference ANR-11-IDEX-0004-02.

580 The work of S. Höche was supported by the U.S. Department of Energy under contract DE-AC02-
581 76SF00515.

582 The work of N. Kauer and C. O'Brien was supported by the STFC grants ST/J000485/1, ST/J005010/1
583 and ST/L000512/1.

584 The work of B. Hespel and E. Vryonidou was supported in part by the National Fund for Scientific
585 Research (F.R.S.-FNRS Belgium) under a FRIA grant and the European Union as part of the FP7 Marie
586 Curie Initial Training Network MCnetITN (PITN-GA-2012-315877).

587 The work of N. Greiner was supported by the Swiss National Science Foundation under contract
588 PZ00P2_154829.

589 The work of Y. Li was supported by Fermilab, which is operated by Fermi Research Alliance,
590 LLC under Contract No. DE-AC02-07CH11359 with the United States Department of Energy.

591 E. Maina is supported by the Research Executive Agency (REA) of the European Union under the
592 Grant Agreement PITN-GA-2012-316704 (HiggsTools).

593 U. Ellwanger acknowledges support from the European Union Initial Training Networks Higgs-
594 Tools (PITN-GA-2012-316704), INVISIBLES (PITN-GA-2011-289442), the ERC advanced grant
595 Higgs@LHC, and from the grant H2020-MSCA-RISE-2014 No. 645722 (NonMinimalHiggs).

596 S. Plätzer acknowledges support by a FP7 Marie Curie Intra European Fellowship under Grant
597 Agreement PIEF-GA-2013-628739. This work was supported in part by the European Union as part of
598 the FP7 Marie Curie Initial Training Network MCnetITN (PITN-GA-2012-315877).

⁵⁹⁹ **Appendices**

Table A.1: Total VBF cross sections in the SM for a LHC CM energy of $\sqrt{s} = 7$ TeV, including QCD and EW corrections and their uncertainties for different Higgs-boson masses M_H . For more details see Section 1.3.

M_H [GeV]	σ^{VBF} [fb]	$\Delta_{\text{scale}}[\%]$	$\Delta_{\text{PDF}/\alpha_s/\text{PDF}\oplus\alpha_s}[\%]$	$\sigma_{\text{NNLOQCD}}^{\text{DIS}}$ [fb]	$\delta_{\text{EW}}[\%]$	σ_γ [fb]	$\sigma_{s\text{-channel}}$ [fb]
120.0	1301.6(2)	+0.20 -0.22	$\pm 2.1/\pm 0.4/\pm 2.2$	1344.0(2)	-4.5	17.6	668.7(2)
120.5	1295.5(2)	+0.20 -0.22	$\pm 2.1/\pm 0.4/\pm 2.2$	1337.6(2)	-4.5	17.5	659.7(2)
121.0	1289.3(2)	+0.20 -0.22	$\pm 2.1/\pm 0.4/\pm 2.2$	1331.2(2)	-4.5	17.5	650.9(2)
121.5	1283.2(2)	+0.20 -0.22	$\pm 2.1/\pm 0.4/\pm 2.2$	1324.8(2)	-4.5	17.5	642.1(2)
122.0	1277.2(2)	+0.20 -0.22	$\pm 2.1/\pm 0.4/\pm 2.2$	1318.5(2)	-4.5	17.4	633.5(2)
122.5	1271.1(2)	+0.20 -0.22	$\pm 2.1/\pm 0.4/\pm 2.2$	1312.2(2)	-4.4	17.4	624.9(2)
123.0	1265.1(2)	+0.19 -0.21	$\pm 2.1/\pm 0.4/\pm 2.2$	1305.9(2)	-4.4	17.3	616.7(2)
123.5	1259.2(2)	+0.19 -0.21	$\pm 2.1/\pm 0.4/\pm 2.2$	1299.7(2)	-4.4	17.3	608.4(2)
124.0	1253.2(2)	+0.19 -0.21	$\pm 2.1/\pm 0.4/\pm 2.2$	1293.5(2)	-4.4	17.2	600.1(2)
124.1	1252.1(2)	+0.19 -0.21	$\pm 2.1/\pm 0.4/\pm 2.2$	1292.3(2)	-4.4	17.2	598.6(2)
124.2	1250.9(2)	+0.19 -0.21	$\pm 2.1/\pm 0.4/\pm 2.2$	1291.0(2)	-4.4	17.2	597.0(2)
124.3	1249.7(2)	+0.19 -0.21	$\pm 2.1/\pm 0.4/\pm 2.2$	1289.8(2)	-4.4	17.2	595.4(2)
124.4	1248.5(1)	+0.19 -0.21	$\pm 2.1/\pm 0.4/\pm 2.2$	1288.6(2)	-4.4	17.2	593.8(2)
124.5	1247.3(1)	+0.19 -0.21	$\pm 2.1/\pm 0.4/\pm 2.2$	1287.3(2)	-4.4	17.2	592.2(2)
124.6	1246.2(1)	+0.19 -0.21	$\pm 2.1/\pm 0.4/\pm 2.2$	1286.1(2)	-4.4	17.2	590.8(2)
124.7	1245.0(1)	+0.19 -0.21	$\pm 2.1/\pm 0.4/\pm 2.2$	1284.9(2)	-4.4	17.2	589.0(2)
124.8	1243.8(1)	+0.19 -0.21	$\pm 2.1/\pm 0.4/\pm 2.2$	1283.7(2)	-4.4	17.1	587.6(2)
124.9	1242.6(1)	+0.19 -0.21	$\pm 2.1/\pm 0.4/\pm 2.2$	1282.5(2)	-4.4	17.1	586.0(2)
125.0	1241.5(1)	+0.19 -0.21	$\pm 2.1/\pm 0.4/\pm 2.2$	1281.2(2)	-4.4	17.1	584.5(2)
125.09	1240.3(1)	+0.19 -0.21	$\pm 2.1/\pm 0.4/\pm 2.2$	1280.0(2)	-4.4	17.1	582.8(2)
125.1	1240.3(1)	+0.19 -0.21	$\pm 2.1/\pm 0.4/\pm 2.2$	1280.0(2)	-4.4	17.1	582.9(2)
125.2	1239.1(1)	+0.19 -0.21	$\pm 2.1/\pm 0.4/\pm 2.2$	1278.8(2)	-4.4	17.1	581.2(2)
125.3	1238.0(1)	+0.19 -0.21	$\pm 2.1/\pm 0.4/\pm 2.2$	1277.6(2)	-4.4	17.1	579.7(2)
125.4	1236.8(1)	+0.19 -0.21	$\pm 2.1/\pm 0.4/\pm 2.2$	1276.4(2)	-4.4	17.1	578.1(2)
125.5	1235.7(1)	+0.19 -0.21	$\pm 2.1/\pm 0.4/\pm 2.2$	1275.2(2)	-4.4	17.1	576.6(2)
125.6	1234.5(1)	+0.19 -0.21	$\pm 2.1/\pm 0.4/\pm 2.2$	1273.9(2)	-4.4	17.1	575.2(2)
125.7	1233.3(1)	+0.19 -0.21	$\pm 2.1/\pm 0.4/\pm 2.2$	1272.7(2)	-4.4	17.1	573.7(2)
125.8	1232.2(1)	+0.19 -0.21	$\pm 2.1/\pm 0.4/\pm 2.2$	1271.5(2)	-4.4	17.1	572.1(2)
125.9	1231.0(1)	+0.19 -0.21	$\pm 2.1/\pm 0.4/\pm 2.2$	1270.3(2)	-4.4	17.0	570.5(2)
126.0	1229.9(1)	+0.19 -0.21	$\pm 2.1/\pm 0.4/\pm 2.2$	1269.1(2)	-4.4	17.0	569.1(2)
126.5	1224.1(1)	+0.18 -0.21	$\pm 2.1/\pm 0.4/\pm 2.2$	1263.1(2)	-4.4	17.0	561.5(2)
127.0	1218.4(1)	+0.18 -0.21	$\pm 2.1/\pm 0.4/\pm 2.2$	1257.2(2)	-4.4	16.9	554.2(2)
127.5	1212.7(1)	+0.18 -0.21	$\pm 2.1/\pm 0.4/\pm 2.2$	1251.2(2)	-4.4	16.9	546.8(2)
128.0	1207.1(1)	+0.18 -0.21	$\pm 2.1/\pm 0.4/\pm 2.2$	1245.3(2)	-4.4	16.9	539.9(2)
128.5	1201.4(1)	+0.18 -0.20	$\pm 2.1/\pm 0.4/\pm 2.2$	1239.5(2)	-4.4	16.8	532.9(2)
129.0	1195.9(1)	+0.18 -0.20	$\pm 2.1/\pm 0.4/\pm 2.2$	1233.7(2)	-4.4	16.8	526.0(2)
129.5	1190.3(1)	+0.17 -0.20	$\pm 2.1/\pm 0.4/\pm 2.2$	1227.9(1)	-4.4	16.7	519.1(2)
130.0	1184.8(1)	+0.17 -0.20	$\pm 2.1/\pm 0.4/\pm 2.2$	1222.1(1)	-4.4	16.7	512.2(2)

A SM vector-boson-fusion cross sections

In this appendix the cross-section Tables 1.1 and 1.2 for the SM VBF cross sections shown in Section 1.3 are expanded to a scan over SM Higgs-boson masses. In detail the total cross sections are collected in Tables A.4–?? and the fiducial cross sections in Tables A.5–A.8.

Inclusive cross sections at NNLO QCD computed with the VBF@NNLO code are shown in Tables A.14–?? for the SM M_H scan, and in Tables ??–?? for the energy scan.

Numbers for the extended M_H scan are shown in Tables A.18–?? . WW- and ZZ-fusion contributions are

Table A.2: Total VBF cross sections in the SM for a LHC CM energy of $\sqrt{s} = 8$ TeV, including QCD and EW corrections and their uncertainties for different Higgs-boson masses M_H . For more details see Section 1.3.

M_H [GeV]	σ^{VBF} [fb]	$\Delta_{\text{scale}}[\%]$	$\Delta_{\text{PDF}/\alpha_s/\text{PDF} \oplus \alpha_s}[\%]$	$\sigma_{\text{NNLOQCD}}^{\text{DIS}}$ [fb]	$\delta_{\text{EW}}[\%]$	σ_γ [fb]	$\sigma_{s\text{-channel}}$ [fb]
120.0	1675.7(2)	+0.26 -0.25	$\pm 2.1/\pm 0.4/\pm 2.2$	1733.7(2)	-4.7	22.7	811.7(3)
120.5	1668.1(2)	+0.26 -0.25	$\pm 2.1/\pm 0.4/\pm 2.2$	1725.8(2)	-4.7	22.6	800.5(3)
121.0	1660.5(2)	+0.26 -0.25	$\pm 2.1/\pm 0.4/\pm 2.2$	1717.8(2)	-4.7	22.6	790.0(3)
121.5	1652.9(2)	+0.26 -0.25	$\pm 2.1/\pm 0.4/\pm 2.2$	1709.9(2)	-4.6	22.5	779.3(3)
122.0	1645.4(2)	+0.26 -0.25	$\pm 2.1/\pm 0.4/\pm 2.2$	1702.1(2)	-4.6	22.5	768.7(3)
122.5	1637.9(2)	+0.26 -0.24	$\pm 2.1/\pm 0.4/\pm 2.2$	1694.3(2)	-4.6	22.4	759.0(3)
123.0	1630.5(2)	+0.25 -0.24	$\pm 2.1/\pm 0.4/\pm 2.2$	1686.5(2)	-4.6	22.3	748.9(2)
123.5	1623.2(2)	+0.25 -0.24	$\pm 2.1/\pm 0.4/\pm 2.2$	1678.8(2)	-4.6	22.3	739.2(2)
124.0	1615.8(2)	+0.25 -0.24	$\pm 2.1/\pm 0.4/\pm 2.2$	1671.1(2)	-4.6	22.2	729.3(3)
124.1	1614.4(2)	+0.25 -0.24	$\pm 2.1/\pm 0.4/\pm 2.2$	1669.6(2)	-4.6	22.2	727.3(3)
124.2	1612.9(2)	+0.25 -0.24	$\pm 2.1/\pm 0.4/\pm 2.2$	1668.1(2)	-4.6	22.2	725.5(3)
124.3	1611.4(2)	+0.25 -0.24	$\pm 2.1/\pm 0.4/\pm 2.2$	1666.6(2)	-4.6	22.2	723.5(2)
124.4	1610.0(2)	+0.25 -0.24	$\pm 2.1/\pm 0.4/\pm 2.2$	1665.0(2)	-4.6	22.2	721.8(3)
124.5	1608.5(2)	+0.25 -0.24	$\pm 2.1/\pm 0.4/\pm 2.2$	1663.5(2)	-4.6	22.2	719.9(3)
124.6	1607.1(2)	+0.25 -0.24	$\pm 2.1/\pm 0.4/\pm 2.2$	1662.0(2)	-4.6	22.2	717.9(3)
124.7	1605.6(2)	+0.25 -0.24	$\pm 2.1/\pm 0.4/\pm 2.2$	1660.5(2)	-4.6	22.1	716.1(2)
124.8	1604.2(2)	+0.25 -0.24	$\pm 2.1/\pm 0.4/\pm 2.2$	1659.0(2)	-4.6	22.1	714.2(3)
124.9	1602.8(2)	+0.25 -0.24	$\pm 2.1/\pm 0.4/\pm 2.2$	1657.5(2)	-4.6	22.1	712.4(3)
125.0	1601.3(2)	+0.25 -0.24	$\pm 2.1/\pm 0.4/\pm 2.2$	1656.0(2)	-4.6	22.1	710.4(3)
125.09	1599.8(2)	+0.25 -0.24	$\pm 2.1/\pm 0.4/\pm 2.2$	1654.4(2)	-4.6	22.1	708.7(3)
125.1	1599.8(2)	+0.25 -0.24	$\pm 2.1/\pm 0.4/\pm 2.2$	1654.4(2)	-4.6	22.1	708.7(3)
125.2	1598.4(2)	+0.25 -0.24	$\pm 2.1/\pm 0.4/\pm 2.2$	1652.9(2)	-4.6	22.1	706.5(2)
125.3	1597.0(2)	+0.25 -0.24	$\pm 2.1/\pm 0.4/\pm 2.2$	1651.4(2)	-4.6	22.1	704.8(3)
125.4	1595.5(2)	+0.25 -0.24	$\pm 2.1/\pm 0.4/\pm 2.2$	1649.9(2)	-4.6	22.1	703.0(3)
125.5	1594.1(2)	+0.25 -0.24	$\pm 2.1/\pm 0.4/\pm 2.2$	1648.4(2)	-4.6	22.1	701.2(3)
125.6	1592.7(2)	+0.25 -0.24	$\pm 2.1/\pm 0.4/\pm 2.2$	1646.9(2)	-4.6	22.0	699.3(3)
125.7	1591.2(2)	+0.25 -0.24	$\pm 2.1/\pm 0.4/\pm 2.2$	1645.4(2)	-4.6	22.0	697.5(3)
125.8	1589.8(2)	+0.25 -0.24	$\pm 2.1/\pm 0.4/\pm 2.2$	1643.9(2)	-4.6	22.0	695.6(3)
125.9	1588.4(2)	+0.25 -0.24	$\pm 2.1/\pm 0.4/\pm 2.2$	1642.4(2)	-4.6	22.0	693.7(3)
126.0	1587.0(2)	+0.24 -0.24	$\pm 2.1/\pm 0.4/\pm 2.2$	1640.9(2)	-4.6	22.0	692.0(3)
126.5	1579.8(2)	+0.24 -0.24	$\pm 2.1/\pm 0.4/\pm 2.2$	1633.5(2)	-4.6	21.9	683.1(3)
127.0	1572.8(2)	+0.24 -0.24	$\pm 2.1/\pm 0.4/\pm 2.2$	1626.1(2)	-4.6	21.9	674.2(3)
127.5	1565.7(2)	+0.24 -0.24	$\pm 2.1/\pm 0.4/\pm 2.2$	1618.7(2)	-4.6	21.8	665.4(2)
128.0	1558.7(2)	+0.24 -0.24	$\pm 2.1/\pm 0.4/\pm 2.2$	1611.4(2)	-4.6	21.8	656.9(2)
128.5	1551.7(2)	+0.24 -0.24	$\pm 2.1/\pm 0.4/\pm 2.2$	1604.2(2)	-4.6	21.7	648.5(2)
129.0	1544.8(2)	+0.24 -0.23	$\pm 2.1/\pm 0.4/\pm 2.2$	1596.9(2)	-4.6	21.7	640.2(2)
129.5	1537.9(2)	+0.24 -0.23	$\pm 2.1/\pm 0.4/\pm 2.2$	1589.8(2)	-4.6	21.6	631.9(2)
130.0	1531.1(2)	+0.23 -0.23	$\pm 2.1/\pm 0.4/\pm 2.2$	1582.6(2)	-4.6	21.5	623.7(2)

Table A.3: Total VBF cross sections in the SM for a LHC CM energy of $\sqrt{s} = 13$ TeV, including QCD and EW corrections and their uncertainties for different Higgs-boson masses M_H . For more details see Section 1.3.

M_H [GeV]	σ^{VBF} [fb]	$\Delta_{\text{scale}}[\%]$	$\Delta_{\text{PDF}/\alpha_s/\text{PDF} \oplus \alpha_s}[\%]$	$\sigma_{\text{NNLOQCD}}^{\text{DIS}}$ [fb]	$\delta_{\text{EW}}[\%]$	σ_γ [fb]	$\sigma_{s\text{-channel}}$ [fb]
120.0	3935.2(7)	+0.44 -0.33	$\pm 2.1/\pm 0.5/\pm 2.1$	4100.8(7)	-5.3	53.0	1567.0(6)
120.5	3919.4(7)	+0.44 -0.33	$\pm 2.1/\pm 0.5/\pm 2.1$	4084.2(7)	-5.3	52.9	1546.0(7)
121.0	3903.9(7)	+0.44 -0.33	$\pm 2.1/\pm 0.5/\pm 2.1$	4067.8(7)	-5.3	52.8	1525.7(6)
121.5	3888.3(7)	+0.44 -0.33	$\pm 2.1/\pm 0.5/\pm 2.1$	4051.5(7)	-5.3	52.7	1506.7(6)
122.0	3873.0(7)	+0.44 -0.33	$\pm 2.1/\pm 0.5/\pm 2.1$	4035.2(7)	-5.3	52.5	1487.6(6)
122.5	3857.6(7)	+0.43 -0.33	$\pm 2.1/\pm 0.5/\pm 2.1$	4019.0(7)	-5.3	52.4	1468.2(6)
123.0	3842.3(7)	+0.43 -0.33	$\pm 2.1/\pm 0.5/\pm 2.1$	4003.0(7)	-5.3	52.3	1449.3(5)
123.5	3827.0(7)	+0.43 -0.33	$\pm 2.1/\pm 0.5/\pm 2.1$	3987.0(7)	-5.3	52.2	1430.8(5)
124.0	3811.9(7)	+0.43 -0.33	$\pm 2.1/\pm 0.5/\pm 2.1$	3971.1(7)	-5.3	52.1	1412.9(5)
124.1	3808.9(7)	+0.43 -0.33	$\pm 2.1/\pm 0.5/\pm 2.1$	3967.9(7)	-5.3	52.1	1409.4(5)
124.2	3805.9(7)	+0.43 -0.33	$\pm 2.1/\pm 0.5/\pm 2.1$	3964.7(7)	-5.3	52.0	1405.8(5)
124.3	3802.9(7)	+0.43 -0.33	$\pm 2.1/\pm 0.5/\pm 2.1$	3961.6(7)	-5.3	52.0	1401.9(5)
124.4	3799.9(7)	+0.43 -0.33	$\pm 2.1/\pm 0.5/\pm 2.1$	3958.4(7)	-5.3	52.0	1398.4(5)
124.5	3796.9(7)	+0.43 -0.33	$\pm 2.1/\pm 0.5/\pm 2.1$	3955.2(7)	-5.3	52.0	1395.1(5)
124.6	3793.9(7)	+0.43 -0.33	$\pm 2.1/\pm 0.5/\pm 2.1$	3952.1(7)	-5.3	51.9	1391.5(5)
124.7	3790.9(7)	+0.43 -0.33	$\pm 2.1/\pm 0.5/\pm 2.1$	3948.9(7)	-5.3	51.9	1388.0(5)
124.8	3788.0(6)	+0.43 -0.33	$\pm 2.1/\pm 0.5/\pm 2.1$	3945.8(7)	-5.3	51.9	1384.9(5)
124.9	3785.0(6)	+0.43 -0.33	$\pm 2.1/\pm 0.5/\pm 2.1$	3942.7(7)	-5.3	51.9	1381.5(5)
125.0	3782.0(6)	+0.43 -0.33	$\pm 2.1/\pm 0.5/\pm 2.1$	3939.5(7)	-5.3	51.9	1378.1(5)
125.09	3779.0(6)	+0.43 -0.33	$\pm 2.1/\pm 0.5/\pm 2.1$	3936.4(7)	-5.3	51.8	1374.5(5)
125.1	3779.1(6)	+0.43 -0.33	$\pm 2.1/\pm 0.5/\pm 2.1$	3936.4(7)	-5.3	51.8	1373.9(5)
125.2	3775.9(6)	+0.43 -0.33	$\pm 2.1/\pm 0.5/\pm 2.1$	3933.2(7)	-5.3	51.8	1370.5(5)
125.3	3773.0(6)	+0.43 -0.33	$\pm 2.1/\pm 0.5/\pm 2.1$	3930.1(7)	-5.3	51.8	1367.2(5)
125.4	3769.9(6)	+0.43 -0.33	$\pm 2.1/\pm 0.5/\pm 2.1$	3927.0(7)	-5.3	51.8	1364.0(5)
125.5	3767.0(6)	+0.43 -0.33	$\pm 2.1/\pm 0.5/\pm 2.1$	3923.9(7)	-5.3	51.7	1360.0(5)
125.6	3764.2(6)	+0.43 -0.33	$\pm 2.1/\pm 0.5/\pm 2.1$	3920.7(7)	-5.3	51.7	1356.7(5)
125.7	3761.1(6)	+0.43 -0.33	$\pm 2.1/\pm 0.5/\pm 2.1$	3917.6(7)	-5.3	51.7	1353.3(5)
125.8	3758.1(6)	+0.43 -0.33	$\pm 2.1/\pm 0.5/\pm 2.1$	3914.5(7)	-5.3	51.7	1349.8(5)
125.9	3755.1(6)	+0.43 -0.32	$\pm 2.1/\pm 0.5/\pm 2.1$	3911.4(7)	-5.3	51.6	1346.5(5)
126.0	3752.2(6)	+0.43 -0.32	$\pm 2.1/\pm 0.5/\pm 2.1$	3908.3(7)	-5.3	51.6	1343.2(5)
126.5	3737.5(6)	+0.42 -0.32	$\pm 2.1/\pm 0.5/\pm 2.1$	3892.8(7)	-5.3	51.5	1326.4(5)
127.0	3723.0(6)	+0.42 -0.32	$\pm 2.1/\pm 0.5/\pm 2.1$	3877.4(7)	-5.3	51.4	1310.2(5)
127.5	3708.4(6)	+0.42 -0.32	$\pm 2.1/\pm 0.5/\pm 2.1$	3862.1(7)	-5.3	51.3	1293.4(5)
128.0	3693.9(6)	+0.42 -0.32	$\pm 2.1/\pm 0.5/\pm 2.1$	3846.8(7)	-5.3	51.2	1277.6(5)
128.5	3679.5(6)	+0.42 -0.32	$\pm 2.1/\pm 0.5/\pm 2.1$	3831.7(7)	-5.3	51.0	1261.8(5)
129.0	3665.1(6)	+0.42 -0.32	$\pm 2.1/\pm 0.5/\pm 2.1$	3816.6(7)	-5.3	50.9	1246.4(5)
129.5	3650.8(6)	+0.42 -0.32	$\pm 2.1/\pm 0.5/\pm 2.1$	3801.6(7)	-5.3	50.8	1231.0(5)
130.0	3636.7(6)	+0.42 -0.32	$\pm 2.1/\pm 0.5/\pm 2.1$	3786.7(7)	-5.3	50.7	1216.1(5)

Table A.4: Total VBF cross sections in the SM for a LHC CM energy of $\sqrt{s} = 14$ TeV, including QCD and EW corrections and their uncertainties for different Higgs-boson masses M_H . For more details see Section 1.3.

M_H [GeV]	σ^{VBF} [fb]	$\Delta_{\text{scale}}[\%]$	$\Delta_{\text{PDF}/\alpha_s/\text{PDF} \oplus \alpha_s}[\%]$	$\sigma_{\text{NNLOQCD}}^{\text{DIS}}$ [fb]	$\delta_{\text{EW}}[\%]$	σ_γ [fb]	$\sigma_{s\text{-channel}}$ [fb]
120.0	4448.4(8)	+0.46 -0.34	$\pm 2.1/\pm 0.5/\pm 2.1$	4640.4(8)	-5.4	59.8	1722.3(6)
120.5	4430.8(8)	+0.46 -0.34	$\pm 2.1/\pm 0.5/\pm 2.1$	4622.1(8)	-5.4	59.7	1700.5(7)
121.0	4413.6(8)	+0.46 -0.34	$\pm 2.1/\pm 0.5/\pm 2.1$	4603.8(8)	-5.4	59.5	1678.6(6)
121.5	4396.3(8)	+0.46 -0.34	$\pm 2.1/\pm 0.5/\pm 2.1$	4585.6(8)	-5.4	59.4	1657.0(6)
122.0	4379.0(8)	+0.46 -0.34	$\pm 2.1/\pm 0.5/\pm 2.1$	4567.6(8)	-5.4	59.3	1636.0(6)
122.5	4362.0(8)	+0.46 -0.34	$\pm 2.1/\pm 0.5/\pm 2.1$	4549.6(8)	-5.4	59.2	1615.1(6)
123.0	4345.0(8)	+0.46 -0.34	$\pm 2.1/\pm 0.5/\pm 2.1$	4531.8(8)	-5.4	59.0	1594.4(6)
123.5	4328.3(8)	+0.46 -0.34	$\pm 2.1/\pm 0.5/\pm 2.1$	4514.0(8)	-5.4	58.9	1574.4(6)
124.0	4311.4(8)	+0.45 -0.34	$\pm 2.1/\pm 0.5/\pm 2.1$	4496.3(8)	-5.4	58.8	1554.3(6)
124.1	4308.0(8)	+0.45 -0.34	$\pm 2.1/\pm 0.5/\pm 2.1$	4492.8(8)	-5.4	58.7	1550.3(6)
124.2	4304.8(8)	+0.45 -0.34	$\pm 2.1/\pm 0.5/\pm 2.1$	4489.3(8)	-5.4	58.7	1546.8(6)
124.3	4301.4(8)	+0.45 -0.34	$\pm 2.1/\pm 0.5/\pm 2.1$	4485.8(8)	-5.4	58.7	1542.9(6)
124.4	4298.2(8)	+0.45 -0.34	$\pm 2.1/\pm 0.5/\pm 2.1$	4482.2(8)	-5.4	58.7	1538.9(6)
124.5	4294.8(8)	+0.45 -0.34	$\pm 2.1/\pm 0.5/\pm 2.1$	4478.7(8)	-5.4	58.6	1535.2(6)
124.6	4291.4(8)	+0.45 -0.34	$\pm 2.1/\pm 0.5/\pm 2.1$	4475.2(8)	-5.4	58.6	1531.4(6)
124.7	4288.2(8)	+0.45 -0.34	$\pm 2.1/\pm 0.5/\pm 2.1$	4471.7(8)	-5.4	58.6	1527.4(6)
124.8	4284.9(8)	+0.45 -0.34	$\pm 2.1/\pm 0.5/\pm 2.1$	4468.2(8)	-5.4	58.6	1524.0(6)
124.9	4281.4(8)	+0.45 -0.34	$\pm 2.1/\pm 0.5/\pm 2.1$	4464.7(8)	-5.4	58.5	1519.7(6)
125.0	4278.0(8)	+0.45 -0.34	$\pm 2.1/\pm 0.5/\pm 2.1$	4461.2(8)	-5.4	58.5	1515.9(6)
125.09	4274.8(8)	+0.45 -0.34	$\pm 2.1/\pm 0.5/\pm 2.1$	4457.8(8)	-5.4	58.5	1512.5(6)
125.1	4274.9(8)	+0.45 -0.34	$\pm 2.1/\pm 0.5/\pm 2.1$	4457.8(8)	-5.4	58.5	1512.2(6)
125.2	4271.5(8)	+0.45 -0.34	$\pm 2.1/\pm 0.5/\pm 2.1$	4454.3(8)	-5.4	58.5	1508.0(6)
125.3	4268.2(8)	+0.45 -0.34	$\pm 2.1/\pm 0.5/\pm 2.1$	4450.8(8)	-5.4	58.4	1504.3(6)
125.4	4264.9(8)	+0.45 -0.34	$\pm 2.1/\pm 0.5/\pm 2.1$	4447.3(8)	-5.4	58.4	1500.8(6)
125.5	4261.6(7)	+0.45 -0.34	$\pm 2.1/\pm 0.5/\pm 2.1$	4443.8(8)	-5.4	58.4	1497.0(6)
125.6	4258.2(7)	+0.45 -0.34	$\pm 2.1/\pm 0.5/\pm 2.1$	4440.4(8)	-5.4	58.4	1493.7(6)
125.7	4255.0(7)	+0.45 -0.34	$\pm 2.1/\pm 0.5/\pm 2.1$	4436.9(8)	-5.4	58.3	1489.5(6)
125.8	4251.6(7)	+0.45 -0.34	$\pm 2.1/\pm 0.5/\pm 2.1$	4433.4(8)	-5.4	58.3	1485.8(6)
125.9	4248.5(7)	+0.45 -0.34	$\pm 2.1/\pm 0.5/\pm 2.1$	4430.0(8)	-5.4	58.3	1481.7(5)
126.0	4245.1(7)	+0.45 -0.34	$\pm 2.1/\pm 0.5/\pm 2.1$	4426.5(8)	-5.4	58.3	1478.5(6)
126.5	4228.8(7)	+0.45 -0.33	$\pm 2.1/\pm 0.5/\pm 2.1$	4409.3(8)	-5.4	58.1	1459.8(6)
127.0	4212.6(7)	+0.45 -0.33	$\pm 2.1/\pm 0.5/\pm 2.1$	4392.2(8)	-5.4	58.0	1441.8(6)
127.5	4196.4(7)	+0.45 -0.33	$\pm 2.1/\pm 0.5/\pm 2.1$	4375.2(8)	-5.4	57.9	1424.0(6)
128.0	4180.4(7)	+0.44 -0.33	$\pm 2.1/\pm 0.5/\pm 2.1$	4358.2(8)	-5.4	57.8	1406.6(5)
128.5	4164.4(7)	+0.44 -0.33	$\pm 2.1/\pm 0.5/\pm 2.1$	4341.3(8)	-5.4	57.6	1389.1(6)
129.0	4148.4(7)	+0.44 -0.33	$\pm 2.1/\pm 0.5/\pm 2.1$	4324.6(8)	-5.4	57.5	1371.7(6)
129.5	4132.5(7)	+0.44 -0.33	$\pm 2.1/\pm 0.5/\pm 2.1$	4307.9(8)	-5.4	57.4	1355.1(5)
130.0	4116.8(7)	+0.44 -0.33	$\pm 2.1/\pm 0.5/\pm 2.1$	4291.3(8)	-5.4	57.3	1338.8(6)

Table A.5: Fiducial VBF cross sections in the SM for a LHC CM energy of $\sqrt{s} = 7$ TeV, including QCD and EW corrections and their uncertainties for different Higgs-boson masses M_H . For more details see Section 1.3. The numbers in the $\sigma_{\text{NNLOQCD}}^{\text{DIS}}$ column have been obtained from a linear interpolation. The interpolation was performed by fitting the cross section for $M_H = \{120.0, 122.5, 125.0, 127.5, 130.0\}$ GeV to a linear function. The scale uncertainty in the column Δ_{scale} was only computed for $M_H = 125.0$ GeV.

$M_H[\text{GeV}]$	$\sigma^{\text{VBF}}[\text{fb}]$	$\Delta_{\text{scale}}[\%]$	$\Delta_{\text{PDF}/\alpha_s/\text{PDF} \oplus \alpha_s}[\%]$	$\sigma_{\text{NNLOQCD}}^{\text{DIS}}[\text{fb}]$	$\delta_{\text{EW}}[\%]$	$\sigma_\gamma[\text{fb}]$	$\sigma_{s\text{-chan}}[\text{fb}]$
120.0	625.8(9)	$^{+1.3}_{-1.6}$	$\pm 2.3 / \pm 0.3 / \pm 2.3$	655.7(10)	-6.1	10.1	9.3
120.5	623.5(8)	$^{+1.3}_{-1.6}$	$\pm 2.3 / \pm 0.3 / \pm 2.3$	653.2(9)	-6.1	10.1	9.2
121.0	621.2(8)	$^{+1.3}_{-1.6}$	$\pm 2.3 / \pm 0.3 / \pm 2.3$	650.7(8)	-6.1	10.1	9.1
121.5	618.8(7)	$^{+1.3}_{-1.6}$	$\pm 2.3 / \pm 0.3 / \pm 2.3$	648.2(8)	-6.1	10.1	9.0
122.0	616.4(7)	$^{+1.3}_{-1.6}$	$\pm 2.3 / \pm 0.3 / \pm 2.3$	645.7(7)	-6.1	10.0	8.8
122.5	614.1(6)	$^{+1.3}_{-1.6}$	$\pm 2.3 / \pm 0.3 / \pm 2.3$	643.2(6)	-6.1	10.0	8.7
123.0	611.7(6)	$^{+1.3}_{-1.6}$	$\pm 2.3 / \pm 0.3 / \pm 2.3$	640.7(6)	-6.1	10.0	8.6
123.5	609.4(5)	$^{+1.3}_{-1.6}$	$\pm 2.3 / \pm 0.3 / \pm 2.3$	638.3(6)	-6.1	10.0	8.5
124.0	607.1(5)	$^{+1.3}_{-1.6}$	$\pm 2.3 / \pm 0.3 / \pm 2.3$	635.8(5)	-6.1	9.9	8.4
124.1	606.6(5)	$^{+1.3}_{-1.6}$	$\pm 2.3 / \pm 0.3 / \pm 2.3$	635.3(5)	-6.1	9.9	8.4
124.2	606.2(5)	$^{+1.3}_{-1.6}$	$\pm 2.3 / \pm 0.3 / \pm 2.3$	634.8(5)	-6.1	9.9	8.4
124.3	605.7(5)	$^{+1.3}_{-1.6}$	$\pm 2.3 / \pm 0.3 / \pm 2.3$	634.3(5)	-6.1	9.9	8.4
124.4	605.2(5)	$^{+1.3}_{-1.6}$	$\pm 2.3 / \pm 0.3 / \pm 2.3$	633.8(5)	-6.1	9.9	8.3
124.5	604.8(5)	$^{+1.3}_{-1.6}$	$\pm 2.3 / \pm 0.3 / \pm 2.3$	633.3(5)	-6.1	9.9	8.3
124.6	604.3(5)	$^{+1.3}_{-1.6}$	$\pm 2.3 / \pm 0.3 / \pm 2.3$	632.8(5)	-6.1	9.9	8.3
124.7	603.8(5)	$^{+1.3}_{-1.6}$	$\pm 2.3 / \pm 0.3 / \pm 2.3$	632.3(5)	-6.1	9.9	8.3
124.8	603.4(5)	$^{+1.3}_{-1.6}$	$\pm 2.3 / \pm 0.3 / \pm 2.3$	631.8(5)	-6.1	9.9	8.2
124.9	602.9(5)	$^{+1.3}_{-1.6}$	$\pm 2.3 / \pm 0.3 / \pm 2.3$	631.3(5)	-6.1	9.9	8.2
125.0	602.4(5)	$^{+1.3}_{-1.6}$	$\pm 2.3 / \pm 0.3 / \pm 2.3$	630.8(5)	-6.1	9.9	8.2
125.09	602.0(5)	$^{+1.3}_{-1.6}$	$\pm 2.3 / \pm 0.3 / \pm 2.3$	630.3(5)	-6.1	9.9	8.2
125.1	602.0(5)	$^{+1.3}_{-1.6}$	$\pm 2.3 / \pm 0.3 / \pm 2.3$	630.3(5)	-6.1	9.9	8.2
125.2	601.5(5)	$^{+1.3}_{-1.6}$	$\pm 2.3 / \pm 0.3 / \pm 2.3$	629.8(5)	-6.1	9.9	8.2
125.3	601.1(5)	$^{+1.3}_{-1.6}$	$\pm 2.3 / \pm 0.3 / \pm 2.3$	629.3(5)	-6.1	9.9	8.2
125.4	600.5(5)	$^{+1.3}_{-1.6}$	$\pm 2.3 / \pm 0.3 / \pm 2.3$	628.8(5)	-6.1	9.9	8.1
125.5	600.1(5)	$^{+1.3}_{-1.6}$	$\pm 2.3 / \pm 0.3 / \pm 2.3$	628.3(5)	-6.1	9.9	8.1
125.6	599.7(5)	$^{+1.3}_{-1.6}$	$\pm 2.3 / \pm 0.3 / \pm 2.3$	627.8(5)	-6.1	9.9	8.1
125.7	599.2(5)	$^{+1.3}_{-1.6}$	$\pm 2.3 / \pm 0.3 / \pm 2.3$	627.3(5)	-6.1	9.9	8.1
125.8	598.7(5)	$^{+1.3}_{-1.6}$	$\pm 2.3 / \pm 0.3 / \pm 2.3$	626.8(5)	-6.1	9.9	8.1
125.9	598.2(5)	$^{+1.3}_{-1.6}$	$\pm 2.3 / \pm 0.3 / \pm 2.3$	626.3(5)	-6.1	9.9	8.0
126.0	597.8(5)	$^{+1.3}_{-1.6}$	$\pm 2.3 / \pm 0.3 / \pm 2.3$	625.8(5)	-6.1	9.9	8.0
126.5	595.4(5)	$^{+1.3}_{-1.6}$	$\pm 2.3 / \pm 0.3 / \pm 2.3$	623.3(6)	-6.1	9.8	7.9
127.0	593.1(6)	$^{+1.3}_{-1.6}$	$\pm 2.3 / \pm 0.3 / \pm 2.3$	620.8(6)	-6.0	9.8	7.8
127.5	590.8(6)	$^{+1.3}_{-1.6}$	$\pm 2.3 / \pm 0.3 / \pm 2.3$	618.4(6)	-6.0	9.8	7.7
128.0	588.5(7)	$^{+1.3}_{-1.6}$	$\pm 2.3 / \pm 0.3 / \pm 2.3$	615.9(7)	-6.0	9.8	7.6
128.5	586.1(7)	$^{+1.3}_{-1.6}$	$\pm 2.3 / \pm 0.3 / \pm 2.3$	613.4(8)	-6.0	9.7	7.5
129.0	583.8(8)	$^{+1.3}_{-1.6}$	$\pm 2.3 / \pm 0.3 / \pm 2.3$	610.9(8)	-6.0	9.7	7.5
129.5	581.5(8)	$^{+1.3}_{-1.6}$	$\pm 2.3 / \pm 0.3 / \pm 2.3$	608.4(9)	-6.0	9.7	7.4
130.0	579.1(9)	$^{+1.3}_{-1.6}$	$\pm 2.3 / \pm 0.3 / \pm 2.3$	605.9(10)	-6.0	9.7	7.3

Table A.6: Fiducial VBF cross sections in the SM for a LHC CM energy of $\sqrt{s} = 8$ TeV, including QCD and EW corrections and their uncertainties for different Higgs-boson masses M_H . For more details see Section 1.3. The numbers in the $\sigma_{\text{NNLOQCD}}^{\text{DIS}}$ column have been obtained from a linear interpolation. The interpolation was performed by fitting the cross section for $M_H = \{120.0, 122.5, 125.0, 127.5, 130.0\}$ GeV to a linear function. The scale uncertainty in the column Δ_{scale} was only computed for $M_H = 125.0$ GeV.

M_H [GeV]	σ^{VBF} [fb]	$\Delta_{\text{scale}}[\%]$	$\Delta_{\text{PDF}/\alpha_s/\text{PDF}\oplus\alpha_s}[\%]$	$\sigma_{\text{NNLOQCD}}^{\text{DIS}}$ [fb]	$\delta_{\text{EW}}[\%]$	σ_γ [fb]	$\sigma_{s\text{-chan}}$ [fb]
120.0	824.9(11)	$^{+1.3}_{-1.5}$	$\pm 2.3/\pm 0.3/\pm 2.3$	865.7(12)	-6.3	13.4	12.4
120.5	821.9(11)	$^{+1.3}_{-1.5}$	$\pm 2.3/\pm 0.3/\pm 2.3$	862.6(11)	-6.3	13.3	12.3
121.0	819.1(10)	$^{+1.3}_{-1.5}$	$\pm 2.3/\pm 0.3/\pm 2.3$	859.5(11)	-6.3	13.3	12.2
121.5	816.2(9)	$^{+1.3}_{-1.5}$	$\pm 2.3/\pm 0.3/\pm 2.3$	856.4(10)	-6.2	13.3	12.0
122.0	813.3(8)	$^{+1.3}_{-1.5}$	$\pm 2.3/\pm 0.3/\pm 2.3$	853.3(9)	-6.2	13.2	11.9
122.5	810.4(8)	$^{+1.3}_{-1.5}$	$\pm 2.3/\pm 0.3/\pm 2.3$	850.2(8)	-6.2	13.2	11.7
123.0	807.5(7)	$^{+1.3}_{-1.5}$	$\pm 2.3/\pm 0.3/\pm 2.3$	847.1(8)	-6.2	13.2	11.6
123.5	804.7(7)	$^{+1.3}_{-1.5}$	$\pm 2.3/\pm 0.3/\pm 2.3$	844.1(7)	-6.2	13.1	11.4
124.0	801.6(6)	$^{+1.3}_{-1.5}$	$\pm 2.3/\pm 0.3/\pm 2.3$	841.0(7)	-6.2	13.1	11.3
124.1	801.1(6)	$^{+1.3}_{-1.5}$	$\pm 2.3/\pm 0.3/\pm 2.3$	840.3(7)	-6.2	13.1	11.3
124.2	800.6(6)	$^{+1.3}_{-1.5}$	$\pm 2.3/\pm 0.3/\pm 2.3$	839.7(7)	-6.2	13.1	11.2
124.3	799.9(6)	$^{+1.3}_{-1.5}$	$\pm 2.3/\pm 0.3/\pm 2.3$	839.1(7)	-6.2	13.1	11.2
124.4	799.4(6)	$^{+1.3}_{-1.5}$	$\pm 2.3/\pm 0.3/\pm 2.3$	838.5(7)	-6.2	13.1	11.2
124.5	798.9(6)	$^{+1.3}_{-1.5}$	$\pm 2.3/\pm 0.3/\pm 2.3$	837.9(7)	-6.2	13.1	11.2
124.6	798.2(6)	$^{+1.3}_{-1.5}$	$\pm 2.3/\pm 0.3/\pm 2.3$	837.2(7)	-6.2	13.1	11.1
124.7	797.6(6)	$^{+1.3}_{-1.5}$	$\pm 2.3/\pm 0.3/\pm 2.3$	836.6(7)	-6.2	13.1	11.1
124.8	797.1(6)	$^{+1.3}_{-1.5}$	$\pm 2.3/\pm 0.3/\pm 2.3$	836.0(7)	-6.2	13.1	11.1
124.9	796.6(6)	$^{+1.3}_{-1.5}$	$\pm 2.3/\pm 0.3/\pm 2.3$	835.4(7)	-6.2	13.1	11.1
125.0	795.9(6)	$^{+1.3}_{-1.5}$	$\pm 2.3/\pm 0.3/\pm 2.3$	834.8(7)	-6.2	13.1	11.1
125.09	795.4(6)	$^{+1.3}_{-1.5}$	$\pm 2.3/\pm 0.3/\pm 2.3$	834.1(7)	-6.2	13.1	11.0
125.1	795.3(6)	$^{+1.3}_{-1.5}$	$\pm 2.3/\pm 0.3/\pm 2.3$	834.1(7)	-6.2	13.1	11.0
125.2	794.8(6)	$^{+1.3}_{-1.5}$	$\pm 2.3/\pm 0.3/\pm 2.3$	833.5(7)	-6.2	13.0	11.0
125.3	794.3(6)	$^{+1.3}_{-1.5}$	$\pm 2.3/\pm 0.3/\pm 2.3$	832.9(7)	-6.2	13.0	11.0
125.4	793.6(6)	$^{+1.3}_{-1.5}$	$\pm 2.3/\pm 0.3/\pm 2.3$	832.3(7)	-6.2	13.0	10.9
125.5	793.0(6)	$^{+1.3}_{-1.5}$	$\pm 2.3/\pm 0.3/\pm 2.3$	831.7(7)	-6.2	13.0	10.9
125.6	792.4(6)	$^{+1.3}_{-1.5}$	$\pm 2.3/\pm 0.3/\pm 2.3$	831.1(7)	-6.2	13.0	10.9
125.7	791.8(6)	$^{+1.3}_{-1.5}$	$\pm 2.3/\pm 0.3/\pm 2.3$	830.4(7)	-6.2	13.0	10.8
125.8	791.2(6)	$^{+1.3}_{-1.5}$	$\pm 2.3/\pm 0.3/\pm 2.3$	829.8(7)	-6.2	13.0	10.8
125.9	790.7(6)	$^{+1.3}_{-1.5}$	$\pm 2.3/\pm 0.3/\pm 2.3$	829.2(7)	-6.2	13.0	10.8
126.0	790.1(6)	$^{+1.3}_{-1.5}$	$\pm 2.3/\pm 0.3/\pm 2.3$	828.6(7)	-6.2	13.0	10.8
126.5	787.1(7)	$^{+1.3}_{-1.5}$	$\pm 2.3/\pm 0.3/\pm 2.3$	825.5(7)	-6.2	13.0	10.7
127.0	784.3(7)	$^{+1.3}_{-1.5}$	$\pm 2.3/\pm 0.3/\pm 2.3$	822.4(8)	-6.2	12.9	10.5
127.5	781.5(8)	$^{+1.3}_{-1.5}$	$\pm 2.3/\pm 0.3/\pm 2.3$	819.3(8)	-6.2	12.9	10.4
128.0	778.5(8)	$^{+1.3}_{-1.5}$	$\pm 2.3/\pm 0.3/\pm 2.3$	816.2(9)	-6.2	12.9	10.3
128.5	775.7(9)	$^{+1.3}_{-1.5}$	$\pm 2.3/\pm 0.3/\pm 2.3$	813.1(10)	-6.2	12.8	10.2
129.0	772.8(10)	$^{+1.3}_{-1.5}$	$\pm 2.3/\pm 0.3/\pm 2.3$	810.0(11)	-6.2	12.8	10.0
129.5	769.8(11)	$^{+1.3}_{-1.5}$	$\pm 2.3/\pm 0.3/\pm 2.3$	806.9(11)	-6.2	12.8	9.9
130.0	766.9(11)	$^{+1.3}_{-1.5}$	$\pm 2.3/\pm 0.3/\pm 2.3$	803.8(12)	-6.2	12.8	9.8

Table A.7: Fiducial VBF cross sections in the SM for a LHC CM energy of $\sqrt{s} = 13$ TeV, including QCD and EW corrections and their uncertainties for different Higgs-boson masses M_H . For more details see Section 1.3. The numbers in the $\sigma_{\text{NNLOQCD}}^{\text{DIS}}$ column have been obtained from a linear interpolation. The interpolation was performed by fitting the cross section for $M_H = \{120.0, 122.5, 125.0, 127.5, 130.0\}$ GeV to a linear function. The scale uncertainty in the column Δ_{scale} was only computed for $M_H = 125.0$ GeV.

M_H [GeV]	σ^{VBF} [fb]	$\Delta_{\text{scale}}\%$	$\Delta_{\text{PDF}/\alpha_s/\text{PDF}+\alpha_s}\%$	$\sigma_{\text{NNLOQCD}}^{\text{DIS}}$ [fb]	$\delta_{\text{EW}}\%$	σ_γ [fb]	$\sigma_{s\text{-chan}}$ [fb]
120.0	2038.9(45)	$^{+1.3}_{-1.2}$	$\pm 2.1/\pm 0.4/\pm 2.2$	2152.8(48)	-6.8	33.0	32.4
120.5	2032.3(41)	$^{+1.3}_{-1.2}$	$\pm 2.1/\pm 0.4/\pm 2.2$	2145.9(44)	-6.8	32.9	32.1
121.0	2026.3(36)	$^{+1.3}_{-1.2}$	$\pm 2.1/\pm 0.4/\pm 2.2$	2139.1(39)	-6.8	32.8	31.7
121.5	2020.0(32)	$^{+1.3}_{-1.2}$	$\pm 2.1/\pm 0.4/\pm 2.2$	2132.2(35)	-6.8	32.8	31.3
122.0	2013.4(28)	$^{+1.3}_{-1.2}$	$\pm 2.1/\pm 0.4/\pm 2.2$	2125.4(30)	-6.8	32.7	30.9
122.5	2007.1(24)	$^{+1.3}_{-1.2}$	$\pm 2.1/\pm 0.4/\pm 2.2$	2118.5(26)	-6.8	32.6	30.6
123.0	2000.5(20)	$^{+1.3}_{-1.2}$	$\pm 2.1/\pm 0.4/\pm 2.2$	2111.7(21)	-6.8	32.6	30.2
123.5	1994.5(16)	$^{+1.3}_{-1.2}$	$\pm 2.1/\pm 0.4/\pm 2.2$	2104.8(17)	-6.8	32.5	29.9
124.0	1987.9(13)	$^{+1.3}_{-1.2}$	$\pm 2.1/\pm 0.4/\pm 2.2$	2097.9(14)	-6.8	32.4	29.6
124.1	1986.9(12)	$^{+1.3}_{-1.2}$	$\pm 2.1/\pm 0.4/\pm 2.2$	2096.6(13)	-6.8	32.4	29.5
124.2	1985.3(12)	$^{+1.3}_{-1.2}$	$\pm 2.1/\pm 0.4/\pm 2.2$	2095.2(12)	-6.8	32.4	29.5
124.3	1984.2(11)	$^{+1.3}_{-1.2}$	$\pm 2.1/\pm 0.4/\pm 2.2$	2093.8(12)	-6.8	32.4	29.4
124.4	1982.7(11)	$^{+1.3}_{-1.2}$	$\pm 2.1/\pm 0.4/\pm 2.2$	2092.5(11)	-6.8	32.4	29.3
124.5	1981.4(10)	$^{+1.3}_{-1.2}$	$\pm 2.1/\pm 0.4/\pm 2.2$	2091.1(11)	-6.8	32.4	29.2
124.6	1980.4(10)	$^{+1.3}_{-1.2}$	$\pm 2.1/\pm 0.4/\pm 2.2$	2089.7(11)	-6.8	32.4	29.2
124.7	1979.2(10)	$^{+1.3}_{-1.2}$	$\pm 2.1/\pm 0.4/\pm 2.2$	2088.4(10)	-6.8	32.4	29.1
124.8	1977.6(9)	$^{+1.3}_{-1.2}$	$\pm 2.1/\pm 0.4/\pm 2.2$	2087.0(10)	-6.8	32.3	29.0
124.9	1976.4(9)	$^{+1.3}_{-1.2}$	$\pm 2.1/\pm 0.4/\pm 2.2$	2085.6(10)	-6.8	32.3	29.0
125.0	1975.4(9)	$^{+1.3}_{-1.2}$	$\pm 2.1/\pm 0.4/\pm 2.2$	2084.2(10)	-6.8	32.3	29.0
125.09	1974.0(9)	$^{+1.3}_{-1.2}$	$\pm 2.1/\pm 0.4/\pm 2.2$	2082.9(10)	-6.8	32.3	28.9
125.1	1974.1(9)	$^{+1.3}_{-1.2}$	$\pm 2.1/\pm 0.4/\pm 2.2$	2082.9(10)	-6.8	32.3	28.9
125.2	1972.8(9)	$^{+1.3}_{-1.2}$	$\pm 2.1/\pm 0.4/\pm 2.2$	2081.5(10)	-6.8	32.3	28.8
125.3	1971.4(10)	$^{+1.3}_{-1.2}$	$\pm 2.1/\pm 0.4/\pm 2.2$	2080.1(10)	-6.8	32.3	28.7
125.4	1970.1(10)	$^{+1.3}_{-1.2}$	$\pm 2.1/\pm 0.4/\pm 2.2$	2078.8(11)	-6.8	32.3	28.7
125.5	1968.8(10)	$^{+1.3}_{-1.2}$	$\pm 2.1/\pm 0.4/\pm 2.2$	2077.4(11)	-6.8	32.2	28.6
125.6	1967.6(11)	$^{+1.3}_{-1.2}$	$\pm 2.1/\pm 0.4/\pm 2.2$	2076.0(11)	-6.8	32.2	28.5
125.7	1966.2(11)	$^{+1.3}_{-1.2}$	$\pm 2.1/\pm 0.4/\pm 2.2$	2074.6(12)	-6.8	32.2	28.5
125.8	1965.1(12)	$^{+1.3}_{-1.2}$	$\pm 2.1/\pm 0.4/\pm 2.2$	2073.3(12)	-6.8	32.2	28.4
125.9	1963.6(12)	$^{+1.3}_{-1.2}$	$\pm 2.1/\pm 0.4/\pm 2.2$	2071.9(13)	-6.8	32.2	28.4
126.0	1962.6(13)	$^{+1.3}_{-1.2}$	$\pm 2.1/\pm 0.4/\pm 2.2$	2070.5(14)	-6.8	32.2	28.3
126.5	1956.2(16)	$^{+1.3}_{-1.2}$	$\pm 2.1/\pm 0.4/\pm 2.2$	2063.7(17)	-6.8	32.1	27.9
127.0	1949.7(20)	$^{+1.3}_{-1.2}$	$\pm 2.1/\pm 0.4/\pm 2.2$	2056.8(21)	-6.8	32.1	27.6
127.5	1943.5(24)	$^{+1.3}_{-1.2}$	$\pm 2.1/\pm 0.4/\pm 2.2$	2050.0(26)	-6.8	32.0	27.4
128.0	1937.2(28)	$^{+1.3}_{-1.2}$	$\pm 2.1/\pm 0.4/\pm 2.2$	2043.1(30)	-6.7	31.9	27.1
128.5	1930.7(32)	$^{+1.3}_{-1.2}$	$\pm 2.1/\pm 0.4/\pm 2.2$	2036.3(35)	-6.7	31.9	26.8
129.0	1924.4(36)	$^{+1.3}_{-1.2}$	$\pm 2.1/\pm 0.4/\pm 2.2$	2029.4(39)	-6.7	31.8	26.5
129.5	1917.7(41)	$^{+1.3}_{-1.2}$	$\pm 2.1/\pm 0.4/\pm 2.2$	2022.6(44)	-6.8	31.7	26.2
130.0	1911.5(45)	$^{+1.3}_{-1.2}$	$\pm 2.1/\pm 0.4/\pm 2.2$	2015.7(48)	-6.7	31.7	25.9

Table A.8: Fiducial VBF cross sections in the SM for a LHC CM energy of $\sqrt{s} = 14$ TeV, including QCD and EW corrections and their uncertainties for different Higgs-boson masses M_H . For more details see Section 1.3. The numbers in the $\sigma_{\text{NNLOQCD}}^{\text{DIS}}$ column have been obtained from a linear interpolation. The interpolation was performed by fitting the cross section for $M_H = \{120.0, 122.5, 125.0, 127.5, 130.0\}$ GeV to a linear function. The scale uncertainty in the column Δ_{scale} was only computed for $M_H = 125.0$ GeV.

M_H [GeV]	σ^{VBF} [fb]	$\Delta_{\text{scale}}[\%]$	$\Delta_{\text{PDF}/\alpha_s/\text{PDF} \oplus \alpha_s}[\%]$	$\sigma_{\text{NNLOQCD}}^{\text{DIS}}$ [fb]	$\delta_{\text{EW}}[\%]$	σ_γ [fb]	$\sigma_{s\text{-chan}}$ [fb]
120.0	2301.6(48)	$^{+1.5}_{-1.3}$	$\pm 2.1 / \pm 0.4 / \pm 2.1$	2432.4(51)	-6.9	37.4	37.0
120.5	2294.9(45)	$^{+1.5}_{-1.3}$	$\pm 2.1 / \pm 0.4 / \pm 2.1$	2425.4(48)	-6.9	37.3	36.6
121.0	2288.6(41)	$^{+1.5}_{-1.3}$	$\pm 2.1 / \pm 0.4 / \pm 2.1$	2418.3(44)	-6.9	37.2	36.2
121.5	2282.0(38)	$^{+1.5}_{-1.3}$	$\pm 2.1 / \pm 0.4 / \pm 2.1$	2411.3(41)	-6.9	37.1	35.8
122.0	2275.5(35)	$^{+1.5}_{-1.3}$	$\pm 2.1 / \pm 0.4 / \pm 2.1$	2404.3(38)	-6.9	37.1	35.4
122.5	2269.1(33)	$^{+1.5}_{-1.3}$	$\pm 2.1 / \pm 0.4 / \pm 2.1$	2397.3(35)	-6.9	37.0	35.0
123.0	2262.8(31)	$^{+1.5}_{-1.3}$	$\pm 2.1 / \pm 0.4 / \pm 2.1$	2390.3(33)	-6.9	36.9	34.6
123.5	2256.0(29)	$^{+1.5}_{-1.3}$	$\pm 2.1 / \pm 0.4 / \pm 2.1$	2383.2(31)	-6.9	36.9	34.2
124.0	2249.8(27)	$^{+1.5}_{-1.3}$	$\pm 2.1 / \pm 0.4 / \pm 2.1$	2376.2(29)	-6.9	36.8	33.8
124.1	2248.5(27)	$^{+1.5}_{-1.3}$	$\pm 2.1 / \pm 0.4 / \pm 2.1$	2374.8(29)	-6.9	36.8	33.7
124.2	2247.3(27)	$^{+1.5}_{-1.3}$	$\pm 2.1 / \pm 0.4 / \pm 2.1$	2373.4(29)	-6.9	36.8	33.7
124.3	2245.9(27)	$^{+1.5}_{-1.3}$	$\pm 2.1 / \pm 0.4 / \pm 2.1$	2372.0(29)	-6.9	36.7	33.6
124.4	2244.2(26)	$^{+1.5}_{-1.3}$	$\pm 2.1 / \pm 0.4 / \pm 2.1$	2370.6(28)	-6.9	36.7	33.5
124.5	2243.1(26)	$^{+1.5}_{-1.3}$	$\pm 2.1 / \pm 0.4 / \pm 2.1$	2369.2(28)	-6.9	36.7	33.4
124.6	2241.9(26)	$^{+1.5}_{-1.3}$	$\pm 2.1 / \pm 0.4 / \pm 2.1$	2367.8(28)	-6.9	36.7	33.4
124.7	2240.5(26)	$^{+1.5}_{-1.3}$	$\pm 2.1 / \pm 0.4 / \pm 2.1$	2366.4(28)	-6.9	36.7	33.3
124.8	2239.0(26)	$^{+1.5}_{-1.3}$	$\pm 2.1 / \pm 0.4 / \pm 2.1$	2365.0(28)	-6.9	36.7	33.2
124.9	2237.5(26)	$^{+1.5}_{-1.3}$	$\pm 2.1 / \pm 0.4 / \pm 2.1$	2363.6(28)	-6.9	36.7	33.1
125.0	2236.6(26)	$^{+1.5}_{-1.3}$	$\pm 2.1 / \pm 0.4 / \pm 2.1$	2362.2(28)	-6.9	36.7	33.1
125.09	2235.3(26)	$^{+1.5}_{-1.3}$	$\pm 2.1 / \pm 0.4 / \pm 2.1$	2360.8(28)	-6.9	36.6	33.0
125.1	2235.2(26)	$^{+1.5}_{-1.3}$	$\pm 2.1 / \pm 0.4 / \pm 2.1$	2360.8(28)	-6.9	36.6	33.0
125.2	2233.8(26)	$^{+1.5}_{-1.3}$	$\pm 2.1 / \pm 0.4 / \pm 2.1$	2359.4(28)	-6.9	36.6	32.9
125.3	2232.6(26)	$^{+1.5}_{-1.3}$	$\pm 2.1 / \pm 0.4 / \pm 2.1$	2358.0(28)	-6.9	36.6	32.9
125.4	2231.4(26)	$^{+1.5}_{-1.3}$	$\pm 2.1 / \pm 0.4 / \pm 2.1$	2356.6(28)	-6.9	36.6	32.8
125.5	2230.0(26)	$^{+1.5}_{-1.3}$	$\pm 2.1 / \pm 0.4 / \pm 2.1$	2355.2(28)	-6.9	36.6	32.7
125.6	2228.6(26)	$^{+1.5}_{-1.3}$	$\pm 2.1 / \pm 0.4 / \pm 2.1$	2353.8(28)	-6.9	36.6	32.6
125.7	2227.5(27)	$^{+1.5}_{-1.3}$	$\pm 2.1 / \pm 0.4 / \pm 2.1$	2352.4(29)	-6.9	36.6	32.6
125.8	2226.1(27)	$^{+1.5}_{-1.3}$	$\pm 2.1 / \pm 0.4 / \pm 2.1$	2351.0(29)	-6.9	36.5	32.5
125.9	2224.7(27)	$^{+1.5}_{-1.3}$	$\pm 2.1 / \pm 0.4 / \pm 2.1$	2349.6(29)	-6.9	36.5	32.4
126.0	2223.5(27)	$^{+1.5}_{-1.3}$	$\pm 2.1 / \pm 0.4 / \pm 2.1$	2348.2(29)	-6.9	36.5	32.3
126.5	2217.0(29)	$^{+1.5}_{-1.3}$	$\pm 2.1 / \pm 0.4 / \pm 2.1$	2341.1(31)	-6.9	36.4	32.0
127.0	2210.3(31)	$^{+1.5}_{-1.3}$	$\pm 2.1 / \pm 0.4 / \pm 2.1$	2334.1(33)	-6.9	36.4	31.6
127.5	2204.0(33)	$^{+1.5}_{-1.3}$	$\pm 2.1 / \pm 0.4 / \pm 2.1$	2327.1(35)	-6.9	36.3	31.3
128.0	2197.6(35)	$^{+1.5}_{-1.3}$	$\pm 2.1 / \pm 0.4 / \pm 2.1$	2320.1(38)	-6.8	36.2	30.9
128.5	2190.9(38)	$^{+1.5}_{-1.3}$	$\pm 2.1 / \pm 0.4 / \pm 2.1$	2313.1(41)	-6.8	36.2	30.6
129.0	2184.5(41)	$^{+1.5}_{-1.3}$	$\pm 2.1 / \pm 0.4 / \pm 2.1$	2306.0(44)	-6.8	36.1	30.3
129.5	2177.9(45)	$^{+1.5}_{-1.3}$	$\pm 2.1 / \pm 0.4 / \pm 2.1$	2299.0(48)	-6.8	36.0	29.9
130.0	2171.5(48)	$^{+1.5}_{-1.3}$	$\pm 2.1 / \pm 0.4 / \pm 2.1$	2292.0(51)	-6.8	35.9	29.6

Table A.9: Inclusive VBF cross sections for a LHC CM energy of $\sqrt{s} = 7$ TeV, at NNLO QCD, with an on shell Higgs or with off-shell effects included in the complex-pole scheme, together with their uncertainties. For more details see Section ??.

M_H [GeV]	σ_{OS}^{VBF} [fb]	$\sigma_{CPS}^{\text{VBF}}$ [fb]	δ_{CPS}	$\Delta_{\text{scale}}[\%]$	$\Delta_{\text{PDF}}[\%]$	$\Delta_{\alpha_s}[\%]$	$\Delta_{\text{PDF} \oplus \alpha_s}[\%]$
120.00	1339	1353	1.0	+0.2 -0.2	± 1.9	± 0.4	± 1.9
120.50	1332	1346	1.1	+0.2 -0.2	± 1.9	± 0.4	± 1.9
121.00	1326	1340	1.1	+0.2 -0.2	± 1.9	± 0.4	± 1.9
121.50	1320	1334	1.1	+0.2 -0.2	± 1.9	± 0.4	± 1.9
122.00	1313	1327	1.1	+0.2 -0.2	± 1.9	± 0.4	± 1.9
122.50	1307	1321	1.1	+0.2 -0.2	± 1.9	± 0.4	± 1.9
123.00	1301	1315	1.1	+0.2 -0.2	± 1.9	± 0.4	± 1.9
123.50	1295	1309	1.1	+0.2 -0.2	± 1.9	± 0.4	± 1.9
124.00	1288	1303	1.2	+0.2 -0.2	± 1.9	± 0.4	± 1.9
124.10	1287	1302	1.2	+0.2 -0.2	± 1.9	± 0.4	± 1.9
124.20	1286	1301	1.2	+0.2 -0.2	± 1.9	± 0.4	± 1.9
124.30	1285	1299	1.1	+0.2 -0.2	± 1.9	± 0.4	± 1.9
124.40	1283	1298	1.2	+0.2 -0.2	± 1.9	± 0.4	± 1.9
124.50	1282	1297	1.2	+0.2 -0.2	± 1.9	± 0.4	± 1.9
124.60	1281	1296	1.2	+0.2 -0.2	± 1.9	± 0.4	± 1.9
124.70	1280	1295	1.2	+0.2 -0.2	± 1.9	± 0.4	± 1.9
124.80	1279	1293	1.1	+0.2 -0.2	± 1.9	± 0.4	± 1.9
124.90	1277	1292	1.2	+0.2 -0.2	± 1.9	± 0.4	± 1.9
125.00	1276	1291	1.2	+0.2 -0.2	± 1.9	± 0.4	± 1.9
125.09	1275	1290	1.2	+0.2 -0.2	± 1.9	± 0.4	± 1.9
125.10	1275	1290	1.2	+0.2 -0.2	± 1.9	± 0.4	± 1.9
125.20	1274	1289	1.2	+0.2 -0.2	± 1.9	± 0.4	± 1.9
125.30	1272	1288	1.3	+0.2 -0.2	± 1.9	± 0.4	± 1.9
125.40	1271	1286	1.2	+0.2 -0.2	± 1.9	± 0.4	± 1.9
125.50	1270	1285	1.2	+0.2 -0.2	± 1.9	± 0.4	± 1.9
125.60	1269	1284	1.2	+0.2 -0.2	± 1.9	± 0.4	± 1.9
125.70	1268	1283	1.2	+0.2 -0.2	± 1.9	± 0.4	± 1.9
125.80	1266	1282	1.3	+0.2 -0.2	± 1.9	± 0.4	± 1.9
125.90	1265	1280	1.2	+0.2 -0.2	± 1.9	± 0.4	± 1.9
126.00	1264	1279	1.2	+0.2 -0.2	± 1.9	± 0.4	± 1.9
126.50	1258	1273	1.2	+0.2 -0.2	± 1.9	± 0.4	± 1.9
127.00	1252	1268	1.3	+0.2 -0.2	± 1.9	± 0.4	± 1.9
127.50	1247	1262	1.2	+0.2 -0.2	± 1.9	± 0.4	± 1.9
128.00	1240	1256	1.3	+0.2 -0.2	± 1.9	± 0.4	± 1.9
128.50	1235	1250	1.2	+0.2 -0.2	± 1.9	± 0.4	± 1.9
129.00	1229	1244	1.2	+0.2 -0.2	± 1.9	± 0.4	± 1.9
129.50	1223	1239	1.3	+0.2 -0.2	± 1.9	± 0.4	± 1.9
130.00	1217	1233	1.3	+0.2 -0.2	± 1.9	± 0.4	± 1.9

607 shown in Tables A.19–A.22 and Tables A.23–A.26. No interpolation of results has been performed.

Table A.10: Inclusive VBF cross sections for a LHC CM energy of $\sqrt{s} = 8$ TeV, at NNLO QCD, with an on shell Higgs or with off-shell effects included in the complex-pole scheme, together with their uncertainties. For more details see Section ??.

$M_H[\text{GeV}]$	$\sigma_{\text{OS}}^{\text{VBF}}[\text{fb}]$	$\sigma_{\text{CPS}}^{\text{VBF}}[\text{fb}]$	δ_{CPS}	$\Delta_{\text{scale}}[\%]$	$\Delta_{\text{PDF}}[\%]$	$\Delta_{\alpha_s}[\%]$	$\Delta_{\text{PDF} \oplus \alpha_s}[\%]$
120.00	1727	1748	1.2	$^{+0.3}_{-0.2}$	± 1.9	± 0.5	± 1.9
120.50	1719	1741	1.3	$^{+0.2}_{-0.2}$	± 1.9	± 0.5	± 1.9
121.00	1711	1733	1.3	$^{+0.3}_{-0.2}$	± 1.9	± 0.5	± 1.9
121.50	1704	1725	1.2	$^{+0.2}_{-0.2}$	± 1.9	± 0.5	± 1.9
122.00	1695	1717	1.3	$^{+0.3}_{-0.2}$	± 1.9	± 0.5	± 1.9
122.50	1688	1710	1.3	$^{+0.2}_{-0.2}$	± 1.9	± 0.5	± 1.9
123.00	1680	1702	1.3	$^{+0.3}_{-0.2}$	± 1.9	± 0.5	± 1.9
123.50	1673	1695	1.3	$^{+0.2}_{-0.2}$	± 1.9	± 0.5	± 1.9
124.00	1665	1687	1.3	$^{+0.3}_{-0.2}$	± 1.9	± 0.5	± 1.9
124.10	1663	1685	1.3	$^{+0.3}_{-0.2}$	± 1.9	± 0.5	± 1.9
124.20	1662	1684	1.3	$^{+0.3}_{-0.2}$	± 1.9	± 0.5	± 1.9
124.30	1660	1682	1.3	$^{+0.3}_{-0.2}$	± 1.9	± 0.5	± 1.9
124.40	1659	1681	1.3	$^{+0.3}_{-0.2}$	± 1.9	± 0.5	± 1.9
124.50	1657	1679	1.3	$^{+0.3}_{-0.2}$	± 1.9	± 0.5	± 1.9
124.60	1656	1678	1.3	$^{+0.3}_{-0.2}$	± 1.9	± 0.5	± 1.9
124.70	1654	1676	1.3	$^{+0.3}_{-0.2}$	± 1.9	± 0.5	± 1.9
124.80	1653	1675	1.3	$^{+0.3}_{-0.2}$	± 1.9	± 0.5	± 1.9
124.90	1651	1673	1.3	$^{+0.3}_{-0.2}$	± 1.9	± 0.5	± 1.9
125.00	1650	1672	1.3	$^{+0.3}_{-0.2}$	± 1.9	± 0.5	± 1.9
125.09	1648	1670	1.3	$^{+0.3}_{-0.2}$	± 1.9	± 0.5	± 1.9
125.10	1648	1670	1.3	$^{+0.3}_{-0.2}$	± 1.9	± 0.5	± 1.9
125.20	1647	1669	1.3	$^{+0.3}_{-0.2}$	± 1.9	± 0.5	± 1.9
125.30	1645	1667	1.3	$^{+0.3}_{-0.2}$	± 1.9	± 0.5	± 1.9
125.40	1644	1666	1.3	$^{+0.3}_{-0.2}$	± 1.9	± 0.5	± 1.9
125.50	1642	1664	1.3	$^{+0.3}_{-0.2}$	± 1.9	± 0.5	± 1.9
125.60	1641	1663	1.3	$^{+0.3}_{-0.2}$	± 1.9	± 0.5	± 1.9
125.70	1639	1661	1.3	$^{+0.3}_{-0.2}$	± 1.9	± 0.5	± 1.9
125.80	1638	1660	1.3	$^{+0.3}_{-0.2}$	± 1.9	± 0.5	± 1.9
125.90	1636	1659	1.4	$^{+0.3}_{-0.2}$	± 1.9	± 0.5	± 1.9
126.00	1635	1657	1.3	$^{+0.3}_{-0.2}$	± 1.9	± 0.5	± 1.9
126.50	1628	1650	1.4	$^{+0.2}_{-0.2}$	± 1.9	± 0.5	± 1.9
127.00	1620	1643	1.4	$^{+0.2}_{-0.2}$	± 1.9	± 0.4	± 1.9
127.50	1613	1635	1.4	$^{+0.2}_{-0.2}$	± 1.9	± 0.4	± 1.9
128.00	1605	1629	1.5	$^{+0.2}_{-0.2}$	± 1.9	± 0.4	± 1.9
128.50	1599	1621	1.4	$^{+0.2}_{-0.2}$	± 1.9	± 0.4	± 1.9
129.00	1591	1614	1.4	$^{+0.2}_{-0.2}$	± 1.9	± 0.4	± 1.9
129.50	1584	1607	1.5	$^{+0.2}_{-0.2}$	± 1.9	± 0.4	± 1.9
130.00	1577	1600	1.5	$^{+0.2}_{-0.2}$	± 1.9	± 0.4	± 1.9

Table A.11: Inclusive VBF cross sections for a LHC CM energy of $\sqrt{s} = 13$ TeV, at NNLO QCD, with an on shell Higgs or with off-shell effects included in the complex-pole scheme, together with their uncertainties. For more details see Section ??.

$M_H[\text{GeV}]$	$\sigma_{\text{OS}}^{\text{VBF}}[\text{fb}]$	$\sigma_{\text{CPS}}^{\text{VBF}}[\text{fb}]$	δ_{CPS}	$\Delta_{\text{scale}}[\%]$	$\Delta_{\text{PDF}}[\%]$	$\Delta_{\alpha_s}[\%]$	$\Delta_{\text{PDF} \oplus \alpha_s}[\%]$
120.00	4086	4162	1.9	+0.5 -0.2	±1.8	±0.6	±1.9
120.50	4072	4148	1.9	+0.4 -0.3	±1.8	±0.6	±1.9
121.00	4053	4130	1.9	+0.5 -0.2	±1.8	±0.6	±1.9
121.50	4039	4110	1.8	+0.4 -0.3	±1.8	±0.6	±1.9
122.00	4020	4098	1.9	+0.5 -0.2	±1.8	±0.6	±1.9
122.50	4007	4082	1.9	+0.4 -0.3	±1.8	±0.6	±1.9
123.00	3988	4068	2.0	+0.5 -0.2	±1.8	±0.6	±1.9
123.50	3975	4054	2.0	+0.4 -0.3	±1.8	±0.6	±1.9
124.00	3957	4041	2.1	+0.5 -0.2	±1.8	±0.6	±1.9
124.10	3953	4038	2.2	+0.5 -0.2	±1.8	±0.6	±1.9
124.20	3950	4034	2.1	+0.5 -0.2	±1.8	±0.6	±1.9
124.30	3947	4029	2.1	+0.5 -0.2	±1.8	±0.6	±1.9
124.40	3944	4026	2.1	+0.5 -0.2	±1.8	±0.6	±1.9
124.50	3941	4024	2.1	+0.5 -0.2	±1.8	±0.6	±1.9
124.60	3938	4021	2.1	+0.5 -0.2	±1.8	±0.6	±1.9
124.70	3935	4021	2.2	+0.5 -0.2	±1.8	±0.6	±1.9
124.80	3931	4017	2.2	+0.5 -0.2	±1.8	±0.6	±1.9
124.90	3928	4015	2.2	+0.5 -0.2	±1.8	±0.6	±1.9
125.00	3925	4013	2.2	+0.5 -0.2	±1.8	±0.6	±1.9
125.09	3922	4006	2.1	+0.5 -0.2	±1.8	±0.6	±1.9
125.10	3922	4005	2.1	+0.5 -0.2	±1.8	±0.6	±1.9
125.20	3919	4005	2.2	+0.5 -0.2	±1.8	±0.6	±1.9
125.30	3916	4000	2.1	+0.5 -0.2	±1.8	±0.6	±1.9
125.40	3913	4000	2.2	+0.5 -0.2	±1.8	±0.6	±1.9
125.50	3910	3997	2.2	+0.5 -0.2	±1.8	±0.6	±1.9
125.60	3906	3994	2.3	+0.5 -0.2	±1.8	±0.6	±1.9
125.70	3903	3991	2.3	+0.5 -0.2	±1.8	±0.6	±1.9
125.80	3900	3988	2.3	+0.5 -0.2	±1.8	±0.6	±1.9
125.90	3897	3985	2.3	+0.5 -0.2	±1.8	±0.6	±1.9
126.00	3894	3982	2.3	+0.5 -0.2	±1.8	±0.6	±1.9
126.50	3881	3968	2.2	+0.4 -0.3	±1.8	±0.6	±1.9
127.00	3863	3954	2.4	+0.5 -0.2	±1.8	±0.6	±1.9
127.50	3851	3939	2.3	+0.4 -0.3	±1.8	±0.6	±1.9
128.00	3833	3924	2.4	+0.5 -0.2	±1.8	±0.6	±1.9
128.50	3820	3911	2.4	+0.4 -0.3	±1.8	±0.6	±1.9
129.00	3803	3895	2.4	+0.5 -0.2	±1.8	±0.6	±1.9
129.50	3790	3882	2.4	+0.4 -0.3	±1.8	±0.6	±1.9
130.00	3773	3868	2.5	+0.4 -0.2	±1.8	±0.6	±1.9

Table A.12: Inclusive VBF cross sections for a LHC CM energy of $\sqrt{s} = 14$ TeV, at NNLO QCD, with an on shell Higgs or with off-shell effects included in the complex-pole scheme, together with their uncertainties. For more details see Section ??.

$M_H[\text{GeV}]$	$\sigma_{\text{OS}}^{\text{VBF}}[\text{fb}]$	$\sigma_{\text{CPS}}^{\text{VBF}}[\text{fb}]$	δ_{CPS}	$\Delta_{\text{scale}}[\%]$	$\Delta_{\text{PDF}}[\%]$	$\Delta_{\alpha_s}[\%]$	$\Delta_{\text{PDF} \oplus \alpha_s}[\%]$
120.00	4623	4718	2.1	+0.5 -0.2	±1.8	±0.6	±1.9
120.50	4608	4700	2.0	+0.4 -0.3	±1.8	±0.6	±1.9
121.00	4587	4687	2.2	+0.5 -0.2	±1.8	±0.6	±1.9
121.50	4572	4673	2.2	+0.4 -0.3	±1.8	±0.6	±1.9
122.00	4551	4651	2.2	+0.5 -0.2	±1.8	±0.6	±1.9
122.50	4536	4634	2.2	+0.4 -0.3	±1.8	±0.6	±1.9
123.00	4515	4605	2.0	+0.5 -0.2	±1.8	±0.6	±1.9
123.50	4501	4590	2.0	+0.4 -0.3	±1.8	±0.6	±1.9
124.00	4480	4577	2.2	+0.5 -0.2	±1.8	±0.6	±1.9
124.10	4476	4572	2.1	+0.5 -0.2	±1.8	±0.6	±1.9
124.20	4473	4569	2.1	+0.5 -0.2	±1.8	±0.6	±1.9
124.30	4469	4563	2.1	+0.5 -0.2	±1.8	±0.6	±1.9
124.40	4466	4562	2.1	+0.5 -0.2	±1.8	±0.6	±1.9
124.50	4462	4561	2.2	+0.5 -0.2	±1.8	±0.6	±1.9
124.60	4459	4559	2.2	+0.5 -0.2	±1.8	±0.6	±1.9
124.70	4455	4556	2.3	+0.5 -0.2	±1.8	±0.6	±1.9
124.80	4452	4552	2.2	+0.5 -0.2	±1.8	±0.6	±1.9
124.90	4448	4549	2.3	+0.5 -0.2	±1.8	±0.6	±1.9
125.00	4445	4547	2.3	+0.5 -0.2	±1.8	±0.6	±1.9
125.09	4442	4543	2.3	+0.5 -0.2	±1.8	±0.6	±1.9
125.10	4441	4542	2.3	+0.5 -0.2	±1.8	±0.6	±1.9
125.20	4438	4540	2.3	+0.5 -0.2	±1.8	±0.6	±1.9
125.30	4434	4538	2.3	+0.5 -0.2	±1.8	±0.6	±1.9
125.40	4431	4536	2.4	+0.5 -0.2	±1.8	±0.6	±1.9
125.50	4428	4533	2.4	+0.5 -0.2	±1.8	±0.6	±1.9
125.60	4424	4531	2.4	+0.5 -0.2	±1.8	±0.6	±1.9
125.70	4421	4528	2.4	+0.5 -0.2	±1.8	±0.6	±1.9
125.80	4417	4525	2.4	+0.5 -0.2	±1.8	±0.6	±1.9
125.90	4414	4522	2.4	+0.5 -0.2	±1.8	±0.6	±1.9
126.00	4410	4519	2.5	+0.5 -0.2	±1.8	±0.6	±1.9
126.50	4396	4505	2.5	+0.4 -0.3	±1.8	±0.6	±1.9
127.00	4376	4488	2.6	+0.5 -0.2	±1.8	±0.6	±1.9
127.50	4362	4472	2.5	+0.4 -0.3	±1.8	±0.6	±1.9
128.00	4342	4454	2.6	+0.5 -0.2	±1.8	±0.6	±1.9
128.50	4329	4438	2.5	+0.4 -0.3	±1.8	±0.6	±1.9
129.00	4309	4423	2.6	+0.5 -0.2	±1.8	±0.6	±1.9
129.50	4295	4407	2.6	+0.4 -0.3	±1.8	±0.6	±1.9
130.00	4276	4388	2.6	+0.5 -0.2	±1.8	±0.6	±1.9

Table A.13: Inclusive VBF cross sections for a Higgs boson mass of $M_H = 125$ GeV, at NNLO QCD, with an on shell Higgs or with off-shell effects included in the complex-pole scheme, together with their uncertainties. For more details see Section ??.

M_H [GeV]	σ_{OS}^{VBF} [fb]	$\sigma_{CPS}^{\text{VBF}}$ [fb]	δ_{CPS}	$\Delta_{\text{scale}}[\%]$	$\Delta_{\text{PDF}}[\%]$	$\Delta_{\alpha_s}[\%]$	$\Delta_{\text{PDF} \oplus \alpha_s}[\%]$
6.0	938	947	0.9	+0.2 -0.1	± 1.9	± 0.4	± 2.0
6.5	1102	1114	1.1	+0.2 -0.1	± 1.9	± 0.4	± 1.9
7.0	1276	1291	1.2	+0.2 -0.2	± 1.9	± 0.4	± 1.9
7.5	1459	1477	1.2	+0.2 -0.2	± 1.9	± 0.4	± 1.9
8.0	1650	1672	1.3	+0.3 -0.2	± 1.9	± 0.5	± 1.9
8.5	1848	1873	1.4	+0.3 -0.2	± 1.9	± 0.5	± 1.9
9.0	2054	2083	1.4	+0.3 -0.2	± 1.8	± 0.5	± 1.9
9.5	2267	2300	1.5	+0.3 -0.2	± 1.8	± 0.5	± 1.9
10.0	2487	2529	1.7	+0.4 -0.2	± 1.8	± 0.5	± 1.9
10.5	2713	2758	1.7	+0.4 -0.2	± 1.8	± 0.5	± 1.9
11.0	2944	2997	1.8	+0.4 -0.2	± 1.8	± 0.5	± 1.9
11.5	3182	3240	1.8	+0.4 -0.2	± 1.8	± 0.5	± 1.9
12.0	3424	3486	1.8	+0.4 -0.2	± 1.8	± 0.6	± 1.9
12.5	3672	3740	1.9	+0.4 -0.2	± 1.8	± 0.6	± 1.9
13.0	3925	4013	2.2	+0.5 -0.2	± 1.8	± 0.6	± 1.9
13.5	4183	4276	2.2	+0.5 -0.2	± 1.8	± 0.6	± 1.9
14.0	4445	4547	2.3	+0.5 -0.2	± 1.8	± 0.6	± 1.9
14.5	4711	4823	2.4	+0.5 -0.2	± 1.8	± 0.6	± 1.9
15.0	4982	5079	1.9	+0.5 -0.3	± 1.8	± 0.6	± 1.9

Table A.14: Inclusive VBF cross sections for a Higgs boson mass of $M_H = 125.09$ GeV, at NNLO QCD, with an on shell Higgs or with off-shell effects included in the complex-pole scheme, together with their uncertainties. For more details see Section ??.

M_H [GeV]	σ_{OS}^{VBF} [fb]	$\sigma_{CPS}^{\text{VBF}}$ [fb]	δ_{CPS}	$\Delta_{\text{scale}}[\%]$	$\Delta_{\text{PDF}}[\%]$	$\Delta_{\alpha_s}[\%]$	$\Delta_{\text{PDF} \oplus \alpha_s}[\%]$
6.0	937	946	0.9	+0.2 -0.1	± 1.9	± 0.4	± 2.0
6.5	1101	1113	1.1	+0.2 -0.1	± 1.9	± 0.4	± 1.9
7.0	1275	1290	1.2	+0.2 -0.2	± 1.9	± 0.4	± 1.9
7.5	1457	1476	1.3	+0.2 -0.2	± 1.9	± 0.4	± 1.9
8.0	1648	1670	1.3	+0.3 -0.2	± 1.9	± 0.5	± 1.9
8.5	1847	1872	1.4	+0.3 -0.2	± 1.9	± 0.5	± 1.9
9.0	2052	2081	1.4	+0.3 -0.2	± 1.8	± 0.5	± 1.9
9.5	2265	2299	1.5	+0.3 -0.2	± 1.8	± 0.5	± 1.9
10.0	2485	2527	1.7	+0.4 -0.2	± 1.8	± 0.5	± 1.9
10.5	2710	2759	1.8	+0.4 -0.2	± 1.8	± 0.5	± 1.9
11.0	2942	2992	1.7	+0.4 -0.2	± 1.8	± 0.5	± 1.9
11.5	3179	3232	1.7	+0.4 -0.2	± 1.8	± 0.5	± 1.9
12.0	3422	3480	1.7	+0.4 -0.2	± 1.8	± 0.6	± 1.9
12.5	3670	3740	1.9	+0.4 -0.2	± 1.8	± 0.6	± 1.9
13.0	3922	4006	2.1	+0.5 -0.2	± 1.8	± 0.6	± 1.9
13.5	4180	4267	2.1	+0.5 -0.2	± 1.8	± 0.6	± 1.9
14.0	4442	4543	2.3	+0.5 -0.2	± 1.8	± 0.6	± 1.9
14.5	4708	4813	2.2	+0.5 -0.2	± 1.8	± 0.6	± 1.9
15.0	4979	5093	2.3	+0.5 -0.3	± 1.8	± 0.6	± 1.9

Table A.15: Inclusive VBF cross sections for a LHC CM energy of $\sqrt{s} = 7$ TeV, at NNLO QCD, with an on shell Higgs, for the extended M_H scan, together with their uncertainties. For more details see Section ??.

M_H [GeV]	σ_{OS}^{VBF} [fb]	$\sigma_{CPS}^{\text{VBF}}$ [fb]	δ_{CPS}	$\Delta_{\text{scale}}[\%]$	$\Delta_{\text{PDF}}[\%]$	$\Delta_{\alpha_s}[\%]$	$\Delta_{\text{PDF} \oplus \alpha_s}[\%]$
10	$4.452 \cdot 10^3$	$\begin{array}{l} +0.9 \\ -0.5 \end{array}$	± 1.8	± 0.7	± 2.0		
15	$4.224 \cdot 10^3$	$\begin{array}{l} +0.8 \\ -0.4 \end{array}$	± 1.8	± 0.7	± 2.0		
20	$3.994 \cdot 10^3$	$\begin{array}{l} +0.8 \\ -0.4 \end{array}$	± 1.8	± 0.7	± 2.0		
25	$3.768 \cdot 10^3$	$\begin{array}{l} +0.7 \\ -0.4 \end{array}$	± 1.8	± 0.7	± 2.0		
30	$3.555 \cdot 10^3$	$\begin{array}{l} +0.6 \\ -0.4 \end{array}$	± 1.8	± 0.6	± 1.9		
35	$3.350 \cdot 10^3$	$\begin{array}{l} +0.6 \\ -0.3 \end{array}$	± 1.8	± 0.6	± 1.9		
40	$3.157 \cdot 10^3$	$\begin{array}{l} +0.6 \\ -0.3 \end{array}$	± 1.8	± 0.6	± 1.9		
45	$2.977 \cdot 10^3$	$\begin{array}{l} +0.6 \\ -0.3 \end{array}$	± 1.8	± 0.6	± 1.9		
50	$2.808 \cdot 10^3$	$\begin{array}{l} +0.5 \\ -0.3 \end{array}$	± 1.8	± 0.6	± 1.9		
55	$2.651 \cdot 10^3$	$\begin{array}{l} +0.5 \\ -0.3 \end{array}$	± 1.8	± 0.6	± 1.9		
60	$2.504 \cdot 10^3$	$\begin{array}{l} +0.5 \\ -0.3 \end{array}$	± 1.8	± 0.6	± 1.9		
65	$2.367 \cdot 10^3$	$\begin{array}{l} +0.4 \\ -0.2 \end{array}$	± 1.8	± 0.5	± 1.9		
70	$2.240 \cdot 10^3$	$\begin{array}{l} +0.4 \\ -0.2 \end{array}$	± 1.8	± 0.5	± 1.9		
75	$2.120 \cdot 10^3$	$\begin{array}{l} +0.4 \\ -0.2 \end{array}$	± 1.9	± 0.5	± 1.9		
80	$2.009 \cdot 10^3$	$\begin{array}{l} +0.4 \\ -0.2 \end{array}$	± 1.9	± 0.5	± 1.9		
85	$1.905 \cdot 10^3$	$\begin{array}{l} +0.3 \\ -0.2 \end{array}$	± 1.9	± 0.5	± 1.9		
90	$1.807 \cdot 10^3$	$\begin{array}{l} +0.3 \\ -0.2 \end{array}$	± 1.9	± 0.5	± 1.9		
95	$1.716 \cdot 10^3$	$\begin{array}{l} +0.3 \\ -0.2 \end{array}$	± 1.9	± 0.5	± 1.9		
100	$1.631 \cdot 10^3$	$\begin{array}{l} +0.3 \\ -0.2 \end{array}$	± 1.9	± 0.5	± 1.9		
105	$1.550 \cdot 10^3$	$\begin{array}{l} +0.3 \\ -0.2 \end{array}$	± 1.9	± 0.5	± 1.9		
110	$1.475 \cdot 10^3$	$\begin{array}{l} +0.2 \\ -0.2 \end{array}$	± 1.9	± 0.4	± 1.9		
115	$1.405 \cdot 10^3$	$\begin{array}{l} +0.2 \\ -0.2 \end{array}$	± 1.9	± 0.4	± 1.9		
120	$1.339 \cdot 10^3$	$\begin{array}{l} +0.2 \\ -0.2 \end{array}$	± 1.9	± 0.4	± 1.9		
125	$1.276 \cdot 10^3$	$\begin{array}{l} +0.2 \\ -0.2 \end{array}$	± 1.9	± 0.4	± 1.9		
130	$1.217 \cdot 10^3$	$\begin{array}{l} +0.2 \\ -0.2 \end{array}$	± 1.9	± 0.4	± 1.9		
135	$1.162 \cdot 10^3$	$\begin{array}{l} +0.2 \\ -0.1 \end{array}$	± 1.9	± 0.4	± 1.9		
140	$1.110 \cdot 10^3$	$\begin{array}{l} +0.2 \\ -0.1 \end{array}$	± 1.9	± 0.4	± 1.9		
145	$1.061 \cdot 10^3$	$\begin{array}{l} +0.2 \\ -0.1 \end{array}$	± 1.9	± 0.4	± 1.9		
150	$1.014 \cdot 10^3$	$\begin{array}{l} +0.2 \\ -0.1 \end{array}$	± 1.9	± 0.4	± 2.0		
160	$9.285 \cdot 10^2$	$\begin{array}{l} +0.2 \\ -0.1 \end{array}$	± 1.9	± 0.4	± 2.0		
170	$8.518 \cdot 10^2$	$\begin{array}{l} +0.2 \\ -0.1 \end{array}$	± 1.9	± 0.3	± 2.0		
180	$7.830 \cdot 10^2$	$\begin{array}{l} +0.2 \\ -0.1 \end{array}$	± 1.9	± 0.3	± 2.0		
190	$7.210 \cdot 10^2$	$\begin{array}{l} +0.2 \\ -0.1 \end{array}$	± 2.0	± 0.3	± 2.0		
200	$6.650 \cdot 10^2$	$\begin{array}{l} +0.2 \\ -0.1 \end{array}$	± 2.0	± 0.3	± 2.0		
210	$6.143 \cdot 10^2$	$\begin{array}{l} +0.2 \\ -0.1 \end{array}$	± 2.0	± 0.3	± 2.0		
220	$5.684 \cdot 10^2$	$\begin{array}{l} +0.3 \\ -0.1 \end{array}$	± 2.0	± 0.3	± 2.0		
230	$5.266 \cdot 10^2$	$\begin{array}{l} +0.3 \\ -0.1 \end{array}$	± 2.0	± 0.3	± 2.0		
240	$4.886 \cdot 10^2$	$\begin{array}{l} +0.3 \\ -0.1 \end{array}$	± 2.0	± 0.3	± 2.0		
250	$4.539 \cdot 10^2$	$\begin{array}{l} +0.3 \\ -0.2 \end{array}$	± 2.0	± 0.2	± 2.0		
260	$4.222 \cdot 10^2$	$\begin{array}{l} +0.3 \\ -0.2 \end{array}$	± 2.0	± 0.2	± 2.1		
270	$3.932 \cdot 10^2$	$\begin{array}{l} +0.3 \\ -0.2 \end{array}$	± 2.1	± 0.2	± 2.1		
280	$3.666 \cdot 10^2$	$\begin{array}{l} +0.3 \\ -0.2 \end{array}$	± 2.1	± 0.2	± 2.1		
290	$3.421 \cdot 10^2$	$\begin{array}{l} +0.3 \\ -0.2 \end{array}$	± 2.1	± 0.2	± 2.1		
300	$3.196 \cdot 10^2$	$\begin{array}{l} +0.3 \\ -0.3 \end{array}$	± 2.1	± 0.2	± 2.1		
310	$2.989 \cdot 10^2$	$\begin{array}{l} +0.3 \\ -0.3 \end{array}$	± 2.1	± 0.2	± 2.1		
320	$2.798 \cdot 10^2$	$\begin{array}{l} +0.3 \\ -0.3 \end{array}$	± 2.1	± 0.2	± 2.1		
330	$2.621 \cdot 10^2$	$\begin{array}{l} +0.3 \\ -0.3 \end{array}$	± 2.1	± 0.2	± 2.2		
340	$2.457 \cdot 10^2$	$\begin{array}{l} +0.3 \\ -0.4 \end{array}$	± 2.2	± 0.2	± 2.2		
350	$2.306 \cdot 10^2$	$\begin{array}{l} +0.3 \\ -0.4 \end{array}$	± 2.2	± 0.1	± 2.2		
360	$2.166 \cdot 10^2$	$\begin{array}{l} +0.3 \\ -0.4 \end{array}$	± 2.2	± 0.1	± 2.2		
370	$2.035 \cdot 10^2$	$\begin{array}{l} +0.3 \\ -0.4 \end{array}$	± 2.2	± 0.1	± 2.2		
380	$1.914 \cdot 10^2$	$\begin{array}{l} +0.3 \\ -0.4 \end{array}$	± 2.2	± 0.1	± 2.2		
390	$1.802 \cdot 10^2$	$\begin{array}{l} +0.3 \\ -0.5 \end{array}$	± 2.2	± 0.1	± 2.2		
400	$1.697 \cdot 10^2$	$\begin{array}{l} +0.3 \\ -0.5 \end{array}$	± 2.3	± 0.1	± 2.3		
410	$1.599 \cdot 10^2$	$\begin{array}{l} +0.3 \\ -0.5 \end{array}$	± 2.3	± 0.1	± 2.3		
420	$1.508 \cdot 10^2$	$\begin{array}{l} +0.3 \\ -0.5 \end{array}$	± 2.3	± 0.1	± 2.3		
430	$1.423 \cdot 10^2$	$\begin{array}{l} +0.3 \\ -0.5 \end{array}$	± 2.3	± 0.1	± 2.3		

Table A.16: Inclusive VBF cross sections for a LHC CM energy of $\sqrt{s} = 8$ TeV, at NNLO QCD, with an on shell Higgs, for the extended M_H scan, together with their uncertainties. For more details see Section ??.

M_H [GeV]	σ_{OS}^{VBF} [fb]	$\sigma_{CPS}^{\text{VBF}}$ [fb]	δ_{CPS}	$\Delta_{\text{scale}}[\%]$	$\Delta_{\text{PDF}}[\%]$	$\Delta_{\alpha_s}[\%]$	$\Delta_{\text{PDF} \oplus \alpha_s}[\%]$
10	$5.474 \cdot 10^3$	$+0.9$ -0.5	± 1.8	± 0.8	± 2.0		
15	$5.208 \cdot 10^3$	$+0.8$ -0.5	± 1.8	± 0.7	± 2.0		
20	$4.934 \cdot 10^3$	$+0.8$ -0.5	± 1.8	± 0.7	± 2.0		
25	$4.667 \cdot 10^3$	$+0.8$ -0.4	± 1.8	± 0.7	± 2.0		
30	$4.413 \cdot 10^3$	$+0.7$ -0.4	± 1.8	± 0.7	± 1.9		
35	$4.169 \cdot 10^3$	$+0.7$ -0.4	± 1.8	± 0.7	± 1.9		
40	$3.938 \cdot 10^3$	$+0.6$ -0.3	± 1.8	± 0.6	± 1.9		
45	$3.722 \cdot 10^3$	$+0.6$ -0.3	± 1.8	± 0.6	± 1.9		
50	$3.519 \cdot 10^3$	$+0.6$ -0.3	± 1.8	± 0.6	± 1.9		
55	$3.329 \cdot 10^3$	$+0.5$ -0.3	± 1.8	± 0.6	± 1.9		
60	$3.152 \cdot 10^3$	$+0.5$ -0.3	± 1.8	± 0.6	± 1.9		
65	$2.986 \cdot 10^3$	$+0.5$ -0.3	± 1.8	± 0.6	± 1.9		
70	$2.831 \cdot 10^3$	$+0.5$ -0.3	± 1.8	± 0.6	± 1.9		
75	$2.686 \cdot 10^3$	$+0.4$ -0.2	± 1.8	± 0.5	± 1.9		
80	$2.550 \cdot 10^3$	$+0.4$ -0.2	± 1.8	± 0.5	± 1.9		
85	$2.423 \cdot 10^3$	$+0.4$ -0.2	± 1.8	± 0.5	± 1.9		
90	$2.304 \cdot 10^3$	$+0.4$ -0.2	± 1.8	± 0.5	± 1.9		
95	$2.192 \cdot 10^3$	$+0.4$ -0.2	± 1.8	± 0.5	± 1.9		
100	$2.087 \cdot 10^3$	$+0.3$ -0.2	± 1.8	± 0.5	± 1.9		
105	$1.988 \cdot 10^3$	$+0.3$ -0.2	± 1.8	± 0.5	± 1.9		
110	$1.896 \cdot 10^3$	$+0.3$ -0.2	± 1.9	± 0.5	± 1.9		
115	$1.809 \cdot 10^3$	$+0.3$ -0.2	± 1.9	± 0.5	± 1.9		
120	$1.727 \cdot 10^3$	$+0.3$ -0.2	± 1.9	± 0.5	± 1.9		
125	$1.650 \cdot 10^3$	$+0.3$ -0.2	± 1.9	± 0.5	± 1.9		
130	$1.577 \cdot 10^3$	$+0.2$ -0.2	± 1.9	± 0.4	± 1.9		
135	$1.508 \cdot 10^3$	$+0.3$ -0.2	± 1.9	± 0.4	± 1.9		
140	$1.443 \cdot 10^3$	$+0.3$ -0.2	± 1.9	± 0.4	± 1.9		
145	$1.382 \cdot 10^3$	$+0.2$ -0.2	± 1.9	± 0.4	± 1.9		
150	$1.323 \cdot 10^3$	$+0.2$ -0.1	± 1.9	± 0.4	± 1.9		
160	$1.216 \cdot 10^3$	$+0.3$ -0.1	± 1.9	± 0.4	± 1.9		
170	$1.120 \cdot 10^3$	$+0.3$ -0.1	± 1.9	± 0.4	± 1.9		
180	$1.033 \cdot 10^3$	$+0.3$ -0.1	± 1.9	± 0.4	± 1.9		
190	$9.549 \cdot 10^2$	$+0.2$ -0.1	± 1.9	± 0.4	± 2.0		
200	$8.839 \cdot 10^2$	$+0.2$ -0.1	± 1.9	± 0.3	± 2.0		
210	$8.195 \cdot 10^2$	$+0.2$ -0.1	± 1.9	± 0.3	± 2.0		
220	$7.609 \cdot 10^2$	$+0.3$ -0.1	± 1.9	± 0.3	± 2.0		
230	$7.074 \cdot 10^2$	$+0.3$ -0.1	± 2.0	± 0.3	± 2.0		
240	$6.587 \cdot 10^2$	$+0.3$ -0.1	± 2.0	± 0.3	± 2.0		
250	$6.140 \cdot 10^2$	$+0.3$ -0.1	± 2.0	± 0.3	± 2.0		
260	$5.731 \cdot 10^2$	$+0.3$ -0.1	± 2.0	± 0.3	± 2.0		
270	$5.356 \cdot 10^2$	$+0.3$ -0.1	± 2.0	± 0.3	± 2.0		
280	$5.011 \cdot 10^2$	$+0.3$ -0.1	± 2.0	± 0.3	± 2.0		
290	$4.692 \cdot 10^2$	$+0.3$ -0.2	± 2.0	± 0.2	± 2.0		
300	$4.399 \cdot 10^2$	$+0.3$ -0.2	± 2.0	± 0.2	± 2.1		
310	$4.128 \cdot 10^2$	$+0.3$ -0.2	± 2.0	± 0.2	± 2.1		
320	$3.877 \cdot 10^2$	$+0.3$ -0.2	± 2.1	± 0.2	± 2.1		
330	$3.644 \cdot 10^2$	$+0.3$ -0.2	± 2.1	± 0.2	± 2.1		
340	$3.428 \cdot 10^2$	$+0.3$ -0.2	± 2.1	± 0.2	± 2.1		
350	$3.228 \cdot 10^2$	$+0.3$ -0.3	± 2.1	± 0.2	± 2.1		
360	$3.042 \cdot 10^2$	$+0.3$ -0.3	± 2.1	± 0.2	± 2.1		
370	$2.868 \cdot 10^2$	$+0.3$ -0.3	± 2.1	± 0.2	± 2.1		
380	$2.707 \cdot 10^2$	$+0.3$ -0.3	± 2.1	± 0.2	± 2.1		
390	$2.556 \cdot 10^2$	$+0.3$ -0.3	± 2.2	± 0.2	± 2.2		
400	$2.415 \cdot 10^2$	$+0.3$ -0.4	± 2.2	± 0.2	± 2.2		
410	$2.284 \cdot 10^2$	$+0.3$ -0.4	± 2.2	± 0.1	± 2.2		
420	$2.161 \cdot 10^2$	$+0.3$ -0.4	± 2.2	± 0.1	± 2.2		
430	$2.046 \cdot 10^2$	$+0.3$ -0.4	± 2.2	± 0.1	± 2.2		

Table A.17: Inclusive VBF cross sections for a LHC CM energy of $\sqrt{s} = 13$ TeV, at NNLO QCD, with an on shell Higgs, for the extended M_H scan, together with their uncertainties. For more details see Section ??.

M_H [GeV]	$\sigma_{\text{OS}}^{\text{VBF}}$ [fb]	$\sigma_{\text{CPS}}^{\text{VBF}}$ [fb]	δ_{CPS}	$\Delta_{\text{scale}}[\%]$	$\Delta_{\text{PDF}}[\%]$	$\Delta_{\alpha_s}[\%]$	$\Delta_{\text{PDF} \oplus \alpha_s}[\%]$
10	$1.121 \cdot 10^4$	$+1.0$ -0.7	± 1.8	± 0.9	± 2.0		
15	$1.074 \cdot 10^4$	$+1.0$ -0.6	± 1.8	± 0.8	± 2.0		
20	$1.025 \cdot 10^4$	$+0.9$ -0.6	± 1.8	± 0.8	± 2.0		
25	$9.769 \cdot 10^3$	$+0.8$ -0.6	± 1.8	± 0.8	± 2.0		
30	$9.299 \cdot 10^3$	$+0.9$ -0.5	± 1.8	± 0.8	± 2.0		
35	$8.847 \cdot 10^3$	$+0.8$ -0.5	± 1.8	± 0.8	± 1.9		
40	$8.419 \cdot 10^3$	$+0.8$ -0.5	± 1.8	± 0.7	± 1.9		
45	$8.011 \cdot 10^3$	$+0.8$ -0.4	± 1.8	± 0.7	± 1.9		
50	$7.627 \cdot 10^3$	$+0.8$ -0.4	± 1.8	± 0.7	± 1.9		
55	$7.264 \cdot 10^3$	$+0.7$ -0.4	± 1.8	± 0.7	± 1.9		
60	$6.924 \cdot 10^3$	$+0.7$ -0.4	± 1.8	± 0.7	± 1.9		
65	$6.603 \cdot 10^3$	$+0.7$ -0.4	± 1.8	± 0.7	± 1.9		
70	$6.301 \cdot 10^3$	$+0.7$ -0.4	± 1.8	± 0.7	± 1.9		
75	$6.016 \cdot 10^3$	$+0.6$ -0.3	± 1.8	± 0.7	± 1.9		
80	$5.748 \cdot 10^3$	$+0.6$ -0.3	± 1.8	± 0.6	± 1.9		
85	$5.496 \cdot 10^3$	$+0.6$ -0.3	± 1.8	± 0.6	± 1.9		
90	$5.258 \cdot 10^3$	$+0.6$ -0.3	± 1.8	± 0.6	± 1.9		
95	$5.034 \cdot 10^3$	$+0.6$ -0.3	± 1.8	± 0.6	± 1.9		
100	$4.822 \cdot 10^3$	$+0.5$ -0.3	± 1.8	± 0.6	± 1.9		
105	$4.623 \cdot 10^3$	$+0.5$ -0.3	± 1.8	± 0.6	± 1.9		
110	$4.434 \cdot 10^3$	$+0.5$ -0.2	± 1.8	± 0.6	± 1.9		
115	$4.255 \cdot 10^3$	$+0.5$ -0.2	± 1.8	± 0.6	± 1.9		
120	$4.086 \cdot 10^3$	$+0.5$ -0.2	± 1.8	± 0.6	± 1.9		
125	$3.925 \cdot 10^3$	$+0.5$ -0.2	± 1.8	± 0.6	± 1.9		
130	$3.773 \cdot 10^3$	$+0.4$ -0.2	± 1.8	± 0.6	± 1.9		
135	$3.629 \cdot 10^3$	$+0.4$ -0.2	± 1.8	± 0.6	± 1.9		
140	$3.492 \cdot 10^3$	$+0.4$ -0.2	± 1.8	± 0.5	± 1.9		
145	$3.362 \cdot 10^3$	$+0.4$ -0.2	± 1.8	± 0.5	± 1.9		
150	$3.239 \cdot 10^3$	$+0.4$ -0.2	± 1.8	± 0.5	± 1.9		
160	$3.010 \cdot 10^3$	$+0.4$ -0.2	± 1.8	± 0.5	± 1.9		
170	$2.802 \cdot 10^3$	$+0.4$ -0.2	± 1.8	± 0.5	± 1.9		
180	$2.612 \cdot 10^3$	$+0.3$ -0.2	± 1.8	± 0.5	± 1.9		
190	$2.440 \cdot 10^3$	$+0.3$ -0.2	± 1.8	± 0.5	± 1.9		
200	$2.282 \cdot 10^3$	$+0.3$ -0.2	± 1.8	± 0.5	± 1.9		
210	$2.138 \cdot 10^3$	$+0.3$ -0.2	± 1.8	± 0.5	± 1.9		
220	$2.006 \cdot 10^3$	$+0.3$ -0.2	± 1.8	± 0.5	± 1.9		
230	$1.884 \cdot 10^3$	$+0.3$ -0.1	± 1.8	± 0.4	± 1.9		
240	$1.772 \cdot 10^3$	$+0.3$ -0.1	± 1.8	± 0.4	± 1.9		
250	$1.669 \cdot 10^3$	$+0.3$ -0.1	± 1.8	± 0.4	± 1.9		
260	$1.573 \cdot 10^3$	$+0.3$ -0.1	± 1.9	± 0.4	± 1.9		
270	$1.485 \cdot 10^3$	$+0.3$ -0.1	± 1.9	± 0.4	± 1.9		
280	$1.403 \cdot 10^3$	$+0.3$ -0.1	± 1.9	± 0.4	± 1.9		
290	$1.326 \cdot 10^3$	$+0.3$ -0.1	± 1.9	± 0.4	± 1.9		
300	$1.256 \cdot 10^3$	$+0.3$ -0.1	± 1.9	± 0.4	± 1.9		
310	$1.190 \cdot 10^3$	$+0.3$ -0.1	± 1.9	± 0.4	± 1.9		
320	$1.128 \cdot 10^3$	$+0.3$ -0.1	± 1.9	± 0.4	± 1.9		
330	$1.071 \cdot 10^3$	$+0.3$ -0.1	± 1.9	± 0.4	± 1.9		
340	$1.017 \cdot 10^3$	$+0.3$ -0.1	± 1.9	± 0.4	± 1.9		
350	$9.666 \cdot 10^2$	$+0.3$ -0.1	± 1.9	± 0.3	± 1.9		
360	$9.194 \cdot 10^2$	$+0.3$ -0.1	± 1.9	± 0.3	± 1.9		
370	$8.752 \cdot 10^2$	$+0.3$ -0.1	± 1.9	± 0.3	± 2.0		
380	$8.337 \cdot 10^2$	$+0.3$ -0.1	± 1.9	± 0.3	± 2.0		
390	$7.947 \cdot 10^2$	$+0.3$ -0.1	± 1.9	± 0.3	± 2.0		
400	$7.580 \cdot 10^2$	$+0.3$ -0.1	± 1.9	± 0.3	± 2.0		
410	$7.235 \cdot 10^2$	$+0.3$ -0.0	± 2.0	± 0.3	± 2.0		
420	$6.909 \cdot 10^2$	$+0.3$ -0.0	± 2.0	± 0.3	± 2.0		
430	$6.602 \cdot 10^2$	$+0.3$ -0.0	± 2.0	± 0.3	± 2.0		

Table A.18: Inclusive VBF cross sections for a LHC CM energy of $\sqrt{s} = 14$ TeV, at NNLO QCD, with an on shell Higgs, for the extended M_H scan, together with their uncertainties. For more details see Section ??.

M_H [GeV]	σ_{OS}^{VBF} [fb]	$\sigma_{CPS}^{\text{VBF}}$ [fb]	δ_{CPS}	$\Delta_{\text{scale}}[\%]$	$\Delta_{\text{PDF}}[\%]$	$\Delta_{\alpha_s}[\%]$	$\Delta_{\text{PDF} \oplus \alpha_s}[\%]$
10	$1.246 \cdot 10^4$	$+1.0$ -0.7	± 1.8	± 0.9	± 2.0		
15	$1.194 \cdot 10^4$	$+1.0$ -0.6	± 1.8	± 0.9	± 2.0		
20	$1.140 \cdot 10^4$	$+0.9$ -0.6	± 1.8	± 0.8	± 2.0		
25	$1.088 \cdot 10^4$	$+0.9$ -0.6	± 1.8	± 0.8	± 2.0		
30	$1.037 \cdot 10^4$	$+0.9$ -0.5	± 1.8	± 0.8	± 2.0		
35	$9.872 \cdot 10^3$	$+0.8$ -0.5	± 1.8	± 0.8	± 2.0		
40	$9.401 \cdot 10^3$	$+0.8$ -0.5	± 1.8	± 0.8	± 1.9		
45	$8.955 \cdot 10^3$	$+0.8$ -0.5	± 1.8	± 0.7	± 1.9		
50	$8.533 \cdot 10^3$	$+0.8$ -0.4	± 1.8	± 0.7	± 1.9		
55	$8.136 \cdot 10^3$	$+0.7$ -0.4	± 1.8	± 0.7	± 1.9		
60	$7.761 \cdot 10^3$	$+0.7$ -0.4	± 1.8	± 0.7	± 1.9		
65	$7.408 \cdot 10^3$	$+0.7$ -0.4	± 1.8	± 0.7	± 1.9		
70	$7.075 \cdot 10^3$	$+0.7$ -0.4	± 1.8	± 0.7	± 1.9		
75	$6.761 \cdot 10^3$	$+0.7$ -0.4	± 1.8	± 0.7	± 1.9		
80	$6.465 \cdot 10^3$	$+0.6$ -0.3	± 1.8	± 0.7	± 1.9		
85	$6.186 \cdot 10^3$	$+0.6$ -0.3	± 1.8	± 0.7	± 1.9		
90	$5.922 \cdot 10^3$	$+0.6$ -0.3	± 1.8	± 0.6	± 1.9		
95	$5.674 \cdot 10^3$	$+0.6$ -0.3	± 1.8	± 0.6	± 1.9		
100	$5.440 \cdot 10^3$	$+0.6$ -0.3	± 1.8	± 0.6	± 1.9		
105	$5.219 \cdot 10^3$	$+0.6$ -0.3	± 1.8	± 0.6	± 1.9		
110	$5.009 \cdot 10^3$	$+0.5$ -0.3	± 1.8	± 0.6	± 1.9		
115	$4.811 \cdot 10^3$	$+0.5$ -0.3	± 1.8	± 0.6	± 1.9		
120	$4.623 \cdot 10^3$	$+0.5$ -0.2	± 1.8	± 0.6	± 1.9		
125	$4.445 \cdot 10^3$	$+0.5$ -0.2	± 1.8	± 0.6	± 1.9		
130	$4.276 \cdot 10^3$	$+0.5$ -0.2	± 1.8	± 0.6	± 1.9		
135	$4.115 \cdot 10^3$	$+0.5$ -0.2	± 1.8	± 0.6	± 1.9		
140	$3.963 \cdot 10^3$	$+0.5$ -0.2	± 1.8	± 0.6	± 1.9		
145	$3.818 \cdot 10^3$	$+0.4$ -0.2	± 1.8	± 0.6	± 1.9		
150	$3.681 \cdot 10^3$	$+0.4$ -0.2	± 1.8	± 0.6	± 1.9		
160	$3.425 \cdot 10^3$	$+0.4$ -0.2	± 1.8	± 0.5	± 1.9		
170	$3.193 \cdot 10^3$	$+0.4$ -0.2	± 1.8	± 0.5	± 1.9		
180	$2.981 \cdot 10^3$	$+0.4$ -0.2	± 1.8	± 0.5	± 1.9		
190	$2.788 \cdot 10^3$	$+0.3$ -0.2	± 1.8	± 0.5	± 1.9		
200	$2.611 \cdot 10^3$	$+0.3$ -0.2	± 1.8	± 0.5	± 1.9		
210	$2.449 \cdot 10^3$	$+0.3$ -0.2	± 1.8	± 0.5	± 1.9		
220	$2.301 \cdot 10^3$	$+0.3$ -0.2	± 1.8	± 0.5	± 1.9		
230	$2.164 \cdot 10^3$	$+0.3$ -0.2	± 1.8	± 0.5	± 1.9		
240	$2.038 \cdot 10^3$	$+0.3$ -0.2	± 1.8	± 0.5	± 1.9		
250	$1.921 \cdot 10^3$	$+0.3$ -0.1	± 1.8	± 0.4	± 1.9		
260	$1.813 \cdot 10^3$	$+0.3$ -0.1	± 1.8	± 0.4	± 1.9		
270	$1.714 \cdot 10^3$	$+0.3$ -0.1	± 1.8	± 0.4	± 1.9		
280	$1.621 \cdot 10^3$	$+0.3$ -0.1	± 1.9	± 0.4	± 1.9		
290	$1.535 \cdot 10^3$	$+0.3$ -0.1	± 1.9	± 0.4	± 1.9		
300	$1.454 \cdot 10^3$	$+0.3$ -0.1	± 1.9	± 0.4	± 1.9		
310	$1.380 \cdot 10^3$	$+0.3$ -0.1	± 1.9	± 0.4	± 1.9		
320	$1.310 \cdot 10^3$	$+0.3$ -0.1	± 1.9	± 0.4	± 1.9		
330	$1.245 \cdot 10^3$	$+0.3$ -0.1	± 1.9	± 0.4	± 1.9		
340	$1.184 \cdot 10^3$	$+0.3$ -0.1	± 1.9	± 0.4	± 1.9		
350	$1.126 \cdot 10^3$	$+0.3$ -0.1	± 1.9	± 0.4	± 1.9		
360	$1.073 \cdot 10^3$	$+0.3$ -0.1	± 1.9	± 0.4	± 1.9		
370	$1.022 \cdot 10^3$	$+0.3$ -0.1	± 1.9	± 0.4	± 1.9		
380	$9.749 \cdot 10^2$	$+0.3$ -0.1	± 1.9	± 0.3	± 1.9		
390	$9.303 \cdot 10^2$	$+0.3$ -0.1	± 1.9	± 0.3	± 1.9		
400	$8.884 \cdot 10^2$	$+0.3$ -0.1	± 1.9	± 0.3	± 2.0		
410	$8.488 \cdot 10^2$	$+0.3$ -0.1	± 1.9	± 0.3	± 2.0		
420	$8.115 \cdot 10^2$	$+0.3$ -0.1	± 1.9	± 0.3	± 2.0		
430	$7.763 \cdot 10^2$	$+0.3$ -0.1	± 1.9	± 0.3	± 2.0		

Table A.19: Inclusive VBF cross sections for a LHC CM energy of $\sqrt{s} = 7$ TeV, at NNLO QCD, with an on shell Higgs, for the extended M_H scan, together with their uncertainties. Only the WW-fusion contribution is included. For more details see Section ??.

M_H [GeV]	σ_{OS}^{VBF} [fb]	$\sigma_{CPS}^{\text{VBF}}$ [fb]	δ_{CPS}	$\Delta_{\text{scale}}[\%]$	$\Delta_{\text{PDF}}[\%]$	$\Delta_{\alpha_s}[\%]$	$\Delta_{\text{PDF} \oplus \alpha_s}[\%]$
10	$3.361 \cdot 10^3$	$+0.8$ -0.5	± 1.9	± 0.7	± 2.0		
15	$3.186 \cdot 10^3$	$+0.7$ -0.5	± 1.9	± 0.7	± 2.0		
20	$3.008 \cdot 10^3$	$+0.7$ -0.4	± 1.9	± 0.7	± 2.0		
25	$2.835 \cdot 10^3$	$+0.7$ -0.4	± 1.9	± 0.6	± 2.0		
30	$2.671 \cdot 10^3$	$+0.6$ -0.4	± 1.9	± 0.6	± 2.0		
35	$2.515 \cdot 10^3$	$+0.6$ -0.3	± 1.9	± 0.6	± 2.0		
40	$2.367 \cdot 10^3$	$+0.6$ -0.3	± 1.9	± 0.6	± 2.0		
45	$2.230 \cdot 10^3$	$+0.5$ -0.3	± 1.9	± 0.6	± 2.0		
50	$2.101 \cdot 10^3$	$+0.5$ -0.3	± 1.9	± 0.6	± 2.0		
55	$1.982 \cdot 10^3$	$+0.5$ -0.3	± 1.9	± 0.5	± 2.0		
60	$1.871 \cdot 10^3$	$+0.4$ -0.3	± 1.9	± 0.5	± 2.0		
65	$1.767 \cdot 10^3$	$+0.4$ -0.3	± 1.9	± 0.5	± 2.0		
70	$1.671 \cdot 10^3$	$+0.4$ -0.3	± 1.9	± 0.5	± 2.0		
75	$1.581 \cdot 10^3$	$+0.4$ -0.3	± 1.9	± 0.5	± 2.0		
80	$1.496 \cdot 10^3$	$+0.3$ -0.2	± 1.9	± 0.5	± 2.0		
85	$1.418 \cdot 10^3$	$+0.3$ -0.2	± 1.9	± 0.5	± 2.0		
90	$1.345 \cdot 10^3$	$+0.3$ -0.2	± 1.9	± 0.5	± 2.0		
95	$1.276 \cdot 10^3$	$+0.3$ -0.2	± 1.9	± 0.4	± 2.0		
100	$1.212 \cdot 10^3$	$+0.3$ -0.2	± 1.9	± 0.4	± 2.0		
105	$1.152 \cdot 10^3$	$+0.2$ -0.2	± 1.9	± 0.4	± 2.0		
110	$1.095 \cdot 10^3$	$+0.2$ -0.2	± 1.9	± 0.4	± 2.0		
115	$1.043 \cdot 10^3$	$+0.2$ -0.2	± 1.9	± 0.4	± 2.0		
120	$9.929 \cdot 10^2$	$+0.2$ -0.2	± 1.9	± 0.4	± 2.0		
125	$9.462 \cdot 10^2$	$+0.2$ -0.2	± 1.9	± 0.4	± 2.0		
130	$9.023 \cdot 10^2$	$+0.2$ -0.2	± 1.9	± 0.4	± 2.0		
135	$8.609 \cdot 10^2$	$+0.2$ -0.2	± 1.9	± 0.4	± 2.0		
140	$8.219 \cdot 10^2$	$+0.2$ -0.1	± 1.9	± 0.4	± 2.0		
145	$7.852 \cdot 10^2$	$+0.2$ -0.1	± 2.0	± 0.4	± 2.0		
150	$7.505 \cdot 10^2$	$+0.2$ -0.1	± 2.0	± 0.4	± 2.0		
160	$6.867 \cdot 10^2$	$+0.2$ -0.1	± 2.0	± 0.3	± 2.0		
170	$6.296 \cdot 10^2$	$+0.2$ -0.1	± 2.0	± 0.3	± 2.0		
180	$5.784 \cdot 10^2$	$+0.2$ -0.1	± 2.0	± 0.3	± 2.0		
190	$5.323 \cdot 10^2$	$+0.2$ -0.1	± 2.0	± 0.3	± 2.0		
200	$4.907 \cdot 10^2$	$+0.2$ -0.1	± 2.0	± 0.3	± 2.0		
210	$4.531 \cdot 10^2$	$+0.2$ -0.1	± 2.0	± 0.3	± 2.0		
220	$4.191 \cdot 10^2$	$+0.2$ -0.1	± 2.0	± 0.3	± 2.1		
230	$3.881 \cdot 10^2$	$+0.2$ -0.1	± 2.1	± 0.2	± 2.1		
240	$3.600 \cdot 10^2$	$+0.2$ -0.2	± 2.1	± 0.2	± 2.1		
250	$3.343 \cdot 10^2$	$+0.2$ -0.2	± 2.1	± 0.2	± 2.1		
260	$3.108 \cdot 10^2$	$+0.2$ -0.2	± 2.1	± 0.2	± 2.1		
270	$2.894 \cdot 10^2$	$+0.2$ -0.2	± 2.1	± 0.2	± 2.1		
280	$2.697 \cdot 10^2$	$+0.2$ -0.3	± 2.1	± 0.2	± 2.1		
290	$2.516 \cdot 10^2$	$+0.2$ -0.3	± 2.1	± 0.2	± 2.2		
300	$2.350 \cdot 10^2$	$+0.2$ -0.3	± 2.2	± 0.2	± 2.2		
310	$2.197 \cdot 10^2$	$+0.2$ -0.3	± 2.2	± 0.2	± 2.2		
320	$2.056 \cdot 10^2$	$+0.2$ -0.4	± 2.2	± 0.2	± 2.2		
330	$1.925 \cdot 10^2$	$+0.3$ -0.4	± 2.2	± 0.1	± 2.2		
340	$1.805 \cdot 10^2$	$+0.3$ -0.4	± 2.2	± 0.1	± 2.2		
350	$1.693 \cdot 10^2$	$+0.3$ -0.4	± 2.2	± 0.1	± 2.3		
360	$1.589 \cdot 10^2$	$+0.3$ -0.4	± 2.3	± 0.1	± 2.3		
370	$1.493 \cdot 10^2$	$+0.3$ -0.5	± 2.3	± 0.1	± 2.3		
380	$1.404 \cdot 10^2$	$+0.3$ -0.5	± 2.3	± 0.1	± 2.3		
390	$1.321 \cdot 10^2$	$+0.3$ -0.5	± 2.3	± 0.1	± 2.3		
400	$1.244 \cdot 10^2$	$+0.3$ -0.5	± 2.3	± 0.1	± 2.3		
410	$1.172 \cdot 10^2$	$+0.3$ -0.5	± 2.4	± 0.1	± 2.4		
420	$1.105 \cdot 10^2$	$+0.3$ -0.5	± 2.4	± 0.1	± 2.4		

Table A.20: Inclusive VBF cross sections for a LHC CM energy of $\sqrt{s} = 8$ TeV, at NNLO QCD, with an on shell Higgs, for the extended M_H scan, together with their uncertainties. Only the WW-fusion contribution is included. For more details see Section ??.

M_H [GeV]	σ_{OS}^{VBF} [fb]	$\sigma_{CPS}^{\text{VBF}}$ [fb]	δ_{CPS}	$\Delta_{\text{scale}}[\%]$	$\Delta_{\text{PDF}}[\%]$	$\Delta_{\alpha_s}[\%]$	$\Delta_{\text{PDF} \oplus \alpha_s}[\%]$
10	$4.121 \cdot 10^3$	$^{+0.8}_{-0.6}$	± 1.9	± 0.7	± 2.0		
15	$3.915 \cdot 10^3$	$^{+0.8}_{-0.5}$	± 1.9	± 0.7	± 2.0		
20	$3.706 \cdot 10^3$	$^{+0.7}_{-0.5}$	± 1.9	± 0.7	± 2.0		
25	$3.502 \cdot 10^3$	$^{+0.7}_{-0.4}$	± 1.9	± 0.7	± 2.0		
30	$3.307 \cdot 10^3$	$^{+0.7}_{-0.4}$	± 1.9	± 0.7	± 2.0		
35	$3.120 \cdot 10^3$	$^{+0.6}_{-0.4}$	± 1.9	± 0.6	± 2.0		
40	$2.945 \cdot 10^3$	$^{+0.6}_{-0.3}$	± 1.9	± 0.6	± 2.0		
45	$2.781 \cdot 10^3$	$^{+0.6}_{-0.3}$	± 1.9	± 0.6	± 2.0		
50	$2.627 \cdot 10^3$	$^{+0.6}_{-0.3}$	± 1.9	± 0.6	± 1.9		
55	$2.483 \cdot 10^3$	$^{+0.5}_{-0.3}$	± 1.9	± 0.6	± 1.9		
60	$2.349 \cdot 10^3$	$^{+0.5}_{-0.3}$	± 1.9	± 0.6	± 1.9		
65	$2.223 \cdot 10^3$	$^{+0.5}_{-0.3}$	± 1.9	± 0.5	± 1.9		
70	$2.107 \cdot 10^3$	$^{+0.4}_{-0.3}$	± 1.9	± 0.5	± 1.9		
75	$1.997 \cdot 10^3$	$^{+0.4}_{-0.3}$	± 1.9	± 0.5	± 1.9		
80	$1.895 \cdot 10^3$	$^{+0.4}_{-0.3}$	± 1.9	± 0.5	± 1.9		
85	$1.800 \cdot 10^3$	$^{+0.4}_{-0.3}$	± 1.9	± 0.5	± 1.9		
90	$1.710 \cdot 10^3$	$^{+0.4}_{-0.3}$	± 1.9	± 0.5	± 1.9		
95	$1.626 \cdot 10^3$	$^{+0.3}_{-0.2}$	± 1.9	± 0.5	± 1.9		
100	$1.548 \cdot 10^3$	$^{+0.3}_{-0.2}$	± 1.9	± 0.5	± 1.9		
105	$1.474 \cdot 10^3$	$^{+0.3}_{-0.2}$	± 1.9	± 0.5	± 1.9		
110	$1.405 \cdot 10^3$	$^{+0.3}_{-0.2}$	± 1.9	± 0.5	± 1.9		
115	$1.339 \cdot 10^3$	$^{+0.3}_{-0.2}$	± 1.9	± 0.4	± 1.9		
120	$1.278 \cdot 10^3$	$^{+0.2}_{-0.2}$	± 1.9	± 0.4	± 1.9		
125	$1.220 \cdot 10^3$	$^{+0.2}_{-0.2}$	± 1.9	± 0.4	± 2.0		
130	$1.166 \cdot 10^3$	$^{+0.2}_{-0.2}$	± 1.9	± 0.4	± 2.0		
135	$1.115 \cdot 10^3$	$^{+0.2}_{-0.2}$	± 1.9	± 0.4	± 2.0		
140	$1.067 \cdot 10^3$	$^{+0.2}_{-0.2}$	± 1.9	± 0.4	± 2.0		
145	$1.021 \cdot 10^3$	$^{+0.2}_{-0.2}$	± 1.9	± 0.4	± 2.0		
150	$9.775 \cdot 10^2$	$^{+0.2}_{-0.2}$	± 1.9	± 0.4	± 2.0		
160	$8.978 \cdot 10^2$	$^{+0.2}_{-0.1}$	± 1.9	± 0.4	± 2.0		
170	$8.263 \cdot 10^2$	$^{+0.2}_{-0.1}$	± 1.9	± 0.4	± 2.0		
180	$7.619 \cdot 10^2$	$^{+0.2}_{-0.1}$	± 2.0	± 0.3	± 2.0		
190	$7.037 \cdot 10^2$	$^{+0.2}_{-0.1}$	± 2.0	± 0.3	± 2.0		
200	$6.511 \cdot 10^2$	$^{+0.2}_{-0.1}$	± 2.0	± 0.3	± 2.0		
210	$6.034 \cdot 10^2$	$^{+0.2}_{-0.1}$	± 2.0	± 0.3	± 2.0		
220	$5.601 \cdot 10^2$	$^{+0.2}_{-0.1}$	± 2.0	± 0.3	± 2.0		
230	$5.206 \cdot 10^2$	$^{+0.2}_{-0.1}$	± 2.0	± 0.3	± 2.0		
240	$4.845 \cdot 10^2$	$^{+0.2}_{-0.1}$	± 2.0	± 0.3	± 2.0		
250	$4.515 \cdot 10^2$	$^{+0.2}_{-0.1}$	± 2.0	± 0.3	± 2.0		
260	$4.213 \cdot 10^2$	$^{+0.2}_{-0.1}$	± 2.0	± 0.3	± 2.1		
270	$3.936 \cdot 10^2$	$^{+0.2}_{-0.1}$	± 2.1	± 0.2	± 2.1		
280	$3.681 \cdot 10^2$	$^{+0.2}_{-0.2}$	± 2.1	± 0.2	± 2.1		
290	$3.447 \cdot 10^2$	$^{+0.2}_{-0.2}$	± 2.1	± 0.2	± 2.1		
300	$3.230 \cdot 10^2$	$^{+0.2}_{-0.2}$	± 2.1	± 0.2	± 2.1		
310	$3.030 \cdot 10^2$	$^{+0.2}_{-0.2}$	± 2.1	± 0.2	± 2.1		
320	$2.845 \cdot 10^2$	$^{+0.2}_{-0.2}$	± 2.1	± 0.2	± 2.1		
330	$2.674 \cdot 10^2$	$^{+0.2}_{-0.3}$	± 2.1	± 0.2	± 2.1		
340	$2.515 \cdot 10^2$	$^{+0.3}_{-0.3}$	± 2.1	± 0.2	± 2.2		
350	$2.367 \cdot 10^2$	$^{+0.3}_{-0.3}$	± 2.2	± 0.2	± 2.2		
360	$2.230 \cdot 10^2$	$^{+0.3}_{-0.3}$	± 2.2	± 0.2	± 2.2		
370	$2.103 \cdot 10^2$	$^{+0.3}_{-0.3}$	± 2.2	± 0.2	± 2.2		
380	$1.984 \cdot 10^2$	$^{+0.3}_{-0.4}$	± 2.2	Ix	± 0.1	± 2.2	
390	$1.873 \cdot 10^2$	$^{+0.3}_{-0.4}$	± 2.2		± 0.1	± 2.2	
400	$1.770 \cdot 10^2$	$^{+0.3}_{-0.4}$	± 2.2		± 0.1	± 2.2	
410	$1.673 \cdot 10^2$	$^{+0.3}_{-0.4}$	± 2.3		± 0.1	± 2.3	
420	$1.583 \cdot 10^2$	$^{+0.3}_{-0.4}$	± 2.3		± 0.1	± 2.3	

Table A.21: Inclusive VBF cross sections for a LHC CM energy of $\sqrt{s} = 13$ TeV, at NNLO QCD, with an on shell Higgs, for the extended M_H scan, together with their uncertainties. Only the WW-fusion contribution is included. For more details see Section ??.

M_H [GeV]	$\sigma_{\text{OS}}^{\text{VBF}}$ [fb]	$\sigma_{\text{CPS}}^{\text{VBF}}$ [fb]	δ_{CPS}	$\Delta_{\text{scale}}[\%]$	$\Delta_{\text{PDF}}[\%]$	$\Delta_{\alpha_s}[\%]$	$\Delta_{\text{PDF} \oplus \alpha_s}[\%]$
10	$8.357 \cdot 10^3$	$+0.9$ -0.7	± 1.9	± 0.8	± 2.0		
15	$7.995 \cdot 10^3$	$+0.9$ -0.7	± 1.9	± 0.8	± 2.0		
20	$7.623 \cdot 10^3$	$+0.9$ -0.6	± 1.8	± 0.8	± 2.0		
25	$7.260 \cdot 10^3$	$+0.8$ -0.6	± 1.8	± 0.8	± 2.0		
30	$6.902 \cdot 10^3$	$+0.8$ -0.5	± 1.8	± 0.8	± 2.0		
35	$6.562 \cdot 10^3$	$+0.8$ -0.5	± 1.8	± 0.7	± 2.0		
40	$6.238 \cdot 10^3$	$+0.8$ -0.5	± 1.8	± 0.7	± 2.0		
45	$5.932 \cdot 10^3$	$+0.7$ -0.4	± 1.8	± 0.7	± 2.0		
50	$5.643 \cdot 10^3$	$+0.7$ -0.4	± 1.8	± 0.7	± 2.0		
55	$5.371 \cdot 10^3$	$+0.7$ -0.4	± 1.8	± 0.7	± 1.9		
60	$5.116 \cdot 10^3$	$+0.7$ -0.4	± 1.8	± 0.7	± 1.9		
65	$4.876 \cdot 10^3$	$+0.7$ -0.3	± 1.8	± 0.7	± 1.9		
70	$4.649 \cdot 10^3$	$+0.6$ -0.3	± 1.8	± 0.6	± 1.9		
75	$4.437 \cdot 10^3$	$+0.6$ -0.3	± 1.8	± 0.6	± 1.9		
80	$4.237 \cdot 10^3$	$+0.6$ -0.3	± 1.8	± 0.6	± 1.9		
85	$4.049 \cdot 10^3$	$+0.6$ -0.3	± 1.8	± 0.6	± 1.9		
90	$3.872 \cdot 10^3$	$+0.6$ -0.3	± 1.8	± 0.6	± 1.9		
95	$3.705 \cdot 10^3$	$+0.5$ -0.3	± 1.8	± 0.6	± 1.9		
100	$3.548 \cdot 10^3$	$+0.5$ -0.3	± 1.8	± 0.6	± 1.9		
105	$3.399 \cdot 10^3$	$+0.5$ -0.3	± 1.8	± 0.6	± 1.9		
110	$3.259 \cdot 10^3$	$+0.5$ -0.3	± 1.8	± 0.6	± 1.9		
115	$3.126 \cdot 10^3$	$+0.5$ -0.3	± 1.8	± 0.6	± 1.9		
120	$3.001 \cdot 10^3$	$+0.5$ -0.3	± 1.8	± 0.6	± 1.9		
125	$2.882 \cdot 10^3$	$+0.5$ -0.3	± 1.8	± 0.5	± 1.9		
130	$2.770 \cdot 10^3$	$+0.4$ -0.2	± 1.8	± 0.5	± 1.9		
135	$2.663 \cdot 10^3$	$+0.4$ -0.2	± 1.8	± 0.5	± 1.9		
140	$2.562 \cdot 10^3$	$+0.4$ -0.2	± 1.8	± 0.5	± 1.9		
145	$2.466 \cdot 10^3$	$+0.4$ -0.2	± 1.8	± 0.5	± 1.9		
150	$2.375 \cdot 10^3$	$+0.4$ -0.2	± 1.8	± 0.5	± 1.9		
160	$2.206 \cdot 10^3$	$+0.4$ -0.2	± 1.8	± 0.5	± 1.9		
170	$2.052 \cdot 10^3$	$+0.3$ -0.2	± 1.8	± 0.5	± 1.9		
180	$1.913 \cdot 10^3$	$+0.3$ -0.2	± 1.9	± 0.5	± 1.9		
190	$1.786 \cdot 10^3$	$+0.3$ -0.2	± 1.9	± 0.5	± 1.9		
200	$1.670 \cdot 10^3$	$+0.3$ -0.2	± 1.9	± 0.5	± 1.9		
210	$1.564 \cdot 10^3$	$+0.3$ -0.2	± 1.9	± 0.4	± 1.9		
220	$1.467 \cdot 10^3$	$+0.2$ -0.2	± 1.9	± 0.4	± 1.9		
230	$1.378 \cdot 10^3$	$+0.2$ -0.2	± 1.9	± 0.4	± 1.9		
240	$1.295 \cdot 10^3$	$+0.2$ -0.2	± 1.9	± 0.4	± 1.9		
250	$1.220 \cdot 10^3$	$+0.2$ -0.1	± 1.9	± 0.4	± 1.9		
260	$1.150 \cdot 10^3$	$+0.2$ -0.1	± 1.9	± 0.4	± 1.9		
270	$1.085 \cdot 10^3$	$+0.2$ -0.1	± 1.9	± 0.4	± 1.9		
280	$1.025 \cdot 10^3$	$+0.2$ -0.1	± 1.9	± 0.4	± 1.9		
290	$9.689 \cdot 10^2$	$+0.2$ -0.1	± 1.9	± 0.4	± 2.0		
300	$9.170 \cdot 10^2$	$+0.3$ -0.1	± 1.9	± 0.4	± 2.0		
310	$8.687 \cdot 10^2$	$+0.3$ -0.1	± 1.9	± 0.4	± 2.0		
320	$8.237 \cdot 10^2$	$+0.3$ -0.1	± 1.9	± 0.3	± 2.0		
330	$7.816 \cdot 10^2$	$+0.3$ -0.1	± 1.9	± 0.3	± 2.0		
340	$7.423 \cdot 10^2$	$+0.3$ -0.1	± 2.0	± 0.3	± 2.0		
350	$7.055 \cdot 10^2$	$+0.3$ -0.1	± 2.0	± 0.3	± 2.0		
360	$6.711 \cdot 10^2$	$+0.3$ -0.1	± 2.0	± 0.3	± 2.0		
370	$6.388 \cdot 10^2$	$+0.3$ -0.1	± 2.0	± 0.3	± 2.0		
380	$6.084 \cdot 10^2$	$+0.3$ -0.1	± 2.0	$1x\pm 0.3$	± 2.0		
390	$5.799 \cdot 10^2$	$+0.3$ -0.1	± 2.0	± 0.3	± 2.0		
400	$5.531 \cdot 10^2$	$+0.3$ -0.1	± 2.0	± 0.3	± 2.0		
410	$5.278 \cdot 10^2$	$+0.3$ -0.1	± 2.0	± 0.3	± 2.0		
420	$5.040 \cdot 10^2$	$+0.3$ -0.1	± 2.0	± 0.3	± 2.0		

Table A.22: Inclusive VBF cross sections for a LHC CM energy of $\sqrt{s} = 14$ TeV, at NNLO QCD, with an on shell Higgs, for the extended M_H scan, together with their uncertainties. Only the WW-fusion contribution is included. For more details see Section ??.

M_H [GeV]	$\sigma_{\text{OS}}^{\text{VBF}}$ [fb]	$\sigma_{\text{CPS}}^{\text{VBF}}$ [fb]	δ_{CPS}	$\Delta_{\text{scale}}[\%]$	$\Delta_{\text{PDF}}[\%]$	$\Delta_{\alpha_s}[\%]$	$\Delta_{\text{PDF} \oplus \alpha_s}[\%]$
10	$9.269 \cdot 10^3$	$+0.9$ -0.7	± 1.9	± 0.9	± 2.0		
15	$8.876 \cdot 10^3$	$+0.9$ -0.7	± 1.9	± 0.8	± 2.0		
20	$8.472 \cdot 10^3$	$+0.9$ -0.6	± 1.8	± 0.8	± 2.0		
25	$8.075 \cdot 10^3$	$+0.9$ -0.6	± 1.8	± 0.8	± 2.0		
30	$7.686 \cdot 10^3$	$+0.8$ -0.6	± 1.8	± 0.8	± 2.0		
35	$7.311 \cdot 10^3$	$+0.8$ -0.5	± 1.8	± 0.8	± 2.0		
40	$6.957 \cdot 10^3$	$+0.8$ -0.5	± 1.8	± 0.7	± 2.0		
45	$6.622 \cdot 10^3$	$+0.8$ -0.4	± 1.8	± 0.7	± 2.0		
50	$6.305 \cdot 10^3$	$+0.7$ -0.4	± 1.8	± 0.7	± 2.0		
55	$6.007 \cdot 10^3$	$+0.7$ -0.4	± 1.8	± 0.7	± 1.9		
60	$5.727 \cdot 10^3$	$+0.7$ -0.4	± 1.8	± 0.7	± 1.9		
65	$5.463 \cdot 10^3$	$+0.7$ -0.4	± 1.8	± 0.7	± 1.9		
70	$5.214 \cdot 10^3$	$+0.7$ -0.3	± 1.8	± 0.7	± 1.9		
75	$4.979 \cdot 10^3$	$+0.6$ -0.3	± 1.8	± 0.7	± 1.9		
80	$4.759 \cdot 10^3$	$+0.6$ -0.3	± 1.8	± 0.6	± 1.9		
85	$4.551 \cdot 10^3$	$+0.6$ -0.3	± 1.8	± 0.6	± 1.9		
90	$4.356 \cdot 10^3$	$+0.6$ -0.3	± 1.8	± 0.6	± 1.9		
95	$4.172 \cdot 10^3$	$+0.6$ -0.3	± 1.8	± 0.6	± 1.9		
100	$3.998 \cdot 10^3$	$+0.6$ -0.3	± 1.8	± 0.6	± 1.9		
105	$3.833 \cdot 10^3$	$+0.5$ -0.3	± 1.8	± 0.6	± 1.9		
110	$3.678 \cdot 10^3$	$+0.5$ -0.3	± 1.8	± 0.6	± 1.9		
115	$3.531 \cdot 10^3$	$+0.5$ -0.3	± 1.8	± 0.6	± 1.9		
120	$3.392 \cdot 10^3$	$+0.5$ -0.3	± 1.8	± 0.6	± 1.9		
125	$3.260 \cdot 10^3$	$+0.5$ -0.3	± 1.8	± 0.6	± 1.9		
130	$3.135 \cdot 10^3$	$+0.5$ -0.2	± 1.8	± 0.6	± 1.9		
135	$3.016 \cdot 10^3$	$+0.5$ -0.2	± 1.8	± 0.5	± 1.9		
140	$2.904 \cdot 10^3$	$+0.4$ -0.2	± 1.8	± 0.5	± 1.9		
145	$2.797 \cdot 10^3$	$+0.4$ -0.2	± 1.8	± 0.5	± 1.9		
150	$2.696 \cdot 10^3$	$+0.4$ -0.2	± 1.8	± 0.5	± 1.9		
160	$2.507 \cdot 10^3$	$+0.4$ -0.2	± 1.8	± 0.5	± 1.9		
170	$2.336 \cdot 10^3$	$+0.4$ -0.2	± 1.8	± 0.5	± 1.9		
180	$2.181 \cdot 10^3$	$+0.3$ -0.2	± 1.8	± 0.5	± 1.9		
190	$2.039 \cdot 10^3$	$+0.3$ -0.2	± 1.8	± 0.5	± 1.9		
200	$1.909 \cdot 10^3$	$+0.3$ -0.2	± 1.9	± 0.5	± 1.9		
210	$1.790 \cdot 10^3$	$+0.3$ -0.2	± 1.9	± 0.5	± 1.9		
220	$1.681 \cdot 10^3$	$+0.3$ -0.2	± 1.9	± 0.4	± 1.9		
230	$1.581 \cdot 10^3$	$+0.2$ -0.2	± 1.9	± 0.4	± 1.9		
240	$1.488 \cdot 10^3$	$+0.2$ -0.2	± 1.9	± 0.4	± 1.9		
250	$1.403 \cdot 10^3$	$+0.2$ -0.2	± 1.9	± 0.4	± 1.9		
260	$1.324 \cdot 10^3$	$+0.2$ -0.2	± 1.9	± 0.4	± 1.9		
270	$1.251 \cdot 10^3$	$+0.2$ -0.1	± 1.9	± 0.4	± 1.9		
280	$1.183 \cdot 10^3$	$+0.2$ -0.1	± 1.9	± 0.4	± 1.9		
290	$1.120 \cdot 10^3$	$+0.2$ -0.1	± 1.9	± 0.4	± 1.9		
300	$1.061 \cdot 10^3$	$+0.2$ -0.1	± 1.9	± 0.4	± 1.9		
310	$1.007 \cdot 10^3$	$+0.2$ -0.1	± 1.9	± 0.4	± 1.9		
320	$9.556 \cdot 10^2$	$+0.2$ -0.1	± 1.9	± 0.4	± 2.0		
330	$9.079 \cdot 10^2$	$+0.3$ -0.1	± 1.9	± 0.4	± 2.0		
340	$8.632 \cdot 10^2$	$+0.3$ -0.1	± 1.9	± 0.3	± 2.0		
350	$8.214 \cdot 10^2$	$+0.3$ -0.1	± 1.9	± 0.3	± 2.0		
360	$7.822 \cdot 10^2$	$+0.3$ -0.1	± 1.9	± 0.3	± 2.0		
370	$7.455 \cdot 10^2$	$+0.3$ -0.1	± 2.0	± 0.3	± 2.0		
380	$7.108 \cdot 10^2$	$+0.3$ -0.1	± 2.0	$1xii \pm 0.3$	± 2.0		
390	$6.783 \cdot 10^2$	$+0.3$ -0.1	± 2.0	± 0.3	± 2.0		
400	$6.477 \cdot 10^2$	$+0.3$ -0.1	± 2.0	± 0.3	± 2.0		
410	$6.188 \cdot 10^2$	$+0.3$ -0.1	± 2.0	± 0.3	± 2.0		
420	$5.916 \cdot 10^2$	$+0.3$ -0.1	± 2.0	± 0.3	± 2.0		

Table A.23: Inclusive VBF cross sections for a LHC CM energy of $\sqrt{s} = 7$ TeV, at NNLO QCD, with an on shell Higgs, for the extended M_H scan, together with their uncertainties. Only the ZZ-fusion contribution is included. For more details see Section ??.

M_H [GeV]	σ_{OS}^{VBF} [fb]	$\sigma_{CPS}^{\text{VBF}}$ [fb]	δ_{CPS}	$\Delta_{\text{scale}}[\%]$	$\Delta_{\text{PDF}}[\%]$	$\Delta_{\alpha_s}[\%]$	$\Delta_{\text{PDF} \oplus \alpha_s}[\%]$
10	$1.120 \cdot 10^3$	$+0.9$ -0.5	± 1.7	± 0.8	± 1.9		
15	$1.065 \cdot 10^3$	$+0.9$ -0.5	± 1.7	± 0.8	± 1.9		
20	$1.010 \cdot 10^3$	$+0.8$ -0.5	± 1.7	± 0.7	± 1.9		
25	$9.552 \cdot 10^2$	$+0.8$ -0.4	± 1.7	± 0.7	± 1.9		
30	$9.026 \cdot 10^2$	$+0.8$ -0.4	± 1.7	± 0.7	± 1.9		
35	$8.529 \cdot 10^2$	$+0.7$ -0.4	± 1.7	± 0.7	± 1.9		
40	$8.055 \cdot 10^2$	$+0.7$ -0.3	± 1.7	± 0.7	± 1.8		
45	$7.609 \cdot 10^2$	$+0.7$ -0.3	± 1.7	± 0.7	± 1.8		
50	$7.191 \cdot 10^2$	$+0.6$ -0.3	± 1.7	± 0.6	± 1.8		
55	$6.799 \cdot 10^2$	$+0.6$ -0.3	± 1.7	± 0.6	± 1.8		
60	$6.432 \cdot 10^2$	$+0.6$ -0.3	± 1.7	± 0.6	± 1.8		
65	$6.090 \cdot 10^2$	$+0.5$ -0.3	± 1.7	± 0.6	± 1.8		
70	$5.769 \cdot 10^2$	$+0.5$ -0.3	± 1.7	± 0.6	± 1.8		
75	$5.469 \cdot 10^2$	$+0.5$ -0.3	± 1.7	± 0.6	± 1.8		
80	$5.188 \cdot 10^2$	$+0.5$ -0.3	± 1.7	± 0.6	± 1.8		
85	$4.925 \cdot 10^2$	$+0.5$ -0.2	± 1.7	± 0.6	± 1.8		
90	$4.679 \cdot 10^2$	$+0.4$ -0.2	± 1.7	± 0.5	± 1.8		
95	$4.448 \cdot 10^2$	$+0.4$ -0.2	± 1.8	± 0.5	± 1.8		
100	$4.231 \cdot 10^2$	$+0.4$ -0.2	± 1.8	± 0.5	± 1.8		
105	$4.028 \cdot 10^2$	$+0.4$ -0.2	± 1.8	± 0.5	± 1.8		
110	$3.836 \cdot 10^2$	$+0.3$ -0.2	± 1.8	± 0.5	± 1.8		
115	$3.656 \cdot 10^2$	$+0.3$ -0.2	± 1.8	± 0.5	± 1.8		
120	$3.486 \cdot 10^2$	$+0.3$ -0.2	± 1.8	± 0.5	± 1.8		
125	$3.327 \cdot 10^2$	$+0.3$ -0.2	± 1.8	± 0.5	± 1.8		
130	$3.176 \cdot 10^2$	$+0.3$ -0.2	± 1.8	± 0.5	± 1.8		
135	$3.034 \cdot 10^2$	$+0.3$ -0.2	± 1.8	± 0.5	± 1.8		
140	$2.900 \cdot 10^2$	$+0.3$ -0.2	± 1.8	± 0.5	± 1.8		
145	$2.773 \cdot 10^2$	$+0.3$ -0.2	± 1.8	± 0.4	± 1.8		
150	$2.654 \cdot 10^2$	$+0.3$ -0.2	± 1.8	± 0.4	± 1.9		
160	$2.433 \cdot 10^2$	$+0.3$ -0.2	± 1.8	± 0.4	± 1.9		
170	$2.235 \cdot 10^2$	$+0.3$ -0.1	± 1.8	± 0.4	± 1.9		
180	$2.057 \cdot 10^2$	$+0.3$ -0.1	± 1.8	± 0.4	± 1.9		
190	$1.896 \cdot 10^2$	$+0.3$ -0.1	± 1.8	± 0.4	± 1.9		
200	$1.751 \cdot 10^2$	$+0.3$ -0.1	± 1.8	± 0.4	± 1.9		
210	$1.619 \cdot 10^2$	$+0.3$ -0.1	± 1.9	± 0.4	± 1.9		
220	$1.499 \cdot 10^2$	$+0.3$ -0.1	± 1.9	± 0.3	± 1.9		
230	$1.391 \cdot 10^2$	$+0.3$ -0.1	± 1.9	± 0.3	± 1.9		
240	$1.291 \cdot 10^2$	$+0.3$ -0.1	± 1.9	± 0.3	± 1.9		
250	$1.201 \cdot 10^2$	$+0.3$ -0.1	± 1.9	± 0.3	± 1.9		
260	$1.118 \cdot 10^2$	$+0.3$ -0.1	± 1.9	± 0.3	± 1.9		
270	$1.042 \cdot 10^2$	$+0.3$ -0.1	± 1.9	± 0.3	± 1.9		
280	$9.719 \cdot 10^1$	$+0.3$ -0.1	± 1.9	± 0.3	± 1.9		
290	$9.078 \cdot 10^1$	$+0.3$ -0.1	± 1.9	± 0.3	± 1.9		
300	$8.486 \cdot 10^1$	$+0.3$ -0.2	± 1.9	± 0.3	± 2.0		
310	$7.941 \cdot 10^1$	$+0.3$ -0.2	± 2.0	± 0.2	± 2.0		
320	$7.438 \cdot 10^1$	$+0.3$ -0.2	± 2.0	± 0.2	± 2.0		
330	$6.973 \cdot 10^1$	$+0.3$ -0.2	± 2.0	± 0.2	± 2.0		
340	$6.542 \cdot 10^1$	$+0.3$ -0.2	± 2.0	± 0.2	± 2.0		
350	$6.143 \cdot 10^1$	$+0.3$ -0.3	± 2.0	± 0.2	± 2.0		
360	$5.772 \cdot 10^1$	$+0.3$ -0.3	± 2.0	± 0.2	± 2.0		
370	$5.428 \cdot 10^1$	$+0.3$ -0.3	± 2.0	± 0.2	± 2.0		
380	$5.108 \cdot 10^1$	$+0.3$ -0.3	± 2.0	± 0.2	± 2.0		
390	$4.811 \cdot 10^1$	$+0.3$ -0.3	± 2.0	± 0.2	± 2.0		
400	$4.533 \cdot 10^1$	$+0.3$ -0.3	± 2.0	± 0.2	± 2.1		
410	$4.275 \cdot 10^1$	$+0.3$ -0.4	± 2.1	± 0.1	± 2.1		
420	$4.033 \cdot 10^1$	$+0.3$ -0.4	± 2.1	± 0.1	± 2.1		
				± 2.0	$\text{lxi} \pm 0.2$		

Table A.24: Inclusive VBF cross sections for a LHC CM energy of $\sqrt{s} = 8$ TeV, at NNLO QCD, with an on shell Higgs, for the extended M_H scan, together with their uncertainties. Only the ZZ-fusion contribution is included. For more details see Section ??.

M_H [GeV]	σ_{OS}^{VBF} [fb]	$\sigma_{CPS}^{\text{VBF}}$ [fb]	δ_{CPS}	$\Delta_{\text{scale}}[\%]$	$\Delta_{\text{PDF}}[\%]$	$\Delta_{\alpha_s}[\%]$	$\Delta_{\text{PDF} \oplus \alpha_s}[\%]$
10	$1.386 \cdot 10^3$	$+^{+1.0}_{-0.6}$	± 1.7	± 0.8	± 1.9		
15	$1.321 \cdot 10^3$	$+^{+0.9}_{-0.5}$	± 1.7	± 0.8	± 1.9		
20	$1.255 \cdot 10^3$	$+^{+0.9}_{-0.5}$	± 1.7	± 0.8	± 1.9		
25	$1.190 \cdot 10^3$	$+^{+0.8}_{-0.4}$	± 1.7	± 0.8	± 1.9		
30	$1.127 \cdot 10^3$	$+^{+0.8}_{-0.4}$	± 1.7	± 0.7	± 1.9		
35	$1.068 \cdot 10^3$	$+^{+0.8}_{-0.4}$	± 1.7	± 0.7	± 1.9		
40	$1.011 \cdot 10^3$	$+^{+0.7}_{-0.4}$	± 1.7	± 0.7	± 1.8		
45	$9.569 \cdot 10^2$	$+^{+0.7}_{-0.3}$	± 1.7	± 0.7	± 1.8		
50	$9.063 \cdot 10^2$	$+^{+0.7}_{-0.3}$	± 1.7	± 0.7	± 1.8		
55	$8.588 \cdot 10^2$	$+^{+0.7}_{-0.3}$	± 1.7	± 0.7	± 1.8		
60	$8.143 \cdot 10^2$	$+^{+0.6}_{-0.3}$	± 1.7	± 0.6	± 1.8		
65	$7.726 \cdot 10^2$	$+^{+0.6}_{-0.3}$	± 1.7	± 0.6	± 1.8		
70	$7.334 \cdot 10^2$	$+^{+0.6}_{-0.3}$	± 1.7	± 0.6	± 1.8		
75	$6.967 \cdot 10^2$	$+^{+0.6}_{-0.3}$	± 1.7	± 0.6	± 1.8		
80	$6.623 \cdot 10^2$	$+^{+0.5}_{-0.3}$	± 1.7	± 0.6	± 1.8		
85	$6.301 \cdot 10^2$	$+^{+0.5}_{-0.3}$	± 1.7	± 0.6	± 1.8		
90	$5.998 \cdot 10^2$	$+^{+0.5}_{-0.3}$	± 1.7	± 0.6	± 1.8		
95	$5.713 \cdot 10^2$	$+^{+0.5}_{-0.3}$	± 1.7	± 0.6	± 1.8		
100	$5.445 \cdot 10^2$	$+^{+0.5}_{-0.3}$	± 1.7	± 0.6	± 1.8		
105	$5.193 \cdot 10^2$	$+^{+0.4}_{-0.2}$	± 1.7	± 0.6	± 1.8		
110	$4.955 \cdot 10^2$	$+^{+0.4}_{-0.2}$	± 1.7	± 0.5	± 1.8		
115	$4.732 \cdot 10^2$	$+^{+0.4}_{-0.2}$	± 1.7	± 0.5	± 1.8		
120	$4.521 \cdot 10^2$	$+^{+0.4}_{-0.2}$	± 1.7	± 0.5	± 1.8		
125	$4.322 \cdot 10^2$	$+^{+0.4}_{-0.2}$	± 1.8	± 0.5	± 1.8		
130	$4.134 \cdot 10^2$	$+^{+0.3}_{-0.2}$	± 1.8	± 0.5	± 1.8		
135	$3.957 \cdot 10^2$	$+^{+0.3}_{-0.2}$	± 1.8	± 0.5	± 1.8		
140	$3.789 \cdot 10^2$	$+^{+0.3}_{-0.2}$	± 1.8	± 0.5	± 1.8		
145	$3.630 \cdot 10^2$	$+^{+0.3}_{-0.2}$	± 1.8	± 0.5	± 1.8		
150	$3.480 \cdot 10^2$	$+^{+0.3}_{-0.2}$	± 1.8	± 0.5	± 1.8		
160	$3.202 \cdot 10^2$	$+^{+0.3}_{-0.2}$	± 1.8	± 0.5	± 1.8		
170	$2.952 \cdot 10^2$	$+^{+0.3}_{-0.2}$	± 1.8	± 0.4	± 1.8		
180	$2.726 \cdot 10^2$	$+^{+0.3}_{-0.2}$	± 1.8	± 0.4	± 1.8		
190	$2.522 \cdot 10^2$	$+^{+0.3}_{-0.1}$	± 1.8	± 0.4	± 1.9		
200	$2.337 \cdot 10^2$	$+^{+0.3}_{-0.1}$	± 1.8	± 0.4	± 1.9		
210	$2.169 \cdot 10^2$	$+^{+0.3}_{-0.1}$	± 1.8	± 0.4	± 1.9		
220	$2.015 \cdot 10^2$	$+^{+0.3}_{-0.1}$	± 1.8	± 0.4	± 1.9		
230	$1.875 \cdot 10^2$	$+^{+0.3}_{-0.1}$	± 1.8	± 0.4	± 1.9		
240	$1.747 \cdot 10^2$	$+^{+0.3}_{-0.1}$	± 1.8	± 0.4	± 1.9		
250	$1.630 \cdot 10^2$	$+^{+0.3}_{-0.1}$	± 1.9	± 0.4	± 1.9		
260	$1.523 \cdot 10^2$	$+^{+0.3}_{-0.1}$	± 1.9	± 0.3	± 1.9		
270	$1.424 \cdot 10^2$	$+^{+0.3}_{-0.1}$	± 1.9	± 0.3	± 1.9		
280	$1.333 \cdot 10^2$	$+^{+0.3}_{-0.1}$	± 1.9	± 0.3	± 1.9		
290	$1.249 \cdot 10^2$	$+^{+0.3}_{-0.1}$	± 1.9	± 0.3	± 1.9		
300	$1.172 \cdot 10^2$	$+^{+0.3}_{-0.1}$	± 1.9	± 0.3	± 1.9		
310	$1.100 \cdot 10^2$	$+^{+0.3}_{-0.1}$	± 1.9	± 0.3	± 1.9		
320	$1.034 \cdot 10^2$	$+^{+0.3}_{-0.1}$	± 1.9	± 0.3	± 1.9		
330	$9.723 \cdot 10^1$	$+^{+0.3}_{-0.1}$	± 1.9	± 0.3	± 1.9		
340	$9.152 \cdot 10^1$	$+^{+0.3}_{-0.1}$	± 1.9	± 0.3	± 1.9		
350	$8.622 \cdot 10^1$	$+^{+0.3}_{-0.2}$	± 1.9	± 0.2	± 2.0		
360	$8.128 \cdot 10^1$	$+^{+0.3}_{-0.2}$	± 2.0	± 0.2	± 2.0		
370	$7.669 \cdot 10^1$	$+^{+0.3}_{-0.2}$	± 2.0	± 0.2	± 2.0		
380	$7.240 \cdot 10^1$	$+^{+0.3}_{-0.2}$	± 2.0	± 0.2	± 2.0		
390	$6.840 \cdot 10^1$	$+^{+0.3}_{-0.2}$	± 2.0	± 0.2	± 2.0		
400	$6.467 \cdot 10^1$	$+^{+0.3}_{-0.2}$	± 2.0	± 0.2	± 2.0		
410	$6.118 \cdot 10^1$	$+^{+0.3}_{-0.3}$	± 2.0	± 0.2	± 2.0		
420	$5.791 \cdot 10^1$	$+^{+0.3}_{-0.3}$	± 2.0	± 0.2	± 2.0		

Table A.25: Inclusive VBF cross sections for a LHC CM energy of $\sqrt{s} = 13$ TeV, at NNLO QCD, with an on shell Higgs, for the extended M_H scan, together with their uncertainties. Only the ZZ-fusion contribution is included. For more details see Section ??.

M_H [GeV]	σ_{OS}^{VBF} [fb]	$\sigma_{CPS}^{\text{VBF}}$ [fb]	δ_{CPS}	$\Delta_{\text{scale}}[\%]$	$\Delta_{\text{PDF}}[\%]$	$\Delta_{\alpha_s}[\%]$	$\Delta_{\text{PDF} \oplus \alpha_s}[\%]$
10	$2.903 \cdot 10^3$	$+^{+1.0}_{-0.7}$	± 1.7	± 0.9	± 1.9		
15	$2.788 \cdot 10^3$	$+^{+1.0}_{-0.7}$	± 1.7	± 0.9	± 1.9		
20	$2.667 \cdot 10^3$	$+^{+1.0}_{-0.6}$	± 1.7	± 0.9	± 1.9		
25	$2.546 \cdot 10^3$	$+^{+1.0}_{-0.6}$	± 1.7	± 0.9	± 1.9		
30	$2.429 \cdot 10^3$	$+^{+0.9}_{-0.6}$	± 1.7	± 0.8	± 1.9		
35	$2.316 \cdot 10^3$	$+^{+0.9}_{-0.5}$	± 1.7	± 0.8	± 1.9		
40	$2.208 \cdot 10^3$	$+^{+0.9}_{-0.5}$	± 1.7	± 0.8	± 1.9		
45	$2.105 \cdot 10^3$	$+^{+0.9}_{-0.5}$	± 1.7	± 0.8	± 1.9		
50	$2.007 \cdot 10^3$	$+^{+0.8}_{-0.4}$	± 1.7	± 0.8	± 1.8		
55	$1.915 \cdot 10^3$	$+^{+0.8}_{-0.4}$	± 1.7	± 0.8	± 1.8		
60	$1.827 \cdot 10^3$	$+^{+0.8}_{-0.4}$	± 1.7	± 0.8	± 1.8		
65	$1.745 \cdot 10^3$	$+^{+0.8}_{-0.4}$	± 1.7	± 0.7	± 1.8		
70	$1.667 \cdot 10^3$	$+^{+0.7}_{-0.4}$	± 1.7	± 0.7	± 1.8		
75	$1.594 \cdot 10^3$	$+^{+0.7}_{-0.3}$	± 1.7	± 0.7	± 1.8		
80	$1.524 \cdot 10^3$	$+^{+0.7}_{-0.3}$	± 1.7	± 0.7	± 1.8		
85	$1.459 \cdot 10^3$	$+^{+0.7}_{-0.3}$	± 1.7	± 0.7	± 1.8		
90	$1.397 \cdot 10^3$	$+^{+0.7}_{-0.3}$	± 1.7	± 0.7	± 1.8		
95	$1.339 \cdot 10^3$	$+^{+0.7}_{-0.3}$	± 1.7	± 0.7	± 1.8		
100	$1.284 \cdot 10^3$	$+^{+0.6}_{-0.3}$	± 1.7	± 0.7	± 1.8		
105	$1.231 \cdot 10^3$	$+^{+0.6}_{-0.3}$	± 1.7	± 0.7	± 1.8		
110	$1.182 \cdot 10^3$	$+^{+0.6}_{-0.3}$	± 1.7	± 0.7	± 1.8		
115	$1.135 \cdot 10^3$	$+^{+0.6}_{-0.3}$	± 1.7	± 0.6	± 1.8		
120	$1.091 \cdot 10^3$	$+^{+0.6}_{-0.3}$	± 1.7	± 0.6	± 1.8		
125	$1.049 \cdot 10^3$	$+^{+0.6}_{-0.3}$	± 1.7	± 0.6	± 1.8		
130	$1.009 \cdot 10^3$	$+^{+0.5}_{-0.3}$	± 1.7	± 0.6	± 1.8		
135	$9.706 \cdot 10^2$	$+^{+0.5}_{-0.3}$	± 1.7	± 0.6	± 1.8		
140	$9.345 \cdot 10^2$	$+^{+0.5}_{-0.3}$	± 1.7	± 0.6	± 1.8		
145	$9.002 \cdot 10^2$	$+^{+0.5}_{-0.3}$	± 1.7	± 0.6	± 1.8		
150	$8.676 \cdot 10^2$	$+^{+0.5}_{-0.2}$	± 1.7	± 0.6	± 1.8		
160	$8.069 \cdot 10^2$	$+^{+0.5}_{-0.2}$	± 1.7	± 0.6	± 1.8		
170	$7.518 \cdot 10^2$	$+^{+0.4}_{-0.2}$	± 1.7	± 0.6	± 1.8		
180	$7.016 \cdot 10^2$	$+^{+0.4}_{-0.2}$	± 1.7	± 0.6	± 1.8		
190	$6.557 \cdot 10^2$	$+^{+0.4}_{-0.2}$	± 1.7	± 0.6	± 1.8		
200	$6.137 \cdot 10^2$	$+^{+0.4}_{-0.2}$	± 1.7	± 0.5	± 1.8		
210	$5.753 \cdot 10^2$	$+^{+0.4}_{-0.2}$	± 1.7	± 0.5	± 1.8		
220	$5.400 \cdot 10^2$	$+^{+0.3}_{-0.2}$	± 1.7	± 0.5	± 1.8		
230	$5.075 \cdot 10^2$	$+^{+0.3}_{-0.2}$	± 1.7	± 0.5	± 1.8		
240	$4.775 \cdot 10^2$	$+^{+0.3}_{-0.2}$	± 1.7	± 0.5	± 1.8		
250	$4.498 \cdot 10^2$	$+^{+0.3}_{-0.2}$	± 1.7	± 0.5	± 1.8		
260	$4.242 \cdot 10^2$	$+^{+0.3}_{-0.2}$	± 1.7	± 0.5	± 1.8		
270	$4.005 \cdot 10^2$	$+^{+0.3}_{-0.2}$	± 1.7	± 0.5	± 1.8		
280	$3.785 \cdot 10^2$	$+^{+0.3}_{-0.1}$	± 1.8	± 0.5	± 1.8		
290	$3.581 \cdot 10^2$	$+^{+0.3}_{-0.1}$	± 1.8	± 0.5	± 1.8		
300	$3.391 \cdot 10^2$	$+^{+0.3}_{-0.1}$	± 1.8	± 0.4	± 1.8		
310	$3.213 \cdot 10^2$	$+^{+0.3}_{-0.1}$	± 1.8	± 0.4	± 1.8		
320	$3.048 \cdot 10^2$	$+^{+0.3}_{-0.1}$	± 1.8	± 0.4	± 1.8		
330	$2.893 \cdot 10^2$	$+^{+0.3}_{-0.1}$	± 1.8	± 0.4	± 1.8		
340	$2.749 \cdot 10^2$	$+^{+0.3}_{-0.1}$	± 1.8	± 0.4	± 1.8		
350	$2.614 \cdot 10^2$	$+^{+0.3}_{-0.1}$	± 1.8	± 0.4	± 1.8		
360	$2.487 \cdot 10^2$	$+^{+0.3}_{-0.1}$	± 1.8	± 0.4	± 1.8		
370	$2.368 \cdot 10^2$	$+^{+0.3}_{-0.1}$	± 1.8	± 0.4	± 1.8		
380	$2.256 \cdot 10^2$	$+^{+0.3}_{-0.1}$	± 1.8	$1x\pm 0.4$	± 1.9		
390	$2.151 \cdot 10^2$	$+^{+0.3}_{-0.1}$	± 1.8	± 0.4	± 1.9		
400	$2.052 \cdot 10^2$	$+^{+0.3}_{-0.1}$	± 1.8	± 0.4	± 1.9		
410	$1.959 \cdot 10^2$	$+^{+0.3}_{-0.1}$	± 1.8	± 0.4	± 1.9		
420	$1.871 \cdot 10^2$	$+^{+0.3}_{-0.1}$	± 1.8	± 0.4	± 1.9		

Table A.26: Inclusive VBF cross sections for a LHC CM energy of $\sqrt{s} = 14$ TeV, at NNLO QCD, with an on shell Higgs, for the extended M_H scan, together with their uncertainties. Only the ZZ-fusion contribution is included. For more details see Section ??.

M_H [GeV]	σ_{OS}^{VBF} [fb]	$\sigma_{CPS}^{\text{VBF}}$ [fb]	δ_{CPS}	$\Delta_{\text{scale}}[\%]$	$\Delta_{\text{PDF}}[\%]$	$\Delta_{\alpha_s}[\%]$	$\Delta_{\text{PDF} \oplus \alpha_s}[\%]$
10	$3.235 \cdot 10^3$	$^{+1.1}_{-0.7}$	± 1.7	± 0.9	± 2.0		
15	$3.110 \cdot 10^3$	$^{+1.0}_{-0.7}$	± 1.7	± 0.9	± 1.9		
20	$2.977 \cdot 10^3$	$^{+1.0}_{-0.6}$	± 1.7	± 0.9	± 1.9		
25	$2.845 \cdot 10^3$	$^{+1.0}_{-0.6}$	± 1.7	± 0.9	± 1.9		
30	$2.718 \cdot 10^3$	$^{+0.9}_{-0.6}$	± 1.7	± 0.9	± 1.9		
35	$2.593 \cdot 10^3$	$^{+0.9}_{-0.6}$	± 1.7	± 0.8	± 1.9		
40	$2.474 \cdot 10^3$	$^{+0.9}_{-0.5}$	± 1.7	± 0.8	± 1.9		
45	$2.361 \cdot 10^3$	$^{+0.9}_{-0.5}$	± 1.7	± 0.8	± 1.9		
50	$2.253 \cdot 10^3$	$^{+0.9}_{-0.5}$	± 1.7	± 0.8	± 1.9		
55	$2.151 \cdot 10^3$	$^{+0.8}_{-0.4}$	± 1.7	± 0.8	± 1.8		
60	$2.055 \cdot 10^3$	$^{+0.8}_{-0.4}$	± 1.7	± 0.8	± 1.8		
65	$1.964 \cdot 10^3$	$^{+0.8}_{-0.4}$	± 1.7	± 0.8	± 1.8		
70	$1.878 \cdot 10^3$	$^{+0.8}_{-0.4}$	± 1.7	± 0.7	± 1.8		
75	$1.797 \cdot 10^3$	$^{+0.7}_{-0.4}$	± 1.7	± 0.7	± 1.8		
80	$1.720 \cdot 10^3$	$^{+0.7}_{-0.3}$	± 1.7	± 0.7	± 1.8		
85	$1.647 \cdot 10^3$	$^{+0.7}_{-0.3}$	± 1.7	± 0.7	± 1.8		
90	$1.579 \cdot 10^3$	$^{+0.7}_{-0.3}$	± 1.7	± 0.7	± 1.8		
95	$1.514 \cdot 10^3$	$^{+0.7}_{-0.3}$	± 1.7	± 0.7	± 1.8		
100	$1.452 \cdot 10^3$	$^{+0.7}_{-0.3}$	± 1.7	± 0.7	± 1.8		
105	$1.394 \cdot 10^3$	$^{+0.6}_{-0.3}$	± 1.7	± 0.7	± 1.8		
110	$1.340 \cdot 10^3$	$^{+0.6}_{-0.3}$	± 1.7	± 0.7	± 1.8		
115	$1.288 \cdot 10^3$	$^{+0.6}_{-0.3}$	± 1.7	± 0.7	± 1.8		
120	$1.238 \cdot 10^3$	$^{+0.6}_{-0.3}$	± 1.7	± 0.7	± 1.8		
125	$1.191 \cdot 10^3$	$^{+0.6}_{-0.3}$	± 1.7	± 0.7	± 1.8		
130	$1.146 \cdot 10^3$	$^{+0.6}_{-0.3}$	± 1.7	± 0.6	± 1.8		
135	$1.104 \cdot 10^3$	$^{+0.6}_{-0.3}$	± 1.7	± 0.6	± 1.8		
140	$1.064 \cdot 10^3$	$^{+0.5}_{-0.3}$	± 1.7	± 0.6	± 1.8		
145	$1.025 \cdot 10^3$	$^{+0.5}_{-0.3}$	± 1.7	± 0.6	± 1.8		
150	$9.889 \cdot 10^2$	$^{+0.5}_{-0.3}$	± 1.7	± 0.6	± 1.8		
160	$9.210 \cdot 10^2$	$^{+0.5}_{-0.2}$	± 1.7	± 0.6	± 1.8		
170	$8.592 \cdot 10^2$	$^{+0.5}_{-0.2}$	± 1.7	± 0.6	± 1.8		
180	$8.029 \cdot 10^2$	$^{+0.5}_{-0.2}$	± 1.7	± 0.6	± 1.8		
190	$7.514 \cdot 10^2$	$^{+0.4}_{-0.2}$	± 1.7	± 0.6	± 1.8		
200	$7.041 \cdot 10^2$	$^{+0.4}_{-0.2}$	± 1.7	± 0.6	± 1.8		
210	$6.608 \cdot 10^2$	$^{+0.4}_{-0.2}$	± 1.7	± 0.5	± 1.8		
220	$6.210 \cdot 10^2$	$^{+0.4}_{-0.2}$	± 1.7	± 0.5	± 1.8		
230	$5.844 \cdot 10^2$	$^{+0.4}_{-0.2}$	± 1.7	± 0.5	± 1.8		
240	$5.506 \cdot 10^2$	$^{+0.3}_{-0.2}$	± 1.7	± 0.5	± 1.8		
250	$5.193 \cdot 10^2$	$^{+0.3}_{-0.2}$	± 1.7	± 0.5	± 1.8		
260	$4.904 \cdot 10^2$	$^{+0.3}_{-0.2}$	± 1.7	± 0.5	± 1.8		
270	$4.635 \cdot 10^2$	$^{+0.3}_{-0.2}$	± 1.7	± 0.5	± 1.8		
280	$4.385 \cdot 10^2$	$^{+0.3}_{-0.2}$	± 1.7	± 0.5	± 1.8		
290	$4.153 \cdot 10^2$	$^{+0.3}_{-0.2}$	± 1.7	± 0.5	± 1.8		
300	$3.937 \cdot 10^2$	$^{+0.3}_{-0.2}$	± 1.7	± 0.5	± 1.8		
310	$3.736 \cdot 10^2$	$^{+0.3}_{-0.1}$	± 1.8	± 0.5	± 1.8		
320	$3.547 \cdot 10^2$	$^{+0.3}_{-0.1}$	± 1.8	± 0.5	± 1.8		
330	$3.372 \cdot 10^2$	$^{+0.3}_{-0.1}$	± 1.8	± 0.4	± 1.8		
340	$3.207 \cdot 10^2$	$^{+0.3}_{-0.1}$	± 1.8	± 0.4	± 1.8		
350	$3.052 \cdot 10^2$	$^{+0.3}_{-0.1}$	± 1.8	± 0.4	± 1.8		
360	$2.907 \cdot 10^2$	$^{+0.3}_{-0.1}$	± 1.8	± 0.4	± 1.8		
370	$2.771 \cdot 10^2$	$^{+0.3}_{-0.1}$	± 1.8	± 0.4	± 1.8		
380	$2.643 \cdot 10^2$	$^{+0.3}_{-0.1}$	± 1.8	± 0.4	± 1.8		
390	$2.523 \cdot 10^2$	$^{+0.3}_{-0.1}$	± 1.8	± 0.4	± 1.8		
400	$2.409 \cdot 10^2$	$^{+0.3}_{-0.1}$	± 1.8	± 0.4	± 1.8		
410	$2.302 \cdot 10^2$	$^{+0.3}_{-0.1}$	± 1.8	± 0.4	± 1.8		
420	$2.201 \cdot 10^2$	$^{+0.3}_{-0.1}$	± 1.8	± 0.4	± 1.9		

Table B.1: Total $W^+(\rightarrow l^+ \nu_l)H$ cross sections including QCD and EW corrections and their uncertainties for a proton–proton collision energy $\sqrt{s} = 7$ TeV and a Higgs-boson masses.

M_H [GeV]	σ [fb]	$\Delta_{\text{scale}}[\%]$	$\Delta_{\text{PDF}/\alpha_s/\text{PDF}\oplus\alpha_s}[\%]$	$\sigma_{\text{NNLOQCD}}^{\text{DY}}$ [fb]	$\sigma_{\text{t-loop}}$ [fb]	$\delta_{\text{EW}}[\%]$	σ_γ [fb]
120.0	46.85	$^{+0.6}_{-0.9}$	$\pm 1.8/\pm 0.6/\pm 1.9$	48.90	0.47	-7.0	$0.91^{+1.13}_{-0.11}$
120.5	46.22	$^{+0.6}_{-1.0}$	$\pm 1.8/\pm 0.6/\pm 1.9$	48.24	0.46	-7.0	$0.90^{+1.12}_{-0.11}$
121.0	45.57	$^{+0.7}_{-0.9}$	$\pm 1.9/\pm 0.6/\pm 1.9$	47.56	0.46	-7.0	$0.90^{+1.12}_{-0.10}$
121.5	44.95	$^{+0.7}_{-0.9}$	$\pm 1.9/\pm 0.6/\pm 2.0$	46.92	0.45	-7.1	$0.90^{+1.12}_{-0.10}$
122.0	44.38	$^{+0.7}_{-0.9}$	$\pm 1.9/\pm 0.6/\pm 2.0$	46.32	0.45	-7.1	$0.90^{+1.12}_{-0.10}$
122.5	43.80	$^{+0.6}_{-0.9}$	$\pm 1.9/\pm 0.6/\pm 2.0$	45.72	0.44	-7.1	$0.89^{+1.11}_{-0.10}$
123.0	43.22	$^{+0.7}_{-0.9}$	$\pm 1.9/\pm 0.6/\pm 2.0$	45.11	0.44	-7.1	$0.89^{+1.11}_{-0.10}$
123.5	42.63	$^{+0.7}_{-0.9}$	$\pm 1.9/\pm 0.6/\pm 2.0$	44.50	0.43	-7.2	$0.89^{+1.11}_{-0.10}$
124.0	42.07	$^{+0.7}_{-0.8}$	$\pm 1.9/\pm 0.7/\pm 2.0$	43.91	0.43	-7.2	$0.88^{+1.11}_{-0.10}$
124.1	41.96	$^{+0.7}_{-0.8}$	$\pm 1.9/\pm 0.7/\pm 2.0$	43.80	0.43	-7.2	$0.88^{+1.10}_{-0.10}$
124.2	41.84	$^{+0.7}_{-0.8}$	$\pm 1.9/\pm 0.7/\pm 2.0$	43.67	0.42	-7.2	$0.88^{+1.10}_{-0.10}$
124.3	41.75	$^{+0.7}_{-0.9}$	$\pm 1.9/\pm 0.7/\pm 2.0$	43.58	0.42	-7.2	$0.88^{+1.10}_{-0.10}$
124.4	41.65	$^{+0.7}_{-0.9}$	$\pm 1.9/\pm 0.7/\pm 2.0$	43.47	0.42	-7.2	$0.88^{+1.10}_{-0.10}$
124.5	41.54	$^{+0.6}_{-0.9}$	$\pm 1.9/\pm 0.7/\pm 2.0$	43.36	0.42	-7.2	$0.88^{+1.10}_{-0.10}$
124.6	41.45	$^{+0.6}_{-1.0}$	$\pm 1.9/\pm 0.7/\pm 2.0$	43.26	0.42	-7.2	$0.88^{+1.10}_{-0.10}$
124.7	41.32	$^{+0.7}_{-0.9}$	$\pm 1.9/\pm 0.7/\pm 2.0$	43.13	0.42	-7.2	$0.88^{+1.10}_{-0.10}$
124.8	41.21	$^{+0.7}_{-0.9}$	$\pm 1.9/\pm 0.7/\pm 2.0$	43.01	0.42	-7.2	$0.88^{+1.10}_{-0.10}$
124.9	41.10	$^{+0.7}_{-0.9}$	$\pm 1.9/\pm 0.7/\pm 2.0$	42.90	0.42	-7.2	$0.88^{+1.10}_{-0.10}$
125.0	40.99	$^{+0.7}_{-0.9}$	$\pm 1.9/\pm 0.7/\pm 2.0$	42.78	0.42	-7.2	$0.88^{+1.10}_{-0.10}$
125.09	40.88	$^{+0.7}_{-0.8}$	$\pm 1.9/\pm 0.7/\pm 2.0$	42.68	0.42	-7.2	$0.88^{+1.10}_{-0.10}$
125.1	40.89	$^{+0.7}_{-0.9}$	$\pm 1.9/\pm 0.7/\pm 2.0$	42.67	0.42	-7.2	$0.88^{+1.10}_{-0.10}$
125.2	40.79	$^{+0.6}_{-0.9}$	$\pm 1.9/\pm 0.7/\pm 2.0$	42.57	0.42	-7.2	$0.88^{+1.10}_{-0.10}$
125.3	40.68	$^{+0.6}_{-0.9}$	$\pm 1.9/\pm 0.7/\pm 2.0$	42.46	0.42	-7.2	$0.88^{+1.10}_{-0.10}$
125.4	40.56	$^{+0.7}_{-0.9}$	$\pm 1.9/\pm 0.7/\pm 2.0$	42.34	0.42	-7.2	$0.88^{+1.10}_{-0.10}$
125.5	40.47	$^{+0.6}_{-0.9}$	$\pm 1.9/\pm 0.7/\pm 2.0$	42.24	0.41	-7.2	$0.88^{+1.10}_{-0.10}$
125.6	40.36	$^{+0.6}_{-0.9}$	$\pm 1.9/\pm 0.7/\pm 2.0$	42.13	0.41	-7.3	$0.87^{+1.10}_{-0.10}$
125.7	40.26	$^{+0.6}_{-0.9}$	$\pm 1.9/\pm 0.7/\pm 2.0$	42.02	0.41	-7.3	$0.87^{+1.10}_{-0.10}$
125.8	40.15	$^{+0.7}_{-0.9}$	$\pm 1.9/\pm 0.7/\pm 2.0$	41.90	0.41	-7.3	$0.87^{+1.10}_{-0.10}$
125.9	40.03	$^{+0.7}_{-0.9}$	$\pm 1.9/\pm 0.7/\pm 2.0$	41.78	0.41	-7.3	$0.87^{+1.10}_{-0.10}$
126.0	39.93	$^{+0.7}_{-0.9}$	$\pm 1.9/\pm 0.7/\pm 2.0$	41.68	0.41	-7.3	$0.87^{+1.10}_{-0.10}$
126.5	39.41	$^{+0.7}_{-0.9}$	$\pm 1.9/\pm 0.7/\pm 2.0$	41.14	0.40	-7.3	$0.87^{+1.09}_{-0.10}$
127.0	38.91	$^{+0.7}_{-0.9}$	$\pm 1.9/\pm 0.7/\pm 2.0$	40.61	0.40	-7.3	$0.87^{+1.09}_{-0.10}$
127.5	38.40	$^{+0.6}_{-0.9}$	$\pm 1.9/\pm 0.7/\pm 2.0$	40.08	0.40	-7.3	$0.86^{+1.09}_{-0.10}$
128.0	37.91	$^{+0.7}_{-0.9}$	$\pm 1.9/\pm 0.6/\pm 2.0$	39.57	0.39	-7.4	$0.86^{+1.09}_{-0.10}$
128.5	37.42	$^{+0.7}_{-0.9}$	$\pm 1.9/\pm 0.6/\pm 2.0$	39.06	0.39	-7.4	$0.86^{+1.08}_{-0.10}$
129.0	36.94	$^{+0.7}_{-0.9}$	$\pm 1.9/\pm 0.6/\pm 2.0$	38.56	0.38	-7.4	$0.86^{+1.08}_{-0.10}$
129.5	36.48	$^{+0.6}_{-1.0}$	$\pm 1.9/\pm 0.6/\pm 2.0$	38.08	0.38	-7.4	$0.85^{+1.08}_{-0.10}$
130.0	36.01	$^{+0.6}_{-0.9}$	$\pm 1.9/\pm 0.6/\pm 2.0$	37.59	0.37	-7.5	$0.85^{+1.08}_{-0.09}$

B SM Higgs-strahlung cross sections

Here we expand Tables 1.3–1.6, which contain predictions for total and fiducial Higgs-strahlung cross sections in the SM for $M_H = 125$ GeV, to a scan over SM Higgs-boson masses. In detail the total cross sections for the production of $W^+(\rightarrow l^+ \nu_l)H$, $W^-(\rightarrow l^- \bar{\nu}_l)H$, $Z(\rightarrow l^+ l^-)H$, and $Z(\rightarrow \nu \bar{\nu})H$ final states are summarized in Tables B.1–B.16.

Table B.2: Total $W^+(\rightarrow l^+ \nu_l)H$ cross sections including QCD and EW corrections and their uncertainties for a proton–proton collision energy $\sqrt{s} = 8$ TeV and a Higgs-boson masses.

M_H [GeV]	σ [fb]	$\Delta_{\text{scale}}[\%]$	$\Delta_{\text{PDF}/\alpha_s/\text{PDF}+\alpha_s}[\%]$	$\sigma_{\text{NNLOQCD}}^{\text{DY}}$ [fb]	$\sigma_{\text{t-loop}}$ [fb]	$\delta_{\text{EW}}[\%]$	σ_γ [fb]
120.0	56.46	+0.6 -0.8	$\pm 1.8/\pm 0.7/\pm 2.0$	58.79	0.59	-7.0	$1.21^{+1.44}_{-0.15}$
120.5	55.73	+0.5 -0.9	$\pm 1.8/\pm 0.7/\pm 2.0$	58.04	0.59	-7.1	$1.21^{+1.43}_{-0.15}$
121.0	54.97	+0.6 -0.8	$\pm 1.8/\pm 0.7/\pm 2.0$	57.24	0.58	-7.1	$1.21^{+1.43}_{-0.15}$
121.5	54.24	+0.6 -0.8	$\pm 1.8/\pm 0.7/\pm 2.0$	56.48	0.58	-7.1	$1.20^{+1.42}_{-0.14}$
122.0	53.52	+0.6 -0.8	$\pm 1.8/\pm 0.7/\pm 2.0$	55.73	0.56	-7.1	$1.20^{+1.41}_{-0.14}$
122.5	52.84	+0.6 -0.8	$\pm 1.8/\pm 0.7/\pm 2.0$	55.02	0.56	-7.2	$1.20^{+1.41}_{-0.14}$
123.0	52.14	+0.6 -0.9	$\pm 1.8/\pm 0.8/\pm 2.0$	54.29	0.55	-7.2	$1.19^{+1.40}_{-0.14}$
123.5	51.46	+0.6 -0.9	$\pm 1.8/\pm 0.8/\pm 2.0$	53.58	0.55	-7.2	$1.19^{+1.39}_{-0.14}$
124.0	50.79	+0.7 -0.8	$\pm 1.8/\pm 0.8/\pm 2.0$	52.88	0.54	-7.2	$1.19^{+1.39}_{-0.14}$
124.1	50.67	+0.6 -0.8	$\pm 1.8/\pm 0.8/\pm 2.0$	52.75	0.54	-7.2	$1.19^{+1.39}_{-0.14}$
124.2	50.54	+0.6 -0.9	$\pm 1.8/\pm 0.8/\pm 2.0$	52.63	0.54	-7.2	$1.18^{+1.39}_{-0.14}$
124.3	50.42	+0.6 -0.9	$\pm 1.8/\pm 0.8/\pm 2.0$	52.50	0.54	-7.2	$1.18^{+1.38}_{-0.14}$
124.4	50.32	+0.5 -0.9	$\pm 1.8/\pm 0.8/\pm 2.0$	52.38	0.54	-7.2	$1.18^{+1.38}_{-0.14}$
124.5	50.17	+0.6 -0.9	$\pm 1.8/\pm 0.8/\pm 2.0$	52.23	0.54	-7.2	$1.18^{+1.38}_{-0.14}$
124.6	50.02	+0.6 -0.9	$\pm 1.8/\pm 0.8/\pm 2.0$	52.09	0.53	-7.3	$1.18^{+1.38}_{-0.14}$
124.7	49.87	+0.7 -0.8	$\pm 1.8/\pm 0.8/\pm 2.0$	51.92	0.53	-7.3	$1.18^{+1.38}_{-0.14}$
124.8	49.77	+0.6 -0.9	$\pm 1.8/\pm 0.8/\pm 2.0$	51.82	0.53	-7.3	$1.18^{+1.38}_{-0.14}$
124.9	49.65	+0.6 -0.9	$\pm 1.8/\pm 0.8/\pm 2.0$	51.69	0.53	-7.3	$1.18^{+1.38}_{-0.14}$
125.0	49.52	+0.6 -0.9	$\pm 1.8/\pm 0.8/\pm 2.0$	51.56	0.53	-7.3	$1.18^{+1.38}_{-0.14}$
125.09	49.40	+0.7 -0.9	$\pm 1.8/\pm 0.8/\pm 2.0$	51.44	0.53	-7.3	$1.18^{+1.38}_{-0.14}$
125.1	49.40	+0.6 -0.9	$\pm 1.8/\pm 0.8/\pm 2.0$	51.43	0.53	-7.3	$1.18^{+1.37}_{-0.14}$
125.2	49.25	+0.7 -0.9	$\pm 1.8/\pm 0.8/\pm 2.0$	51.28	0.53	-7.3	$1.18^{+1.37}_{-0.14}$
125.3	49.11	+0.7 -0.9	$\pm 1.8/\pm 0.8/\pm 2.0$	51.14	0.53	-7.3	$1.18^{+1.37}_{-0.14}$
125.4	48.98	+0.7 -0.9	$\pm 1.8/\pm 0.8/\pm 2.0$	51.00	0.53	-7.3	$1.18^{+1.37}_{-0.14}$
125.5	48.84	+0.7 -0.8	$\pm 1.8/\pm 0.8/\pm 2.0$	50.85	0.52	-7.3	$1.18^{+1.37}_{-0.14}$
125.6	48.73	+0.6 -0.8	$\pm 1.8/\pm 0.8/\pm 2.0$	50.73	0.53	-7.3	$1.18^{+1.37}_{-0.14}$
125.7	48.61	+0.6 -0.9	$\pm 1.8/\pm 0.7/\pm 2.0$	50.62	0.52	-7.3	$1.17^{+1.37}_{-0.14}$
125.8	48.47	+0.7 -0.8	$\pm 1.8/\pm 0.7/\pm 2.0$	50.47	0.52	-7.3	$1.17^{+1.37}_{-0.14}$
125.9	48.36	+0.6 -0.9	$\pm 1.8/\pm 0.7/\pm 2.0$	50.35	0.52	-7.3	$1.17^{+1.37}_{-0.14}$
126.0	48.23	+0.6 -0.9	$\pm 1.8/\pm 0.7/\pm 2.0$	50.21	0.52	-7.3	$1.17^{+1.37}_{-0.14}$
126.5	47.59	+0.7 -0.8	$\pm 1.8/\pm 0.7/\pm 2.0$	49.55	0.52	-7.3	$1.17^{+1.37}_{-0.14}$
127.0	47.00	+0.6 -0.9	$\pm 1.8/\pm 0.7/\pm 2.0$	48.93	0.51	-7.4	$1.17^{+1.36}_{-0.14}$
127.5	46.39	+0.7 -0.8	$\pm 1.8/\pm 0.7/\pm 2.0$	48.29	0.50	-7.4	$1.16^{+1.36}_{-0.14}$
128.0	45.83	+0.6 -0.8	$\pm 1.8/\pm 0.7/\pm 2.0$	47.70	0.50	-7.4	$1.16^{+1.36}_{-0.14}$
128.5	45.26	+0.6 -0.9	$\pm 1.8/\pm 0.7/\pm 2.0$	47.11	0.49	-7.4	$1.16^{+1.35}_{-0.14}$
129.0	44.67	+0.6 -0.9	$\pm 1.9/\pm 0.7/\pm 2.0$	46.51	0.49	-7.5	$1.15^{+1.35}_{-0.13}$
129.5	44.12	+0.6 -0.9	$\pm 1.9/\pm 0.7/\pm 2.0$	45.93	0.48	-7.5	$1.15^{+1.35}_{-0.13}$
130.0	43.57	+0.6 -1.0	$\pm 1.9/\pm 0.7/\pm 2.0$	45.36	0.48	-7.5	$1.15^{+1.34}_{-0.13}$

Table B.3: Total $W^+(\rightarrow l^+ \nu_l)H$ cross sections including QCD and EW corrections and their uncertainties for a proton–proton collision energy $\sqrt{s} = 13$ TeV and a Higgs-boson masses.

M_H [GeV]	σ [fb]	$\Delta_{\text{scale}}[\%]$	$\Delta_{\text{PDF}/\alpha_s/\text{PDF} \oplus \alpha_s}[\%]$	σ_{NNLOQCD} [fb]	$\sigma_{\text{t-loop}}$ [fb]	$\delta_{\text{EW}}[\%]$	σ_γ [fb]
120.0	106.94	$^{+0.6}_{-0.6}$	$\pm 1.6 / \pm 0.9 / \pm 1.8$	110.37	1.33	-7.2	$3.16^{+3.39}_{-0.38}$
120.5	105.60	$^{+0.5}_{-0.7}$	$\pm 1.6 / \pm 0.9 / \pm 1.8$	108.99	1.32	-7.2	$3.15^{+3.39}_{-0.38}$
121.0	104.30	$^{+0.5}_{-0.7}$	$\pm 1.6 / \pm 0.9 / \pm 1.8$	107.63	1.30	-7.2	$3.15^{+3.38}_{-0.38}$
121.5	103.03	$^{+0.4}_{-0.8}$	$\pm 1.6 / \pm 0.9 / \pm 1.8$	106.32	1.29	-7.3	$3.14^{+3.37}_{-0.38}$
122.0	101.77	$^{+0.3}_{-0.8}$	$\pm 1.6 / \pm 0.9 / \pm 1.8$	105.00	1.27	-7.3	$3.13^{+3.37}_{-0.37}$
122.5	100.48	$^{+0.5}_{-0.8}$	$\pm 1.6 / \pm 0.9 / \pm 1.8$	103.65	1.26	-7.3	$3.13^{+3.36}_{-0.37}$
123.0	99.10	$^{+0.6}_{-0.7}$	$\pm 1.6 / \pm 0.9 / \pm 1.8$	102.20	1.25	-7.3	$3.12^{+3.35}_{-0.37}$
123.5	97.81	$^{+0.6}_{-0.7}$	$\pm 1.6 / \pm 0.9 / \pm 1.8$	100.87	1.23	-7.3	$3.11^{+3.35}_{-0.37}$
124.0	96.57	$^{+0.6}_{-0.6}$	$\pm 1.6 / \pm 0.9 / \pm 1.8$	99.58	1.22	-7.4	$3.11^{+3.34}_{-0.37}$
124.1	96.34	$^{+0.5}_{-0.6}$	$\pm 1.6 / \pm 0.9 / \pm 1.8$	99.34	1.22	-7.4	$3.10^{+3.34}_{-0.37}$
124.2	96.10	$^{+0.5}_{-0.6}$	$\pm 1.6 / \pm 0.9 / \pm 1.8$	99.07	1.22	-7.4	$3.10^{+3.34}_{-0.37}$
124.3	95.88	$^{+0.6}_{-0.7}$	$\pm 1.6 / \pm 0.9 / \pm 1.8$	98.86	1.21	-7.4	$3.10^{+3.34}_{-0.37}$
124.4	95.65	$^{+0.6}_{-0.7}$	$\pm 1.6 / \pm 0.9 / \pm 1.8$	98.61	1.22	-7.4	$3.10^{+3.34}_{-0.37}$
124.5	95.36	$^{+0.6}_{-0.6}$	$\pm 1.6 / \pm 0.9 / \pm 1.8$	98.31	1.22	-7.4	$3.10^{+3.33}_{-0.37}$
124.6	95.21	$^{+0.5}_{-0.7}$	$\pm 1.6 / \pm 0.9 / \pm 1.8$	98.15	1.21	-7.4	$3.10^{+3.33}_{-0.37}$
124.7	94.94	$^{+0.6}_{-0.7}$	$\pm 1.6 / \pm 0.9 / \pm 1.8$	97.88	1.20	-7.4	$3.10^{+3.33}_{-0.37}$
124.8	94.71	$^{+0.6}_{-0.8}$	$\pm 1.6 / \pm 0.9 / \pm 1.8$	97.64	1.21	-7.4	$3.09^{+3.33}_{-0.37}$
124.9	94.47	$^{+0.6}_{-0.7}$	$\pm 1.6 / \pm 0.9 / \pm 1.8$	97.38	1.21	-7.4	$3.09^{+3.33}_{-0.37}$
125.0	94.26	$^{+0.5}_{-0.7}$	$\pm 1.6 / \pm 0.9 / \pm 1.8$	97.18	1.20	-7.4	$3.09^{+3.33}_{-0.37}$
125.09	94.04	$^{+0.5}_{-0.7}$	$\pm 1.6 / \pm 0.9 / \pm 1.8$	96.94	1.20	-7.4	$3.09^{+3.33}_{-0.37}$
125.1	94.01	$^{+0.6}_{-0.7}$	$\pm 1.6 / \pm 0.9 / \pm 1.8$	96.91	1.20	-7.4	$3.09^{+3.33}_{-0.37}$
125.2	93.77	$^{+0.6}_{-0.7}$	$\pm 1.6 / \pm 0.9 / \pm 1.8$	96.66	1.19	-7.4	$3.09^{+3.33}_{-0.37}$
125.3	93.54	$^{+0.6}_{-0.8}$	$\pm 1.6 / \pm 0.9 / \pm 1.8$	96.42	1.20	-7.4	$3.09^{+3.32}_{-0.37}$
125.4	93.31	$^{+0.6}_{-0.7}$	$\pm 1.6 / \pm 0.9 / \pm 1.8$	96.18	1.19	-7.4	$3.09^{+3.32}_{-0.37}$
125.5	93.08	$^{+0.6}_{-0.7}$	$\pm 1.6 / \pm 0.9 / \pm 1.8$	95.94	1.19	-7.4	$3.09^{+3.32}_{-0.37}$
125.6	92.84	$^{+0.5}_{-0.6}$	$\pm 1.6 / \pm 0.9 / \pm 1.8$	95.70	1.18	-7.4	$3.08^{+3.32}_{-0.36}$
125.7	92.54	$^{+0.6}_{-0.6}$	$\pm 1.6 / \pm 0.9 / \pm 1.8$	95.37	1.19	-7.4	$3.08^{+3.32}_{-0.36}$
125.8	92.34	$^{+0.7}_{-0.7}$	$\pm 1.6 / \pm 0.9 / \pm 1.8$	95.18	1.17	-7.5	$3.08^{+3.32}_{-0.36}$
125.9	92.20	$^{+0.6}_{-0.8}$	$\pm 1.6 / \pm 0.9 / \pm 1.8$	95.02	1.19	-7.5	$3.08^{+3.32}_{-0.36}$
126.0	91.91	$^{+0.6}_{-0.8}$	$\pm 1.6 / \pm 0.9 / \pm 1.8$	94.74	1.17	-7.5	$3.08^{+3.32}_{-0.36}$
126.5	90.77	$^{+0.6}_{-0.7}$	$\pm 1.6 / \pm 0.9 / \pm 1.8$	93.56	1.16	-7.5	$3.07^{+3.31}_{-0.36}$
127.0	89.75	$^{+0.5}_{-0.7}$	$\pm 1.6 / \pm 0.9 / \pm 1.8$	92.48	1.16	-7.5	$3.06^{+3.31}_{-0.36}$
127.5	88.58	$^{+0.6}_{-0.7}$	$\pm 1.6 / \pm 0.9 / \pm 1.8$	91.26	1.14	-7.5	$3.06^{+3.30}_{-0.36}$
128.0	87.54	$^{+0.5}_{-0.7}$	$\pm 1.6 / \pm 0.9 / \pm 1.8$	90.18	1.13	-7.6	$3.05^{+3.30}_{-0.36}$
128.5	86.47	$^{+0.6}_{-0.7}$	$\pm 1.6 / \pm 0.9 / \pm 1.8$	89.07	1.12	-7.6	$3.04^{+3.29}_{-0.35}$
129.0	85.45	$^{+0.5}_{-0.7}$	$\pm 1.6 / \pm 0.9 / \pm 1.8$	88.00	1.11	-7.6	$3.04^{+3.29}_{-0.35}$
129.5	84.44	$^{+0.5}_{-0.7}$	$\pm 1.6 / \pm 0.9 / \pm 1.8$	86.96	1.10	-7.6	$3.03^{+3.28}_{-0.35}$
130.0	83.49	$^{+0.4}_{-0.8}$	$\pm 1.6 / \pm 0.9 / \pm 1.8$	85.97	1.09	-7.7	$3.02^{+3.28}_{-0.35}$

Table B.4: Total $W^+(\rightarrow l^+ \nu_l)H$ cross sections including QCD and EW corrections and their uncertainties for a proton–proton collision energy $\sqrt{s} = 14$ TeV and a Higgs-boson masses.

M_H [GeV]	σ [fb]	$\Delta_{\text{scale}}[\%]$	$\Delta_{\text{PDF}/\alpha_s/\text{PDF}+\alpha_s}[\%]$	σ_{NNLOQCD} [fb]	$\sigma_{\text{t-loop}}$ [fb]	$\delta_{\text{EW}}[\%]$	σ_γ [fb]
120.0	117.37	$+0.5$ -0.6	$\pm 1.5 / \pm 0.9 / \pm 1.8$	120.96	1.48	-7.2	$3.63^{+3.80}_{-0.43}$
120.5	115.95	$+0.4$ -0.7	$\pm 1.5 / \pm 0.9 / \pm 1.8$	119.46	1.48	-7.2	$3.62^{+3.79}_{-0.43}$
121.0	114.51	$+0.5$ -0.7	$\pm 1.5 / \pm 0.9 / \pm 1.8$	117.96	1.47	-7.2	$3.61^{+3.78}_{-0.43}$
121.5	112.91	$+0.5$ -0.6	$\pm 1.5 / \pm 0.9 / \pm 1.8$	116.32	1.44	-7.3	$3.60^{+3.77}_{-0.43}$
122.0	111.56	$+0.4$ -0.6	$\pm 1.5 / \pm 0.9 / \pm 1.8$	114.90	1.44	-7.3	$3.60^{+3.77}_{-0.43}$
122.5	110.21	$+0.4$ -0.8	$\pm 1.5 / \pm 0.9 / \pm 1.8$	113.50	1.42	-7.3	$3.59^{+3.76}_{-0.43}$
123.0	108.86	$+0.5$ -0.8	$\pm 1.5 / \pm 0.9 / \pm 1.8$	112.10	1.40	-7.3	$3.58^{+3.75}_{-0.43}$
123.5	107.39	$+0.6$ -0.6	$\pm 1.5 / \pm 0.9 / \pm 1.8$	110.56	1.39	-7.4	$3.57^{+3.74}_{-0.43}$
124.0	106.19	$+0.5$ -0.7	$\pm 1.5 / \pm 0.9 / \pm 1.8$	109.32	1.38	-7.4	$3.56^{+3.73}_{-0.43}$
124.1	105.94	$+0.5$ -0.7	$\pm 1.5 / \pm 0.9 / \pm 1.8$	109.06	1.38	-7.4	$3.56^{+3.73}_{-0.43}$
124.2	105.73	$+0.3$ -0.7	$\pm 1.5 / \pm 0.9 / \pm 1.8$	108.84	1.37	-7.4	$3.56^{+3.73}_{-0.43}$
124.3	105.47	$+0.3$ -0.8	$\pm 1.5 / \pm 0.9 / \pm 1.8$	108.56	1.37	-7.4	$3.56^{+3.73}_{-0.43}$
124.4	105.12	$+0.4$ -0.6	$\pm 1.5 / \pm 0.9 / \pm 1.8$	108.20	1.37	-7.4	$3.56^{+3.73}_{-0.43}$
124.5	104.93	$+0.4$ -0.8	$\pm 1.5 / \pm 0.9 / \pm 1.8$	108.01	1.36	-7.4	$3.55^{+3.73}_{-0.43}$
124.6	104.62	$+0.5$ -0.7	$\pm 1.5 / \pm 0.9 / \pm 1.8$	107.70	1.36	-7.4	$3.55^{+3.72}_{-0.43}$
124.7	104.44	$+0.4$ -0.8	$\pm 1.5 / \pm 0.9 / \pm 1.8$	107.51	1.36	-7.4	$3.55^{+3.72}_{-0.43}$
124.8	104.10	$+0.4$ -0.7	$\pm 1.5 / \pm 0.9 / \pm 1.8$	107.15	1.35	-7.4	$3.55^{+3.72}_{-0.43}$
124.9	103.93	$+0.3$ -0.8	$\pm 1.5 / \pm 0.9 / \pm 1.8$	106.97	1.35	-7.4	$3.55^{+3.72}_{-0.43}$
125.0	103.63	$+0.3$ -0.8	$\pm 1.5 / \pm 0.9 / \pm 1.8$	106.65	1.36	-7.4	$3.55^{+3.72}_{-0.43}$
125.09	103.40	$+0.4$ -0.8	$\pm 1.5 / \pm 0.9 / \pm 1.8$	106.42	1.35	-7.4	$3.54^{+3.72}_{-0.43}$
125.1	103.37	$+0.4$ -0.8	$\pm 1.5 / \pm 0.9 / \pm 1.8$	106.39	1.35	-7.4	$3.54^{+3.72}_{-0.43}$
125.2	103.06	$+0.5$ -0.7	$\pm 1.5 / \pm 0.9 / \pm 1.8$	106.06	1.34	-7.4	$3.54^{+3.71}_{-0.43}$
125.3	102.91	$+0.3$ -0.9	$\pm 1.5 / \pm 0.9 / \pm 1.8$	105.91	1.34	-7.4	$3.54^{+3.71}_{-0.43}$
125.4	102.56	$+0.4$ -0.7	$\pm 1.5 / \pm 0.9 / \pm 1.8$	105.56	1.33	-7.5	$3.54^{+3.71}_{-0.43}$
125.5	102.31	$+0.4$ -0.7	$\pm 1.5 / \pm 0.9 / \pm 1.8$	105.27	1.34	-7.5	$3.54^{+3.71}_{-0.43}$
125.6	101.97	$+0.6$ -0.6	$\pm 1.5 / \pm 0.9 / \pm 1.8$	104.91	1.34	-7.5	$3.53^{+3.71}_{-0.42}$
125.7	101.78	$+0.6$ -0.7	$\pm 1.5 / \pm 0.9 / \pm 1.8$	104.73	1.33	-7.5	$3.53^{+3.70}_{-0.42}$
125.8	101.60	$+0.4$ -0.7	$\pm 1.5 / \pm 0.9 / \pm 1.8$	104.54	1.33	-7.5	$3.53^{+3.70}_{-0.42}$
125.9	101.32	$+0.4$ -0.7	$\pm 1.5 / \pm 0.9 / \pm 1.8$	104.27	1.32	-7.5	$3.53^{+3.70}_{-0.42}$
126.0	101.08	$+0.5$ -0.7	$\pm 1.5 / \pm 0.9 / \pm 1.8$	104.01	1.33	-7.5	$3.53^{+3.70}_{-0.42}$
126.5	99.82	$+0.5$ -0.7	$\pm 1.5 / \pm 0.9 / \pm 1.8$	102.70	1.31	-7.5	$3.52^{+3.69}_{-0.42}$
127.0	98.61	$+0.4$ -0.7	$\pm 1.5 / \pm 0.9 / \pm 1.8$	101.44	1.30	-7.5	$3.51^{+3.68}_{-0.42}$
127.5	97.44	$+0.4$ -0.7	$\pm 1.5 / \pm 0.9 / \pm 1.8$	100.23	1.28	-7.6	$3.50^{+3.67}_{-0.42}$
128.0	96.21	$+0.5$ -0.7	$\pm 1.5 / \pm 0.9 / \pm 1.8$	98.95	1.27	-7.6	$3.49^{+3.66}_{-0.42}$
128.5	95.11	$+0.4$ -0.8	$\pm 1.5 / \pm 0.9 / \pm 1.8$	97.81	1.26	-7.6	$3.48^{+3.65}_{-0.41}$
129.0	94.00	$+0.5$ -0.8	$\pm 1.5 / \pm 0.9 / \pm 1.8$	96.67	1.25	-7.6	$3.47^{+3.64}_{-0.41}$
129.5	92.83	$+0.5$ -0.7	$\pm 1.5 / \pm 0.9 / \pm 1.8$	95.44	1.24	-7.7	$3.46^{+3.63}_{-0.41}$
130.0	91.71	$+0.5$ -0.7	$\pm 1.5 / \pm 0.9 / \pm 1.8$	94.30	1.22	-7.7	$3.46^{+3.63}_{-0.41}$

Table B.5: Total $W^- \rightarrow l^- \bar{\nu}_l H$ cross sections including QCD and EW corrections and their uncertainties for a proton–proton collision energy $\sqrt{s} = 7$ TeV and a Higgs-boson masses.

M_H [GeV]	σ [fb]	$\Delta_{\text{scale}}[\%]$	$\Delta_{\text{PDF}/\alpha_s/\text{PDF}+\alpha_s}[\%]$	$\sigma_{\text{NNLOQCD}}^{\text{DY}}$ [fb]	$\sigma_{\text{t-loop}}$ [fb]	$\delta_{\text{EW}}[\%]$	σ_γ [fb]
120.0	26.48	$+0.6$ -0.8	$\pm 2.2/\pm 0.6/\pm 2.3$	27.56	0.27	-6.8	$0.52^{+0.72}_{-0.05}$
120.5	26.10	$+0.6$ -0.8	$\pm 2.2/\pm 0.6/\pm 2.3$	27.17	0.27	-6.8	$0.52^{+0.72}_{-0.05}$
121.0	25.74	$+0.6$ -0.8	$\pm 2.2/\pm 0.6/\pm 2.3$	26.80	0.26	-6.9	$0.52^{+0.72}_{-0.05}$
121.5	25.38	$+0.6$ -0.9	$\pm 2.2/\pm 0.6/\pm 2.3$	26.42	0.26	-6.9	$0.52^{+0.71}_{-0.05}$
122.0	25.03	$+0.7$ -0.9	$\pm 2.2/\pm 0.6/\pm 2.3$	26.06	0.26	-6.9	$0.52^{+0.71}_{-0.05}$
122.5	24.68	$+0.6$ -0.8	$\pm 2.2/\pm 0.6/\pm 2.3$	25.69	0.25	-6.9	$0.52^{+0.71}_{-0.05}$
123.0	24.35	$+0.6$ -0.8	$\pm 2.2/\pm 0.6/\pm 2.3$	25.34	0.25	-7.0	$0.51^{+0.70}_{-0.05}$
123.5	24.02	$+0.6$ -0.9	$\pm 2.2/\pm 0.6/\pm 2.3$	25.00	0.25	-7.0	$0.51^{+0.70}_{-0.05}$
124.0	23.69	$+0.5$ -0.9	$\pm 2.2/\pm 0.6/\pm 2.3$	24.66	0.25	-7.0	$0.51^{+0.70}_{-0.05}$
124.1	23.63	$+0.5$ -0.9	$\pm 2.2/\pm 0.6/\pm 2.3$	24.59	0.25	-7.0	$0.51^{+0.70}_{-0.05}$
124.2	23.57	$+0.5$ -0.9	$\pm 2.2/\pm 0.6/\pm 2.3$	24.53	0.24	-7.0	$0.51^{+0.69}_{-0.05}$
124.3	23.49	$+0.6$ -0.8	$\pm 2.2/\pm 0.6/\pm 2.3$	24.45	0.24	-7.0	$0.51^{+0.69}_{-0.05}$
124.4	23.42	$+0.6$ -0.8	$\pm 2.2/\pm 0.6/\pm 2.3$	24.38	0.24	-7.0	$0.51^{+0.69}_{-0.05}$
124.5	23.38	$+0.5$ -0.9	$\pm 2.2/\pm 0.6/\pm 2.3$	24.33	0.24	-7.0	$0.51^{+0.69}_{-0.05}$
124.6	23.30	$+0.6$ -0.9	$\pm 2.2/\pm 0.6/\pm 2.3$	24.25	0.24	-7.0	$0.51^{+0.69}_{-0.05}$
124.7	23.24	$+0.6$ -0.9	$\pm 2.2/\pm 0.6/\pm 2.3$	24.18	0.24	-7.0	$0.51^{+0.69}_{-0.05}$
124.8	23.17	$+0.6$ -0.9	$\pm 2.2/\pm 0.6/\pm 2.3$	24.12	0.24	-7.0	$0.51^{+0.69}_{-0.05}$
124.9	23.11	$+0.6$ -0.9	$\pm 2.2/\pm 0.6/\pm 2.3$	24.05	0.24	-7.0	$0.51^{+0.69}_{-0.05}$
125.0	23.04	$+0.6$ -0.8	$\pm 2.2/\pm 0.6/\pm 2.3$	23.98	0.24	-7.0	$0.51^{+0.69}_{-0.05}$
125.09	22.98	$+0.6$ -0.8	$\pm 2.2/\pm 0.6/\pm 2.3$	23.92	0.24	-7.0	$0.51^{+0.69}_{-0.05}$
125.1	22.97	$+0.6$ -0.8	$\pm 2.2/\pm 0.6/\pm 2.3$	23.91	0.24	-7.1	$0.51^{+0.69}_{-0.05}$
125.2	22.90	$+0.7$ -0.9	$\pm 2.2/\pm 0.6/\pm 2.3$	23.84	0.24	-7.1	$0.51^{+0.69}_{-0.05}$
125.3	22.85	$+0.6$ -0.9	$\pm 2.2/\pm 0.6/\pm 2.3$	23.78	0.24	-7.0	$0.51^{+0.69}_{-0.05}$
125.4	22.78	$+0.6$ -0.9	$\pm 2.2/\pm 0.6/\pm 2.3$	23.71	0.24	-7.1	$0.51^{+0.69}_{-0.05}$
125.5	22.72	$+0.6$ -0.9	$\pm 2.2/\pm 0.6/\pm 2.3$	23.65	0.24	-7.1	$0.51^{+0.69}_{-0.05}$
125.6	22.66	$+0.6$ -0.9	$\pm 2.2/\pm 0.6/\pm 2.3$	23.58	0.24	-7.1	$0.51^{+0.69}_{-0.05}$
125.7	22.59	$+0.6$ -0.8	$\pm 2.2/\pm 0.6/\pm 2.3$	23.51	0.24	-7.1	$0.50^{+0.69}_{-0.05}$
125.8	22.54	$+0.6$ -0.8	$\pm 2.3/\pm 0.6/\pm 2.3$	23.46	0.23	-7.1	$0.50^{+0.68}_{-0.05}$
125.9	22.48	$+0.6$ -0.9	$\pm 2.3/\pm 0.6/\pm 2.3$	23.40	0.23	-7.1	$0.50^{+0.68}_{-0.05}$
126.0	22.41	$+0.7$ -0.8	$\pm 2.3/\pm 0.6/\pm 2.3$	23.32	0.23	-7.1	$0.50^{+0.68}_{-0.05}$
126.5	22.11	$+0.6$ -0.9	$\pm 2.3/\pm 0.6/\pm 2.3$	23.01	0.23	-7.1	$0.50^{+0.68}_{-0.05}$
127.0	21.82	$+0.6$ -1.0	$\pm 2.3/\pm 0.6/\pm 2.3$	22.71	0.23	-7.1	$0.50^{+0.68}_{-0.05}$
127.5	21.52	$+0.6$ -0.9	$\pm 2.3/\pm 0.6/\pm 2.4$	22.40	0.23	-7.2	$0.50^{+0.68}_{-0.05}$
128.0	21.22	$+0.7$ -0.9	$\pm 2.3/\pm 0.6/\pm 2.4$	22.08	0.22	-7.2	$0.50^{+0.67}_{-0.05}$
128.5	20.94	$+0.7$ -0.9	$\pm 2.3/\pm 0.6/\pm 2.4$	21.79	0.22	-7.2	$0.49^{+0.67}_{-0.05}$
129.0	20.65	$+0.6$ -0.9	$\pm 2.3/\pm 0.6/\pm 2.4$	21.49	0.22	-7.2	$0.49^{+0.67}_{-0.05}$
129.5	20.39	$+0.6$ -0.9	$\pm 2.3/\pm 0.6/\pm 2.4$	21.22	0.22	-7.2	$0.49^{+0.66}_{-0.05}$
130.0	20.10	$+0.7$ -0.9	$\pm 2.3/\pm 0.6/\pm 2.4$	20.92	0.21	-7.3	$0.49^{+0.66}_{-0.05}$

Table B.6: Total $W^- \rightarrow l^- \bar{\nu}_l H$ cross sections including QCD and EW corrections and their uncertainties for a proton–proton collision energy $\sqrt{s} = 8$ TeV and a Higgs-boson masses.

M_H [GeV]	σ [fb]	$\Delta_{\text{scale}}[\%]$	$\Delta_{\text{PDF}/\alpha_s/\text{PDF}+\alpha_s}[\%]$	σ_{NNLOQCD} [fb]	$\sigma_{\text{t-loop}}$ [fb]	$\delta_{\text{EW}}[\%]$	σ_γ [fb]
120.0	32.88	+0.5 -0.9	$\pm 2.1/\pm 0.6/\pm 2.2$	34.15	0.35	-6.9	$0.72^{+0.98}_{-0.07}$
120.5	32.41	+0.5 -0.8	$\pm 2.1/\pm 0.6/\pm 2.2$	33.66	0.35	-6.9	$0.72^{+0.98}_{-0.07}$
121.0	31.96	+0.6 -0.8	$\pm 2.1/\pm 0.6/\pm 2.2$	33.20	0.34	-6.9	$0.72^{+0.97}_{-0.07}$
121.5	31.51	+0.5 -0.8	$\pm 2.1/\pm 0.6/\pm 2.2$	32.73	0.34	-6.9	$0.72^{+0.97}_{-0.07}$
122.0	31.09	+0.5 -0.8	$\pm 2.1/\pm 0.6/\pm 2.2$	32.29	0.34	-7.0	$0.71^{+0.97}_{-0.07}$
122.5	30.67	+0.5 -0.8	$\pm 2.1/\pm 0.6/\pm 2.2$	31.85	0.33	-7.0	$0.71^{+0.96}_{-0.07}$
123.0	30.23	+0.6 -0.8	$\pm 2.1/\pm 0.6/\pm 2.2$	31.39	0.33	-7.0	$0.71^{+0.96}_{-0.07}$
123.5	29.81	+0.6 -0.8	$\pm 2.1/\pm 0.6/\pm 2.2$	30.96	0.32	-7.0	$0.70^{+0.95}_{-0.07}$
124.0	29.44	+0.5 -0.8	$\pm 2.1/\pm 0.6/\pm 2.2$	30.57	0.32	-7.1	$0.70^{+0.95}_{-0.07}$
124.1	29.34	+0.5 -0.8	$\pm 2.1/\pm 0.6/\pm 2.2$	30.48	0.32	-7.1	$0.70^{+0.95}_{-0.07}$
124.2	29.27	+0.5 -0.9	$\pm 2.1/\pm 0.6/\pm 2.2$	30.40	0.32	-7.0	$0.70^{+0.95}_{-0.07}$
124.3	29.20	+0.5 -0.9	$\pm 2.1/\pm 0.6/\pm 2.2$	30.32	0.32	-7.1	$0.70^{+0.95}_{-0.07}$
124.4	29.12	+0.5 -0.9	$\pm 2.1/\pm 0.6/\pm 2.2$	30.24	0.32	-7.1	$0.70^{+0.95}_{-0.07}$
124.5	29.03	+0.5 -0.8	$\pm 2.1/\pm 0.6/\pm 2.2$	30.14	0.32	-7.1	$0.70^{+0.95}_{-0.07}$
124.6	28.96	+0.5 -0.8	$\pm 2.1/\pm 0.6/\pm 2.2$	30.07	0.32	-7.1	$0.70^{+0.95}_{-0.07}$
124.7	28.87	+0.6 -0.8	$\pm 2.1/\pm 0.6/\pm 2.2$	29.98	0.32	-7.1	$0.70^{+0.95}_{-0.07}$
124.8	28.79	+0.6 -0.8	$\pm 2.1/\pm 0.6/\pm 2.2$	29.90	0.31	-7.1	$0.70^{+0.94}_{-0.07}$
124.9	28.70	+0.6 -0.8	$\pm 2.1/\pm 0.6/\pm 2.1$	29.80	0.31	-7.1	$0.70^{+0.94}_{-0.07}$
125.0	28.62	+0.6 -0.8	$\pm 2.1/\pm 0.6/\pm 2.1$	29.71	0.31	-7.1	$0.70^{+0.94}_{-0.07}$
125.09	28.55	+0.6 -0.7	$\pm 2.1/\pm 0.6/\pm 2.1$	29.64	0.31	-7.1	$0.70^{+0.94}_{-0.07}$
125.1	28.55	+0.6 -0.7	$\pm 2.1/\pm 0.6/\pm 2.1$	29.64	0.31	-7.1	$0.70^{+0.94}_{-0.07}$
125.2	28.48	+0.6 -0.8	$\pm 2.1/\pm 0.6/\pm 2.2$	29.57	0.31	-7.1	$0.70^{+0.94}_{-0.07}$
125.3	28.41	+0.5 -0.8	$\pm 2.1/\pm 0.6/\pm 2.2$	29.50	0.31	-7.1	$0.70^{+0.94}_{-0.07}$
125.4	28.32	+0.6 -0.8	$\pm 2.1/\pm 0.6/\pm 2.2$	29.40	0.31	-7.1	$0.69^{+0.94}_{-0.07}$
125.5	28.24	+0.6 -0.7	$\pm 2.1/\pm 0.6/\pm 2.2$	29.33	0.31	-7.1	$0.69^{+0.94}_{-0.07}$
125.6	28.16	+0.6 -0.8	$\pm 2.1/\pm 0.6/\pm 2.2$	29.24	0.31	-7.1	$0.69^{+0.94}_{-0.07}$
125.7	28.09	+0.6 -0.8	$\pm 2.1/\pm 0.6/\pm 2.2$	29.17	0.31	-7.1	$0.69^{+0.94}_{-0.07}$
125.8	28.01	+0.6 -0.7	$\pm 2.1/\pm 0.6/\pm 2.2$	29.08	0.31	-7.1	$0.69^{+0.94}_{-0.07}$
125.9	27.94	+0.6 -0.7	$\pm 2.1/\pm 0.6/\pm 2.2$	29.00	0.31	-7.1	$0.69^{+0.94}_{-0.07}$
126.0	27.87	+0.6 -0.8	$\pm 2.1/\pm 0.6/\pm 2.2$	28.93	0.31	-7.1	$0.69^{+0.94}_{-0.07}$
126.5	27.52	+0.5 -0.8	$\pm 2.1/\pm 0.6/\pm 2.2$	28.57	0.30	-7.2	$0.69^{+0.94}_{-0.07}$
127.0	27.14	+0.6 -0.8	$\pm 2.1/\pm 0.6/\pm 2.2$	28.18	0.30	-7.2	$0.69^{+0.93}_{-0.07}$
127.5	26.79	+0.5 -0.8	$\pm 2.1/\pm 0.6/\pm 2.2$	27.81	0.30	-7.2	$0.69^{+0.93}_{-0.07}$
128.0	26.43	+0.6 -0.9	$\pm 2.1/\pm 0.6/\pm 2.2$	27.44	0.29	-7.2	$0.68^{+0.93}_{-0.07}$
128.5	26.06	+0.6 -0.8	$\pm 2.1/\pm 0.6/\pm 2.2$	27.06	0.29	-7.3	$0.68^{+0.92}_{-0.07}$
129.0	25.74	+0.6 -0.8	$\pm 2.1/\pm 0.6/\pm 2.2$	26.71	0.29	-7.3	$0.68^{+0.92}_{-0.06}$
129.5	25.39	+0.5 -0.8	$\pm 2.1/\pm 0.6/\pm 2.2$	26.36	0.28	-7.3	$0.68^{+0.92}_{-0.06}$
130.0	25.05	+0.6 -0.8	$\pm 2.1/\pm 0.6/\pm 2.2$	26.01	0.28	-7.3	$0.68^{+0.92}_{-0.06}$

Table B.7: Total $W^- \rightarrow l^-\bar{\nu}_l H$ cross sections including QCD and EW corrections and their uncertainties for a proton–proton collision energy $\sqrt{s} = 13$ TeV and a Higgs-boson masses.

M_H [GeV]	σ [fb]	$\Delta_{\text{scale}}[\%]$	$\Delta_{\text{PDF}/\alpha_s/\text{PDF}+\alpha_s}[\%]$	σ_{NNLOQCD} [fb]	$\sigma_{\text{t-loop}}$ [fb]	$\delta_{\text{EW}}[\%]$	σ_γ [fb]
120.0	68.17	+0.4 -0.6	$\pm 1.7/\pm 0.9/\pm 1.9$	70.18	0.86	-7.0	$2.05^{+2.38}_{-0.23}$
120.5	67.25	+0.5 -0.6	$\pm 1.7/\pm 0.8/\pm 1.9$	69.22	0.85	-7.0	$2.05^{+2.37}_{-0.23}$
121.0	66.35	+0.5 -0.6	$\pm 1.8/\pm 0.8/\pm 1.9$	68.29	0.85	-7.1	$2.04^{+2.37}_{-0.23}$
121.5	65.48	+0.5 -0.6	$\pm 1.8/\pm 0.8/\pm 1.9$	67.39	0.83	-7.1	$2.04^{+2.37}_{-0.23}$
122.0	64.60	+0.6 -0.6	$\pm 1.8/\pm 0.8/\pm 1.9$	66.46	0.83	-7.1	$2.03^{+2.36}_{-0.23}$
122.5	63.82	+0.4 -0.7	$\pm 1.8/\pm 0.8/\pm 2.0$	65.66	0.82	-7.1	$2.03^{+2.36}_{-0.23}$
123.0	62.99	+0.5 -0.6	$\pm 1.8/\pm 0.8/\pm 2.0$	64.80	0.81	-7.2	$2.02^{+2.36}_{-0.23}$
123.5	62.19	+0.5 -0.7	$\pm 1.8/\pm 0.8/\pm 2.0$	63.96	0.80	-7.2	$2.02^{+2.35}_{-0.22}$
124.0	61.33	+0.6 -0.6	$\pm 1.8/\pm 0.8/\pm 2.0$	63.08	0.79	-7.2	$2.01^{+2.35}_{-0.22}$
124.1	61.22	+0.5 -0.7	$\pm 1.8/\pm 0.8/\pm 2.0$	62.96	0.80	-7.2	$2.01^{+2.35}_{-0.22}$
124.2	61.04	+0.5 -0.6	$\pm 1.8/\pm 0.8/\pm 2.0$	62.76	0.79	-7.2	$2.01^{+2.35}_{-0.22}$
124.3	60.93	+0.5 -0.6	$\pm 1.8/\pm 0.8/\pm 2.0$	62.65	0.78	-7.2	$2.01^{+2.35}_{-0.22}$
124.4	60.78	+0.4 -0.7	$\pm 1.8/\pm 0.8/\pm 2.0$	62.49	0.79	-7.2	$2.01^{+2.35}_{-0.22}$
124.5	60.57	+0.6 -0.6	$\pm 1.8/\pm 0.8/\pm 2.0$	62.27	0.78	-7.2	$2.01^{+2.35}_{-0.22}$
124.6	60.47	+0.4 -0.7	$\pm 1.8/\pm 0.8/\pm 2.0$	62.17	0.79	-7.2	$2.01^{+2.35}_{-0.22}$
124.7	60.31	+0.4 -0.7	$\pm 1.8/\pm 0.8/\pm 2.0$	62.00	0.78	-7.2	$2.01^{+2.35}_{-0.22}$
124.8	60.18	+0.4 -0.7	$\pm 1.8/\pm 0.8/\pm 2.0$	61.87	0.78	-7.2	$2.01^{+2.34}_{-0.22}$
124.9	60.02	+0.3 -0.7	$\pm 1.8/\pm 0.8/\pm 2.0$	61.71	0.78	-7.2	$2.01^{+2.34}_{-0.22}$
125.0	59.83	+0.4 -0.7	$\pm 1.8/\pm 0.8/\pm 2.0$	61.51	0.78	-7.3	$2.00^{+2.34}_{-0.22}$
125.09	59.67	+0.4 -0.6	$\pm 1.8/\pm 0.8/\pm 2.0$	61.33	0.78	-7.2	$2.00^{+2.34}_{-0.22}$
125.1	59.66	+0.4 -0.6	$\pm 1.8/\pm 0.8/\pm 2.0$	61.34	0.77	-7.3	$2.00^{+2.34}_{-0.22}$
125.2	59.50	+0.5 -0.6	$\pm 1.8/\pm 0.8/\pm 2.0$	61.16	0.77	-7.3	$2.00^{+2.34}_{-0.22}$
125.3	59.33	+0.5 -0.6	$\pm 1.8/\pm 0.8/\pm 2.0$	60.99	0.77	-7.3	$2.00^{+2.34}_{-0.22}$
125.4	59.22	+0.5 -0.8	$\pm 1.8/\pm 0.8/\pm 2.0$	60.88	0.77	-7.3	$2.00^{+2.34}_{-0.22}$
125.5	59.08	+0.4 -0.7	$\pm 1.8/\pm 0.8/\pm 2.0$	60.74	0.77	-7.3	$2.00^{+2.34}_{-0.22}$
125.6	58.91	+0.4 -0.7	$\pm 1.8/\pm 0.8/\pm 2.0$	60.56	0.77	-7.3	$2.00^{+2.33}_{-0.22}$
125.7	58.76	+0.3 -0.7	$\pm 1.8/\pm 0.8/\pm 2.0$	60.41	0.77	-7.3	$2.00^{+2.33}_{-0.22}$
125.8	58.62	+0.4 -0.8	$\pm 1.8/\pm 0.8/\pm 2.0$	60.25	0.77	-7.3	$2.00^{+2.33}_{-0.22}$
125.9	58.45	+0.4 -0.7	$\pm 1.8/\pm 0.8/\pm 2.0$	60.07	0.76	-7.3	$1.99^{+2.33}_{-0.22}$
126.0	58.29	+0.5 -0.7	$\pm 1.8/\pm 0.8/\pm 2.0$	59.91	0.76	-7.3	$1.99^{+2.33}_{-0.22}$
126.5	57.59	+0.5 -0.7	$\pm 1.8/\pm 0.8/\pm 2.0$	59.18	0.75	-7.3	$1.99^{+2.32}_{-0.22}$
127.0	56.80	+0.5 -0.6	$\pm 1.8/\pm 0.8/\pm 1.9$	58.36	0.74	-7.3	$1.98^{+2.32}_{-0.22}$
127.5	56.12	+0.5 -0.6	$\pm 1.8/\pm 0.8/\pm 1.9$	57.66	0.74	-7.4	$1.98^{+2.31}_{-0.22}$
128.0	55.41	+0.4 -0.6	$\pm 1.8/\pm 0.8/\pm 1.9$	56.91	0.73	-7.4	$1.97^{+2.30}_{-0.22}$
128.5	54.74	+0.4 -0.7	$\pm 1.8/\pm 0.8/\pm 1.9$	56.22	0.72	-7.4	$1.97^{+2.29}_{-0.22}$
129.0	54.07	+0.4 -0.7	$\pm 1.8/\pm 0.8/\pm 1.9$	55.53	0.71	-7.4	$1.96^{+2.29}_{-0.21}$
129.5	53.38	+0.5 -0.7	$\pm 1.8/\pm 0.8/\pm 1.9$	54.81	0.71	-7.5	$1.96^{+2.28}_{-0.21}$
130.0	52.70	+0.5 -0.6	$\pm 1.8/\pm 0.8/\pm 1.9$	54.10	0.70	-7.5	$1.95^{+2.27}_{-0.21}$

Table B.8: Total $W^- \rightarrow l^-\bar{\nu}_l H$ cross sections including QCD and EW corrections and their uncertainties for a proton–proton collision energy $\sqrt{s} = 14$ TeV and a Higgs-boson masses.

M_H [GeV]	σ [fb]	$\Delta_{\text{scale}}[\%]$	$\Delta_{\text{PDF}/\alpha_s/\text{PDF}\oplus\alpha_s}[\%]$	$\sigma_{\text{NNLOQCD}}^{\text{DY}}$ [fb]	$\sigma_{\text{t-loop}}$ [fb]	$\delta_{\text{EW}}[\%]$	σ_γ [fb]
120.0	75.77	$+0.4$ -0.6	$\pm 1.7/\pm 0.8/\pm 1.9$	77.89	0.97	-7.0	$2.39^{+2.74}_{-0.26}$
120.5	74.76	$+0.4$ -0.6	$\pm 1.7/\pm 0.8/\pm 1.9$	76.82	0.98	-7.1	$2.38^{+2.73}_{-0.26}$
121.0	73.78	$+0.4$ -0.6	$\pm 1.7/\pm 0.8/\pm 1.9$	75.82	0.96	-7.1	$2.37^{+2.72}_{-0.26}$
121.5	72.89	$+0.3$ -0.7	$\pm 1.7/\pm 0.8/\pm 1.9$	74.91	0.95	-7.1	$2.37^{+2.71}_{-0.26}$
122.0	71.93	$+0.4$ -0.7	$\pm 1.7/\pm 0.8/\pm 1.9$	73.90	0.94	-7.1	$2.36^{+2.70}_{-0.26}$
122.5	71.01	$+0.5$ -0.7	$\pm 1.7/\pm 0.8/\pm 1.9$	72.94	0.93	-7.1	$2.35^{+2.69}_{-0.26}$
123.0	70.10	$+0.4$ -0.7	$\pm 1.7/\pm 0.8/\pm 1.9$	71.99	0.92	-7.2	$2.35^{+2.69}_{-0.26}$
123.5	69.18	$+0.4$ -0.7	$\pm 1.7/\pm 0.8/\pm 1.9$	71.04	0.91	-7.2	$2.34^{+2.68}_{-0.26}$
124.0	68.29	$+0.4$ -0.6	$\pm 1.7/\pm 0.8/\pm 1.9$	70.12	0.90	-7.2	$2.33^{+2.67}_{-0.26}$
124.1	68.11	$+0.4$ -0.6	$\pm 1.7/\pm 0.8/\pm 1.9$	69.94	0.90	-7.2	$2.33^{+2.67}_{-0.26}$
124.2	67.91	$+0.5$ -0.6	$\pm 1.7/\pm 0.8/\pm 1.9$	69.72	0.90	-7.2	$2.33^{+2.67}_{-0.26}$
124.3	67.76	$+0.5$ -0.6	$\pm 1.7/\pm 0.8/\pm 1.9$	69.57	0.90	-7.2	$2.33^{+2.67}_{-0.26}$
124.4	67.60	$+0.5$ -0.6	$\pm 1.7/\pm 0.8/\pm 1.9$	69.40	0.89	-7.2	$2.33^{+2.66}_{-0.26}$
124.5	67.42	$+0.4$ -0.7	$\pm 1.7/\pm 0.8/\pm 1.9$	69.22	0.89	-7.2	$2.33^{+2.66}_{-0.26}$
124.6	67.31	$+0.3$ -0.8	$\pm 1.7/\pm 0.9/\pm 1.9$	69.10	0.89	-7.2	$2.33^{+2.66}_{-0.26}$
124.7	67.07	$+0.4$ -0.6	$\pm 1.7/\pm 0.9/\pm 1.9$	68.85	0.89	-7.3	$2.33^{+2.66}_{-0.26}$
124.8	66.84	$+0.5$ -0.6	$\pm 1.7/\pm 0.9/\pm 1.9$	68.61	0.89	-7.3	$2.32^{+2.66}_{-0.26}$
124.9	66.67	$+0.5$ -0.5	$\pm 1.7/\pm 0.9/\pm 1.9$	68.44	0.89	-7.3	$2.32^{+2.66}_{-0.26}$
125.0	66.49	$+0.5$ -0.6	$\pm 1.7/\pm 0.9/\pm 1.9$	68.24	0.89	-7.3	$2.32^{+2.65}_{-0.26}$
125.09	66.33	$+0.5$ -0.5	$\pm 1.7/\pm 0.9/\pm 1.9$	68.09	0.88	-7.3	$2.32^{+2.65}_{-0.26}$
125.1	66.31	$+0.5$ -0.5	$\pm 1.7/\pm 0.9/\pm 1.9$	68.07	0.88	-7.3	$2.32^{+2.65}_{-0.26}$
125.2	66.23	$+0.4$ -0.7	$\pm 1.7/\pm 0.9/\pm 1.9$	67.98	0.88	-7.3	$2.32^{+2.65}_{-0.26}$
125.3	66.02	$+0.5$ -0.6	$\pm 1.7/\pm 0.9/\pm 1.9$	67.75	0.88	-7.3	$2.32^{+2.65}_{-0.26}$
125.4	65.86	$+0.4$ -0.6	$\pm 1.7/\pm 0.9/\pm 1.9$	67.60	0.88	-7.3	$2.32^{+2.65}_{-0.26}$
125.5	65.72	$+0.4$ -0.6	$\pm 1.7/\pm 0.9/\pm 1.9$	67.46	0.87	-7.3	$2.32^{+2.65}_{-0.26}$
125.6	65.55	$+0.3$ -0.6	$\pm 1.7/\pm 0.9/\pm 1.9$	67.28	0.87	-7.3	$2.32^{+2.65}_{-0.26}$
125.7	65.42	$+0.3$ -0.7	$\pm 1.7/\pm 0.9/\pm 1.9$	67.13	0.87	-7.3	$2.31^{+2.65}_{-0.26}$
125.8	65.22	$+0.4$ -0.7	$\pm 1.7/\pm 0.9/\pm 1.9$	66.92	0.87	-7.3	$2.31^{+2.65}_{-0.26}$
125.9	65.07	$+0.3$ -0.7	$\pm 1.7/\pm 0.9/\pm 1.9$	66.77	0.87	-7.3	$2.31^{+2.65}_{-0.25}$
126.0	64.93	$+0.3$ -0.7	$\pm 1.7/\pm 0.9/\pm 1.9$	66.62	0.87	-7.3	$2.31^{+2.65}_{-0.25}$
126.5	64.09	$+0.3$ -0.7	$\pm 1.7/\pm 0.9/\pm 1.9$	65.76	0.85	-7.3	$2.31^{+2.64}_{-0.25}$
127.0	63.21	$+0.4$ -0.6	$\pm 1.7/\pm 0.9/\pm 1.9$	64.84	0.85	-7.4	$2.30^{+2.64}_{-0.25}$
127.5	62.50	$+0.3$ -0.7	$\pm 1.7/\pm 0.9/\pm 1.9$	64.10	0.84	-7.4	$2.30^{+2.63}_{-0.25}$
128.0	61.68	$+0.5$ -0.7	$\pm 1.7/\pm 0.9/\pm 1.9$	63.25	0.83	-7.4	$2.29^{+2.63}_{-0.25}$
128.5	60.85	$+0.5$ -0.7	$\pm 1.7/\pm 0.9/\pm 1.9$	62.39	0.82	-7.4	$2.29^{+2.63}_{-0.25}$
129.0	60.11	$+0.5$ -0.6	$\pm 1.7/\pm 0.9/\pm 1.9$	61.62	0.82	-7.5	$2.28^{+2.62}_{-0.24}$
129.5	59.39	$+0.5$ -0.7	$\pm 1.7/\pm 0.9/\pm 1.9$	60.87	0.80	-7.5	$2.28^{+2.62}_{-0.24}$
130.0	58.70	$+0.4$ -0.7	$\pm 1.7/\pm 0.9/\pm 1.9$	60.16	0.80	-7.5	$2.27^{+2.61}_{-0.24}$

Table B.9: Total $Z(\rightarrow l^+l^-)H$ cross sections including QCD and EW corrections and their uncertainties for a proton–proton collision energy $\sqrt{s} = 7$ TeV and a Higgs-boson masses.

M_H [GeV]	σ [fb]	$\Delta_{\text{scale}}[\%]$	$\Delta_{\text{PDF}/\alpha_s/\text{PDF}+\alpha_s}[\%]$	$\sigma_{\text{NNLOQCD}}^{\text{DY}}[\text{fb}]$	$\sigma_{\text{NLO+NLL}}^{\text{ggZH}}$ [fb]	$\sigma_{\text{t-loop}}$ [fb]	$\delta_{\text{EW}}[\%]$	σ_γ [fb]
120.0	12.97	+2.5 -2.2	$\pm 1.6/\pm 0.7/\pm 1.7$	12.46	1.00	0.12	-5.1	$0.03^{+0.04}_{-0.00}$
120.5	12.81	+2.4 -2.2	$\pm 1.6/\pm 0.7/\pm 1.7$	12.29	0.99	0.12	-5.1	$0.03^{+0.04}_{-0.00}$
121.0	12.65	+2.5 -2.2	$\pm 1.6/\pm 0.7/\pm 1.7$	12.13	0.99	0.12	-5.1	$0.03^{+0.04}_{-0.00}$
121.5	12.48	+2.5 -2.2	$\pm 1.6/\pm 0.7/\pm 1.7$	11.96	0.98	0.12	-5.1	$0.03^{+0.04}_{-0.00}$
122.0	12.32	+2.6 -2.1	$\pm 1.6/\pm 0.7/\pm 1.7$	11.80	0.98	0.11	-5.1	$0.03^{+0.04}_{-0.00}$
122.5	12.17	+2.6 -2.2	$\pm 1.6/\pm 0.7/\pm 1.7$	11.65	0.97	0.11	-5.1	$0.03^{+0.04}_{-0.00}$
123.0	12.00	+2.7 -2.1	$\pm 1.6/\pm 0.7/\pm 1.7$	11.49	0.96	0.11	-5.1	$0.03^{+0.04}_{-0.00}$
123.5	11.85	+2.6 -2.2	$\pm 1.6/\pm 0.7/\pm 1.7$	11.34	0.96	0.11	-5.1	$0.03^{+0.04}_{-0.00}$
124.0	11.72	+2.6 -2.3	$\pm 1.6/\pm 0.7/\pm 1.7$	11.20	0.96	0.11	-5.1	$0.03^{+0.04}_{-0.00}$
124.1	11.69	+2.6 -2.3	$\pm 1.6/\pm 0.7/\pm 1.7$	11.17	0.95	0.11	-5.1	$0.03^{+0.04}_{-0.00}$
124.2	11.66	+2.5 -2.3	$\pm 1.6/\pm 0.7/\pm 1.7$	11.14	0.95	0.11	-5.1	$0.03^{+0.04}_{-0.00}$
124.3	11.63	+2.6 -2.3	$\pm 1.6/\pm 0.7/\pm 1.7$	11.11	0.95	0.11	-5.1	$0.03^{+0.04}_{-0.00}$
124.4	11.60	+2.5 -2.3	$\pm 1.6/\pm 0.7/\pm 1.7$	11.09	0.95	0.11	-5.1	$0.03^{+0.04}_{-0.00}$
124.5	11.57	+2.7 -2.3	$\pm 1.6/\pm 0.7/\pm 1.7$	11.05	0.95	0.11	-5.2	$0.03^{+0.04}_{-0.00}$
124.6	11.54	+2.6 -2.3	$\pm 1.6/\pm 0.7/\pm 1.7$	11.03	0.95	0.11	-5.2	$0.03^{+0.04}_{-0.00}$
124.7	11.51	+2.6 -2.3	$\pm 1.6/\pm 0.7/\pm 1.7$	11.00	0.95	0.11	-5.2	$0.03^{+0.04}_{-0.00}$
124.8	11.48	+2.6 -2.3	$\pm 1.6/\pm 0.7/\pm 1.7$	10.97	0.94	0.11	-5.2	$0.03^{+0.04}_{-0.00}$
124.9	11.46	+2.6 -2.3	$\pm 1.6/\pm 0.7/\pm 1.7$	10.94	0.94	0.11	-5.2	$0.03^{+0.04}_{-0.00}$
125.0	11.43	+2.6 -2.4	$\pm 1.6/\pm 0.7/\pm 1.7$	10.91	0.94	0.11	-5.2	$0.03^{+0.04}_{-0.00}$
125.09	11.40	+2.6 -2.3	$\pm 1.6/\pm 0.7/\pm 1.7$	10.88	0.94	0.11	-5.2	$0.03^{+0.04}_{-0.00}$
125.1	11.40	+2.6 -2.3	$\pm 1.6/\pm 0.7/\pm 1.7$	10.88	0.94	0.11	-5.2	$0.03^{+0.04}_{-0.00}$
125.2	11.37	+2.6 -2.3	$\pm 1.6/\pm 0.7/\pm 1.7$	10.85	0.94	0.11	-5.2	$0.03^{+0.04}_{-0.00}$
125.3	11.34	+2.7 -2.3	$\pm 1.6/\pm 0.7/\pm 1.7$	10.82	0.94	0.11	-5.2	$0.03^{+0.04}_{-0.00}$
125.4	11.31	+2.7 -2.3	$\pm 1.6/\pm 0.7/\pm 1.7$	10.80	0.94	0.11	-5.2	$0.03^{+0.04}_{-0.00}$
125.5	11.28	+2.6 -2.3	$\pm 1.6/\pm 0.7/\pm 1.7$	10.76	0.94	0.11	-5.2	$0.03^{+0.04}_{-0.00}$
125.6	11.25	+2.6 -2.3	$\pm 1.6/\pm 0.7/\pm 1.7$	10.73	0.94	0.11	-5.2	$0.03^{+0.04}_{-0.00}$
125.7	11.23	+2.6 -2.3	$\pm 1.6/\pm 0.7/\pm 1.7$	10.71	0.94	0.11	-5.2	$0.03^{+0.04}_{-0.00}$
125.8	11.20	+2.6 -2.3	$\pm 1.6/\pm 0.7/\pm 1.7$	10.68	0.94	0.11	-5.2	$0.03^{+0.04}_{-0.00}$
125.9	11.17	+2.6 -2.3	$\pm 1.6/\pm 0.7/\pm 1.7$	10.65	0.93	0.11	-5.2	$0.03^{+0.04}_{-0.00}$
126.0	11.14	+2.6 -2.3	$\pm 1.6/\pm 0.7/\pm 1.7$	10.63	0.93	0.10	-5.2	$0.03^{+0.04}_{-0.00}$
126.5	11.00	+2.7 -2.3	$\pm 1.6/\pm 0.7/\pm 1.7$	10.48	0.93	0.10	-5.2	$0.03^{+0.04}_{-0.00}$
127.0	10.87	+2.7 -2.3	$\pm 1.6/\pm 0.7/\pm 1.7$	10.35	0.92	0.10	-5.2	$0.03^{+0.04}_{-0.00}$
127.5	10.73	+2.7 -2.3	$\pm 1.6/\pm 0.7/\pm 1.7$	10.22	0.92	0.10	-5.2	$0.03^{+0.04}_{-0.00}$
128.0	10.60	+2.7 -2.3	$\pm 1.6/\pm 0.7/\pm 1.7$	10.08	0.91	0.10	-5.2	$0.03^{+0.04}_{-0.00}$
128.5	10.48	+2.7 -2.3	$\pm 1.6/\pm 0.7/\pm 1.7$	9.96	0.91	0.10	-5.2	$0.03^{+0.04}_{-0.00}$
129.0	10.35	+2.7 -2.3	$\pm 1.6/\pm 0.7/\pm 1.7$	9.84	0.90	0.10	-5.2	$0.03^{+0.04}_{-0.00}$
129.5	10.22	+2.7 -2.4	$\pm 1.6/\pm 0.7/\pm 1.7$	9.71	0.89	0.10	-5.2	$0.03^{+0.04}_{-0.00}$
130.0	10.10	+2.7 -2.4	$\pm 1.6/\pm 0.7/\pm 1.7$	9.59	0.89	0.10	-5.2	$0.03^{+0.04}_{-0.00}$

Table B.10: Total $Z(-l^+l^-)H$ cross sections including QCD and EW corrections and their uncertainties for a proton–proton collision energy $\sqrt{s} = 8$ TeV and a Higgs-boson masses.

M_H [GeV]	σ [fb]	$\Delta_{\text{scale}}[\%]$	$\Delta_{\text{PDF}/\alpha_s/\text{PDF} \oplus \alpha_s}[\%]$	$\sigma_{\text{NNLOQCD}}^{\text{DY}}[\text{fb}]$	$\sigma_{\text{NLO+NLL}}^{\text{ggZH}}$ [fb]	$\sigma_{\text{t-loop}}$ [fb]	$\delta_{\text{EW}}[\%]$	σ_γ [fb]
120.0	16.06	$^{+2.6}_{-2.4}$	$\pm 1.5/\pm 0.8/\pm 1.7$	15.24	1.41	0.15	-5.1	$0.04^{+0.05}_{-0.00}$
120.5	15.85	$^{+2.7}_{-2.3}$	$\pm 1.5/\pm 0.8/\pm 1.7$	15.03	1.40	0.15	-5.1	$0.04^{+0.05}_{-0.00}$
121.0	15.66	$^{+2.7}_{-2.3}$	$\pm 1.5/\pm 0.8/\pm 1.7$	14.84	1.39	0.15	-5.1	$0.04^{+0.05}_{-0.00}$
121.5	15.47	$^{+2.7}_{-2.3}$	$\pm 1.5/\pm 0.8/\pm 1.7$	14.65	1.38	0.15	-5.1	$0.04^{+0.05}_{-0.00}$
122.0	15.28	$^{+2.8}_{-2.4}$	$\pm 1.5/\pm 0.8/\pm 1.7$	14.46	1.38	0.15	-5.1	$0.04^{+0.05}_{-0.00}$
122.5	15.09	$^{+2.7}_{-2.4}$	$\pm 1.5/\pm 0.8/\pm 1.7$	14.27	1.37	0.14	-5.2	$0.04^{+0.05}_{-0.00}$
123.0	14.90	$^{+2.8}_{-2.4}$	$\pm 1.5/\pm 0.8/\pm 1.7$	14.08	1.36	0.14	-5.2	$0.04^{+0.05}_{-0.00}$
123.5	14.71	$^{+2.8}_{-2.4}$	$\pm 1.5/\pm 0.8/\pm 1.7$	13.90	1.35	0.14	-5.2	$0.04^{+0.05}_{-0.00}$
124.0	14.54	$^{+2.8}_{-2.4}$	$\pm 1.5/\pm 0.8/\pm 1.7$	13.72	1.35	0.14	-5.2	$0.04^{+0.05}_{-0.00}$
124.1	14.50	$^{+2.8}_{-2.4}$	$\pm 1.5/\pm 0.8/\pm 1.7$	13.68	1.34	0.14	-5.2	$0.04^{+0.05}_{-0.00}$
124.2	14.46	$^{+2.8}_{-2.4}$	$\pm 1.5/\pm 0.8/\pm 1.7$	13.65	1.34	0.14	-5.2	$0.04^{+0.05}_{-0.00}$
124.3	14.43	$^{+2.7}_{-2.4}$	$\pm 1.5/\pm 0.8/\pm 1.7$	13.62	1.34	0.14	-5.2	$0.04^{+0.05}_{-0.00}$
124.4	14.40	$^{+2.8}_{-2.5}$	$\pm 1.5/\pm 0.8/\pm 1.7$	13.58	1.34	0.14	-5.2	$0.04^{+0.05}_{-0.00}$
124.5	14.36	$^{+2.7}_{-2.5}$	$\pm 1.5/\pm 0.8/\pm 1.7$	13.55	1.34	0.14	-5.2	$0.04^{+0.05}_{-0.00}$
124.6	14.32	$^{+2.8}_{-2.5}$	$\pm 1.5/\pm 0.8/\pm 1.7$	13.51	1.34	0.14	-5.2	$0.04^{+0.05}_{-0.00}$
124.7	14.28	$^{+2.9}_{-2.4}$	$\pm 1.5/\pm 0.8/\pm 1.7$	13.47	1.33	0.14	-5.2	$0.04^{+0.05}_{-0.00}$
124.8	14.25	$^{+2.9}_{-2.4}$	$\pm 1.5/\pm 0.8/\pm 1.7$	13.43	1.33	0.14	-5.2	$0.04^{+0.05}_{-0.00}$
124.9	14.21	$^{+2.9}_{-2.4}$	$\pm 1.5/\pm 0.8/\pm 1.7$	13.40	1.33	0.14	-5.2	$0.04^{+0.05}_{-0.00}$
125.0	14.18	$^{+2.9}_{-2.4}$	$\pm 1.5/\pm 0.8/\pm 1.7$	13.36	1.33	0.14	-5.2	$0.04^{+0.05}_{-0.00}$
125.09	14.15	$^{+2.8}_{-2.4}$	$\pm 1.5/\pm 0.8/\pm 1.7$	13.34	1.33	0.14	-5.2	$0.04^{+0.05}_{-0.00}$
125.1	14.15	$^{+2.8}_{-2.5}$	$\pm 1.5/\pm 0.8/\pm 1.7$	13.34	1.33	0.14	-5.2	$0.04^{+0.05}_{-0.00}$
125.2	14.11	$^{+2.8}_{-2.5}$	$\pm 1.5/\pm 0.8/\pm 1.7$	13.30	1.33	0.14	-5.2	$0.04^{+0.05}_{-0.00}$
125.3	14.07	$^{+2.9}_{-2.4}$	$\pm 1.5/\pm 0.8/\pm 1.7$	13.26	1.33	0.14	-5.2	$0.04^{+0.05}_{-0.00}$
125.4	14.04	$^{+2.8}_{-2.4}$	$\pm 1.5/\pm 0.8/\pm 1.7$	13.23	1.32	0.14	-5.2	$0.04^{+0.05}_{-0.00}$
125.5	14.01	$^{+2.8}_{-2.5}$	$\pm 1.5/\pm 0.8/\pm 1.7$	13.20	1.32	0.14	-5.2	$0.04^{+0.05}_{-0.00}$
125.6	13.98	$^{+2.8}_{-2.5}$	$\pm 1.5/\pm 0.8/\pm 1.7$	13.16	1.32	0.13	-5.2	$0.04^{+0.05}_{-0.00}$
125.7	13.94	$^{+2.8}_{-2.5}$	$\pm 1.5/\pm 0.7/\pm 1.7$	13.13	1.32	0.14	-5.2	$0.04^{+0.05}_{-0.00}$
125.8	13.91	$^{+2.7}_{-2.6}$	$\pm 1.5/\pm 0.7/\pm 1.7$	13.10	1.32	0.14	-5.2	$0.04^{+0.05}_{-0.00}$
125.9	13.88	$^{+2.8}_{-2.6}$	$\pm 1.5/\pm 0.7/\pm 1.7$	13.07	1.32	0.14	-5.2	$0.04^{+0.05}_{-0.00}$
126.0	13.84	$^{+2.8}_{-2.5}$	$\pm 1.5/\pm 0.7/\pm 1.7$	13.03	1.32	0.13	-5.2	$0.04^{+0.05}_{-0.00}$
126.5	13.67	$^{+2.9}_{-2.5}$	$\pm 1.5/\pm 0.7/\pm 1.7$	12.86	1.31	0.13	-5.2	$0.04^{+0.05}_{-0.00}$
127.0	13.51	$^{+2.9}_{-2.5}$	$\pm 1.5/\pm 0.7/\pm 1.7$	12.70	1.30	0.13	-5.2	$0.04^{+0.05}_{-0.00}$
127.5	13.35	$^{+2.8}_{-2.6}$	$\pm 1.5/\pm 0.7/\pm 1.7$	12.54	1.29	0.13	-5.2	$0.04^{+0.05}_{-0.00}$
128.0	13.19	$^{+2.9}_{-2.6}$	$\pm 1.5/\pm 0.7/\pm 1.7$	12.38	1.29	0.13	-5.2	$0.04^{+0.05}_{-0.00}$
128.5	13.02	$^{+3.0}_{-2.5}$	$\pm 1.5/\pm 0.7/\pm 1.7$	12.22	1.28	0.13	-5.2	$0.04^{+0.05}_{-0.00}$
129.0	12.87	$^{+2.9}_{-2.6}$	$\pm 1.5/\pm 0.7/\pm 1.7$	12.07	1.27	0.13	-5.2	$0.04^{+0.05}_{-0.00}$
129.5	12.72	$^{+2.9}_{-2.6}$	$\pm 1.5/\pm 0.7/\pm 1.7$	11.92	1.26	0.13	-5.2	$0.04^{+0.05}_{-0.00}$
130.0	12.56	$^{+3.0}_{-2.6}$	$\pm 1.5/\pm 0.7/\pm 1.7$	11.77	1.25	0.12	-5.3	$0.04^{+0.05}_{-0.00}$

Table B.11: Total $Z(-l^+l^-)H$ cross sections including QCD and EW corrections and their uncertainties for a proton–proton collision energy $\sqrt{s} = 13$ TeV and a Higgs-boson masses.

M_H [GeV]	σ [fb]	$\Delta_{\text{scale}}[\%]$	$\Delta_{\text{PDF}/\alpha_s/\text{PDF}+\alpha_s}[\%]$	$\sigma_{\text{NNLOQCD}}^{\text{DY}}[\text{fb}]$	$\sigma_{\text{NLO+NLL}}^{\text{ggZH}}$ [fb]	$\sigma_{\text{t-loop}}$ [fb]	$\delta_{\text{EW}}[\%]$	σ_γ [fb]
120.0	33.52	+3.4 -3.0	$\pm 1.3/\pm 1.0/\pm 1.6$	30.24	4.38	0.35	-5.2	$0.11^{+0.13}_{-0.01}$
120.5	33.15	+3.4 -3.0	$\pm 1.3/\pm 1.0/\pm 1.6$	29.89	4.36	0.34	-5.2	$0.11^{+0.13}_{-0.01}$
121.0	32.73	+3.5 -3.0	$\pm 1.3/\pm 1.0/\pm 1.6$	29.49	4.32	0.34	-5.2	$0.11^{+0.13}_{-0.01}$
121.5	32.35	+3.6 -3.0	$\pm 1.3/\pm 1.0/\pm 1.6$	29.14	4.28	0.34	-5.2	$0.11^{+0.13}_{-0.01}$
122.0	31.99	+3.6 -3.0	$\pm 1.3/\pm 1.0/\pm 1.6$	28.75	4.29	0.33	-5.2	$0.11^{+0.13}_{-0.01}$
122.5	31.61	+3.6 -3.0	$\pm 1.3/\pm 0.9/\pm 1.6$	28.38	4.27	0.33	-5.2	$0.11^{+0.12}_{-0.01}$
123.0	31.25	+3.6 -3.1	$\pm 1.3/\pm 0.9/\pm 1.6$	28.05	4.23	0.33	-5.2	$0.11^{+0.12}_{-0.01}$
123.5	30.89	+3.5 -3.1	$\pm 1.3/\pm 0.9/\pm 1.6$	27.69	4.22	0.33	-5.2	$0.11^{+0.12}_{-0.01}$
124.0	30.53	+3.6 -3.1	$\pm 1.3/\pm 0.9/\pm 1.6$	27.34	4.19	0.32	-5.2	$0.11^{+0.12}_{-0.01}$
124.1	30.48	+3.7 -3.2	$\pm 1.3/\pm 0.9/\pm 1.6$	27.29	4.19	0.32	-5.3	$0.11^{+0.12}_{-0.01}$
124.2	30.39	+3.8 -3.0	$\pm 1.3/\pm 0.9/\pm 1.6$	27.20	4.19	0.32	-5.3	$0.11^{+0.12}_{-0.01}$
124.3	30.32	+3.7 -3.1	$\pm 1.3/\pm 0.9/\pm 1.6$	27.14	4.18	0.32	-5.3	$0.11^{+0.12}_{-0.01}$
124.4	30.24	+3.7 -3.0	$\pm 1.3/\pm 0.9/\pm 1.6$	27.06	4.17	0.32	-5.3	$0.11^{+0.12}_{-0.01}$
124.5	30.17	+3.8 -3.0	$\pm 1.3/\pm 0.9/\pm 1.6$	27.00	4.17	0.32	-5.3	$0.11^{+0.12}_{-0.01}$
124.6	30.10	+3.8 -3.0	$\pm 1.3/\pm 0.9/\pm 1.6$	26.93	4.16	0.32	-5.3	$0.11^{+0.12}_{-0.01}$
124.7	30.03	+3.8 -3.1	$\pm 1.3/\pm 0.9/\pm 1.6$	26.86	4.17	0.32	-5.3	$0.11^{+0.12}_{-0.01}$
124.8	29.97	+3.7 -3.1	$\pm 1.3/\pm 0.9/\pm 1.6$	26.81	4.15	0.32	-5.3	$0.11^{+0.12}_{-0.01}$
124.9	29.88	+3.9 -3.1	$\pm 1.3/\pm 0.9/\pm 1.6$	26.72	4.14	0.31	-5.3	$0.11^{+0.12}_{-0.01}$
125.0	29.82	+3.8 -3.1	$\pm 1.3/\pm 0.9/\pm 1.6$	26.66	4.14	0.31	-5.3	$0.11^{+0.12}_{-0.01}$
125.09	29.77	+3.8 -3.0	$\pm 1.3/\pm 0.9/\pm 1.6$	26.60	4.14	0.31	-5.3	$0.11^{+0.12}_{-0.01}$
125.1	29.75	+3.9 -3.0	$\pm 1.3/\pm 0.9/\pm 1.6$	26.59	4.14	0.32	-5.3	$0.11^{+0.12}_{-0.01}$
125.2	29.69	+3.8 -3.1	$\pm 1.3/\pm 0.9/\pm 1.6$	26.53	4.13	0.32	-5.3	$0.11^{+0.12}_{-0.01}$
125.3	29.63	+3.8 -3.1	$\pm 1.3/\pm 0.9/\pm 1.6$	26.47	4.13	0.31	-5.3	$0.11^{+0.12}_{-0.01}$
125.4	29.57	+3.8 -3.1	$\pm 1.3/\pm 0.9/\pm 1.6$	26.42	4.13	0.31	-5.3	$0.11^{+0.12}_{-0.01}$
125.5	29.50	+3.7 -3.1	$\pm 1.3/\pm 0.9/\pm 1.6$	26.34	4.12	0.31	-5.3	$0.11^{+0.12}_{-0.01}$
125.6	29.44	+3.8 -3.1	$\pm 1.3/\pm 0.9/\pm 1.6$	26.28	4.13	0.31	-5.3	$0.11^{+0.12}_{-0.01}$
125.7	29.36	+3.8 -3.0	$\pm 1.3/\pm 0.9/\pm 1.6$	26.22	4.11	0.31	-5.3	$0.11^{+0.12}_{-0.01}$
125.8	29.32	+3.7 -3.2	$\pm 1.3/\pm 0.9/\pm 1.6$	26.17	4.11	0.31	-5.3	$0.11^{+0.12}_{-0.01}$
125.9	29.24	+3.8 -3.1	$\pm 1.3/\pm 0.9/\pm 1.6$	26.09	4.11	0.31	-5.3	$0.11^{+0.12}_{-0.01}$
126.0	29.18	+3.8 -3.1	$\pm 1.3/\pm 0.9/\pm 1.6$	26.03	4.11	0.31	-5.3	$0.11^{+0.12}_{-0.01}$
126.5	28.84	+3.7 -3.2	$\pm 1.3/\pm 0.9/\pm 1.6$	25.70	4.09	0.31	-5.3	$0.11^{+0.12}_{-0.01}$
127.0	28.50	+3.7 -3.2	$\pm 1.3/\pm 0.9/\pm 1.6$	25.38	4.06	0.30	-5.3	$0.11^{+0.12}_{-0.01}$
127.5	28.17	+3.8 -3.2	$\pm 1.3/\pm 0.9/\pm 1.6$	25.05	4.04	0.30	-5.3	$0.11^{+0.12}_{-0.01}$
128.0	27.85	+3.9 -3.1	$\pm 1.3/\pm 0.9/\pm 1.6$	24.75	4.02	0.30	-5.3	$0.11^{+0.12}_{-0.01}$
128.5	27.54	+3.9 -3.2	$\pm 1.3/\pm 0.9/\pm 1.6$	24.46	3.98	0.29	-5.3	$0.11^{+0.12}_{-0.01}$
129.0	27.24	+3.8 -3.2	$\pm 1.3/\pm 0.9/\pm 1.6$	24.16	3.97	0.29	-5.3	$0.10^{+0.12}_{-0.01}$
129.5	26.93	+3.9 -3.2	$\pm 1.3/\pm 0.9/\pm 1.6$	23.85	3.95	0.29	-5.3	$0.10^{+0.12}_{-0.01}$
130.0	26.65	+3.9 -3.2	$\pm 1.3/\pm 0.9/\pm 1.6$	23.59	3.93	0.29	-5.3	$0.10^{+0.12}_{-0.01}$

Table B.12: Total $Z(-l^+l^-)H$ cross sections including QCD and EW corrections and their uncertainties for a proton–proton collision energy $\sqrt{s} = 14$ TeV and a Higgs-boson masses.

M_H [GeV]	σ [fb]	$\Delta_{\text{scale}}[\%]$	$\Delta_{\text{PDF}/\alpha_s/\text{PDF}+\alpha_s}[\%]$	$\sigma_{\text{NNLOQCD}}^{\text{DY}}[\text{fb}]$	$\sigma_{\text{NLO+NLL}}^{\text{ggZH}}$ [fb]	$\sigma_{\text{t-loop}}$ [fb]	$\delta_{\text{EW}}[\%]$	σ_γ [fb]
120.0	37.31	+3.6 -3.0	$\pm 1.3/\pm 1.0/\pm 1.7$	33.39	5.14	0.39	-5.2	$0.13^{+0.14}_{-0.01}$
120.5	36.90	+3.7 -3.1	$\pm 1.3/\pm 1.0/\pm 1.7$	32.99	5.12	0.39	-5.2	$0.13^{+0.14}_{-0.01}$
121.0	36.46	+3.6 -3.1	$\pm 1.3/\pm 1.0/\pm 1.7$	32.57	5.08	0.38	-5.2	$0.13^{+0.14}_{-0.01}$
121.5	36.06	+3.5 -3.1	$\pm 1.3/\pm 1.0/\pm 1.7$	32.17	5.07	0.38	-5.2	$0.13^{+0.14}_{-0.01}$
122.0	35.64	+3.6 -3.1	$\pm 1.3/\pm 1.0/\pm 1.7$	31.77	5.03	0.38	-5.2	$0.13^{+0.14}_{-0.01}$
122.5	35.25	+3.6 -3.2	$\pm 1.3/\pm 1.0/\pm 1.7$	31.39	5.00	0.37	-5.2	$0.13^{+0.14}_{-0.01}$
123.0	34.82	+3.8 -3.1	$\pm 1.3/\pm 1.0/\pm 1.6$	30.97	4.97	0.37	-5.2	$0.13^{+0.14}_{-0.01}$
123.5	34.41	+3.7 -3.1	$\pm 1.3/\pm 1.0/\pm 1.6$	30.58	4.94	0.37	-5.3	$0.13^{+0.14}_{-0.01}$
124.0	34.03	+3.8 -3.2	$\pm 1.3/\pm 1.0/\pm 1.6$	30.20	4.93	0.36	-5.3	$0.12^{+0.13}_{-0.01}$
124.1	33.95	+3.7 -3.2	$\pm 1.3/\pm 1.0/\pm 1.6$	30.13	4.92	0.36	-5.3	$0.12^{+0.13}_{-0.01}$
124.2	33.86	+3.7 -3.1	$\pm 1.3/\pm 1.0/\pm 1.6$	30.04	4.91	0.36	-5.3	$0.12^{+0.13}_{-0.01}$
124.3	33.80	+3.7 -3.2	$\pm 1.3/\pm 1.0/\pm 1.6$	29.97	4.92	0.36	-5.3	$0.12^{+0.13}_{-0.01}$
124.4	33.70	+3.8 -3.2	$\pm 1.3/\pm 1.0/\pm 1.6$	29.89	4.90	0.36	-5.3	$0.12^{+0.13}_{-0.01}$
124.5	33.65	+3.7 -3.3	$\pm 1.3/\pm 1.0/\pm 1.6$	29.84	4.90	0.36	-5.3	$0.12^{+0.13}_{-0.01}$
124.6	33.55	+3.8 -3.2	$\pm 1.3/\pm 1.0/\pm 1.6$	29.75	4.89	0.36	-5.3	$0.12^{+0.13}_{-0.01}$
124.7	33.49	+3.8 -3.3	$\pm 1.3/\pm 1.0/\pm 1.6$	29.68	4.89	0.36	-5.3	$0.12^{+0.13}_{-0.01}$
124.8	33.40	+3.8 -3.2	$\pm 1.3/\pm 1.0/\pm 1.6$	29.61	4.87	0.36	-5.3	$0.12^{+0.13}_{-0.01}$
124.9	33.32	+3.8 -3.2	$\pm 1.3/\pm 1.0/\pm 1.6$	29.52	4.87	0.36	-5.3	$0.12^{+0.13}_{-0.01}$
125.0	33.27	+3.8 -3.3	$\pm 1.3/\pm 1.0/\pm 1.6$	29.47	4.87	0.36	-5.3	$0.12^{+0.13}_{-0.01}$
125.09	33.19	+3.8 -3.2	$\pm 1.3/\pm 1.0/\pm 1.6$	29.39	4.87	0.36	-5.3	$0.12^{+0.13}_{-0.01}$
125.1	33.18	+3.9 -3.3	$\pm 1.3/\pm 1.0/\pm 1.6$	29.39	4.86	0.36	-5.3	$0.12^{+0.13}_{-0.01}$
125.2	33.11	+3.8 -3.2	$\pm 1.3/\pm 1.0/\pm 1.6$	29.31	4.87	0.35	-5.3	$0.12^{+0.13}_{-0.01}$
125.3	33.04	+3.8 -3.3	$\pm 1.3/\pm 1.0/\pm 1.6$	29.25	4.86	0.35	-5.3	$0.12^{+0.13}_{-0.01}$
125.4	32.96	+3.9 -3.2	$\pm 1.3/\pm 1.0/\pm 1.6$	29.17	4.85	0.35	-5.3	$0.12^{+0.13}_{-0.01}$
125.5	32.88	+3.9 -3.2	$\pm 1.3/\pm 1.0/\pm 1.6$	29.10	4.84	0.35	-5.3	$0.12^{+0.13}_{-0.01}$
125.6	32.82	+3.8 -3.3	$\pm 1.3/\pm 1.0/\pm 1.6$	29.04	4.84	0.35	-5.3	$0.12^{+0.13}_{-0.01}$
125.7	32.73	+3.9 -3.3	$\pm 1.3/\pm 1.0/\pm 1.6$	28.95	4.84	0.35	-5.3	$0.12^{+0.13}_{-0.01}$
125.8	32.65	+3.9 -3.2	$\pm 1.3/\pm 1.0/\pm 1.6$	28.87	4.83	0.35	-5.3	$0.12^{+0.13}_{-0.01}$
125.9	32.58	+3.9 -3.2	$\pm 1.3/\pm 1.0/\pm 1.6$	28.81	4.82	0.35	-5.3	$0.12^{+0.13}_{-0.01}$
126.0	32.48	+4.0 -3.2	$\pm 1.3/\pm 1.0/\pm 1.6$	28.71	4.82	0.35	-5.3	$0.12^{+0.13}_{-0.01}$
126.5	32.14	+4.0 -3.3	$\pm 1.3/\pm 1.0/\pm 1.6$	28.39	4.79	0.35	-5.3	$0.12^{+0.13}_{-0.01}$
127.0	31.79	+4.1 -3.3	$\pm 1.3/\pm 1.0/\pm 1.6$	28.04	4.77	0.34	-5.3	$0.12^{+0.13}_{-0.01}$
127.5	31.44	+4.0 -3.3	$\pm 1.3/\pm 1.0/\pm 1.6$	27.71	4.74	0.34	-5.3	$0.12^{+0.13}_{-0.01}$
128.0	31.07	+4.1 -3.2	$\pm 1.3/\pm 1.0/\pm 1.6$	27.36	4.71	0.34	-5.3	$0.12^{+0.13}_{-0.01}$
128.5	30.76	+4.0 -3.4	$\pm 1.3/\pm 1.0/\pm 1.6$	27.06	4.69	0.34	-5.3	$0.12^{+0.13}_{-0.01}$
129.0	30.44	+3.9 -3.4	$\pm 1.3/\pm 1.0/\pm 1.6$	26.75	4.66	0.33	-5.3	$0.12^{+0.13}_{-0.01}$
129.5	30.08	+3.9 -3.4	$\pm 1.3/\pm 1.0/\pm 1.6$	26.41	4.64	0.33	-5.3	$0.12^{+0.14}_{-0.01}$
130.0	29.72	+4.1 -3.4	$\pm 1.3/\pm 1.0/\pm 1.6$	26.07	4.60	0.32	-5.4	$0.12^{+0.14}_{-0.01}$

Table B.13: Total $Z(\rightarrow\nu\bar{\nu})H$ cross sections including QCD and EW corrections and their uncertainties for a proton–proton collision energy $\sqrt{s} = 7$ TeV and a Higgs-boson masses.

$M_H[\text{GeV}]$	$\sigma[\text{fb}]$	$\Delta_{\text{scale}}[\%]$	$\Delta_{\text{PDF}/\alpha_s/\text{PDF} \oplus \alpha_s}[\%]$	$\sigma_{\text{NNLOQCD}}^{\text{DY}}[\text{fb}]$	$\sigma_{\text{NLO+NLL}}^{\text{ggZH}}[\text{fb}]$	$\sigma_{\text{t-loop}}[\text{fb}]$	$\delta_{\text{EW}}[\%]$	$\sigma_\gamma[\text{fb}]$
120.0	77.40	$^{+2.5}_{-2.2}$	$\pm 1.6 / \pm 0.7 / \pm 1.7$	73.87	5.92	0.71	-4.2	-0.00
120.5	76.43	$^{+2.4}_{-2.2}$	$\pm 1.6 / \pm 0.7 / \pm 1.7$	72.90	5.89	0.70	-4.2	-0.00
121.0	75.46	$^{+2.5}_{-2.2}$	$\pm 1.6 / \pm 0.7 / \pm 1.7$	71.93	5.86	0.69	-4.2	-0.00
121.5	74.48	$^{+2.5}_{-2.2}$	$\pm 1.6 / \pm 0.7 / \pm 1.7$	70.95	5.83	0.69	-4.2	-0.00
122.0	73.51	$^{+2.6}_{-2.1}$	$\pm 1.6 / \pm 0.7 / \pm 1.7$	70.00	5.78	0.68	-4.2	-0.00
122.5	72.59	$^{+2.6}_{-2.2}$	$\pm 1.6 / \pm 0.7 / \pm 1.7$	69.08	5.76	0.67	-4.2	-0.00
123.0	71.62	$^{+2.7}_{-2.1}$	$\pm 1.6 / \pm 0.7 / \pm 1.7$	68.12	5.72	0.66	-4.2	-0.00
123.5	70.73	$^{+2.6}_{-2.2}$	$\pm 1.6 / \pm 0.7 / \pm 1.7$	67.24	5.68	0.66	-4.2	-0.00
124.0	69.90	$^{+2.6}_{-2.3}$	$\pm 1.6 / \pm 0.7 / \pm 1.7$	66.40	5.67	0.65	-4.2	-0.00
124.1	69.73	$^{+2.6}_{-2.3}$	$\pm 1.6 / \pm 0.7 / \pm 1.7$	66.23	5.66	0.65	-4.2	-0.00
124.2	69.58	$^{+2.5}_{-2.3}$	$\pm 1.6 / \pm 0.7 / \pm 1.7$	66.08	5.66	0.65	-4.2	-0.00
124.3	69.37	$^{+2.6}_{-2.3}$	$\pm 1.6 / \pm 0.7 / \pm 1.7$	65.88	5.64	0.65	-4.2	-0.00
124.4	69.23	$^{+2.5}_{-2.3}$	$\pm 1.6 / \pm 0.7 / \pm 1.7$	65.74	5.64	0.64	-4.2	-0.00
124.5	69.01	$^{+2.7}_{-2.3}$	$\pm 1.6 / \pm 0.7 / \pm 1.7$	65.52	5.63	0.64	-4.2	-0.00
124.6	68.88	$^{+2.6}_{-2.3}$	$\pm 1.6 / \pm 0.7 / \pm 1.7$	65.39	5.63	0.64	-4.2	-0.00
124.7	68.69	$^{+2.6}_{-2.3}$	$\pm 1.6 / \pm 0.7 / \pm 1.7$	65.21	5.61	0.64	-4.2	-0.00
124.8	68.50	$^{+2.6}_{-2.3}$	$\pm 1.6 / \pm 0.7 / \pm 1.7$	65.03	5.60	0.64	-4.3	-0.00
124.9	68.35	$^{+2.6}_{-2.3}$	$\pm 1.6 / \pm 0.7 / \pm 1.7$	64.87	5.60	0.64	-4.3	-0.00
125.0	68.18	$^{+2.6}_{-2.4}$	$\pm 1.6 / \pm 0.7 / \pm 1.7$	64.70	5.59	0.64	-4.3	-0.00
125.09	68.02	$^{+2.6}_{-2.3}$	$\pm 1.6 / \pm 0.7 / \pm 1.7$	64.53	5.60	0.63	-4.3	-0.00
125.1	68.00	$^{+2.6}_{-2.3}$	$\pm 1.6 / \pm 0.7 / \pm 1.7$	64.51	5.59	0.64	-4.3	-0.00
125.2	67.82	$^{+2.6}_{-2.3}$	$\pm 1.6 / \pm 0.7 / \pm 1.7$	64.34	5.59	0.64	-4.3	-0.00
125.3	67.65	$^{+2.7}_{-2.3}$	$\pm 1.6 / \pm 0.7 / \pm 1.7$	64.17	5.58	0.63	-4.3	-0.00
125.4	67.49	$^{+2.7}_{-2.3}$	$\pm 1.6 / \pm 0.7 / \pm 1.7$	64.02	5.57	0.63	-4.3	-0.00
125.5	67.28	$^{+2.6}_{-2.3}$	$\pm 1.6 / \pm 0.7 / \pm 1.7$	63.81	5.56	0.63	-4.3	-0.00
125.6	67.13	$^{+2.6}_{-2.3}$	$\pm 1.6 / \pm 0.7 / \pm 1.7$	63.65	5.56	0.63	-4.3	-0.00
125.7	66.97	$^{+2.6}_{-2.3}$	$\pm 1.6 / \pm 0.7 / \pm 1.7$	63.50	5.56	0.63	-4.3	-0.00
125.8	66.83	$^{+2.6}_{-2.3}$	$\pm 1.6 / \pm 0.7 / \pm 1.7$	63.35	5.55	0.63	-4.3	-0.00
125.9	66.62	$^{+2.6}_{-2.3}$	$\pm 1.6 / \pm 0.7 / \pm 1.7$	63.16	5.54	0.62	-4.3	-0.00
126.0	66.48	$^{+2.6}_{-2.3}$	$\pm 1.6 / \pm 0.7 / \pm 1.7$	63.02	5.53	0.62	-4.3	-0.00
126.5	65.62	$^{+2.7}_{-2.3}$	$\pm 1.6 / \pm 0.7 / \pm 1.7$	62.17	5.50	0.62	-4.3	-0.00
127.0	64.82	$^{+2.7}_{-2.3}$	$\pm 1.6 / \pm 0.7 / \pm 1.7$	61.38	5.47	0.61	-4.3	-0.00
127.5	64.03	$^{+2.7}_{-2.3}$	$\pm 1.6 / \pm 0.7 / \pm 1.7$	60.58	5.44	0.61	-4.3	-0.00
128.0	63.24	$^{+2.7}_{-2.3}$	$\pm 1.6 / \pm 0.7 / \pm 1.7$	59.80	5.40	0.60	-4.3	-0.00
128.5	62.48	$^{+2.7}_{-2.3}$	$\pm 1.6 / \pm 0.7 / \pm 1.7$	59.06	5.37	0.59	-4.3	-0.00
129.0	61.72	$^{+2.7}_{-2.3}$	$\pm 1.6 / \pm 0.7 / \pm 1.7$	58.32	5.33	0.59	-4.3	-0.00
129.5	60.97	$^{+2.7}_{-2.4}$	$\pm 1.6 / \pm 0.7 / \pm 1.7$	57.57	5.31	0.58	-4.3	-0.00
130.0	60.22	$^{+2.7}_{-2.4}$	$\pm 1.6 / \pm 0.7 / \pm 1.7$	56.84	5.27	0.58	-4.3	-0.00

Table B.14: Total $Z(\rightarrow\nu\bar{\nu})H$ cross sections including QCD and EW corrections and their uncertainties for a proton–proton collision energy $\sqrt{s} = 8$ TeV and a Higgs-boson masses.

$M_H[\text{GeV}]$	$\sigma[\text{fb}]$	$\Delta_{\text{scale}}[\%]$	$\Delta_{\text{PDF}/\alpha_s/\text{PDF} \oplus \alpha_s}[\%]$	$\sigma_{\text{NNLOQCD}}^{\text{DY}}[\text{fb}]$	$\sigma_{\text{NLO+NLL}}^{\text{ggZH}}[\text{fb}]$	$\sigma_{\text{t-loop}}[\text{fb}]$	$\delta_{\text{EW}}[\%]$	$\sigma_\gamma[\text{fb}]$
120.0	95.81	$^{+2.6}_{-2.4}$	$\pm 1.5/\pm 0.8/\pm 1.7$	90.37	8.35	0.90	-4.2	-0.00
120.5	94.56	$^{+2.7}_{-2.3}$	$\pm 1.5/\pm 0.8/\pm 1.7$	89.13	8.30	0.89	-4.2	-0.00
121.0	93.41	$^{+2.7}_{-2.3}$	$\pm 1.5/\pm 0.8/\pm 1.7$	87.99	8.26	0.88	-4.2	-0.00
121.5	92.27	$^{+2.7}_{-2.3}$	$\pm 1.5/\pm 0.8/\pm 1.7$	86.87	8.21	0.87	-4.2	-0.00
122.0	91.12	$^{+2.8}_{-2.4}$	$\pm 1.5/\pm 0.8/\pm 1.7$	85.72	8.17	0.86	-4.2	-0.00
122.5	90.01	$^{+2.7}_{-2.4}$	$\pm 1.5/\pm 0.8/\pm 1.7$	84.62	8.12	0.86	-4.2	-0.00
123.0	88.85	$^{+2.8}_{-2.4}$	$\pm 1.5/\pm 0.8/\pm 1.7$	83.48	8.07	0.85	-4.3	-0.00
123.5	87.74	$^{+2.8}_{-2.4}$	$\pm 1.5/\pm 0.8/\pm 1.7$	82.40	8.02	0.84	-4.3	-0.00
124.0	86.69	$^{+2.8}_{-2.4}$	$\pm 1.5/\pm 0.8/\pm 1.7$	81.35	7.98	0.83	-4.3	-0.00
124.1	86.47	$^{+2.8}_{-2.4}$	$\pm 1.5/\pm 0.8/\pm 1.7$	81.13	7.97	0.83	-4.3	-0.00
124.2	86.27	$^{+2.8}_{-2.4}$	$\pm 1.5/\pm 0.8/\pm 1.7$	80.94	7.96	0.82	-4.3	-0.00
124.3	86.07	$^{+2.7}_{-2.4}$	$\pm 1.5/\pm 0.8/\pm 1.7$	80.74	7.96	0.82	-4.3	-0.00
124.4	85.87	$^{+2.8}_{-2.5}$	$\pm 1.5/\pm 0.8/\pm 1.7$	80.54	7.94	0.83	-4.3	-0.00
124.5	85.65	$^{+2.7}_{-2.5}$	$\pm 1.5/\pm 0.8/\pm 1.7$	80.33	7.93	0.82	-4.3	-0.00
124.6	85.42	$^{+2.8}_{-2.5}$	$\pm 1.5/\pm 0.8/\pm 1.7$	80.09	7.92	0.83	-4.3	-0.00
124.7	85.19	$^{+2.9}_{-2.4}$	$\pm 1.5/\pm 0.8/\pm 1.7$	79.88	7.91	0.82	-4.3	-0.00
124.8	84.97	$^{+2.9}_{-2.4}$	$\pm 1.5/\pm 0.8/\pm 1.7$	79.66	7.90	0.81	-4.3	-0.00
124.9	84.76	$^{+2.9}_{-2.4}$	$\pm 1.5/\pm 0.8/\pm 1.7$	79.46	7.89	0.81	-4.3	-0.00
125.0	84.56	$^{+2.9}_{-2.4}$	$\pm 1.5/\pm 0.8/\pm 1.7$	79.25	7.89	0.81	-4.3	-0.00
125.09	84.40	$^{+2.8}_{-2.4}$	$\pm 1.5/\pm 0.8/\pm 1.7$	79.09	7.89	0.81	-4.3	-0.00
125.1	84.40	$^{+2.8}_{-2.5}$	$\pm 1.5/\pm 0.8/\pm 1.7$	79.08	7.89	0.81	-4.3	-0.00
125.2	84.16	$^{+2.8}_{-2.5}$	$\pm 1.5/\pm 0.8/\pm 1.7$	78.86	7.87	0.81	-4.3	-0.00
125.3	83.94	$^{+2.9}_{-2.4}$	$\pm 1.5/\pm 0.8/\pm 1.7$	78.64	7.86	0.81	-4.3	-0.00
125.4	83.73	$^{+2.8}_{-2.4}$	$\pm 1.5/\pm 0.8/\pm 1.7$	78.44	7.85	0.81	-4.3	-0.00
125.5	83.56	$^{+2.8}_{-2.5}$	$\pm 1.5/\pm 0.8/\pm 1.7$	78.26	7.84	0.81	-4.3	-0.00
125.6	83.36	$^{+2.8}_{-2.5}$	$\pm 1.5/\pm 0.8/\pm 1.7$	78.07	7.84	0.80	-4.3	-0.00
125.7	83.13	$^{+2.8}_{-2.5}$	$\pm 1.5/\pm 0.7/\pm 1.7$	77.84	7.83	0.80	-4.3	-0.00
125.8	82.98	$^{+2.7}_{-2.6}$	$\pm 1.5/\pm 0.7/\pm 1.7$	77.70	7.82	0.80	-4.3	-0.00
125.9	82.79	$^{+2.8}_{-2.6}$	$\pm 1.5/\pm 0.7/\pm 1.7$	77.49	7.82	0.80	-4.3	-0.00
126.0	82.54	$^{+2.8}_{-2.5}$	$\pm 1.5/\pm 0.7/\pm 1.7$	77.26	7.80	0.80	-4.3	-0.00
126.5	81.53	$^{+2.9}_{-2.5}$	$\pm 1.5/\pm 0.7/\pm 1.7$	76.27	7.75	0.79	-4.3	-0.00
127.0	80.54	$^{+2.9}_{-2.5}$	$\pm 1.5/\pm 0.7/\pm 1.7$	75.29	7.71	0.78	-4.3	-0.00
127.5	79.60	$^{+2.8}_{-2.6}$	$\pm 1.5/\pm 0.7/\pm 1.7$	74.36	7.67	0.78	-4.3	-0.00
128.0	78.67	$^{+2.9}_{-2.6}$	$\pm 1.5/\pm 0.7/\pm 1.7$	73.44	7.63	0.77	-4.3	-0.00
128.5	77.63	$^{+3.0}_{-2.5}$	$\pm 1.5/\pm 0.7/\pm 1.7$	72.45	7.57	0.76	-4.3	-0.00
129.0	76.75	$^{+2.9}_{-2.6}$	$\pm 1.5/\pm 0.7/\pm 1.7$	71.57	7.54	0.75	-4.3	-0.00
129.5	75.82	$^{+2.9}_{-2.6}$	$\pm 1.5/\pm 0.7/\pm 1.7$	70.66	7.49	0.74	-4.3	-0.00
130.0	74.90	$^{+3.0}_{-2.6}$	$\pm 1.5/\pm 0.7/\pm 1.7$	69.77	7.43	0.73	-4.4	-0.00

Table B.15: Total $Z(\rightarrow\nu\bar{\nu})H$ cross sections including QCD and EW corrections and their uncertainties for a proton–proton collision energy $\sqrt{s} = 13$ TeV and a Higgs-boson masses.

$M_H[\text{GeV}]$	$\sigma[\text{fb}]$	$\Delta_{\text{scale}}[\%]$	$\Delta_{\text{PDF}/\alpha_s/\text{PDF}\oplus\alpha_s}[\%]$	$\sigma_{\text{NNLOQCD}}^{\text{DY}}[\text{fb}]$	$\sigma_{\text{NLO+NLL}}^{\text{ggZH}}[\text{fb}]$	$\sigma_{\text{t-loop}}[\text{fb}]$	$\delta_{\text{EW}}[\%]$	$\sigma_\gamma[\text{fb}]$
120.0	199.71	+3.4 -3.0	$\pm 1.3/\pm 1.0/\pm 1.6$	179.34	26.00	2.07	-4.3	-0.00
120.5	197.49	+3.4 -3.0	$\pm 1.3/\pm 1.0/\pm 1.6$	177.22	25.85	2.04	-4.3	-0.00
121.0	195.02	+3.5 -3.0	$\pm 1.3/\pm 1.0/\pm 1.6$	174.89	25.64	2.02	-4.3	-0.00
121.5	192.73	+3.6 -3.0	$\pm 1.3/\pm 1.0/\pm 1.6$	172.77	25.40	2.01	-4.3	-0.00
122.0	190.57	+3.6 -3.0	$\pm 1.3/\pm 1.0/\pm 1.6$	170.51	25.45	1.98	-4.3	-0.00
122.5	188.29	+3.6 -3.0	$\pm 1.3/\pm 0.9/\pm 1.6$	168.30	25.31	1.97	-4.3	-0.00
123.0	186.15	+3.6 -3.1	$\pm 1.3/\pm 0.9/\pm 1.6$	166.32	25.10	1.93	-4.3	-0.00
123.5	184.00	+3.5 -3.1	$\pm 1.3/\pm 0.9/\pm 1.6$	164.18	25.02	1.93	-4.3	-0.00
124.0	181.88	+3.6 -3.1	$\pm 1.3/\pm 0.9/\pm 1.6$	162.15	24.86	1.92	-4.3	-0.00
124.1	181.59	+3.7 -3.2	$\pm 1.3/\pm 0.9/\pm 1.6$	161.86	24.87	1.91	-4.4	-0.00
124.2	181.01	+3.8 -3.0	$\pm 1.3/\pm 0.9/\pm 1.6$	161.32	24.82	1.89	-4.4	-0.00
124.3	180.60	+3.7 -3.1	$\pm 1.3/\pm 0.9/\pm 1.6$	160.91	24.80	1.89	-4.4	-0.00
124.4	180.13	+3.7 -3.0	$\pm 1.3/\pm 0.9/\pm 1.6$	160.49	24.74	1.89	-4.4	-0.00
124.5	179.72	+3.8 -3.0	$\pm 1.3/\pm 0.9/\pm 1.6$	160.10	24.71	1.89	-4.4	-0.00
124.6	179.27	+3.8 -3.0	$\pm 1.3/\pm 0.9/\pm 1.6$	159.68	24.67	1.88	-4.4	-0.00
124.7	178.90	+3.8 -3.1	$\pm 1.3/\pm 0.9/\pm 1.6$	159.26	24.70	1.88	-4.4	-0.00
124.8	178.51	+3.7 -3.1	$\pm 1.3/\pm 0.9/\pm 1.6$	158.96	24.61	1.88	-4.4	-0.00
124.9	178.00	+3.9 -3.1	$\pm 1.3/\pm 0.9/\pm 1.6$	158.47	24.58	1.86	-4.4	-0.00
125.0	177.62	+3.8 -3.1	$\pm 1.3/\pm 0.9/\pm 1.6$	158.10	24.57	1.85	-4.4	-0.00
125.09	177.30	+3.8 -3.0	$\pm 1.3/\pm 0.9/\pm 1.6$	157.77	24.55	1.86	-4.4	-0.00
125.1	177.22	+3.9 -3.0	$\pm 1.3/\pm 0.9/\pm 1.6$	157.70	24.54	1.87	-4.4	-0.00
125.2	176.81	+3.8 -3.1	$\pm 1.3/\pm 0.9/\pm 1.6$	157.34	24.47	1.87	-4.4	-0.00
125.3	176.48	+3.8 -3.1	$\pm 1.3/\pm 0.9/\pm 1.6$	157.00	24.48	1.86	-4.4	-0.00
125.4	176.15	+3.8 -3.1	$\pm 1.3/\pm 0.9/\pm 1.6$	156.67	24.46	1.87	-4.4	-0.00
125.5	175.68	+3.7 -3.1	$\pm 1.3/\pm 0.9/\pm 1.6$	156.21	24.44	1.86	-4.4	-0.00
125.6	175.36	+3.8 -3.1	$\pm 1.3/\pm 0.9/\pm 1.6$	155.85	24.48	1.85	-4.4	-0.00
125.7	174.88	+3.8 -3.0	$\pm 1.3/\pm 0.9/\pm 1.6$	155.47	24.36	1.85	-4.4	-0.00
125.8	174.63	+3.7 -3.2	$\pm 1.3/\pm 0.9/\pm 1.6$	155.18	24.40	1.85	-4.4	-0.00
125.9	174.16	+3.8 -3.1	$\pm 1.3/\pm 0.9/\pm 1.6$	154.74	24.36	1.83	-4.4	-0.00
126.0	173.80	+3.8 -3.1	$\pm 1.3/\pm 0.9/\pm 1.6$	154.36	24.37	1.83	-4.4	-0.00
126.5	171.76	+3.7 -3.2	$\pm 1.3/\pm 0.9/\pm 1.6$	152.40	24.23	1.81	-4.4	-0.00
127.0	169.73	+3.7 -3.2	$\pm 1.3/\pm 0.9/\pm 1.6$	150.49	24.07	1.79	-4.4	-0.00
127.5	167.75	+3.8 -3.2	$\pm 1.3/\pm 0.9/\pm 1.6$	148.56	23.94	1.78	-4.4	-0.00
128.0	165.85	+3.9 -3.1	$\pm 1.3/\pm 0.9/\pm 1.6$	146.74	23.81	1.77	-4.4	-0.00
128.5	164.02	+3.9 -3.2	$\pm 1.3/\pm 0.9/\pm 1.6$	145.06	23.62	1.75	-4.4	-0.00
129.0	162.22	+3.8 -3.2	$\pm 1.3/\pm 0.9/\pm 1.6$	143.28	23.55	1.73	-4.4	-0.00
129.5	160.33	+3.9 -3.2	$\pm 1.3/\pm 0.9/\pm 1.6$	141.45	23.44	1.72	-4.4	-0.00
130.0	158.65	+3.9 -3.2	$\pm 1.3/\pm 0.9/\pm 1.6$	139.88	23.29	1.70	-4.4	-0.00

Table B.16: Total $Z(\rightarrow\nu\bar{\nu})H$ cross sections including QCD and EW corrections and their uncertainties for a proton–proton collision energy $\sqrt{s} = 14$ TeV and a Higgs-boson masses.

$M_H[\text{GeV}]$	$\sigma[\text{fb}]$	$\Delta_{\text{scale}}[\%]$	$\Delta_{\text{PDF}/\alpha_s/\text{PDF}\oplus\alpha_s}[\%]$	$\sigma_{\text{NNLOQCD}}^{\text{DY}}[\text{fb}]$	$\sigma_{\text{NLO+NLL}}^{\text{ggZH}}[\text{fb}]$	$\sigma_{\text{t-loop}}[\text{fb}]$	$\delta_{\text{EW}}[\%]$	$\sigma_\gamma[\text{fb}]$
120.0	222.28	+3.6 -3.0	$\pm 1.3/\pm 1.0/\pm 1.7$	198.00	30.48	2.33	-4.3	-0.00
120.5	219.82	+3.7 -3.1	$\pm 1.3/\pm 1.0/\pm 1.7$	195.63	30.34	2.29	-4.3	-0.00
121.0	217.19	+3.6 -3.1	$\pm 1.3/\pm 1.0/\pm 1.7$	193.16	30.10	2.27	-4.3	-0.00
121.5	214.80	+3.5 -3.1	$\pm 1.3/\pm 1.0/\pm 1.7$	190.76	30.04	2.25	-4.3	-0.00
122.0	212.29	+3.6 -3.1	$\pm 1.3/\pm 1.0/\pm 1.7$	188.38	29.84	2.23	-4.3	-0.00
122.5	209.94	+3.6 -3.2	$\pm 1.3/\pm 1.0/\pm 1.7$	186.16	29.64	2.22	-4.3	-0.00
123.0	207.36	+3.8 -3.1	$\pm 1.3/\pm 1.0/\pm 1.6$	183.66	29.50	2.19	-4.3	-0.00
123.5	204.93	+3.7 -3.1	$\pm 1.3/\pm 1.0/\pm 1.6$	181.35	29.29	2.19	-4.4	-0.00
124.0	202.68	+3.8 -3.2	$\pm 1.3/\pm 1.0/\pm 1.6$	179.10	29.24	2.15	-4.4	-0.00
124.1	202.20	+3.7 -3.2	$\pm 1.3/\pm 1.0/\pm 1.6$	178.68	29.16	2.15	-4.4	-0.00
124.2	201.67	+3.7 -3.1	$\pm 1.3/\pm 1.0/\pm 1.6$	178.16	29.13	2.15	-4.4	-0.00
124.3	201.31	+3.7 -3.2	$\pm 1.3/\pm 1.0/\pm 1.6$	177.75	29.18	2.13	-4.4	-0.00
124.4	200.70	+3.8 -3.2	$\pm 1.3/\pm 1.0/\pm 1.6$	177.24	29.06	2.13	-4.4	-0.00
124.5	200.38	+3.7 -3.3	$\pm 1.3/\pm 1.0/\pm 1.6$	176.93	29.04	2.14	-4.4	-0.00
124.6	199.83	+3.8 -3.2	$\pm 1.3/\pm 1.0/\pm 1.6$	176.43	28.98	2.12	-4.4	-0.00
124.7	199.45	+3.8 -3.3	$\pm 1.3/\pm 1.0/\pm 1.6$	176.03	29.00	2.12	-4.4	-0.00
124.8	198.90	+3.8 -3.2	$\pm 1.3/\pm 1.0/\pm 1.6$	175.57	28.90	2.11	-4.4	-0.00
124.9	198.43	+3.8 -3.2	$\pm 1.3/\pm 1.0/\pm 1.6$	175.07	28.91	2.12	-4.4	-0.00
125.0	198.12	+3.8 -3.3	$\pm 1.3/\pm 1.0/\pm 1.6$	174.77	28.88	2.11	-4.4	-0.00
125.09	197.64	+3.8 -3.2	$\pm 1.3/\pm 1.0/\pm 1.6$	174.28	28.86	2.12	-4.4	-0.00
125.1	197.58	+3.9 -3.3	$\pm 1.3/\pm 1.0/\pm 1.6$	174.25	28.85	2.11	-4.4	-0.00
125.2	197.16	+3.8 -3.2	$\pm 1.3/\pm 1.0/\pm 1.6$	173.81	28.86	2.10	-4.4	-0.00
125.3	196.76	+3.8 -3.3	$\pm 1.3/\pm 1.0/\pm 1.6$	173.44	28.82	2.10	-4.4	-0.00
125.4	196.26	+3.9 -3.2	$\pm 1.3/\pm 1.0/\pm 1.6$	172.97	28.77	2.09	-4.4	-0.00
125.5	195.81	+3.9 -3.2	$\pm 1.3/\pm 1.0/\pm 1.6$	172.56	28.72	2.10	-4.4	-0.00
125.6	195.44	+3.8 -3.3	$\pm 1.3/\pm 1.0/\pm 1.6$	172.22	28.68	2.09	-4.4	-0.00
125.7	194.93	+3.9 -3.3	$\pm 1.3/\pm 1.0/\pm 1.6$	171.70	28.68	2.08	-4.4	-0.00
125.8	194.42	+3.9 -3.2	$\pm 1.3/\pm 1.0/\pm 1.6$	171.22	28.63	2.08	-4.4	-0.00
125.9	194.00	+3.9 -3.2	$\pm 1.3/\pm 1.0/\pm 1.6$	170.82	28.60	2.08	-4.4	-0.00
126.0	193.44	+4.0 -3.2	$\pm 1.3/\pm 1.0/\pm 1.6$	170.28	28.56	2.08	-4.4	-0.00
126.5	191.38	+4.0 -3.3	$\pm 1.3/\pm 1.0/\pm 1.6$	168.33	28.40	2.05	-4.4	-0.00
127.0	189.28	+4.1 -3.3	$\pm 1.3/\pm 1.0/\pm 1.6$	166.30	28.28	2.03	-4.4	-0.00
127.5	187.21	+4.0 -3.3	$\pm 1.3/\pm 1.0/\pm 1.6$	164.34	28.10	2.02	-4.4	-0.00
128.0	185.00	+4.1 -3.2	$\pm 1.3/\pm 1.0/\pm 1.6$	162.26	27.92	2.00	-4.4	-0.00
128.5	183.14	+4.0 -3.4	$\pm 1.3/\pm 1.0/\pm 1.6$	160.44	27.82	1.99	-4.4	-0.00
129.0	181.22	+3.9 -3.4	$\pm 1.3/\pm 1.0/\pm 1.6$	158.65	27.66	1.95	-4.4	-0.00
129.5	179.09	+3.9 -3.4	$\pm 1.3/\pm 1.0/\pm 1.6$	156.62	27.50	1.94	-4.4	-0.00
130.0	176.91	+4.1 -3.4	$\pm 1.3/\pm 1.0/\pm 1.6$	154.61	27.27	1.92	-4.5	-0.00

References

- [1] LHC Higgs Cross Section Working Group, S. Dittmaier, et al., *Handbook of LHC Higgs Cross Sections: 1. Inclusive Observables*, arXiv:1101.0593 [hep-ph].
- [2] LHC Higgs Cross Section Working Group, S. Dittmaier, et al., *Handbook of LHC Higgs Cross Sections: 2. Differential Distributions*, CERN-2012-002 (CERN, Geneva, 2012) , arXiv:1201.3084 [hep-ph].
- [3] LHC Higgs Cross Section Working Group, S. Heinemeyer, C. Mariotti, G. Passarino, and R. Tanaka (Eds.), *Handbook of LHC Higgs Cross Sections: 3. Higgs Properties*, CERN-2013-004 (CERN, Geneva, 2013) , arXiv:1307.1347 [hep-ph].
- [4] A. Denner, S. Dittmaier, S. Kallweit, and A. Mück, *HAWK 2.0: A Monte Carlo program for Higgs production in vector-boson fusion and Higgs strahlung at hadron colliders*, Comput. Phys. Commun. **195** (2015) 161–171, arXiv:1412.5390 [hep-ph].
- [5] A. Denner, S. Dittmaier, and A. Mück, *HAWK: A Monte Carlo generator for the production of Higgs bosons Attached to Weak bosons at hadron colliders*, <http://omnibus.uni-freiburg.de/~sd565/programs/hawk/hawk.html>, 2010.
- [6] M. Ciccolini, A. Denner, and S. Dittmaier, *Strong and electroweak corrections to the production of Higgs + 2jets via weak interactions at the LHC*, Phys. Rev. Lett. **99** (2007) 161803, arXiv:0707.0381 [hep-ph].
- [7] M. Ciccolini, A. Denner, and S. Dittmaier, *Electroweak and QCD corrections to Higgs production via vector-boson fusion at the LHC*, Phys. Rev. **D77** (2008) 013002, arXiv:0710.4749 [hep-ph].
- [8] A. Denner, S. Dittmaier, S. Kallweit, and A. Mück, *Electroweak corrections to Higgs-strahlung off W/Z bosons at the Tevatron and the LHC with HAWK*, JHEP **1203** (2012) 075, arXiv:1112.5142 [hep-ph].
- [9] S. Frixione, P. Torrielli, and M. Zaro, *Higgs production through vector-boson fusion at the NLO matched with parton showers*, Phys. Lett. **B726** (2013) 273–282, arXiv:1304.7927 [hep-ph].
- [10] J. Alwall, R. Frederix, S. Frixione, V. Hirschi, F. Maltoni, O. Mattelaer, H. S. Shao, T. Stelzer, P. Torrielli, and M. Zaro, *The automated computation of tree-level and next-to-leading order differential cross sections, and their matching to parton shower simulations*, JHEP **07** (2014) 079, arXiv:1405.0301 [hep-ph].
- [11] P. Nason and C. Oleari, *NLO Higgs boson production via vector-boson fusion matched with shower in POWHEG*, JHEP **02** (2010) 037, arXiv:0911.5299 [hep-ph].
- [12] T. Figy, V. Hankele, and D. Zeppenfeld, *Next-to-leading order QCD corrections to Higgs plus three jet production in vector-boson fusion*, JHEP **02** (2008) 076, arXiv:0710.5621 [hep-ph].
- [13] B. Jäger, F. Schissler, and D. Zeppenfeld, *Parton-shower effects on Higgs boson production via vector-boson fusion in association with three jets*, JHEP **07** (2014) 125, arXiv:1405.6950 [hep-ph].
- [14] P. Bolzoni, F. Maltoni, S.-O. Moch, and M. Zaro, *Higgs production via vector-boson fusion at NNLO in QCD*, Phys. Rev. Lett. **105** (2010) 011801, arXiv:1003.4451 [hep-ph].
- [15] M. Cacciari, F. A. Dreyer, A. Karlberg, G. P. Salam, and G. Zanderighi, *Fully Differential Vector-Boson-Fusion Higgs Production at Next-to-Next-to-Leading Order*, Phys. Rev. Lett. **115** (2015) no. 8, 082002, arXiv:1506.02660 [hep-ph].
- [16] K. Arnold et al., *VBFNLO: A Parton level Monte Carlo for processes with electroweak bosons*, Comput. Phys. Commun. **180** (2009) 1661–1670, arXiv:0811.4559 [hep-ph].
- [17] T. Figy, C. Oleari, and D. Zeppenfeld, *Next-to-leading order jet distributions for Higgs boson production via weak boson fusion*, Phys. Rev. **D68** (2003) 073005, arXiv:hep-ph/0306109 [hep-ph].

- [18] V. Hankele, G. Klamke, D. Zeppenfeld, and T. Figy, *Anomalous Higgs boson couplings in vector boson fusion at the CERN LHC*, Phys. Rev. **D74** (2006) 095001, arXiv:hep-ph/0609075 [hep-ph].
- [19] T. Figy, S. Palmer, and G. Weiglein, *Higgs Production via Weak Boson Fusion in the Standard Model and the MSSM*, JHEP **02** (2012) 105, arXiv:1012.4789 [hep-ph].
- [20] P. Bolzoni, F. Maltoni, S.-O. Moch, and M. Zaro, *Vector boson fusion at NNLO in QCD: SM Higgs and beyond*, Phys. Rev. **D85** (2012) 035002, arXiv:1109.3717 [hep-ph].
- [21] T. Han, G. Valencia, and S. Willenbrock, *Structure function approach to vector boson scattering in p p collisions*, Phys. Rev. Lett. **69** (1992) 3274–3277, arXiv:hep-ph/9206246 [hep-ph].
- [22] W. A. Bardeen, A. J. Buras, D. W. Duke, and T. Muta, *Deep Inelastic Scattering Beyond the Leading Order in Asymptotically Free Gauge Theories*, Phys. Rev. **D18** (1978) 3998.
- [23] D. I. Kazakov, A. V. Kotikov, G. Parente, O. A. Sampayo, and J. Sanchez Guillen, *Complete quartic ($\alpha(s)^{**2}$) correction to the deep inelastic longitudinal structure function $F(L)$ in QCD*, Phys. Rev. Lett. **65** (1990) 1535–1538. [Erratum: Phys. Rev. Lett. 65, 2921 (1990)].
- [24] E. B. Zijlstra and W. L. van Neerven, *Order $\alpha(s)^{**2}$ correction to the structure function $F_3(x, Q^{**2})$ in deep inelastic neutrino - hadron scattering*, Phys. Lett. **B297** (1992) 377–384.
- [25] E. B. Zijlstra and W. L. van Neerven, *Order $\alpha(s)^{**2}$ QCD corrections to the deep inelastic proton structure functions F_2 and $F(L)$* , Nucl. Phys. **B383** (1992) 525–574.
- [26] S. Moch and J. A. M. Vermaasen, *Deep inelastic structure functions at two loops*, Nucl. Phys. **B573** (2000) 853–907, arXiv:hep-ph/9912355 [hep-ph].
- [27] W. L. van Neerven and J. A. M. Vermaasen, *The Role of the Five Point Function in Radiative Corrections to Two Photon Physics*, Phys. Lett. **B142** (1984) 80.
- [28] J. Blumlein, G. J. van Oldenborgh, and R. Ruckl, *QCD and QED corrections to Higgs boson production in charged current e p scattering*, Nucl. Phys. **B395** (1993) 35–59, arXiv:hep-ph/9209219 [hep-ph].
- [29] R. V. Harlander, J. Vollinga, and M. M. Weber, *Gluon-Induced Weak Boson Fusion*, Phys. Rev. **D77** (2008) 053010, arXiv:0801.3355 [hep-ph].
- [30] J. Butterworth et al., *PDF4LHC recommendations for LHC Run II*, J. Phys. **G43** (2016) 023001, arXiv:1510.03865 [hep-ph].
- [31] NNPDF Collaboration, R. D. Ball et al., *Parton distributions with QED corrections*, Nucl. Phys. **B877** (2013) 290–320, arXiv:1308.0598 [hep-ph].
- [32] M. Cacciari, G. P. Salam, and G. Soyez, *The Anti- $k(t)$ jet clustering algorithm*, JHEP **0804** (2008) 063, arXiv:0802.1189 [hep-ph].
- [33] R. Frederix and S. Frixione, *Merging meets matching in MC@NLO*, JHEP **12** (2012) 061, arXiv:1209.6215 [hep-ph].
- [34] R. Frederix, S. Frixione, A. Papaefstathiou, S. Prestel, and P. Torrielli, *A study of multi-jet production in association with an electroweak vector boson*, arXiv:1511.00847 [hep-ph].
- [35] G. Ferrera, M. Grazzini, and F. Tramontano, *Higher-order QCD effects for associated WH production and decay at the LHC*, JHEP **04** (2014) 039, arXiv:1312.1669 [hep-ph].
- [36] G. Ferrera, M. Grazzini, and F. Tramontano, *Associated ZH production at hadron colliders: the fully differential NNLO QCD calculation*, Phys. Lett. **B740** (2015) 51–55, arXiv:1407.4747 [hep-ph].
- [37] A. Djouadi, J. Kalinowski, and M. Spira, *HDECAY: A Program for Higgs boson decays in the standard model and its supersymmetric extension*, Comput. Phys. Commun. **108** (1998) 56–74, arXiv:hep-ph/9704448 [hep-ph]. <http://people.web.psi.ch/spira/hdecay/>.
- [38] J. Gaunt, M. Stahlhofen, F. J. Tackmann, and J. R. Walsh, *N-jettiness Subtractions for NNLO QCD Calculations*, JHEP **09** (2015) 058, arXiv:1505.04794 [hep-ph].

- [39] R. Boughezal, C. Focke, X. Liu, and F. Petriello, *W-boson production in association with a jet at next-to-next-to-leading order in perturbative QCD*, *Phys. Rev. Lett.* **115** (2015) no. 6, 062002, [arXiv:1504.02131 \[hep-ph\]](#).
- [40] R. Boughezal, C. Focke, W. Giele, X. Liu, and F. Petriello, *Higgs boson production in association with a jet at NNLO using jettiness subtraction*, *Phys. Lett.* **B748** (2015) 5–8, [arXiv:1505.03893 \[hep-ph\]](#).
- [41] R. Boughezal, J. M. Campbell, R. K. Ellis, C. Focke, W. T. Giele, X. Liu, and F. Petriello, *Z-boson production in association with a jet at next-to-next-to-leading order in perturbative QCD*, [arXiv:1512.01291 \[hep-ph\]](#).
- [42] J. M. Campbell and R. K. Ellis, *An Update on vector boson pair production at hadron colliders*, *Phys. Rev.* **D60** (1999) 113006, [arXiv:hep-ph/9905386 \[hep-ph\]](#).
- [43] J. M. Campbell, R. K. Ellis, and C. Williams, *Vector boson pair production at the LHC*, *JHEP* **1107** (2011) 018, [arXiv:1105.0020 \[hep-ph\]](#).
- [44] J. M. Campbell, R. K. Ellis, and W. T. Giele, *A Multi-Threaded Version of MCFM*, *Eur. Phys. J.* **C75** (2015) no. 6, 246, [arXiv:1503.06182 \[physics.comp-ph\]](#).
- [45] J. M. Campbell, R. K. Ellis, and C. Williams, *Associated production of a Higgs boson at NNLO*, [arXiv:1601.00658 \[hep-ph\]](#).
- [46] G. Ferrera, M. Grazzini, and F. Tramontano, *Associated WH production at hadron colliders: a fully exclusive QCD calculation at NNLO*, *Phys. Rev. Lett.* **107** (2011) 152003, [arXiv:1107.1164 \[hep-ph\]](#).
- [47] O. Brein, R. V. Harlander, and T. J. Zirke, *vh@nnlo - Higgs Strahlung at hadron colliders*, [arXiv:1210.5347 \[hep-ph\]](#).
- [48] R. V. Harlander, S. Liebler, and T. Zirke, *Higgs Strahlung at the Large Hadron Collider in the 2-Higgs-Doublet Model*, *JHEP* **02** (2014) 023, [arXiv:1307.8122 \[hep-ph\]](#).
- [49] R. Hamberg, W. L. van Neerven, and T. Matsuura, *A Complete calculation of the order $\alpha - s^2$ correction to the Drell-Yan K factor*, *Nucl. Phys.* **B359** (1991) 343–405. [Erratum: Nucl. Phys.B644,403(2002)].
- [50] O. Brein, A. Djouadi, and R. Harlander, *NNLO QCD corrections to the Higgs-strahlung processes at a hadron collider*, *Phys.Lett.* **B579** (2004) 149–156, [arXiv:hep-ph/0307206 \[hep-ph\]](#).
- [51] O. Brein, R. Harlander, M. Wiesemann, and T. Zirke, *Top-Quark Mediated Effects in Hadronic Higgs-Strahlung*, *Eur. Phys. J.* **C72** (2012) 1868, [arXiv:1111.0761 \[hep-ph\]](#).
- [52] B. A. Kniehl, *Elastic e p scattering and the Weizsäcker-Williams approximation*, *Phys. Lett.* **B254** (1991) 267–273.
- [53] D. A. Dicus and C. Kao, *Higgs Boson - Z^0 Production From Gluon Fusion*, *Phys. Rev.* **D38** (1988) 1008. [Erratum: Phys. Rev.D42,2412(1990)].
- [54] B. A. Kniehl and C. P. Palisoc, *Associated production of Z and neutral Higgs bosons at the CERN Large Hadron Collider*, *Phys. Rev.* **D85** (2012) 075027, [arXiv:1112.1575 \[hep-ph\]](#).
- [55] L. Altenkamp, S. Dittmaier, R. V. Harlander, H. Rzehak, and T. J. E. Zirke, *Gluon-induced Higgs-strahlung at next-to-leading order QCD*, *JHEP* **02** (2013) 078, [arXiv:1211.5015 \[hep-ph\]](#).
- [56] R. V. Harlander, A. Kulesza, V. Theeuwes, and T. Zirke, *Soft gluon resummation for gluon-induced Higgs Strahlung*, *JHEP* **11** (2014) 082, [arXiv:1410.0217 \[hep-ph\]](#).
- [57] A. D. Martin, R. G. Roberts, W. J. Stirling, and R. S. Thorne, *Parton distributions incorporating QED contributions*, *Eur. Phys. J.* **C39** (2005) 155, [arXiv:hep-ph/0411040](#).
- [58] S. Carrazza, S. Forte, Z. Kassabov, and J. Rojo, *Specialized minimal PDFs for optimized LHC calculations*, [arXiv:1602.00005 \[hep-ph\]](#).
- [59] F. Campanario, T. M. Figy, S. Plätzer, and M. Sjödahl, *Electroweak Higgs Boson Plus Three Jet*

- 754 *Production at Next-to-Leading-Order QCD*, Phys. Rev. Lett. **111** (2013) no. 21, 211802,
 755 arXiv:1308.2932 [hep-ph].
- 756 [60] F. Campanario, *Towards $pp \rightarrow VVjj$ at NLO QCD: Bosonic contributions to triple vector boson
 757 production plus jet*, JHEP **10** (2011) 070, arXiv:1105.0920 [hep-ph].
- 758 [61] J. Bellm et al., *Herwig 7.0 / Herwig++ 3.0 Release Note*, arXiv:1512.01178 [hep-ph].
- 759 [62] S. Plätzer and S. Gieseke, *Dipole Showers and Automated NLO Matching in Herwig++*, Eur.
 760 Phys. J. **C72** (2012) 2187, arXiv:1109.6256 [hep-ph].
- 761 [63] H.-L. Lai, M. Guzzi, J. Huston, Z. Li, P. M. Nadolsky, et al., *New parton distributions for collider
 762 physics*, Phys. Rev. D **82** (2010) 074024, arXiv:1007.2241 [hep-ph].
- 763 [64] Rivet Collaboration. <http://rivet.hepforge.org/analyses>.
- 764 [65] K. Hamilton, P. Nason, E. Re, and G. Zanderighi, *NNLOPS simulation of Higgs boson production*,
 765 JHEP **10** (2013) 222, arXiv:1309.0017 [hep-ph].
- 766 [66] A. Karlberg, E. Re, and G. Zanderighi, *NNLOPS accurate Drell-Yan production*, JHEP **09** (2014)
 767 134, arXiv:1407.2940 [hep-ph].
- 768 [67] G. Luisoni, P. Nason, C. Oleari, and F. Tramontano, *$HW^\pm/HZ + 0$ and 1 jet at NLO with the
 769 POWHEG BOX interfaced to GoSam and their merging within MiNLO*, JHEP **10** (2013) 083,
 770 arXiv:1306.2542 [hep-ph].
- 771 [68] J. C. Collins and D. E. Soper, *Angular Distribution of Dileptons in High-Energy Hadron
 772 Collisions*, Phys. Rev. **D16** (1977) 2219.
- 773 [69] M. Cacciari and G. P. Salam, *Dispelling the N^3 myth for the k_t jet-finder*, Phys. Lett. **B641** (2006)
 774 57–61, arXiv:hep-ph/0512210 [hep-ph].
- 775 [70] M. Cacciari, G. P. Salam, and G. Soyez, *FastJet User Manual*, Eur. Phys. J. **C72** (2012) 1896,
 776 arXiv:1111.6097 [hep-ph].
- 777 [71] L. A. Harland-Lang, A. D. Martin, P. Motylinski, and R. S. Thorne, *Parton distributions in the
 778 LHC era: MMHT 2014 PDFs*, Eur. Phys. J. **C75** (2015) 204, arXiv:1412.3989 [hep-ph].
- 779 [72] T. Sjostrand, S. Mrenna, and P. Z. Skands, *A Brief Introduction to PYTHIA 8.1*,
 780 Comput.Phys.Commun. **178** (2008) 852–867, arXiv:0710.3820 [hep-ph].
- 781 [73] P. Skands, S. Carrazza, and J. Rojo, *Tuning PYTHIA 8.1: the Monash 2013 Tune*, European
 782 Physical Journal **74** (2014) 3024, arXiv:1404.5630 [hep-ph].
- 783 [74] P. Nason and C. Oleari, *Generation cuts and Born suppression in POWHEG*, arXiv:1303.3922
 784 [hep-ph].